Development of an *in vitro* co-culture model of the human small intestine in homeostatic or inflamed state and its application in nanotoxicological research.

Angela Agnes Margarete Kämpfer

Submitted for the degree of Doctor of Philosophy

Heriot-Watt University

School of Engineering and Physical Sciences

December 2016

Abstract

The use of nanomaterials in consumer products and medical research continues to increase. This trend is concerning, especially for orally consumed products, since studies on the effects of oral exposure to nanomaterials remain inconclusive. The limited availability of appropriate *in vitro* models impedes research, even though questions arising from the increasing prevalence of chronic inflammatory conditions of the intestine need to be addressed urgently.

This project aimed to develop an *in vitro* co-culture model of Caco-2 and PMA-differentiated THP-1 cells to mimic the human intestine in both homeostatic and controlled inflamed states. The two co-culture models were characterised for cytotoxic (barrier integrity, membrane integrity, and metabolic activity) and inflammatory parameters (cytokines, nitric oxide). After establishing the co-culture protocols, the models were used to study the cytotoxic and inflammatory effects of different nanomaterials (silver and copper oxide nanoparticles) in relation to the health status at the time of exposure. Additionally, the co-cultures were applied to investigate the barrier crossing of radio-labelled gold nanoparticles.

Especially for silver nanoparticles strikingly different effects were noted between the two conditions. Overall, the effects were more pronounced in the inflamed co-culture supporting the hypothesis of increased susceptibility to nanomaterials in subjects with impaired health.

To my mum.

Acknowledgements

I would like to thank my supervisors, Dr. Agnieszka Kinsner-Ovaskainen from the Nanobiosciences Unit of the Joint Research Centre, and Prof. Vicki Stone from the Nano-Safety Group at Heriot-Watt University Edinburgh (UK), for their outstanding support, guidance, and continuous trust.

Thanks also to my (former) superiors at the Nanobiosciences Unit, namely Dr. Hermann Stamm, Dr. Birgit Sokull-Klüttgen, and Dr. François Rossi, for having given me the possibility to pursue this PhD project at the Joint Research Centre and always having encouraged and promoted my professional and personal development.

Furthermore, I would like to express my gratitude to Dr. Roel Schins from the IUF Leibniz Institute for Environmental Medicine Düsseldorf. Without his help, this project could not have been realised to the extent it is now.

In addition, I would like to acknowledge my colleagues at the JRC and the Nanobiosciences Unit in particular, for their tireless support, both professionally and privately, especially Dr. Sabrina Gioria, Dr. Patricia Urbán, Dr. David Asturiol, Dr. Rita La Spina, Dr. Isaac Ojea Jiménez, Dr. Uwe Holzwarth, and Paula Caldeira.

My most grateful thanks are expressed to my family and friends who always believed in me, even when I did not myself, especially to Maarten Kieft, whose unconditional support over these years was invaluable.

ACADEMIC REGISTRY

Research Thesis Submission

Name*:*	Angela Kämpfer		
School:	School of Engineering and Physical Sciences		
Version: *(i.e. First, Resubmission, Final)*	Final	Degree Sought:	PhD

Declaration

In accordance with the appropriate regulations I hereby submit my thesis and I declare that:

1) the thesis embodies the results of my own work and has been composed by myself
2) where appropriate, I have made acknowledgement of the work of others and have made reference to work carried out in collaboration with other persons
3) the thesis is the correct version of the thesis for submission and is the same version as any electronic versions submitted*.
4) my thesis for the award referred to, deposited in the Heriot-Watt University Library, should be made available for loan or photocopying and be available via the Institutional Repository, subject to such conditions as the Librarian may require
5) I understand that as a student of the University I am required to abide by the Regulations of the University and to conform to its discipline.
6) I confirm that the thesis has been verified against plagiarism via an approved plagiarism detection application e.g. Turnitin.

* *Please note that it is the responsibility of the candidate to ensure that the correct version of the thesis is submitted.*

Signature of Candidate*:*		Date:	

Submission

Submitted By *(name in capitals):*	
Signature of Individual Submitting:	
Date Submitted:	

For Completion in the Student Service Centre (SSC)

Received in the SSC by *(name in capitals):*			
Method of Submission *(Handed in to SSC; posted through internal/external mail):*			
E-thesis Submitted (**mandatory for final theses)**			
Signature:		Date:	

Table of Contents

Abbreviations

[^{195}Au]AuNPs	Gold nanoparticles containing a small ratio of radioactive ^{195}Au
Ag^+	Silver ions
$AgNO_3$	Silver nitrate
AgNPs	Silver nanoparticles
AJs	Adherence junctions
AP	Apical
BL	Basolateral
BSA	Bovine serum albumin
CCM	Cell culture medium
CuO	Copper oxide
DCs	Dendritic cells
$_D$Caco-2	Differentiated Caco-2 cells
e/n/iNOS	Endothelial, neuronal, inducible nitric oxide synthase
FBS	Foetal bovine serum
FI	Fluorescence intensity
GALT	Gut-associated lymphoid tissue
GI-tract	Gastrointestinal tract
HBSS	Hank's balanced salt solution
IBD	Inflammatory bowel disease
IECs	Intestinal epithelial cells
IFN-γ	Interferon gamma
IL	Interleukin
(i)MΦ	(intestinal) macrophage
LDH	Lactate dehydrogenase
LPS	Lipopolysaccharides
LY	Lucifer Yellow
M-cells	Microfold cells
NMs	Nanomaterials
NO	Nitric oxide
NO_2^-	Nitrite
NPs	Nanoparticles
PBS	Phosphate buffered saline
RT	Room temperature
StDev	Standard deviation
TEER	Transepithelial electrical resistance
TGF-β	Transforming growth factor beta
TJs	Tight junctions
TNF-α	Tumour necrosis factor alpha
PMA	Phorbol 12-myristate 13-acetate
$_{UD}$Caco-2	Undifferentiated Caco-2 cells
ZO-1	Zonula occludens-1

1. Introduction

The use of nanotechnology in the manufacture of consumer goods and medical products remains, financially and technologically, one of the most promising advancements of the 21st century (Kaur et al., 2014). Prognoses concerning the two key areas of nanotechnology, nanomedicine and the agribusiness sector, estimated a market value of $81 billion and $1 trillion between 2020 and 2030, respectively (Kaur et al., 2014; Sabourin and Ayande, 2015). Nanotechnology is expected to revolutionise various areas of life, including the production and processing of food, technological innovations, and medical advancements.

Since years, the use of nanomaterials (NMs) in consumer products increases continuously. In 2016, the 'Nanotechnology Consumer Products Inventory', the largest database for NM-containing consumer products, lists more than 1,800 products claiming to contain NMs (Consumer Products Inventory, 2016). In parallel, the production volume of NMs increases, currently reaching between 550 to 5,500 tons / year for the three most synthesised materials, titanium dioxide (TiO_2), silicium dioxide (SiO_2), and zinc oxide (ZnO) (Bondarenko et al., 2013). At the same time, the number of studies investigating the safety of NMs increased exponentially over the last 15 years (Krug, 2014). Albeit relentless efforts of countless research groups hardly any unequivocal conclusions regarding the potential impacts of NMs on human health and the environment could be drawn to date.

The increasing presence of NMs in products for oral consumption, including food, beverages, and nanomedical products, is concerning since it affects a vast number of individuals on a regular and long-term basis. The intestine is the largest interface between the exogenous and endogenous environment and the main side for the digestion, uptake of nutrients, and water regulation (Kvietys and Granger, 2010). Under homeostatic conditions the intestinal barrier provides a 'gate' function that, in co-operation with constituents of the innate immune system, keeps exogenous antigens from entering the organism. In conditions affecting intestinal health, e.g. acute and chronic inflammation, these functions are impaired, which can have far-reaching implications for the whole organism (Levine and Burakoff, 2011).

Recently, the efforts to investigate the uptake, fate, and effects of orally ingested NMs have increased. The impact of pre-existing health conditions on NM-induced effects remain, however, neglected (Fröhlich and Roblegg, 2012; Lefebvre et al., 2015).

Extensive research on the effects of air pollution demonstrated an increased vulnerability in susceptible groups, e.g. patients with chronic obstructive pulmonary disorder (Sunyer et al., 2000; Löndahl et al., 2012). In this context, the increasing prevalence and incidences of inflammatory bowel diseases (IBD) (a summarising term for chronic inflammatory conditions characterised by alternating active and remission periods) raises concerns (Ponder and Long, 2013). Similar to subjects with chronic pulmonary disorders, IBD patients might face greater risks arising from the oral exposure to NMs than the average population. One of the main challenges in addressing these questions is the limited availability of appropriate *in vitro* models (Lefebvre et al., 2015).

1.1 Anatomy and functions of the gastrointestinal tract

The human gastrointestinal (GI)-tract is a continuous luminal space framed by mucosal epithelia ranging from the oral cavity over the stomach and intestine to the anus. The functional differences of the subunits are reflected in phenotypical distinctions on morphological and biochemical level. As a whole, the GI-tract is responsible for the mechanical and biochemical digestion of food components from macromolecular to absorbable micromolecular size. The digestive process begins in the oral cavity with the physical impact of the teeth and initial enzymatic breakdown of dietary starch and fats. Apart from the allocation of digestive enzymes the secreted saliva supports the formation of a food bolus and allows it to pass from the oral cavity to the stomach via the oesophagus. Whereas important steps of degradation of proteins are completed in the stomach, the enzymatic digestion and absorption of carbohydrates, fats and proteins happens in the small intestine.

With a length of ~6 m the small intestine is the largest part of the GI-tract (Whitney and Rady Rolfes, 2008). To fulfil the task of nutrient absorption with the highest efficacy the small intestine has developed a uniquely specialized surface structure. Its mucosa is pleated in large folds, which in turn have smaller elevations – so-called villi. The great majority of the villous surface is lined with a single-cell layer of absorptive, functionally and morphologically polarised epithelial cells (‘intestinal epithelial cells’ (IECs)). Together with the underlying lamina propria and a layer a smooth muscle cells the epithelium forms the intestinal mucosa.

A schematic overview of the most important IECs and leukocytes is given in Figure 1.1A.

1.1.1 Enterocytes

Enterocytes are the most abundant epithelial cell type in the small intestine and line the majority of its villous surface (Barker, 2014). To maximizing the contact area between the epithelium and chime (i.e. the bolus of partly digested food) enterocytes express micro-villi on their luminal surface forming the so-called 'brush-border' (Shiner and Birbeck, 1961). This anatomy increases the surface area to roughly 300 m^2. The expression of micro-villi and brush border hydrolases, including alkaline phosphatase and sucrose isomaltase, render small intestinal enterocytes unequivocally distinguishable from the other epithelial cell types of the GI-tract (Ranaldi et al., 2003).

The small intestine is one of the fastest renewing tissues in the human body. All enterocytes originate from intestinal stem cells (iSC) located in the crypts surrounding the villi (Figure 1.1A) (Barker, 2014), and subsequently migrate to the tip of the villi within 3-5 days. Throughout this process the cells' anchorage gradually loosens until they are eventually shed at the tip. The loss of cell anchorage induces a specific type of apoptotic cell death termed 'anoikis' (Grossmann et al., 2001).

The enterocyte layer forms the major physical barrier between the exogenous and endogenous environment in the gut. This barrier is, however, selectively permeable *via* transcellular and paracellular pathways: The transcellular uptake is mainly associated with the absorption of dietary compounds, e.g. monosaccharides, amino acids, and fatty acids (Suzuki, 2013), whereas the paracellular permeability is controlled by a junctional complex composed of adherence junctions (AD) and tight junctions (TJ) (Figure 1.1B) (further discussed in Section 1.2.1) (Assimakopoulos et al., 2011).

1.1.2 Non-enterocytic epithelial cells

Apart from the enterocytes, 4 additional epithelial cell types can be distinguished in the small intestine: goblet, endocrine, Paneth and Microfold (M)-cells (Menard et al. 2010). Like enterocytes, all other IECs originate from iSC (Barker, 2014). Whereas enterocytes, goblet, endocrine, and M-cells move towards the tip of the villi, the Paneth cells remain at the base of the crypt (van Es et al., 2005). Paneth cells are mainly

responsible for the synthesis and secretion of anti-microbial peptides (AMP), which act strongly against both Gram-positive and Gram-negative bacteria (Muniz et al., 2012). A high concentration of AMP is secreted directly into the crypt lumen (Bevins and Salzman, 2011) to prevent bacterial invasion of this otherwise vulnerable space (Johansson et al., 2013). Additionally, the AMP disperse in the mucous layer that sheathes the epithelium (Bevins and Salzman, 2011).

The mucus is secreted by goblet cells, which are scattered over the whole epithelium. It is now understood that the mucus lining is more than a static physical barrier to protect the host from luminal antigens. It is a dynamic hurdle that adapts to environmental factors, e.g. the composition of the intestinal microbiota (Deplancke and Gaskins, 2001). In the small intestine, the mucus layer is discontinuous and does not cover the surfaces of M-cells (Deplancke and Gaskins, 2001).

M-cells make up for around 10 % of the follicle-associated epithelium, which covers aggregated lymphoid follicles located in the lamina propria – the so-called Peyer's patches (Mabbott et al., 2013; Jung et al., 2010). Using phagocytotic and transcytotic mechanisms, M-cells enable the translocation of intact macromolecules, e.g. proteins, bacteria, and viruses, from the gut lumen to the underlying Peyer's patches (Neutra et al., 1987; Mabbott et al., 2013).

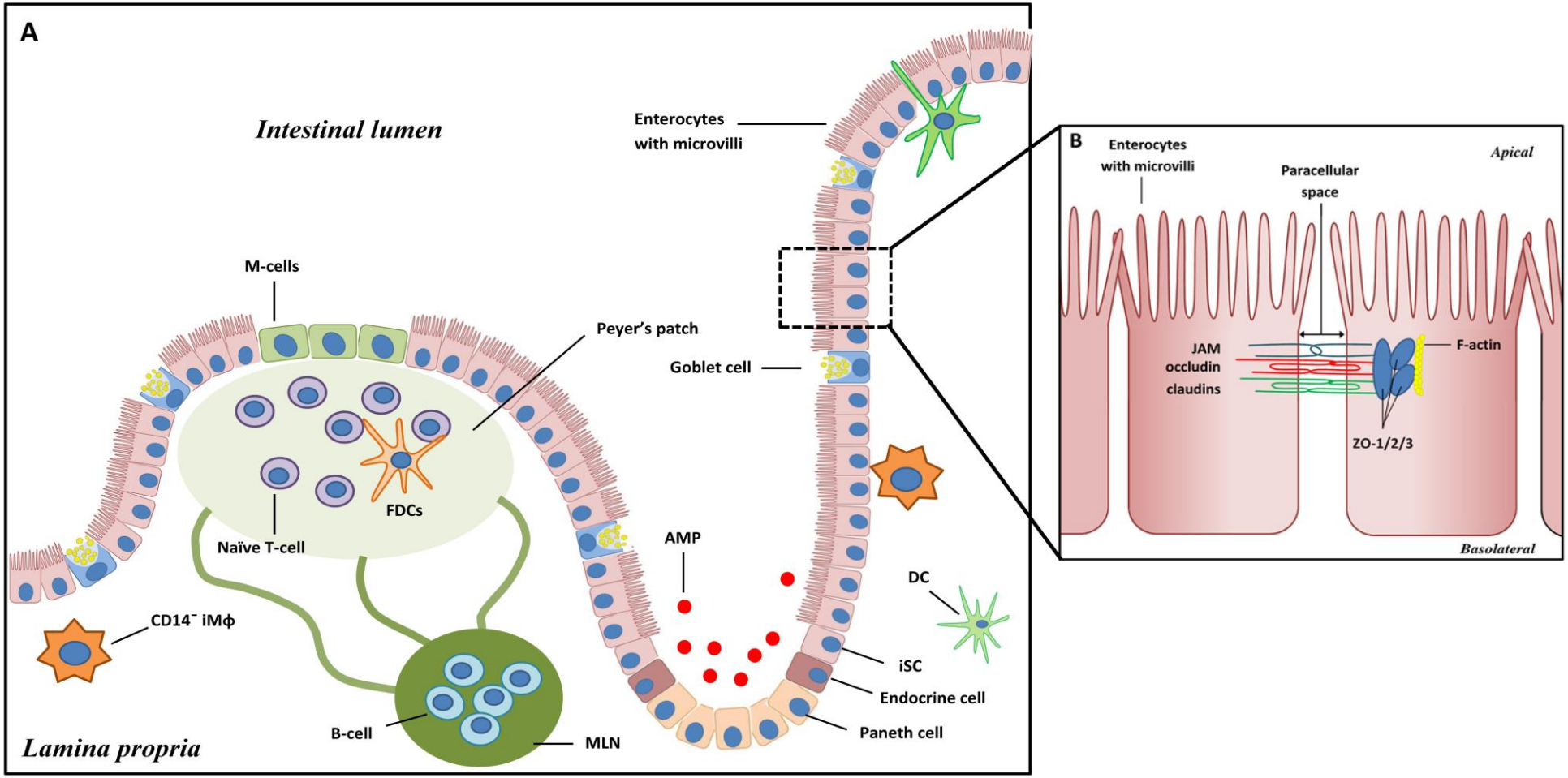

Figure 1.1 Schematic overview of (A) intestinal epithelial cells and the gut-associated lymphoid tissue, and (B) the intestinal TJs

(iMΦ: intestinal macrophages, AMP: anti-microbial peptides, iSC: intestinal stem cells, (F)DCs: (follicular) dendritic cell, MLS: mesenteric lymph node, ZO: Zonula Occludens, JAM: Junctional Adhesion Molecules)

1.1.3 Gut-associated lymphoid tissue

The intestine forms the largest interface between the environment and the human organism. As such, it is in constant contact with a variety of exogenous components, e.g. food-derived macromolecules, and microbial structures of both commensal and pathogenic bacteria that require differential feedback. This feedback can range from tolerance to active immune response (Muniz et al., 2012). The intestine's functions are a tightrope walk between the uptake of nutrients across the intestinal barrier and preventing the intrusion of harmful antigens (Clayburgh et al., 2004). To fulfil this ambivalent role, IECs and the gut-associated lymphoid tissue (GALT) have established a finely-tuned cohabitation. The GALT is composed of aggregated lymphoid tissue (the Peyer's patches and mesenteric lymph nodes (MLN)), as well as individually operating leukocytes (Lorenz and Newberry, 2004). After crossing the follicle-associated epithelium and entering the sub-epithelial dome, luminal macromolecules are phagocytised, presented to and analysed by various types of immune cells, including B-cells, T-cells, dendritic cells (DCs) and macrophages (MΦ) (Rios et al., 2016; Mabbott et al., 2013). DCs travel continuously between compartments of the organised lymphoid tissue to transport antigens from the Peyer's patches to the MLN where they are presented and further immune reactions are decided (Macpherson and Smith, 2006).

Outside of the organised lymphoid tissue individual leukocytes, such as T-cells, MΦ, DCs, and natural killer cells, roam the lamina propria to phagocytise, present, and / or analyse randomly encountered antigens (Coombes and Powrie, 2008; Smythies et al., 2005; Guo et al., 2008). In addition to the uptake of lumenal macromolecules via M-cells, DCs can penetrate the TJs between IECs and sample directly from the intestinal lumen. By expressing several TJ proteins, including occludin, claudin 1, and JAM-A, their interference with the junctions does not cause a disruption of the barrier integrity (Rescigno et al., 2001; Chiba et al., 2008).

1.2 The intestine in healthy and diseased states

The following sub-titles will focus on the major measurable differences between the healthy and diseased intestine and summarise the hallmarks of intestinal inflammation.

1.2.1 Cytokines and chemokines

'Cytokine' is a broad term summarising several groups of small effector proteins that can be released by various cell types, including epithelial cells and leukocytes (Haller et al., 2000; Neurath, 2014). Cytokines are crucial messenger molecules that affect the behaviour of and the communication between cells. They can act in an autocrine, paracrine, and even endocrine manner on the cells that release them, neighbouring cells, and distant cells, respectively (Zhang and An, 2007). Typically, the same cytokine can be secreted by different cell types, and a specific cytokine can act on more than one cell type (Zhang and An, 2007).

Cytokines are commonly distinguished as pro-inflammatory, anti-inflammatory, or chemotactic (chemokines) according to three fields of responsibility, i.e. the induction / maintenance of inflammation, the termination of inflammation, and the recruitment of target cells (Zhang and An, 2007). However, several if not most cytokines can have more than one task depending on additional environmental factors (Müzes et al., 2012; Scheller et al., 2011). Pro-inflammatory cytokines are predominantly synthesised by activated macrophages. Several of these cytokines, e.g. interleukin (IL)-1β, tumour necrosis factor (TNF)-α, and interferon (IFN)-γ, are crucial for the initiation and mediation of inflammatory responses (Zhang and An, 2007). Normally, an infection or damage of the IEC barrier induces a short-term, local acute inflammation under generation of high concentrations of pro-inflammatory cytokines and chemokines, which is followed by a complete recovery of the intestinal wall and its functions (Bamias et al., 2014). However, in some cases, and for reasons that are not yet fully understood, the inflammatory response is not resolved but rather sustained in a chronic manner. The blocking of single cytokines, e.g. TNF-α, has been shown to greatly alleviate the condition of IBD patients (Altwegg and Vincent, 2014). In contrast, the exclusion of others, e.g. IL-1β, rather worsened the condition, which suggests an involvement in the initiation and facilitation of anti-inflammatory and recovery processes like the limitation of leukocyte infiltration (Bamias et al., 2014).

Other cytokines have been shown to be of importance for the preservation and / or recovery of intestinal homeostasis. The chemokines IL-8 and transforming growth factor (TGF)-β, facilitate the recruitment and differentiation of blood monocytes to the lamina propria (Smythies et al., 2006). IL-8 is furthermore involved in the recruitment of neutrophils as first-responders during intestinal inflammation (Fournier and Parkos, 2012). Others, like IL-22, have been attributed a protective role based on the observations that significantly lower levels are recovered in subjects with ongoing inflammatory conditions compared to healthy controls (Bamias et al., 2014).

1.2.2 Nitric oxide

Nitric oxide (NO) can be an important physiological messenger molecule or an indicator for pathophysiological processes depending on the stimulus of its synthesis, its source, as well as the duration and quantity of its release (Forstermann and Sessa, 2012). Under physiological conditions, the generation of nanomolar concentrations of NO by constitutively expressed endothelial and neuronal NOS (eNOS and nNOS, respectively) is meticulously regulated (Kolios et al., 2004). In these cases, NO can be involved in the regulation of blood pressure (Huang et al., 1995), neuronal functions (Prast and Philippu, 2001), and the maintenance of intestinal barrier integrity (Kolios et al., 2004). NO derived from eNOS and nNOS acts as anti-inflammatory mediator by reducing the chemotactic potential of several chemokines and modulation of macrophage-cytokine release towards an anti-inflammatory composition (Kolios et al., 2004). In contrast, the activation of inducible NOS (iNOS) causes the persistent release of micromolar concentrations of NO (Kolios et al., 2004). The ability to release large quantities of NO has been demonstrated to be an important feature of an organism's innate immune response to pathogens (MacMicking et al., 1995; Zeidler et al., 2004). The prolonged and uncontrolled release of NO, however, is suspected to play a role in IBD (Singer et al., 1996) and to contribute to a very early onset of IBD (Dhillon et al., 2014). NO can react further with O_2 or O_2^- and subsequently impose oxidative or nitrosative stress, which can induce DNA damage and enzyme inhibition (Grisham et al., 1999). Furthermore, the excessive generation of NO and the formation of its stable metabolite nitrate (NO_3^-) likely accelerates the growth of less beneficial intestinal bacterial strains, thereby, displacing more favourable ones (Winter et al., 2013).

1.2.3 Intestinal barrier integrity

The integrity of the IEC barrier is essentially controlled by the presence and intactness of TJs sealing the paracellular space between epithelial cells (Figure 1.1B). Whereas the initiation and stabilisation of cell-to-cell contacts is mainly related to the formation of AJ with proteins of the cadherin and catenin families at the core (Hartsock and Nelson, 2008), the TJs determine the selective paracellular permeability to ions, solutes, and water (Suzuki, 2013). At the same time, TJs restrict the passage of any kind of potentially noxious antigens from the lumenal to the serosal side (Edelblum and Turner, 2009). The TJs form the most apical of the junctional structures of adjacent cells and reduce the width between enterocytes to 8-12 and 2-2.5 Å in the jejunum and colon respectively (Bolger et al., 2006). In addition to the charge and size selective 'gate' function (Chiba et al., 2008), TJs hold a 'fence' function, preventing the mixing of apical (AP) and basolateral (BL) membrane proteins and lipids (Hartsock and Nelson, 2008). The integrity of the TJ network and paracellular permeability is often studied by measurement of the transepithelial electrical resistance (TEER) or the translocation of small molecules across the epithelial barrier (Suzuki, 2013).

1.2.3.1 TJ proteins

To date, more than 40 proteins have been identified that are involved in the construction of the TJs (Anderson and Van Itallie, 2009). They can roughly be divided into two types of proteins: (1) transmembrane proteins forming intercellular adhesion structures and (2) intracellular proteins connecting the transmembrane proteins with the actin cytoskeleton (McNeil et al., 2006). Four main transmembrane proteins can be distinguished, namely occludin, claudins, junctional adhesion molecules (JAMs), and tricellulin (Chiba et al., 2008). Occludin has been shown to be dispensable for TJ assembly and the development of a polarised epithelium. However, more detailed analysis revealed histological and functional abnormalities, including inflammation and hyperplasia in the stomach, in occludin knock-out mice suggesting a more complex role of occludin than just involvement in TJs (Saitou et al., 2000). In contrast, proteins of the claudin family are critical for both TJ morphology and function (Van Itallie and Anderson, 2014). Claudins form the structural base of the TJ strands and are, therefore, seen as the backbone of the TJ (Chiba et al., 2008). Whereas some proteins of the

claudin family are involved in the development and maintenance of the barrier, others, e.g. Claudin-2, are essential for the formation of paracellular pores (Yu et al., 2009).

Zonula occludens (ZO) proteins – the main group of intracellular proteins – were the first identified proteins of the TJ and remain one of the best studied group of TJ proteins (Van Itallie and Anderson, 2014). With binding to ZO-1 the transmembrane protein claudin is connected to the actin cytoskeleton (Fannings et al., 1998). For many of their tasks, the members of the ZO-protein family seem to be functionally interchangeable. For instance, the individual depletion of either ZO-1 or ZO-2 only caused mild structural and functional effects on developing epithelia (Umeda et al., 2004). When both proteins were suppressed in parallel the TJ-assembly failed (Umeda et al., 2006). Apart from its involvement in the epithelial barrier integrity ZO-1 actively controls cell proliferation through binding to the ZO-1-associated Y-box (ZONAB) transcription factor (Gottardi et al., 1996; McNeil et al., 2006).

1.2.3.2 Regulation of TJ integrity

The regulation of the TJs has not been fully elucidated to date. Even though one of their main functions is to keep noxious substances from entering the organism, the paracellular permeability can be regulated by a multitude of physiological and pathophysiological stimuli. The main stimuli known to affect the TJ integrity are pathogenic bacteria, cytokines, oxidative stress, and growth factors. These will be presented in more detail under the following sub-headings.

Several different factors that influence the TJ integrity are known to date, including interactions between transmembrane proteins and the actomyosin ring of the cytoskeleton, the phosphorylation of TJ proteins, and the up- or downregulation of TJ proteins (Ulluwishewa et al., 2011; Shen, 2012). The interaction between TJ proteins and the actomyosin ring can be determined by different signalling proteins depending on the type of stimulus. For instance the stimulation of TLR2 activates protein kinase c, which in turn induces a re-distribution of ZO-1 (Cario et al., 2004). In contrast, mitogen-activated protein kinases (MAPK) is mobilised by growth factors (Howe et al., 2005) (Section 1.2.3.2.4). The probably best studied mechanism of TJ regulation, however, involves the phosphorylation of myosin light chain (MLC) through MLC kinase (MLCK), which induces the contraction of the actomyosin ring (Shen, 2012).

A distorted paracellular permeability can affect the gate function of the epithelial barrier and lead to an increased influx of lumenal antigens. Increased intestinal permeability is strongly associated with both acute, e.g. in response to a bacterial infection (Section 1.2.3.2.1), and chronic inflammatory conditions of the intestine. Decreased barrier integrity has been demonstrated in Crohn's disease and *ulcerative colitis* patients, as well as the patients' first grade relatives (Katz et al., 1989; Gerova et al., 2011), but also in individuals with coeliac disease and diabetes Type 1 (van Elburg et al., 1993; Visser et al., 2010). The mechanisms behind the reduction in barrier integrity are best understood for IBD. Biopsy samples from IBD patients showed a significant downregulation of occludin, ZO-1, and claudin-5 and 8, as well as an increase in claudin-2 (Gassler et al., 2001; Zeissig et al., 2007; Weber et al., 2008). It remains unclear, whether the impaired epithelial barrier is the primary cause or a secondary consequence of the disorder.

1.2.3.2.1 Pathogenic bacteria

Various pathogenic bacterial strains target the TJ network to enter the organism (Guttman and Finlay, 2009). In mice, the infection with enterohemorrhagic *E. coli* (EHEC) induced intestinal barrier disruption as measured by reduction in TEER and increase in the mucosal permeability for FITC-labelled dextran. In response to the EHEC infection the distribution and transcription profiles of several TJ proteins were altered (Roxas et al., 2010). Interestingly, whereas EHEC caused an increase in claudin-2 *in vivo*, a significant reduction in claudin-2 expression was reported *in vitro* in a colonic epithelial cell line (T84) (Howe et al., 2005). Another enteroinvasive pathogen – *Shigella* – caused dislocation of ZO-1, occludin, and claudin-1 from the cell boundaries. The disengagement of occludin has been shown to be caused by phosphorylation of the protein. The effects on the TJ network resulted in a significant reduction in barrier integrity, as well as an increase in paracellular flux of molecules as large as 66 kDa (Fiorentino et al., 2014). Direct interactions with TJ proteins have been reported in infections involving the bacterium *Clostridium perfringens*. Shortly after the infection, *Clostridium perfringens* enterotoxin bound to selective proteins of the claudin family and induced a rapid disintegration of the TJ strands, which was reflected in reduced TEER and increased flux of dextran (4-10 kDa) (Sonoda et al., 1999). Whether bacterial endotoxin can affect the barrier integrity is not clear yet as studies have generated contradictive results (Guo et al., 2013; Van De Walle et al., 2010).

1.2.3.2.2 Pro-inflammatory cytokines

Various pro-inflammatory cytokines have been shown to affect the TJ network and paracellular permeability. Interestingly, many of the cytokines seem to induce individual pathways ultimately leading to the barrier disruption. In the presence of both TNF-α and IFN-γ the observed reduction in barrier integrity is associated with increased phosphorylation of MLC. Whereas the phosphorylation of MLC in the presence of IFN-γ is linked to the enhanced expression of Rho associated kinase (ROCK), an increase in MLCK was found in the case of TNF-α exposure (Capaldo and Nusrat, 2009; Wang et al., 2005). For both cytokines, studies reported reduced protein levels of ZO-1 and re-localisation of transmembrane proteins via endocytosis (Bruewer et al., 2003; Marchiando et al., 2010). The disruptive effect was, however, maximised when both cytokines were present in parallel indicating a strong synergistic effect (Wang et al., 2005).

Furthermore, several interleukins (ILs) have been shown to influence the barrier integrity of epithelial cells. In the case of IL-1β exposure, a reduction in occludin on both protein and mRNA level was reported, as well as an up-regulation of MLCK (Capaldo and Nusrat, 2009; Al-Sadi et al., 2010). In contrast to this, the barrier disruption induced by IL-6 was demonstrated to be caused by the activation c-jun N-terminal kinase (JNK) pathway and the subsequent up-regulation of claudin-2 (Al-Sadi et al., 2014).

The reduction in barrier integrity often causes an increased permeability for ions or molecules. However, the individual cytokines seem to affect the permeability differently. The increase in permeability caused by IL-6 was limited to small molecules (<4 Å) but not non-ionic macromolecules (Al-Sadi et al., 2014; Suzuki et al., 2011). On the other hand, IL-1β caused a similar reduction in TEER as IL-6, but allowed an increased flux of molecules as large as 15 Å (Al-Sadi and Ma, 2007). In the presence of either IFN-γ or TNF-α alone, no increased flux of larger molecules (3 kDa dextran) was detected. When epithelial cells were co-exposed to both cytokines, a large increase in permeability was observed for 3 kDa dextran (Wang et al., 2005).

1.2.3.2.3 Reactive oxygen and nitrogen species (ROS/RNS)

In contrast to many pro-inflammatory cytokines, H_2O_2 did not affect the total protein levels of TJ proteins, but causes the increased phosphorylation of ZO-1 and occludin (Basuroy et al., 2006). NO on the other hand, induced delocalisation of ZO-1 and occludin (Cuzzocrea et al., 2000). Several reported observations suggest that NO not only induces intestinal barrier disruption itself but also at least partially mediates the barrier disruption caused by pro-inflammatory cytokines (Xu et al., 2002; Unno et al., 1995).

1.2.3.2.4 Growth Factors

Some have been shown to be able to induce both an increase and decrease in barrier permeability depending on the cell environment (Capaldo and Nusrat, 2009). Whereas TGF-β caused a reduction in TEER in murine uterine epithelial cells (Grant-Tschudy and Wira, 2005), a significant increase in barrier integrity was reported in intestinal epithelial cells (Howe et al., 2005). Furthermore, growth factors appear to have TJ-related protective effects. In Caco-2 cells, the treatment with epithelial growth factor inhibited H_2O_2-associated disruption of the TJs by preventing the dissociation of ZO-1 and occludin from the cytoskeleton (Basuroy et al., 2006). In the cell line T84, TGF-β not only increased the TEER through upregulation of claudin-1, but also protected the epithelial cell layer from EHEC-induced TJ-disruption (Howe et al., 2005).

1.2.4 Macrophage populations

In the homeostatic intestine, different types of leukocytes make up the first line defence of the innate immune system, including DCs and MΦ. These cells are involved in the unspecific protection of the intestinal barrier from harmful antigens and the overall immune regulation in the intestine. Cells of the innate immune system bind encountered antigens through pattern recognitions receptors. Subsequently, the antigen is phagocytised, digested, and parts of its proteins presented via the major histocompatibility complex (MHC), while the cell migrates to the lymph node. There, the antigen is presented to T-cells, which together with B-cells are the main effector cells of the adaptive immune system. The antigen-presentation together with the initiated cytokine release by the innate immune response triggers the T-cell activation

and, thereby, starts the targeted antigen-elimination through the adaptive immune response (Medzhitov, 2007). The different types of leukocytes are distributed over the GALT, the intestinal epithelium, as well as the lamina propria (Habtezion et al., 2016). Within this project, the focus was put on the role of macrophages on intestinal homeostasis and inflammation.

1.2.4.1 Macrophage populations in the homeostatic intestine

Intestinal macrophages (iMΦ) form the largest pool of tissue macrophages within the human body (Smythies et al., 2006). The tissue-resident MΦ are mainly present in the lamina propria, the core of the mucosa, but can also be found to a lesser extent in deeper layers of the intestine – the submucosa and muscularis mucosae (Mowat and Bain, 2011). To sustain the pool, circulating blood monocytes are recruited by IEC-released TGF-β and IL-8 (Smythies et al., 2006; Bain and Mowat, 2014).

Human monocytes are commonly grouped into 'classical', 'non-classical', and 'intermediate' monocytes according to their expression of CD14 and CD16 (Shi and Pamer, 2011):

- Classical: $CD14^{++}CD16^{-}$
- Non-classical: $CD14^{+}CD16^{++}$
- Intermediate: $CD14^{++}CD16^{+}$.

Generally, a 'classical' pro-inflammatory (M1) and an 'alternative' anti-inflammatory (M2)-type differentiation are distinguished (Wang et al., 2014). However, monocytes are known to be able to adapt their phenotype to the environmental circumstances. It was demonstrated in mice that the pool of intestinal tissue macrophages is replenished by recruited classical-type monocytes, which, subsequently, mature into iMΦ (Bain et al., 2014). Functionally, iMΦ are closely related but not identical to anti-inflammatory M2 MΦ (Smith et al., 2011). They are characterised by a systematic inflammatory *anergy*, which describes the lack of pro-inflammatory reactions towards the encounter of non-self antigens (Smythies et al., 2005). This anergy is characterised by a strict down-regulation of the synthesis of TLR-mediated cytokines like IL-1, IL-6, and TNF-α, but not of the phagocytising and bactericidal activity are down-regulated in iMΦ (Smythies et al., 2005). The exact reason for the inflammatory anergy is not clear yet.

iMΦ express Toll-like receptors (TLRs) like TLR2 and 4, which are necessary for the recognition of pathogen-associated molecular patterns (PAMPs) (Mowat und Bain 2014). It was suggested, that the adequate response to stressors is impaired due to a lack or the insufficient expression of other proteins necessary for the recognitions of LPS or the subsequent signal transduction, e.g. CD14 and MyD88 (Smythies et al., 2010; Smith et al., 2011). Yoshioka et al. (2009) found minimal expression of CD14 on the membrane of iMΦ, which the group suggested might be caused by an impaired transport of CD14 from the endoplasmic reticulum to the Golgi apparatus.

In contrast to DCs, iMΦ do not commonly enter the lymphoid tissue. Nevertheless, they can present processed antigens through MHC II to lamina propria T-cells (Mann and Li, 2014; Bain and Mowat, 2014). Altogether, their role can be described as bacterial waste disposal of the innate immune system, which does not rush to action itself but forwards the information (Mowat and Bain, 2011).

1.2.4.2 Macrophage populations in the inflamed intestine

Intestinal inflammation is associated with a significant infiltration of classical monocytes into the lamina propria (Kühl et al., 2015). In the homeostatic intestine, the vast majority of iMΦ lacks the LPS-receptor CD14. However, a small fraction could be identified bearing both macrophage ($CD14^+/CD68^+$) and DC ($CD205^+/CD209^+$) receptors,' which strongly increases in numbers during intestinal inflammation (Kamada et al., 2008). In contrast to $CD14^-$ iMΦ, newly recruited $CD14^+$ macrophages release high concentrations of pro-inflammatory cytokines, including IL-6, TNF-α, IL-1β, and IFN-γ, as well as chemokines to attract additional monocytes (Kamada et al., 2008; Kühl et al., 2015). IL-8, monocyte chemoattractant protein (MCP)-1, and macrophage inflammatory protein (MIP)-1α are the three most abundant chemokines that are involved in the recruitment of blood monocytes to the site of inflammation (Smith et al., 2011; Shi and Pamer, 2011; Banks et al., 2003). For the recruitment of monocytes in both health and disease, MCP-1 seems to be especially important. Whereas the absence of either MCP-1 or its associated receptor causes a significant reduction in the iMΦ pool under homeostatic conditions (Bain et al., 2014), a lack of MCP-1 throughout an infection reduces the monocyte recruitment by up to 50 % (Shi and Pamer, 2011).

1.3 Available approaches for research of the intestine

To study the intestine and its functions various *in vivo*, *ex vivo*, and *in vitro* models are available that differ in applicability and validity. The use of computer-based modelling (so-called *in silico* research) will not be discussed within this project. A non-exhaustive summary of the advantages and disadvantages regarding *in vivo*, *ex vivo*, and *in vitro*-based research models is presented in Table 1.1.

1.3.1 In vivo

The physiology and integrity of the intestine is regulated by the complex interplay of different epithelial and mononuclear cell types, but also the microbiome. Data derived from *in vivo* models offer the great advantage of reflecting the processes within a complete organism rather than a snapshot based on isolated cell types. These results are regarded as the most applicable, especially concerning the integrity and bioavailability of compounds throughout the GI-passage, even though this view is increasingly challenged (Musther et al., 2014). Animal models helped to expand the knowledge regarding digestive processes, absorption, and immune regulation in the intestine under homeostatic conditions. In addition, several models mimicking acute and chronic inflammation are available of which rodent-based models using mice and rats are the most commonly applied (Jiminez et al., 2015). These models are either based on transgenic animal strains or rely on a chemically induced intestinal inflammation (Prattis and Jurjus, 2015; Wirtz et al., 2007). However, results generated using animal studies can only be extrapolated to humans to a limited extent (Musther et al., 2014). Physiological and pathological processes in humans can be tremendously different from those of the experimental species, and the generated results and subsequently drawn conclusions are highly susceptible to flaws and / or biases in the study design (Cerquetella, 2010; Ioannidis, 2012). Furthermore, *in vivo* research is confronted with a generally negative public opinion and demand for the development and use of alternative animal-free methods by the European legislator (Ioannidis, 2012).

1.3.2 Ex vivo

An alternative between *in vivo* and *in vitro* approaches is the use of *ex vivo* cell cultures, which can be divided into biopsy- and stem cell-based approaches. The use of intestinal

biopsy samples has generated numerous insights regarding the intestinal barrier function in health and disease (Piche et al., 2009), the interaction of IECs with enteropathogenic bacteria (Schüller et al., 2009), and material transport across the intestinal barrier (Schmidt et al., 2013). Biopsies-based *ex vivo* research offers the great advantage of providing a short-term organ culture featuring all epithelial cell types (He et al., 2013). This heterogeneous structure of multiple cell types can also present a disadvantage, as it complicates the study of cell type-specific effects (Turner et al., 1997). Furthermore, inter-individual differences between the donors, including variations in genetics, overall health status, or life style choices (e.g. diet, physical activity, consumption of alcohol, caffeine, and nicotine), can cause significant deviations in the outcomes. The main limitation of biopsy sample cultures is the narrow longevity of isolated IECs *ex vivo* (Grossmann et al., 1998). Therefore, efforts were focused on the isolation and maintenance of iSC. For these experiments, intestinal crypts were separated from the intestinal barrier and subsequently grown into three-dimensional organotypic structures in presence of appropriate growth factors (Grabinger et al., 2014). These cultures were found to correlate significantly better with cytotoxicity results generated *in vivo* than cell line-based *in vitro* cultures (Grabinger et al., 2014). Even though stem cell-derived cultures have a significantly increased life span compared to isolated IECs their very limited availability remains a great disadvantage for both approaches. For this project, *ex vivo* cultures were not accessible.

1.3.3 In vitro

In vitro research comprises the use of isolated primary cells and immortalised cell lines to study one or more defined endpoints. For decades, *in vitro* models of the intestinal barrier have been used to study the pharmacological and toxicological effects, as well as the bio-availability of molecules (Sambruy et al., 2001) and particles (Desai et al., 1997). Although the development of primary (Castellanos-Gonzalez et al., 2013) and stem cell-derived (Chopra et al., 2010) intestinal cultures has advanced recently, the application of immortalised cell lines remains favoured due to their easy accessibility, handling, and maintenance. However, the numerous cell types and complex structure defining the small intestine are difficult to mimic *in vitro*. A monoculture of differentiated $_{(D)}$Caco-2 cells showed limited correlation to *ex vivo* permeability of other species (canine, rodent, and non-human primates) for various compounds (e.g. D-glucose, mannitol, progesterone), but promising parallels to human *in vivo* data (Rubas

et al., 1993). Whereas cell monocultures are valuable to study a specific endpoint, e. g. cytotoxicity, their ability to predict downstream impacts in relation to biokinetics and metabolism is limited (Duell et al., 2011; Lilienblum et al., 2008).

Therefore, efforts have focused on the development of more sophisticated intestinal models combining at least two different cell types. Depending on the desired application, developments have aimed for an improved representation of the intestinal barrier (Wikman-Larhed and Artursson, 1995; Hilgendorf et al., 2000; Chen et al., 2010; Schimpel et al., 2014) or the integration of immune cells (Leonard et al., 2010; Susewind et al., 2016). Several groups studied immune responses involving leukocytes with the help of primary cells (Bisping et al., 2001; Leonard et al., 2010; Parlesak et al., 2004). Nevertheless, acquiring and maintaining primary cells is significantly more expensive than the use of cell lines. Furthermore, their accessibility and donor-variability can be problematic in particular regarding the inter-laboratory comparability (Corazza and Wade, 2010).

Additionally to the application of co-cultures, groups recently started to improve the physiological representation of intestinal tissue by culturing cells on three-dimensional scaffolds mimicking the villous structure of the intestine (Chen et al., 2015b; Kim et al., 2014). The newest advancements are so-called ‘gut-on-a-chip’ developments, which can combine different cell types and representative strains from the microbiome, but also account for the physiological structure, peristaltic and sheer stress of the intestinal environment (Lee et al., 2016; Kim et al., 2012a).

The application of these increasingly complex cell models helped generate new insights regarding the regulation of intestinal homeostasis (Parlesak et al., 2004; Nathens et al., 1995), as well as the influence of immune cells on IEC responsiveness to stressors (Wottrich et al., 2004; Susewind et al., 2016) and particles (Moyes et al., 2010). Even though various models involving immune cells are available, none was directly applicable to our interests. Either the models were established using primary cells (Leonard et al., 2010; Bisping et al., 2001) or cell lines of non-human origin (Tanoue et al., 2008). Others were characterised by a spontaneous disruption of the IEC barrier induced by an uncontrolled inflammation-like reaction (Watanabe et al., 2004; Moyes et al., 2010; Kanzato et al., 2001; Satsu et al., 2006). In the most recently presented model by Susewind et al. (2016) the immune cells are embedded in a collagen layer, which can render the application costly. Furthermore, the introduction of a collagen layer might

hinder the accurate detection of messenger molecules, as well as the quantification of NM translocation.

In contrast, the aim of this project was to establish a non-contacting – paracrine – co-culture. For reasons of practicality and accessibility the model was to be based on cell lines rather than primary cells. To maximise the model's applicability to a human exposure scenario cell lines of human origin were favoured.

1.4 Cell lines

1.4.1 Enterocytic cell lines

Over the last 40 years numerous enterocytic cell lines have been established that mainly originated from colon carcinomas (Chantret et al., 1988). One of the most extensively used and best characterised models is the human colon carcinoma cell line Caco-2. Originally isolated from colonic tissue, the cells differentiate spontaneously without external stimulus to enterocyte-like cells once the cells reach confluence (Pinto et al., 1983; Chantret et al., 1988). This differentiation is reflected in the development of a microvillous apical membrane, indicating structural polarisation of the Caco-2 barrier, and the increase in brush border-associated hydrolases (Chantret et al., 1988; Hilgers et al., 1990). Caco-2 cell cultures offer similar transport and permeability characteristics as human intestinal tissue (Lennernas et al., 1996; Rubas et al., 1993). With a size between 4.3-4.6 Å (Watson et al., 2001; Knipp et al., 1997) the TJ pore radius in intact Caco-2 cell layers is slightly larger than in the colon, but only around half the size of the small intestinal TJ radius (Bolger et al., 2006). Even though the cell line does not offer a perfect representation, e.g. concerning drug permeability (Yamaura et al., 2016), it shares a significant amount of proteins and characteristics with human enterocytes and the intestinal barrier (Lenaerts et al., 2007).

1.4.2 Monocyte / macrophage cell lines

In contrast to IECs, the number of available human monocytic or macrophage cell lines is very limited. The THP-1 cell line is one of the most widely used human monocytic cell lines and has been extensively characterised, morphologically and functionally, against peripheral blood mononuclear cells (PBMCs) and PMBC-derived MΦ (Daigneault et al., 2010). The monoblast-like cells can be differentiated into a

macrophage-like phenotype using various stimuli, including phorbol 12-myristate 13-acetate (PMA) and 1α, 25-dihydroxy vitamin D_3 (Tsuchiya, 1980; Tsuchiya et al., 1982). From the basic (M0) macrophage phenotype the cells can be further polarized towards a M1 or M2 phenotype using LPS and IFN-γ or IL-4 and IL-13, respectively (Genin et al., 2015). THP-1 cells have a wide application range as they can be differentiated towards a macrophage-like, as well as a DC-like phenotype (Berges et al., 2005).

Several other groups showed that THP-1 cells are suitable candidates to be introduced in cell line-based co-cultures models of the lung (Kasper et al., 2015) and the intestine (Susewind et al., 2016). It has furthermore been demonstrated that the presence of THP-1 cells can alter the response of a co-culture model towards the exposure to particulate matter compared to monocultures (Alfaro-Moreno et al., 2008; Klein et al., 2013).

Table 1.1 Summary of the general advantages (+) and disadvantages (-) of in vivo-, ex vivo-, and in vitro-based research models

in vivo		*ex vivo*		*in vitro* – primary cells		*in vitro* – cell lines	
+	-	+	-	+	-	+	-
Complex organisms → most realistic	Interspecies differences	Complexity of several cell types	Limited availability, difficult access	Unaltered genetic profile	Limited availability & accessibility	Immortalised → infinite growth	Often tumour-derived cells with altered gene profile
Intact anatomy	Inter-individual differences	Allows mechanistic focus on a specific area	Limited viability	Possibly cells of human origin	Limited life span	Easily obtained and maintained	Prone to mutations
Complete physiological processes	Ethical issues	Higher throughput than *in vivo*	Lack of digestive enzymes	Relatively low costs	Inter-individual differences	Low costs	Limited extrapolation to complex tissues / organisms
	Low public acceptance	Maintained tissue architecture		Less ethical concerns			Differentiation may be necessary
	High costs						Limited anatomical & physiological properties

1.5 Nanomaterials

As early as 1959, Richard Feynman raised the idea to manipulate matter on the atomic scale, which he presented in his famous 'There's plenty of Room at the Bottom' speech. Even though not manageable back then, it created a vision and encouraged an entirely new field of research, which today is commonly known as 'nanotechnology'. Nanotechnology concerns itself with the atomic, molecular, and supramolecular levels of elements and thereof resulting materials to understand and exploit their size-dependent change in behaviour (Boland, 2006). These materials – summarised in the term 'nanomaterials' (NMs) – are characterised by a size of less than 100 nm in at least one dimension (Handy and Shaw, 2007). A more detailed definition, which is used in this project, has recently been recommended by the European Commission (2011) for regulatory purposes clarifying NMs to be any

- *"[…] natural, incidental or manufactured material containing particles,*
- *in an unbound state or as an aggregate or as an agglomerate and where,*
- *for 50 % or more of the particles in the number size distribution, one or more external dimensions is in the size range of 1 nm – 100 nm."*

Usually three major exposure routes are distinguished: inhalation (which to date is seen to be the most likely route of exposure for incidentally generated NPs), dermal uptake through the skin, and absorption of ingested NMs in the GI-tract (Elsaesser and Howard, 2012). Considering the use of NMs in medical products or therapeutics, the direct intravenous and intramuscular exposure to nano-sized objects has to be taken into account additionally (Farokhzad and Langer, 2006). This project will focus on the interactions of NMs with the intestinal barrier and underlying immune cells.

1.5.1 Oral exposure to NMs

NMs are increasingly used in both consumer and industrial products with numerous applications in the food sector. They can be intentionally introduced into food products and beverages or accidentally present as contaminants, e.g. resulting from dissolution and migration from packaging material (Bergin and Witzmann, 2013). The increased incorporation of NMs in a variety of products could cause problems of environmental contamination and, eventually, accumulation of NMs in water and animal products

(Conway et al., 2014; Lu et al., 2016). In a wider context, oral exposure also include the ingestion of inhaled particles after mucocilliary clearance from the respiratory tract (Arora et al., 2012), as well as the ingestion of medical products containing nano-sized components (Bergin and Witzmann, 2013).

Evaluating the average oral uptake of NMs is challenging, as it greatly depends on the diet, the status of processed foods within a diet, as well as the portion size (Lomer et al., 2000). An average daily intake of 10^{12} to 10^{14} micro-and nano-sized particles was estimated with SiO_2 and TiO_2 accounting for the major share (Lomer et al., 2002). For nano-sized SiO_2 particles the daily intake was estimated with 1.8 mg / kg bodyweight, whereas for TiO_2 NPs an oral uptake of roughly 0.07 mg / kg was proposed (Dekkers et al., 2011; Lomer et al., 2000). Concerning Ag, the mean uptake of dietary Ag (i.e. elemental, ionic, and nanoparticulate) was compiled for the French population resulting in the estimation of 1.29-2.65 µg / kg bodyweight (ANSES, 2011). For other NMs, like copper oxide (CuO) no estimations on the oral uptake are available to date. Due to its bactericidal activity, however, CuO is expected to be increasingly used in the future to replace Ag species. To date, the antibacterial properties of CuO only account for a minimal amount of its applications (Bondarenko et al., 2013).

In the food industry, TiO_2 NPs are commonly used as whitening pigment (Weir et al., 2012). SiO_2 NPs are applied as anti-caking agent, and used for the clearance of beer and wine (Yang et al., 2016; Dekkers et al., 2011). Furthermore, the application of NMs offers possibilities to improve the structure of food products, e.g. by increasing the stability of foams and emulsions (Dickinson, 2010) or preserving vulnerable compounds (Freiberger et al., 2015). NMs cam also be used to enhance the nutritional value of food products and nutraceuticals, as well as food supplements (Moncada et al., 2015; Luo et al., 2012; Santos et al., 2013).

Other materials are incorporated into food packaging and food contact materials from which they might – purposely or accidently – be released into the product. The use of nanotechnology in the manufacture of food containers or food contact surfaces generally aims to increase the quality and safety of the product (Silvestre et al., 2011). The applied materials include bactericidal agents like Zn NPs and AgNPs, which serve as shelf life extenders (Perez Espitia et al., 2012; Griffiths, 2015; von Goetz et al., 2013) and antibacterial compounds in water purification systems (Phong et al., 2009). Another aspect to improve food safety is the use of nanotechnology-based ‘intelligent labels’ capable of monitoring the condition of the packaged product and its

environment, e.g. pH, oxygen, CO_2, or pathogens (Kuswandi et al., 2011). Other applications are aimed at improving specific characteristics of the packaging material. The most commonly addressed points are the flexibility of a material, as well as the improvement of its barrier function to enhance the gas barrier properties, e.g. in plastic bottles, and atmospheric stability (Silvestre et al., 2011). Carbon- and silicon based NMs are main components in the sensor development for intelligent food packaging (Vanderroost et al., 2014), whereas polymer-nano-composites (featuring filler materials like nano-clay and SiO_2) enabled major advancements in the improvement of packaging materials (Duncan, 2011). Several studies have demonstrated that NMs used in packaging can migrate from the material into the food product or beverage in the container and might, subsequently, be ingested (von Goetz et al., 2013). Detailed indications regarding their share on the total exposure of consumers are not known.

1.5.2 Fate of orally ingested NMs

The incorporation of NMs as components in a food product or packaging containers makes an oral uptake highly likely. In this context, Ag, metal oxides and metalloids (e.g. SiO_2, ZnO, and TiO_2), as well as gold (Au) if nanomedical applications are taken into account (Fröhlich and Roblegg, 2012), are the materials of main concern.

Nanoparticulate matter can reach the GI-tract via two pathways: directly through oral uptake of nano-sized ingredients or contaminants in food products, beverages, and medical products, or indirectly after mucocilliary clearance from the respiratory tract (Arora et al., 2012). Since the incidental exposure to NMs after clearance from the respiratory tract is difficult to estimate normally only the direct dietary intake is considered in exposure assessments. Even though the exposure likelihood is high and the possibility of particle translocation from the intestinal lumen is recognised since 90 years (Hoet et al., 2004), studies on the uptake of NPs and associated risks have generated few definite answers to date.

1.5.2.1 Overcoming the mucus barrier of the GI-tract

Before overcoming the epithelial monolayer, NMs encounter the mucous lining of the mucosa, which presents an important barrier in the GI-tract. As a visco-adhesive hydrogel, mucus can entrap particles, e.g. through electrostatic interactions, van der

Waals forces, and chain entanglement (Liu et al., 2015). The health condition of the intestinal tissue strongly influences the mucus generation and composition. Both *in vitro* and *in vivo* models of the intestine showed an increased synthesis of mucus in inflamed conditions (Lamprecht et al., 2001; Leonard et al., 2010). Furthermore, an enhanced accumulation of nano-and micro-sized particles was noted at inflamed areas, which was suggested to be related to the mucus generation and composition (Leonard et al., 2010; Maisel et al., 2015). On one side, this knowledge can be used to develop new therapies for the treatment of IBD (Lamprecht et al., 2001; Ali et al., 2013). On the other side, individuals with chronic inflammatory conditions are likely to face different biological responses to NMs compared to healthy subjects (Leonard et al., 2010; Schmidt et al., 2013).

1.5.2.2 Overcoming the intestinal epithelial barrier

Four different pathways have been suggested for the uptake of NMs across the intestinal barrier:

1) Transcellular through enterocytes
2) Transcellular through M-cells
3) Paracellular (Fröhlich and Roblegg, 2012)
4) Persorption through single degrading enterocytes (Hillyer and Albrecht, 2001; Martirosyan et al., 2012).

Whereas the significance of uptake via paracellular processes and persorption remains questionable the transcellular passage of NMs through enterocytes and M-cells is widely acknowledged (Fröhlich and Roblegg, 2012). It has been demonstrated that NMs can enter systemic distribution after the uptake across the gut wall (Florence, 2005; Powell et al., 2010).

Due to the diversity of study outcomes, no broad consensus exists on how NMs interact with the GI-tract and what exactly determines their ability to reach systemic distribution. Several pathways that facilitate the internalisation of NPs into epithelial cells have been identified, including clathrin- and caveolin-mediated endocytosis, clathrin/caveolin-independent endocytosis, pinocytosis, and macropinocytosis (Oh and Park, 2014). Which mechanism is employed for the uptake of a NM appears to critically depend on the particle characteristics, such as size (of primary the particle and

potential aggregates/agglomerates), hydrophobicity, surface modification, and shape (Desai et al., 1997; Win and Feng, 2005; Florence, 2005). Whereas large vesicles of up to 5 µm are formed during macropinocytosis (Oh and Park, 2014) the size of caveolin-mediated caveolae usually ranges between 50 and 80 nm (Iversen et al., 2011). Apart from the size, the particle charge and geometry were shown to influence the uptake mechanisms. Bannunah et al. (2014) observed that the uptake of positively charged particles was mainly facilitated through clathrin-mediated endocytosis, as well as macropinocytosis, whereas the majority of negatively charged particles was internalised via a lipid raft-associated pathway. Alemdaroglu et al. (2008) noted a significantly higher uptake of rod-shaped compared to spherical copolymer micelles in Caco-2 cells.

However, the endocytosis rate of NMs does not necessarily equal their exocytosis, and hence, cannot be applied as a measure for entrance into systemic distribution. For instance Jani et al. (1990) noted size-dependent differences in the uptake of polystyrene particles in the GI-tract of rats. For particles up to 100 nm, higher concentrations of 50 than 100 nm were taken up and systemically distributed. Particles larger than 300 nm were taken up into the intestinal wall but trapped within the Peyer's patches (Jani et al., 1990).

Next to the characteristics of NMs, the diet itself and the physiology of the individual subject, including mucus secretion, pH, and GI-transit time greatly influence the uptake of NMs (Fröhlich and Roblegg, 2012).

1.5.3 Risks and benefits of oral exposure to NMs

The following paragraphs will summarise the potential risks and benefits of orally ingested NMs from a general perspective. More detailed discussions of AgNPs, CuO NPs, and AuNPs will follow in Chapters 4-6.

In vitro studies are widely available in the scientific literature, as both cell lines and commercial NMs are easily accessible and maintainable at comparably low costs. However, the general lack of guidelines and protocols for the design and execution of studies resulted in a multitude of combinations regarding the investigated cell type and chosen cell line and

- cell differentiation
- the NM and its characteristics, e.g. size, geometry, surface modifications, surface charge
- exposure conditions, e.g. time and concentration
- endpoints studied including the choice of assay.

Therefore, it can be difficult to compare across different studies, which can complicate the detection of similarities and differences in the effects and pathways between different NMs and characteristics of NMs.

For several NMs, e.g. SiO_2, ZnO, and TiO_2, the use of moderate exposure concentrations often did not result in measurable adverse effects in short-term exposure studies (McCracken et al., 2013). Some NMs, including TiO_2 NPs, AuNPs, and nano-diamonds, are reported to exhibit very low to no toxicity. No adverse effects on cell viability and gene expression were observed in Caco-2 cells after exposure to 10 µg / mL TiO_2 NPs for up to 72h (Fisichella et al., 2012). The exposure to nano-diamonds (up to 250 µg / mL) induced neither cytotoxicity nor genotoxicity in 6 cell lines or potential target organs, including an intestinal, a kidney, and two liver cell lines (Paget et al., 2014). In contrast, AgNPs were found to significantly reduce cell viability and proliferation in undifferentiated ($_{UD}$)Caco-2 cells at very low exposure concentrations of 1.25 µg / mL (McCracken et al., 2015).

It has been shown *in vivo* that NMs, albeit in a very small fraction, can be absorbed from the GI-tract and systemically distributed (Schleh et al., 2012). The potential effects of orally ingested NMs likely depend on their bioavailability, which can vary significantly between materials. In a 90-day oral exposure study in rats Cho et al. (2013b) observed significant differences in the uptake of ZnO and TiO_2 NPs. Whereas 90 nm ZnO NPs were absorbed and systemically distributed, considerably smaller 26 nm TiO_2 NPs were not (Cho et al., 2013b). In contrast, Nogueira et al. (2012) observed a potential pro-inflammatory effect of sub-chronic exposure to 100 mg / kg bodyweight TiO_2 NPs and MPs in mice. The group noted an increased presence of $CD4^+$ T-cells, as

well as increased levels of pro-inflammatory cytokines like TNF-α, IFN-γ, and IL-12 (Nogueira et al., 2012). Several studies reported indications for the induction of organ-specific toxicity, for instance in response to AgNPs (Kim et al., 2008) or ZnO NPs (Sharma et al., 2012). Most of the available studies used acute or sub-chronic exposure scenarios. Only very few information are available on a potential bio-accumulation of NMs and the induction of chronic toxicity (van der Zande et al., 2012). Furthermore, it remains questionable how these findings translate to a human exposure situation.

To what extend the intestinal physiology can influence the effects of NMs is still unclear. Several *in vivo* studies and one study in human volunteers have shown increased attachment and accumulation of NMs at the site of inflammation within the intestine (Schleh et al., 2012; Schmidt et al., 2013). On the one hand, this might cause an increased uptake of NMs across the intestinal barrier and subsequent systemic distribution. On the other hand, dietary NPs have been suggested to play a role in the induction of intestinal inflammation and even the deterioration of IBD (Martirosyan et al., 2012; Lomer et al., 2002).

Focusing on the benefits of NMs it appears that the great majority are primarily favourable for the manufacturers. The introduction of nano-sized materials to food products is more efficient and effective than the use of the bulk counterpart (Kasaai, 2015). However, both manufacturers and consumers can profit from the use of nanotechnological approaches to improve food safety and quality as mentioned before (Section 1.5.1). One of the most promising developments expected to benefit a wider range of individuals is the use of NMs in medical products and pharmaceuticals. Especially the formulation of drug delivery vehicles to improve targeting, bioavailability, or circulation time of an active substance is a promising application field (de Jong and Borm, 2008).

1.5.4 Unknowns concerning the oral exposure to NMs

The hereinafter presented challenges should be understood as examples and is by no means an exhaustive list.

One of the biggest question marks concerning the oral exposure to NMs is the actual exposure concentration an individual faces. For some NMs average exposure estimations are available (Section 1.5.1), but for most no sound assessment has been

performed. The knowledge of exposure concentrations is of great interest to design studies using realistic exposure scenarios. To date, most studies apply nonsensically high concentrations applied as a single dose / one-time exposure. The results of many *in vivo* studies suggest, though, that the occurrence of chronic toxic effects is substantially more likely than the induction of acute toxicity (Pettibone et al., 2009). In a study by van der Zande et al. (2012), the results showed a low but detectable accumulation of AgNPs in the brain and testes after a 28-day oral exposure study in rats. The detected concentrations were far lower than in the liver or spleen, however, hardly any elimination occurred over a period of 2 months after the last exposure (van der Zande et al., 2012). Results like these strongly call for long-term and repeated-exposure studies to address potential bioaccumulation of NMs and, thereby, induced chronic toxicity.

A topic currently receiving increased interest is the effect of NM-exposure on the intestinal flora. Whereas several studies could show a negative impact of NM-exposure on the composition of the microbiome *in vivo* (Tyagi et al., 2016) and *in vitro* (Taylor et al., 2015) others did not find any significant effects (Wilding et al., 2016). Over the last years, however, the diversity of tasks and importance of the microbiome for the organism, e.g. mental health and weight control (Foster and McVey Neufeld, 2013; Sweeney and Morton, 2013), have become increasingly evident. Hence, reliable and consistent statements are required.

Whereas hardly any effects are known with certainty in the healthy organism even less is known regarding the impact of NM-exposure in the diseased intestine. So far, most exposure experiments are performed in healthy animals and cell cultures mimicking intact tissue, even though the effects of exposure are likely different in individuals with impaired health (de Jong and Borm, 2008). Also concerning the oral uptake of NPs and MPs studies have shown specific effects in IBD patients. For instance Lomer et al. (2002) reported a significant impact of the dietary particle content on the disease activity index of Crohn's disease patients. Furthermore, several studies have observed differences in the adherence and uptake of NMs between healthy and inflamed intestinal tissue (Section 1.5.2.1). However, only few insights have been gained concerning a potentially changed toxicity of NMs in impaired tissue. In this regard, a major limitation is the scarce availability of well-designed and -defined *in vitro* disease models (Lefebvre et al., 2015).

1.6 Aims, objectives, and general hypotheses of the project

The human intestine is constantly in contact with nano-sized objects, including dietary proteins and micelles. Taking into account that both epithelial and immune cells must frequently encounter them, NMs are unlikely to present a danger to human health per se. However, the number of engineered NMs incorporated in food products and packaging material rises continuously. The safety of these materials has been demonstrated using their bulk products, but has generally not taken into account the change in physico-chemical properties when reducing their size to the nanoscale. It is, therefore, unclear how the oral exposure to these NMs affects the human organism compared to their larger-sized counterparts. Even less is known regarding the effects of orally ingested NMs in the diseased compared to the healthy intestine. However, both acute and chronic inflammatory conditions of the intestine present challenges world-wide. Whereas improvements in hygiene and food safety practices slowly reduce the occurrence of foodborne illnesses the prevalence of IBD is rising. In this context, the exposure to NMs must not necessarily mean a hazard, but can also include innovative nanomedical approaches for the treatment of IBD.

The overarching goal of this project was identified to be the development and characterisation of an *in vitro* co-culture model of the human small intestine to progress *in vitro*-based intestinal research models for nanosafety applications. To achieve this goal the following aims (roman numbers) and corresponding objectives (small letters) were defined:

I. Development of an *in vitro* cell line-based co-culture model combining enterocytes and macrophages representing the human small intestine in homeostatic state.
   - I.a THP-1 differentiation protocol and seeding density will be adapted so that no disruption of the Caco2 barrier occurs throughout the co-culture.
   - I.b To assure that THP-1 and Caco-2 cells do not negatively affect each other, the following endpoints will be measured at least once over a time course of 48h: TEER, release of pro-inflammatory cytokines, LDH as marker for necrotic cell death, and NO_2^-.
   - I.c The endpoints will be compared to a Caco-2 monoculture control.

II. Advancement of the homeostatic intestinal model to mimic the diseased intestine by displaying a controlled inflamed state in response to the exposure to a pathophysiological stressor.

II.a The homeostatic co-culture will be triggered to display hallmarks of intestinal inflammation – reduction in barrier integrity, pro-inflammatory cytokine release, LDH release, and NO_2^- synthesis – using a pathophysiological stressor.

II.b The inflammation-like reaction will be induced without altering the previously adapted details, i.e. THP-1 differentiation and seeding density.

II.c The inflammation-like reaction will be assessed regarding the TEER, pro-inflammatory cytokine release, LDH release, and NO_2^- synthesis over a time course of 48h against a Caco-2 monoculture control and the homeostatic co-culture.

III. Application of the two established co-culture models to study the cytotoxic and (pro-)inflammatory effects of NMs in context of the model's health status at the time of exposure.

III.a Both developed co-culture models will be exposed to non-toxic concentrations of NMs that are likely to be orally ingested.

III.b The cytotoxic potential of the NMs will be studied in the cell monocultures prior to the exposure of co-cultures.

III.c In both co-culture conditions the cytotoxic and inflammatory effects of the NMs will be assessed by monitoring TEER, pro-inflammatory cytokine release, LDH release, and NO_2^- synthesis.

III.d All results will be compared to an unexposed Caco-2 monoculture, as well as a corresponding unexposed co-culture control.

IV. Application of the two established co-culture conditions to investigate the effect of the model's health status on the paracellular passage of NMs across the IEC barrier.

IV.a Both developed co-culture models will be exposed to different sizes of radio-labelled AuNPs.

IV.b The effect of the co-culture and the exposure to AuNPs will be monitored by means of TEER and compared to an unexposed Caco-2 monoculture control.

IV.c The activity of the radio-label will be measured in the AP and BL supernatants, as well as in both cell lines.

IV.d The activity distribution in the co-culture models will be compared to an exposed Caco-2 monoculture control and against each other.

The project is based on the hypotheses that

1. Caco-2 and THP-1 cells can cohabit in a paracrine co-culture system to mimic the intestine in homeostatic state.
2. An inflammation-like response displaying hallmarks of intestinal inflammation can be induced in the homeostatic co-culture through the stimulation of the THP-1 cells.
3. The two co-culture models are suitable to study the effects of NMs in relation to the health status of the *in vitro* co-culture at the time of exposure.

The specific hypotheses will be elaborated in the introductory paragraphs of the experimental Chapters 2-6.

2 Development of a co-culture model to mimic the healthy and inflamed human intestine

This chapter will describe the development of the two conditions of the envisaged co-culture model:

1. A homeostatic co-culture of Caco-2 and THP-1 cells to mimic the healthy human intestine (Aim I).
2. An *in vitro* inflammation-like response in a co-culture of Caco-2 and THP-1 cells to resemble the diseased human intestine (Aim II).

The induction of an inflammation-like response should result in the manifestation of the hallmarks of intestinal inflammation – disruption of barrier integrity, cytotoxicity, and release of pro-inflammatory molecules, e.g. cytokines and NO. To obtain highly comparable results from the individual co-culture models the differences between the two set-ups will have to be kept to an absolute minimum.

The development of the co-culture models was based on the following hypotheses:

- THP-1 and Caco-2 cells can cohabit and, therefore, can be used to develop a homeostatic co-culture model.
- The homeostatic co-culture can be disrupted by stimulation of the THP-1 cells with a physiologically relevant stressor.
- The stimulation of THP-1 cells with a stressor causes a significant reduction in barrier integrity compared to the homeostatic co-culture.

2.1 Materials & Methods

2.1.1 Chemicals

Phosphate Buffered Saline (PBS) (20012-019), Minimum Essential Medium (MEM) (31095), Roswell Park Memorial Institute medium (RPMI) (52400), sodium pyruvate (11360), Penicillin / Streptomycin (Pen/Strep) (15150), 2-mercaptoethanol (31350), Trypsin / EDTA (25300-054), and L-Glutamine (35050) were purchased from Thermo Fisher Scientific. D-Glucose (G8769), TritonX-100 (93443), PMA (P1585), formaldehyde (254-9), lipopolysaccharides (LPS) (L4391), Lucifer Yellow (LY)

(L0259), Accutase (A6964), and bovine serum albumin (BSA) (A2153) were obtained from Sigma-Aldrich.

2.1.2 Cell culture

NB: The details concerning the co-culture development will be covered in the results, Sections 2.2.3 and 2.2.4.

Caco-2 cells (DSMZ, ACC169; a kind gift from Dr. Roel Schins) were culture in MEM-based cell culture medium (CCM) substituted with 20 % FBS (Thermo Fisher Scientifc, 26140079), and 1 % Pen/Strep at standard culture conditions (37°C, 5 % CO_2). The cells were sub-cultured at $3x10^5$ cells / 25cm² flask when cell layers reached ~80 % confluence. For co-culture experiments, cells were seeded at a density of $1.8x10^5$ cells / cm² on transparent PET transwell inserts (1 µm pore size; Falcon 353103) and maintained for 18-21 days to allow for barrier formation and differentiation of the cells. Transparent filters were chosen to facilitate the analysis of the cells with light and fluorescence microscopy. Since the model shall eventually be used to study barrier crossing of NMs, filter inserts with a pore-size <1 µm and collagen coating of the filters were avoided, as both might hinder particles to pass into the BL compartment after crossing the Caco-2 cell layer. Apically, cells were maintained in MEM-based CCM, whereas the medium on the BL side was gradually (Table 2.1) changed to RPMI-based THP-1 medium (composition below) without mercaptoethanol. The barrier formation was monitored by regular measurements of TEER every 2 to 3 days of culture (Section 2.1.4), assessment of the translocation of LY across the cell barrier (Section 2.1.5), and immunohistochemical staining of F-actin (cytoskeleton) and the TJ-associated protein ZO-1 (Section 2.1.6).

The early monocytic cell line THP-1 (ATCC, TIB-202) was cultured in RPMI-based CCM substituted with 10 % FBS (Thermo Fisher Scientifc, 10099), 1 % Pen/Strep, 1 % L-Glutamine, 1 nM sodium pyruvate, 0.7 % D-Glucose, and 0.05 mM mercaptoethanol at standard culture conditions. The cells were sub-cultured when reaching a cell density of $8\text{-}10x10^5$ cells / mL. For co-culture experiments, the cells were seeded in 25 cm² culture flasks at a density of $3x10^6$ cells / 6 mL CCM and differentiated with 100 nM PMA (60 µL of a 10 µM stock in PBS). The differentiation with PMA will be discussed in more detail in Section 2.2.2.1. After differentiation, the cells were detached with

Accutase and plated at a density of $1.8x10^5$ cells / well on transwell-suitable 12-well plates.

Table 2.1 Medium composition in the basolateral compartment over 21 days of Caco-2 culture

Days of culture	Caco-2 medium (%)	THP-1 medium (%)
0	100	0
2	100	0
5	66.6	33.6
7	66.6	33.3
9	50	50
12	50	50
14	33.3	66.6
16	33.3	66.6
19	0	100
21	0	100

Both cell lines were tested for their genetic integrity (performed by DSMZ, Braunschweig, Germany). The Caco-2 cell line was confirmed to fully match the testing institute's STR profile. The THP-1 cells were attested a slight deviation from the DSMZ profiles, but fully matched the STR information of the original supplier (ATCC). Both cell lines were negative for contamination with foreign mitochondrial DNA sequences (DSMZ, Braunschweig) and mycoplasma (Minerva Analytix, Berlin).

2.1.3 Adjustments for the inflamed co-culture

To establish the inflamed co-culture several adjustments to the stable co-culture set-up were investigated.

2.1.3.1 LPS-stimulation of THP-1 cells

To induce the release of pro-inflammatory cytokines, 10 ng / mL LPS were added to the BL compartment at the start of the co-culture (T_0) to activate the PMA-differentiated THP-1 cells.

2.1.3.2 Pre-stimulation of THP-1 cells

To allow for an unrestricted activation, the THP-1 cells were exposed before the start of the co-culture. After PMA-differentiation, the cells were plated onto transwell-suitable 12 well plates. The cells were left to re-attach for 1.5h after which the medium was discarded and exchanged for 1.5 mL fresh medium. Subsequently, 10 ng / mL LPS or a combination of LPS and IFN-γ (10 ng / mL each) was added to the well and the cells incubated for 4h at standard culture conditions. After 4h, the co-culture was started by placing the filter inserts with Caco-2 cells on the THP-1-containing wells.

2.1.3.3 IFN-γ priming of Caco-2 cells

To increase their sensitivity to the presence of TNF-α, Caco-2 barriers were primed with IFN-γ as described by Wang et al. (2005). 18-24h before the start of the co-culture, Caco-2 cells were exposed to 10 ng / mL IFN-γ in the BL compartment of the transwell system. Two hours before the start of the co-culture, the exposed cells were washed 2x with 1 mL PBS on the BL side and 1.5 mL fresh CCM were added. The co-culture was initiated as before by placing the primed filters onto transwell-suitable 12 well plates containing PMA-differentiated THP-1 cells.

2.1.4 Monitoring of barrier integrity by TEER

The TEER was measured using an Ohm-meter (Millicell, ERS-2) to monitor the barrier development of the Caco-2 cell layer, as well as to assess the barrier integrity throughout the co-culture with THP-1 cells. To monitor the barrier development, the TEER was measured every 2-3 days from day 2 to 21 post-seeding. For studying the effect of co-culturing Caco-2 and THP-1 cells the TEER was measured just before the co-culture and after 4, 24, and 48h. If applicable, the TEER was also measured after 18h of co-culture. Before measurements were taken, the electrode was sterilised for 15 min in 70 % Ethanol and neutralised in pre-warmed PBS and MEM. The results were corrected for the blank value and multiplied by the filter size to obtain the final results in Ohm per cm^2 ($\Omega \cdot cm^2$).

2.1.5 Barrier permeability assay and calculation of the apparent permeability coefficient

To monitor the Caco-2 barrier development the flux of LY from the AP to the BL compartment was measured at day 2, 4, 6, 12, and 21 post-seeding. The supernatant was removed and the cells washed twice on both AP and BL side with Hank's Balanced Salt Solution containing magnesium and calcium ($HBSS^{+/+}$). Subsequently, 1.6 mL $HBSS^{+/+}$ were added to the BL side and 0.6 mL of 5 mg / mL LY dissolved in $HBSS^{+/+}$ to the AP side. The cells were incubated for 4h at standard culture conditions. From both sides, 100 µL samples were taken immediately after addition of LY and after 4h. The sample volumes were not replaced in the wells. The fluorescence was measured spectrophotometrically (Perkin Elmer, Enspire) at an excitation wavelength of 485 nm and emission wavelength of 530 nm.

To calculate the apparent permeability coefficient (P_{app}) from samples taken after 4h the following equation (2.1) was applied:

$$P_{app} = \frac{dQ/dt}{C_0 * A} \qquad (2.1)$$

With dQ/dt being the permeability rate in µM / s, C_0 the initial concentration of LY in the AP compartment (5 µM), and A the filter surface are in cm^2 (0.9). The result is expressed as cm / s.

2.1.6 Immunocytochemcial staining and analysis

Target proteins of both Caco-2 and THP-1 cells were stained using specific primary antibodies (Abs) coupled with fluorophore-conjugated secondary Abs and imaged with the Zeiss Axiovert 200M in Apotome mode. In Caco-2 cells the development of the (microvillous) cytoskeleton (F-actin, villin) and the TJ network (here ZO-1) were monitored. For THP-1 cells, the influence of PMA exposure on the cytoskeletal structure, as well as the expression of cell surface receptors (CD14 and CD68) were analysed. For immunocytochemical staining the cells were fixed in 3.7 % formaldehyde for 13 min. Subsequently, they were permeabilised with 1 % (Caco-2) or 0.1 % (THP-1) TritonX-100 in PBS for 5 min and blocked against unspecific binding with 3 % BSA in PBS at room temperature (RT). The cells were incubated with the primary Ab (ZO-1: 5 µg / mL [Thermo Fisher, 61-7300]; villin [Sigma, SAB5500190]:

1:100; CD14 [Sigma, C7673] and CD68 [abcam, ab955]: 5 µL / $1x10^6$ cells) for 1.5h at RT. After washing with PBS, the cells were incubated with a mix of AlexaFluor546 (Caco-2 1:300, THP-1 1:2,000), Phalloidin-AlexaFluor488 conjugate (1:40) and DAPI (1:4,000) in PBS for 45 min at 37°C. For analysis using the Zeiss Axiovert microscope the filters were cut out and mounted cells facing up on standard microscopy glass slides. The slides were stored protected from light at 4°C.

A black & white AxioCam MRm (Carl Zeiss; Jena, Germany) was used and pseudocolours were applied after image acquisition. The exposure times for all three channels were set using stained control cells and subsequently applied in the image acquisition of all conditions. The channel focus was adjusted manually for each position. If applicable, the acquired images were analysed using the software ImageJ. All images were treated with the same background subtraction. In case the signal intensity was increased a linear enhancement was applied to the whole file. All corresponding images were treated identically. Further details on the image analysis are given in the individual sections.

2.1.7 Flow cytometry

Flow cytometry was used to study the expression of two cell surface receptors – CD14 and CD68 – on THP-1 cells. The cells were fixed in 3.7 % formaldehyde as undifferentiated control or after differentiation with PMA. For each condition a minimum of $1x10^6$ cells was prepared. The cells were used as unstained control, stained with the primary Ab (CD14 or CD68 as above), stained with the secondary Ab (AlexaFluor 546 at a concentration of 1:100), or stained with both Abs. Since both primary Abs were generated in mice, the receptor stainings had to be performed separately. The unstained and stained cell samples were analysed with flow cytometry (Partec CyFlow Space), kindly performed by Blanka Halamoda-Kenzaoui from the 'Interaction with Biological Systems' (IBS) Competence Group (CG) of the Nanobiosciences (NBS) Unit at the Joint Research Centre (JRC) (Italy). The results are presented as % of gated cells.

2.1.8 Cytokine quantification using Enzyme-Linked Immuno-Sorbent Assay (ELISA)

The release of IL-1β, IL-8, and TNF-α was quantified by a sandwich ELISA using cell-free supernatant collected after 4h exposure to LPS or LPS and IFN-γ, or after 4h of co-culture. The ELISA was run as described by Kinsner et al. (2006). Briefly, the primary Ab (R&D, DY210/201/208) was incubated overnight in coating buffer (0.1 M $NaHCO_3$ in MilliQ H_2O) on high protein-binding 96-well plates (Nunc MaxiSorp). After washing (0.05 % TWEEN20 in PBS) and blocking (3 % BSA / PBS) the supernatant samples were added pure or if necessary diluted (1:2-1:10 in 1 % BSA / PBS) and incubated for 2h. After thorough washing, the secondary Ab was added and incubated for 1.5h at 37°C. After incubation (30 min) with peroxidase (Bio Trend, S207), 100 µL 3,3′,5,5′-Tetramethylbenzidine (Sigma, T0440) were added and the reaction stopped with sulphuric acid (1M) after 10-15 minutes. The absorbance was read spectrophotometrically at 450 nm. In every analysis, a calibration curve and blank was included for each cytokine. The calibration curve was plotted as 4-parameter logfit.

Table 2.2 ELISA upper and lower detection limit according to the manufacturer

Detection limit (in pg / mL)	IL-1β	IL-8	TNF-α	TGF-β1
Upper	250	2,000	1,000	2,000
Lower	3.91	31.2	15.60	31.2

2.1.9 Statistical Analysis

Throughout the entire project, the data analysis was performed with Microsoft Excel and the results were illustrated using GraphPad Prism 6. Variations between results are expressed as standard deviation (StDev). The statistical analysis was done by one-way ANOVA and Dunnett's test, or if applicable unpaired T-test, using Minitab. A value of $p \leq 0.05$ was accepted as statistically significant. In graphs, no symbolic distinction is made between $p \leq 0.05$, ≤ 0.01, ≤ 0.005, and ≤ 0.001.

2.2 Results / Protocols

2.2.1 Caco-2 monoculture

2.2.1.1 Barrier formation and TJ development

The barrier formation was monitored by regular measurements of TEER. The maximum TEER of 510±38 Ω•cm² was reached approximately 12 days post-seeding (Figure 2.1). Subsequently, the barrier resistance decreased again to around 400 Ω•cm². Hereinafter, the TEER results of co-culture and barrier exposure experiments are expressed as percentage of the unexposed Caco-2 monoculture control.

In correspondence to this, the imaging of Caco-2 cells after different culture periods (Figure 2.2) show a clear increase in cell number over 21 days. After 24h of culture (Figure 2.2A) the cells attached and small colonies were formed. The large surrounding F-actin rings suggest a high cellular volume and ample cytosolic space. The TJ-associated protein ZO-1 is exclusively expressed between adjacent cells. On cell membranes facing unoccupied space no ZO-1 expression was observed. After 12 days of culture (Figure 2.2B), two observations were striking. Firstly, the intracellular area was clearly reduced compared to after 24h of culture. Secondly, the cells formed large dome-like structures. The severity of these domes reduced again and was observed infrequently in fully differentiated Caco-2 barriers. After 21 days of culture (Figure 2.2C), a tightly packed cell layer featuring a continuous cytoskeleton and TJ network was formed.

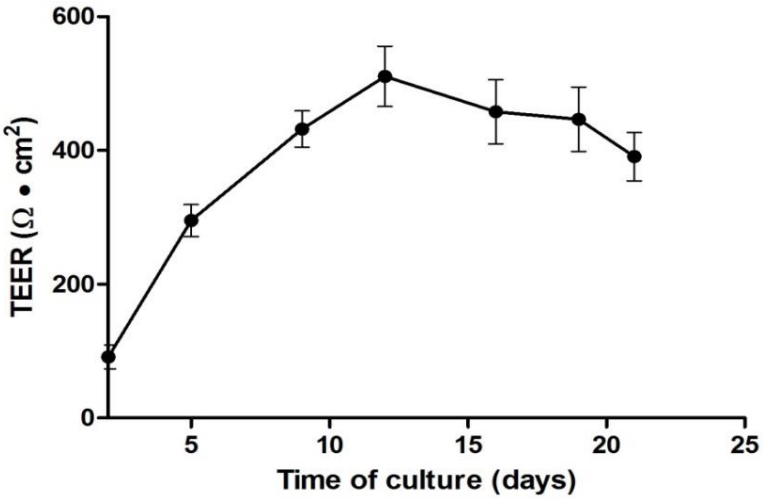

Figure 2.1 Caco-2 barrier development and TJ formation measured as TEER over 21 days of culture

(Day 2-9: Average of N=2; Day 12-21: Average of N≥3 ± StDev)

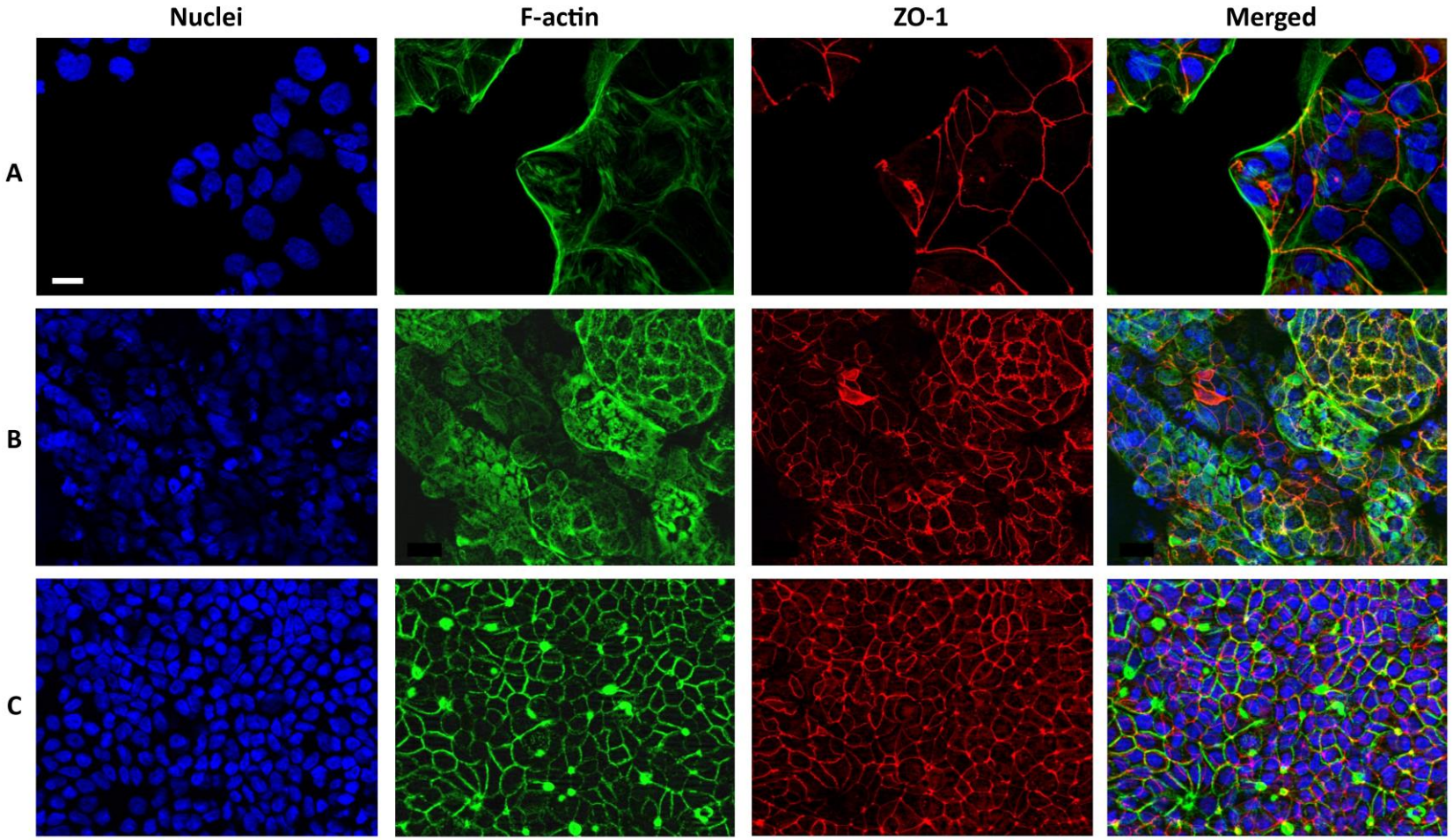

Figure 2.2 Caco-2 barrier development

Imaging of nuclei (blue), F-actin (green), and ZO-1 (red) after (A) 1 day, (B) 12 days, and (C) 21 days of culture (imaged with 40x magnification in Apotome mode, scale bar:20 µm, applies to all images)

Apart from the measurement of TEER, the Caco-2 barrier development was monitored by quantifying the paracellular passage of LY (molecular weight = 521.57) at different time points post-seeding. With increasing formation of the TJ network the translocation of LY across the barrier was expected to be inhibited. The results of LY passage are summarised in Figure 2.3. Over the culture period of 21 days, the P_{app} of LY gradually decreased. The small discrepancy in LY passage between day 4 and 6 is likely related to variations between cultures. Between 6 and 12 days of culture, the Caco-2 barrier becomes almost impermeable to LY and the P_{app}, henceforth, remains low. After 21 days of culture, the translocation of LY from AP to BL compartment was below 1 % over an incubation time of 4h.

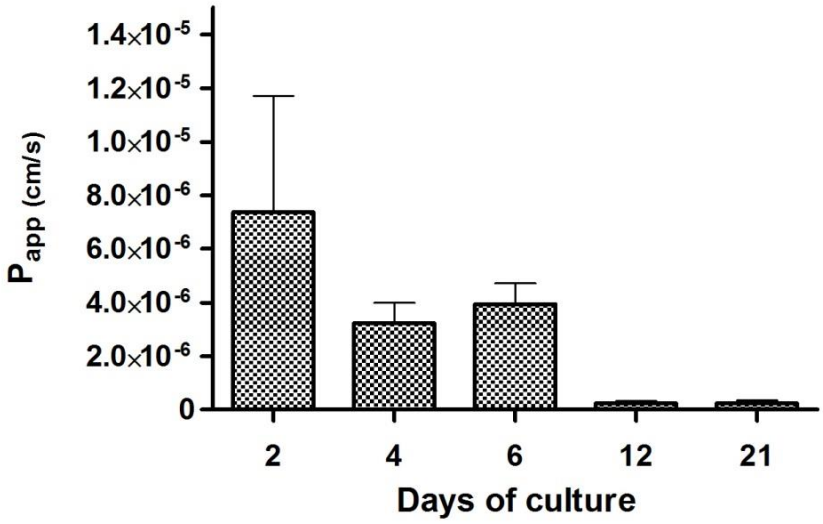

Figure 2.3 LY barrier passage across Caco-2 cells after 2, 4, 6, 12, and 21 days of culture

Results are presented as P_{app} after 4h incubation (Average of N≥2 ± StDev)

2.2.1.2 Caco-2 differentiation

Known as actin-binding / -bundling protein, villin is expected to co-localise to a high extend with F-actin of the cellular cytoskeleton. As shown in Figure 2.4, the fluorescent signal of villin (red) greatly overlays the green signal corresponding to phalloidin-stained F-actin. With increasing culture time the villin-associated fluorescent signal clearly intensifies, confirming an increase in protein expression over time.

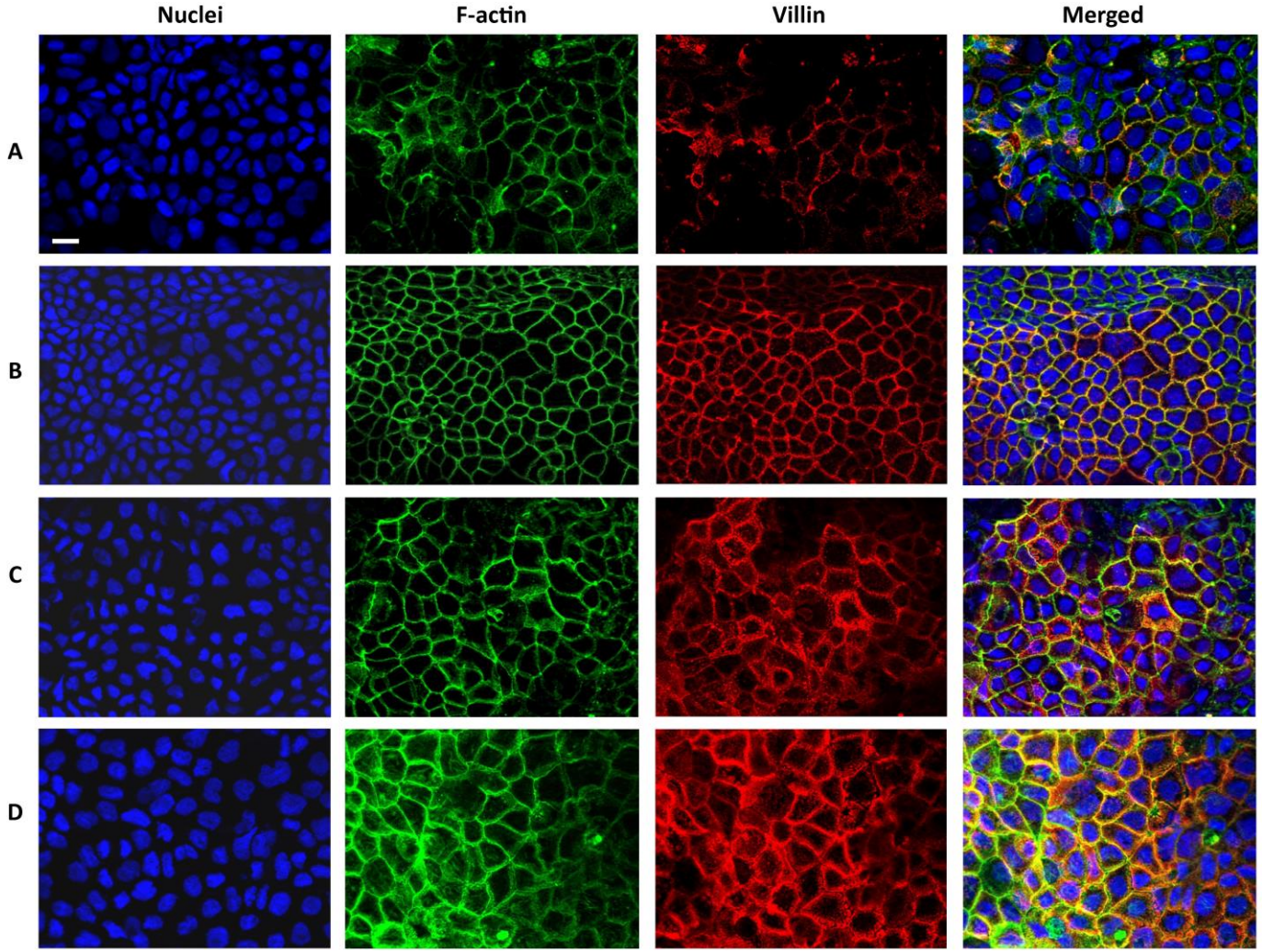

Figure 2.4 Caco-2 villin expression after (A) 2, (B) 5, (C) 13, and (D) 21 days of culture

Fluorescence microscopy analysis in Apoptome mode, 40x magnification, scale bar:20 µm, applies to all images

For the quantitative analysis, the fluorescence intensity (FI) was first normalised to the number of cells and subsequently to the FI measured after 2 days of culture. The results are expressed as fold-increase compared to 2 Days of co-culture (Figure 2.5). Over a period of 21 days of culture, the villin expression of Caco-2 cells increased steadily. At 21 days post-seeding, the FI was ~2.3 times enhanced compared to day 2 (Figure 2.5).

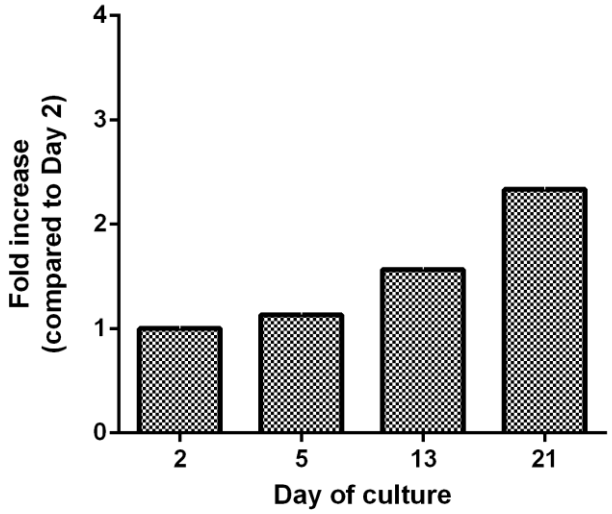

Figure 2.5 Villin expression in Caco-2 cells over 21 days of culture

Measured as increase in villin-associated fluorescence signal normalised to FI after 2 days of culture and cell number (Average of n=2 of one experiment ± StDev)

2.2.2 THP-1

2.2.2.1 PMA-differentiation of THP-1 cells

The monocyte-like THP-1 cells require an external differentiation stimulus, e.g. PMA, to develop macrophage-like characteristics (Tsuchiya et al., 1982). The suspension cells responded to the PMA-treatment by adhering to the plastic surfaces of flasks and well plates. During this process, they underwent a striking morphological change: from compact-spherical (Figure 2.6A&C) to an amoeboid shape forming pseudopodia-like extensions (Figure 2.6B&D). As was observed by optical microscopy, approximately 80-90 % of the cells were firmly attached and the cells' proliferation had ceased after 24h of exposure to PMA.

With flow cytometry and immunohistochemistry the effect of PMA exposure on the expression of two cell surface receptors – CD68 and CD14 – was analysed. The

analysis of undifferentiated THP-1 cells with flow cytometry showed that most cells expressed both surface markers: 85 ± 9 % CD14, 90 ± 0.36 % CD68 (data not shown). Interestingly, after PMA-treatment CD14 was only detected in 70 ± 14 % of the cells, whereas the expression of CD68 was not affected (96 ± 1.3 %) (data not shown).

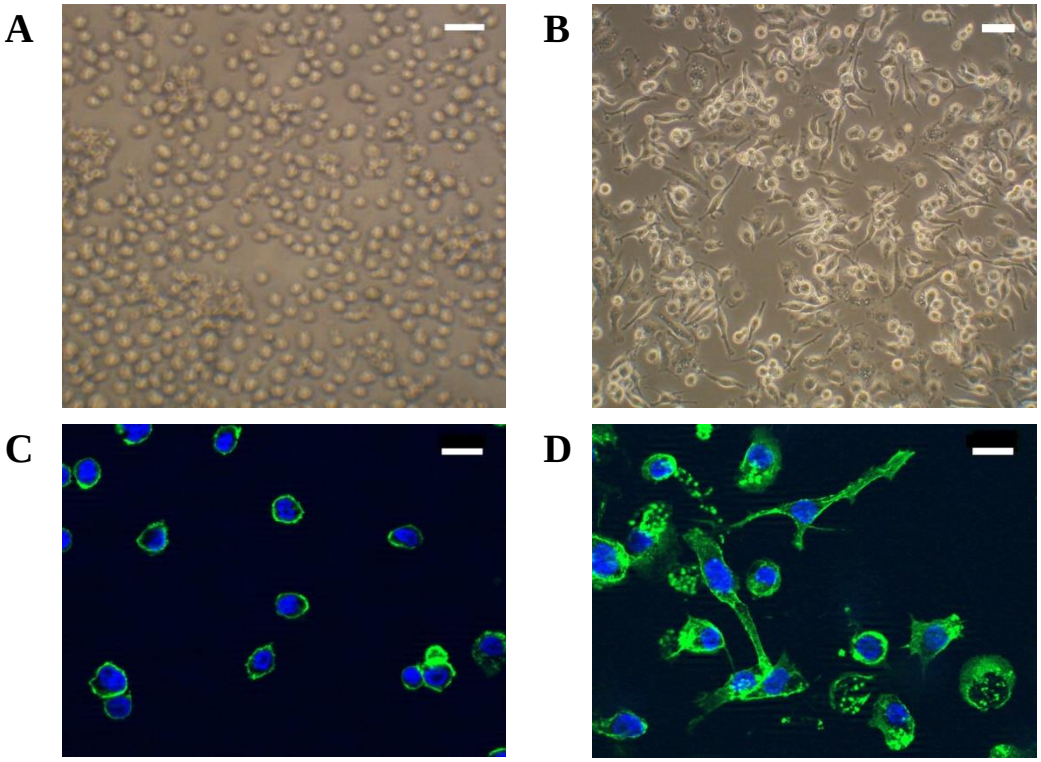

Figure 2.6 Morphology of undifferentiated (A&C) PMA-differentiated (B&D) THP-1 cells

Light microscope 20x magnification; fluorescence microscope (Apotome mode) 40x magnification; blue: DAPI (nuclei), green: Phalloidin AlexaFluor488 conjugated (F-actin); scale bar light microscope: 40 µm; scale bar fluorescence microscope: 20 µm.

To confirm the results obtained with flow cytometry, undifferentiated and PMA-differentiated THP-1 cells were stained, fluorophore-labelled and analysed microscopically (Figure 2.7). For the quantitative analysis, the FI was background-corrected and normalised to the measured area using ImageJ. The results are expressed as FI, which is the intensity per pixel of the measured area. On undifferentiated and PMA-differentiated THP-1 cells CD68 was expressed similarly (FI 19.8 ± 7.3 vs. 15.1 ± 5.6). In line with the flow cytometry outcome the CD14-associated FI was reduced by ~36 % in PMA-treated compared to undifferentiated cells (FI 14.3 ± 5.6 vs. 22.4 ± 7). Since only a very limited number of cells were assessed these results are not representative.

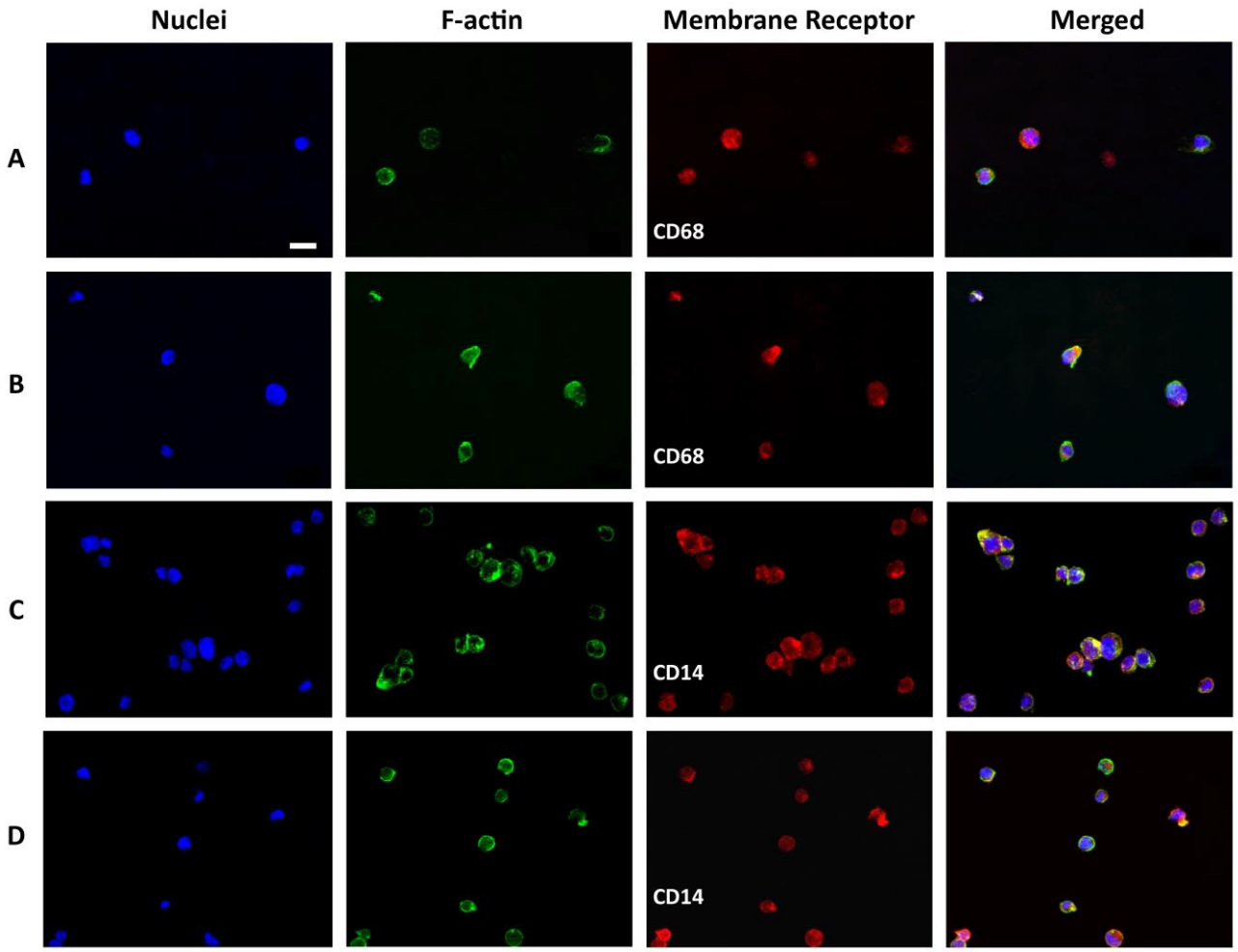

Figure 2.7 Expression of CD68 (A&B) and CD14 (C&D) in undifferentiated (A&C) and PMA-differentiated (B&D) THP-1 cells

Images were acquired in Apotome mode at 40x magnification, scale bar: 20 µm, applies to all images (NB: For differentiation THP-1 cells were exposed to 100 nM PMA for 48h. PMA-treated THP-1 cells were enzymatically detached before fixation. Therefore, the cells do not show the typical amoeboid phenotype associated with PMA-differentiation.)

2.2.2.2 LPS-induced release of pro-inflammatory cytokines

The functionality of the CD14 receptor was confirmed by studying the release of IL-1β, IL-8, and TNF-α from PMA-treated THP-1 cells without stimulation (hereinafter 'unstimulated') and after 4h stimulation with 10 ng / mL LPS.

As shown in Figure 2.8 and Figure 2.9 below, the LPS-induced cytokine release strongly depends on the differentiation status of THP-1 cells. Without stimulation, undifferentiated THP-1 cells released low to undetectable concentrations of pro-inflammatory cytokines (Figure 2.8, black bars). When exposed to LPS, the release of IL-8 (24 vs. 347 pg / mL) and TNF-α (18 vs. 308 pg / mL) increased significantly. The concentration of IL-1β was minimally affected (8 vs. 14 pg / mL) (Figure 2.8, white bars).

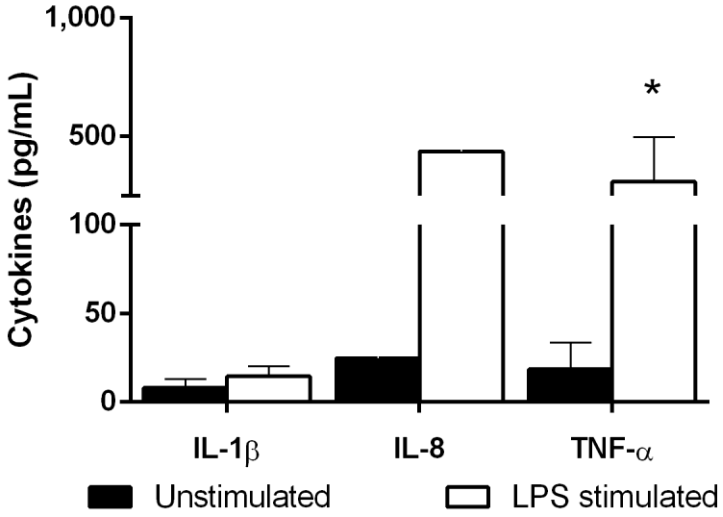

Figure 2.8 Cytokine release of undifferentiated THP-1 cells after 4h exposure to 10 ng/mL LPS

(IL-1ß and TNF-α: Average of N≥3 ± StDev, IL-8: Average of n=3 of one experiment ± StDev)

For initial studies, THP-1 cells were differentiated by exposing the cells to PMA for 24h and subsequent resting for 24h in PMA-free CCM (hereinafter '48h-differentiated'). When differentiated according to the 48h protocol, THP-1 cells readily released considerable concentrations of cytokines without prior LPS stimulation. Especially IL-8 was present at remarkable levels with >3,600 pg / mL (Figure 2.9A, black bars). Both IL-1β and TNF-α were expressed at lower but detectable concentrations (Figure 2.9A, black bars). The exposure to LPS strongly enhanced the release of IL-1β, IL-8, and TNF-α to ~221, 11,328, and 1,037 pg / mL, respectively (Figure 2.9A, white bars).

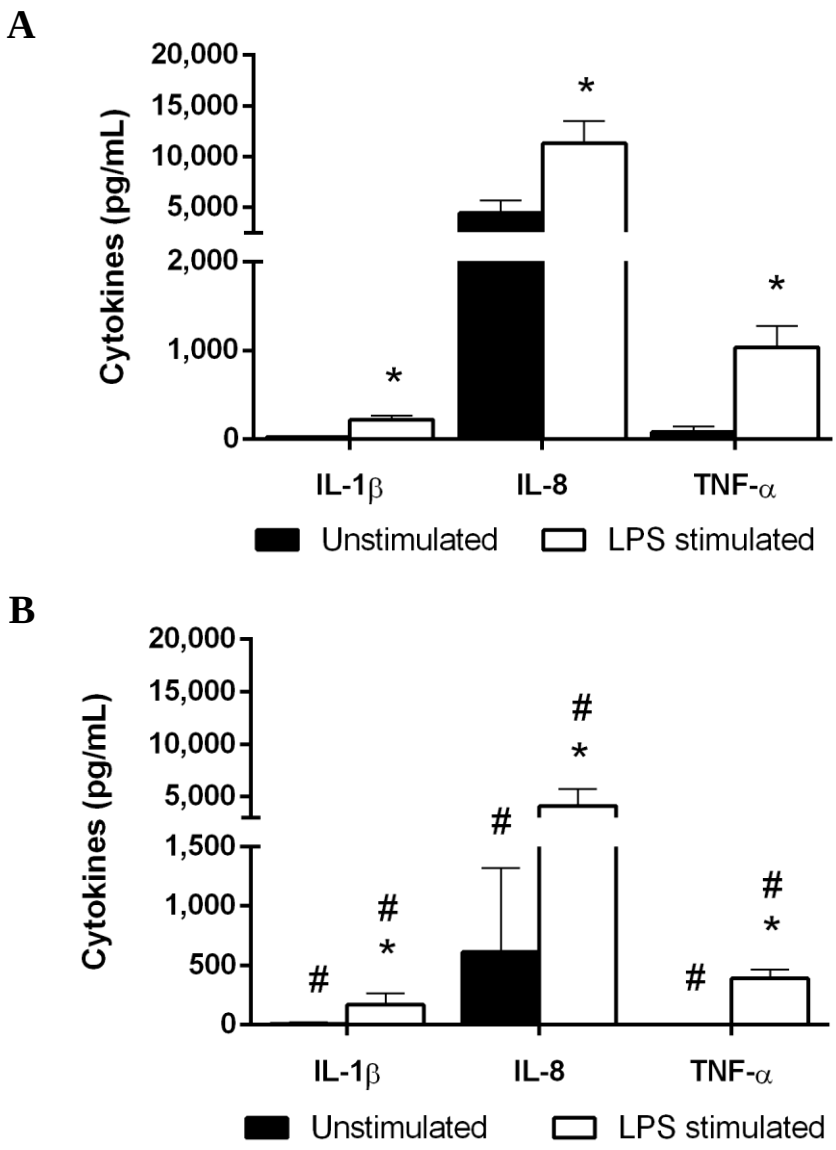

Figure 2.9 Cytokine release of unstimulated and 4h LPS (10 ng / mL) stimulated PMA-differentiated THP-1 cells

*(A) 48h PMA-differentiated THP-1 cells; B) 24h PMA-differentiated THP-1 cells (Average of N≥3 ± StDev; *p≤0.05 compared to cytokine release of unstimulated cells, $^{\#}$p≤0.05 cytokine release of 24h-differentiated compared to 48h-differentiated cells)*

The high background cytokine release of unstimulated THP-1 cells was problematic, since it might negatively affect the Caco-2 barrier integrity. Simplifying the differentiation protocol to a 24h PMA-treatment without subsequent resting (hereinafter '24h-differentiated') significantly decreased the release of IL-1β and IL-8 from unstimulated THP-1 cells by 85 (p=0.04) and 88 % (p≤0.001) to 8.7 and 615 pg / mL, respectively (Figure 2.9B, black bars). The release of TNF-α was completely inhibited. However, the shortened PMA treatment also affected the cells' cytokine response to stimulation with LPS. Significantly lower amounts of IL-8 and TNF-α were released

after 24h-differentiation (Figure 2.9B, white bars) compared to 48h-differentiated THP-1 cells (Figure 2.9A, white bars) (64 and 63 %, respectively). The LPS-induced release of IL-1β was unaffected by the differentiation protocol (Figure 2.9).

To account for the reduction in the cytokine response caused by the change in PMA-differentiation protocol the THP-1 cells were co-stimulated with LPS and IFN-γ (10 ng / mL each). The co-stimulation resulted in a significantly ($p \leq 0.001$) increased release of all three investigated cytokines compared to LPS-stimulation alone (IL-1β: +170 %, IL-8: +300 %, and TNF-α: +210 %) (Figure 2.10).

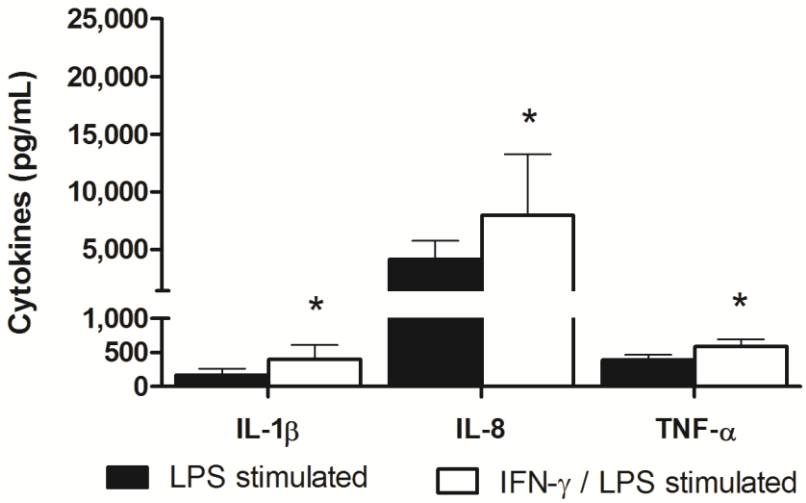

Figure 2.10 Release of IL-1β, IL-8, and TNF-α by 24h-differentiated THP-1 cells after 4h stimulation with 10 ng / mL LPS or 4h co-stimulation with IFN-γ and LPS (10 ng/mL each)

*(Average of N≥3 ± StDev; *p≤0.05 compared to the cytokine release of LPS stimulated cells)Development of a co-culture to mimic the healthy human intestine*

2.2.3.1 Formulation of criteria to be met by the stable co-culture

The first aim of the project was to establish a co-culture of Caco-2 and PMA-differentiated THP-1 cells to mimic the human intestine in homeostatic state (hereinafter 'stable co-culture'). To achieve a homeostatic co-culture it was of utmost importance that the cell lines do not negatively interfere with each other:

1) The co-culture must not activate the THP-1 cells (Moyes et al., 2010).

2) The presence of PMA-differentiated THP-1 cells must not affect the Caco-2 barrier integrity permanently, e.g. via a long-lasting weakening of the TJs, destruction of the cytoskeleton and / or cytotoxic effect (Satsu et al., 2006; Watanabe et al., 2004).

As seen in response to the stimulation with LPS, the activation of THP-1 cells can result in an increased release of pro-inflammatory cytokines, as well as ROS and RNS. Increased concentrations of these compounds can negatively affect the Caco-2 barrier integrity and cell viability (Watanabe et al., 2004; Susewind et al., 2016). Therefore, in the homeostatic 'stable' co-culture the concentrations of pro-inflammatory cytokines and RNS should not exceed the levels measured in unstimulated THP-1 monocultures.

Even if THP-1 cells are not activated in the co-culture, their baseline release of low concentrations of potentially stimulating compounds might affect the Caco-2 barrier negatively. Hence, the barrier integrity measured as TEER should not be significantly lower compared to the Caco-2 monoculture, nor should the apical LDH release, an indicator for necrotic cell death, be notably increased. From observations (data not shown) it was known that changes in the Caco-2 barrier environment can result in temporary TEER reduction. A medium change for instance can reduce the TEER by up to 10 % for several hours. Under normal conditions, these reductions do not represent impaired cellular health or barrier integrity and the TEER was re-established after a maximum of 24h. Presumably, the introduction of an additional cell type is a more serious change to the Caco-2 environment than the exchange of CCM. Therefore, a TEER reduction of ≤10 % in the stable co-culture compared to the Caco-2 monoculture was regarded as acceptable, if the barrier integrity was re-established to ≥95 % after 24h.

In summary, to realistically mimic the homeostatic human intestine the following criteria were developed for a stable co-culture of Caco-2 and THP-1 cells:

- The barrier's TEER decreases less than 10 % compared to the Caco-2 monoculture control over the first 24h of co-culture.
- The TEER is re-established to ≥95 % after 24h of co-culture.
- The concentrations of pro-inflammatory cytokines in the BL compartment do not significantly exceed the cytokine release of 24h-differentiated THP-1 monocultures (Figure 2.9B).
- The LDH release on the AP side is not significantly higher compared to the Caco-2 monoculture.

2.2.3.2 Barrier integrity of unstimulated Caco-2 / THP-1 co-cultures

For the development of the stable co-culture, the primary focus was on meeting the barrier integrity criteria. In a second step, the compliance with cytokine and LDH release was examined, which will be discussed in Chapter 3. A schematic overview of the cell culture and co-culture set-up is given in Figure 2.11.

Before the co-culture, THP-1 cells were 24h PMA-differentiated as described above (Section 2.1.2). The PMA-differentiated THP-1 cells were transferred from the flask to transwell-appropriate well plates at a density of $1.8x10^5$ cells / well. The cells were left undisturbed for 1.5h to re-attach on the plate. To initiate the co-culture, the $_D$Caco-2 cells grown on transwell filters were transferred to the well containing re-attached 24h-differentiated THP-1 cells without additional manipulation of either cell line (Figure 2.11B). To monitor the effect of the presence of THP-1 cells on the Caco-2 barrier the TEER was measured 4, 24, and 48h after the start of the co-culture. As presented in Figure 2.12, the TEER of Caco-2 barriers co-cultured with $1.8x10^5$ 24h-differentiated THP-1 cells (red graph) did not differ significantly from control barriers (blue graph) over a culture period of 48h.

The co-culture was also attempted with 48h-differentiated THP-1 cells (Figure 2.11A). These experiments aimed to confirm the inadequacy of the differentiation protocol for the establishment of a stable co-culture, thereby substantiating the decision for 24h PMA-differentiation of THP-1 cells. After 4h of co-culture, the TEER was equal to both the control and the co-culture with 24h-differentiated THP-1 cells. Subsequently,

the TEER decreased significantly ($p \leq 0.001$) to 80 and 86 % of the control after 24 and 48h, respectively (Figure 2.12).

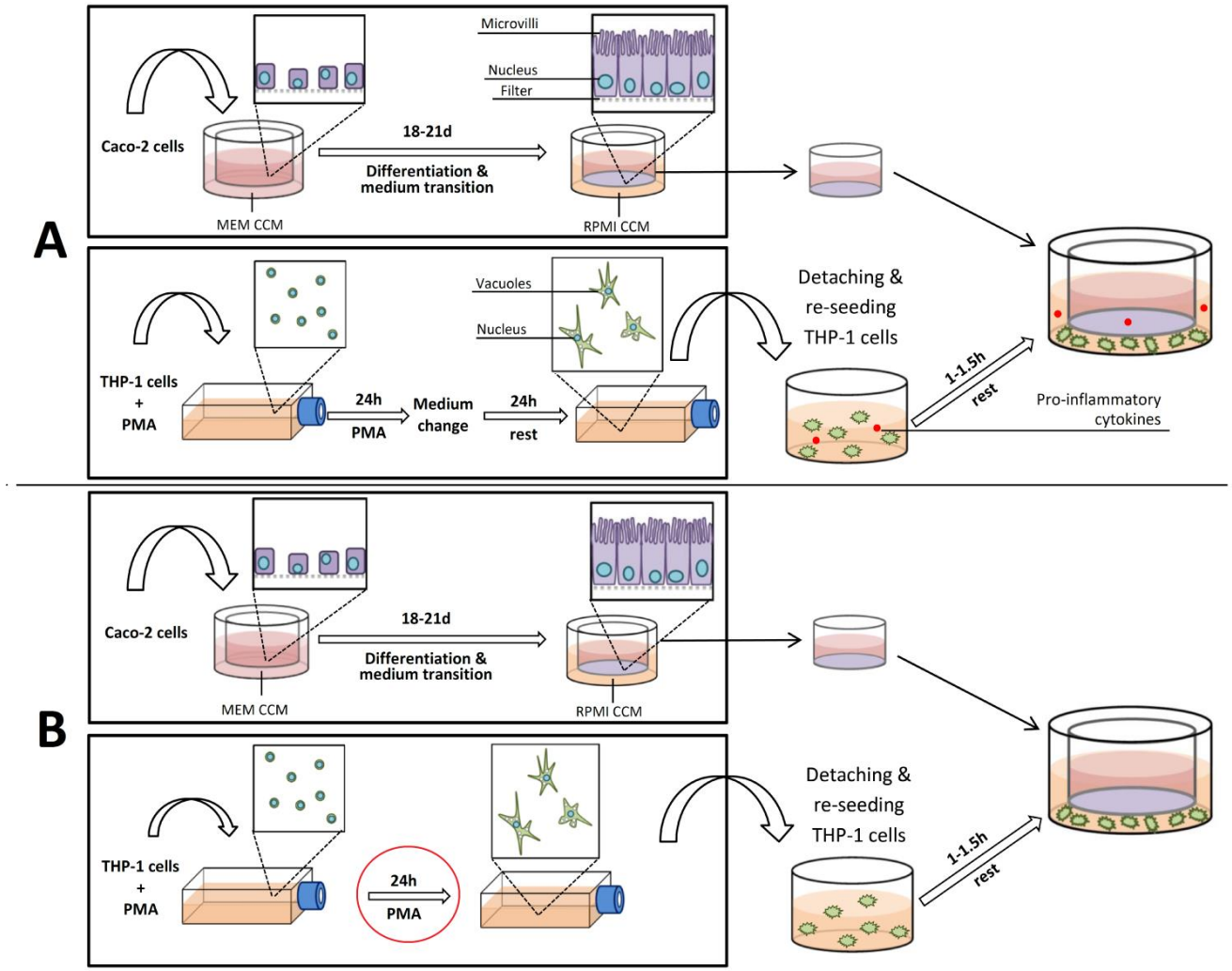

Figure 2.11 Schematic overview: stable co-culture set-up with (A) 48h-differentiated and (B) 24h-differentiated THP-1 cells

(changes to previous set-ups are marked by red circles)

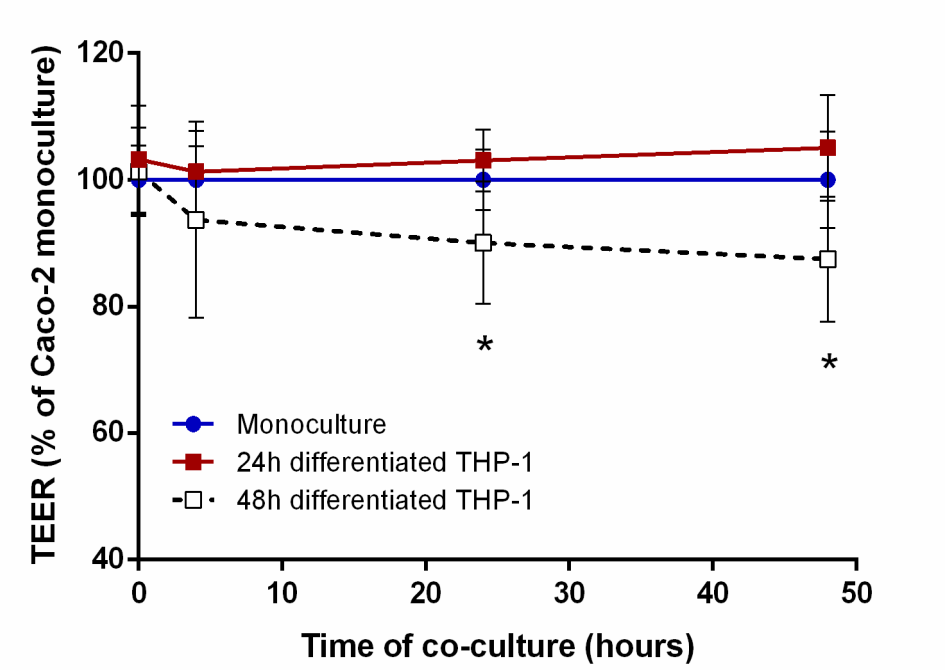

Figure 2.12 Barrier integrity measured as TEER over 48h Caco-2 monoculture (blue graph) or co-culture with 24h (red graph) or 48h (dotted black graph) PMA-differentiated THP-1 cells

*(Average of N=3 ± StDev; *p≤0.05 compared to Caco-2 monoculture)*

2.2.4 Development of a co-culture to mimic the inflamed human intestine

2.2.4.1 Formulation of criteria to be met by the inflamed co-culture

After establishing the conditions for the stable co-culture set-up, the second aim of the project was addressed: The disruption of the stable co-culture through the induction of an inflammation-like response in THP-1 cells (hereinafter 'inflamed'). To keep the two co-culture models as comparable as possible, the number of variables between them had to be pared down to the minimum. Preferably, no major changes should be made to the cell preparations and set-up of the stable co-culture.

Additionally, the *in vitro* inflammation should resemble a biological response as closely as possible. Hence, the following requirements were defined for the establishment of the inflamed model:

- The inflammatory response is induced through a physiologically relevant stressor.
- No substantial or permanent destruction of the Caco-2 barrier must occur.
- Ideally, the system recovers itself and resolves the inflammation-like process without additional manipulation, e.g. medium change.

A major characteristic of intestinal inflammation is the significant reduction in barrier integrity by up to 50 %, which is fully restored after remission (Zeissig et al., 2007). Published studies on monocultures (Van De Walle et al., 2010; Wang et al., 2005) and co-culture models (Susewind et al., 2016; Leonard et al., 2010) of the inflamed intestine achieved TEER reductions between 15-25 % using LPS, IL-1β or a combination of both. As shown by Susewind and colleagues (2016), a fully differentiated Caco-2 barrier is able to cope with moderated barrier disruptions induced by physiologically relevant stressors and can fully re-establish its integrity. Some groups reported TEER reductions of greater than 50 % in disrupted Caco-2 / THP-1 co-cultures (Detzel et al., 2015; Satsu et al., 2006; Moyes et al., 2010). Detzel and colleagues disrupted the barrier substantially using a non-physiological stressor (dimethyl palmitoyl ammonio propanesulfonate (PPS)) to enhance TJ permeability (Detzel et al., 2015). Furthermore, neither Satsu et al. nor Moyes and colleagues intentionally activated the co-culture with a stressor but merely observed the adverse effect of high baseline cytokine release on the Caco-2 cell layer. Altogether, a TEER reduction equal to or greater than 50 % of the monoculture control would be desirable but probably not feasible under the defined requirements. As the LY permeability assay showed the Caco-2 barrier is still leaky 6 days post-seeding with nearly 7 % dye translocation and a TEER of ~300 Ω·cm². At the start of the co-culture at day 21 the TEER is on average 391 ± 59 Ω·cm². Hence, a TEER reduction of 15 % is likely not sufficient as it would only decrease barrier integrity to ~330 Ω·cm², higher than TEER at day 6. Therefore, a minimum TEER reduction of 20-25 % of the Caco-2 monoculture control was aimed for to potentially achieve an increased permeability without permanently disrupting the barrier.

As the model is intended to be used to study the barrier crossing of NMs in healthy and diseased tissue the barrier disruption had to be substantial, and persist for a pro-longed period of time. Other than soluble chemicals, most particles remain in a more or less stable suspension. The stability of this suspension, the disintegration, aggregation, agglomeration, and / or sedimentation of particles depends on the dispersant and particle characteristics, e.g. media viscosity, presence of proteins and ions, particle density and particle size (Teeguarden et al., 2007). Using radio-labelled gold (Au)NPs (Section 6.3.3), we found that particles with an original diameter of 30 nm required at least 6-24h to pass through a cell-free transwell filter in detectable numbers. The density of Au (19.32 g / cm^3) is relatively high compared to other materials, e.g. Ag (10.49 g / cm^3) or SiO_2 (2.65 g / cm^3). Even though the sedimentation is influenced by more parameters than the particle density, it is reasonable to assume that NMs with a lower density than

Au require more time to sediment. Hence, to be able to study the effect of an impaired Caco-2 barrier on the translocation of NMs the TEER reduction should prevail for at least 24h to allow for meaningful barrier crossing studies.

Apart from the reduced barrier integrity, the presence of excess amounts of pro-inflammatory cytokines is a pivotal sign of active inflammatory processes. Depending on the cause and stage of the inflammation both intestinal epithelial cells and various cells of the innate immune system can be the source of the cytokine production (Strober and Fuss, 2011; Blumberg, 2009; Li et al., 1998). Here, LPS will be used as physiologically relevant stressor to activate the PMA-differentiated THP-1 cells. To prove a successful stimulation of an inflammation-like response in the system the concentration of the routinely monitored pro-inflammatory cytokines – IL-1β, IL-8, and TNF-α – should be significantly increased compared to the stable co-culture (Park et al., 2007; Szczepanik et al., 2001).

Altogether, the following criteria were defined to classify a co-culture as 'inflamed':

- The TEER is reduced ≥20-25 % compared to the Caco-2 monoculture control.
- A TEER reduction of minimally 20 % persists for at least 24h.
- The concentrations of the pro-inflammatory cytokines IL-1β, IL-8, and TNF-α significantly exceed the amounts recovered in the stable co-culture after 4h of co-culture.
- Ideally, the TEER is re-established to >90 % of the Caco-2 monoculture control after 48h of co-culture.

2.2.4.2 Results of the individual adjustment steps and additions to the stable co-culture protocol

To not alter the stable co-culture set-up unnecessarily, the adjustments were introduced in individual steps, which will be presented in more detail hereinafter. The co-culture was monitored by measuring the barrier resistance as TEER before the start (T_0), as well as after 4, 24, and 48h of co-culture (T_4-T_{48}). In later stages of the development (Step 2-4), an additional TEER measurement time point after 18h was introduced. The TEER results of all four steps are summarised in Figure 2.13. A schematic description of the cell treatment and co-culture set-up in each step is given in Figure 2.15 and Figure 2.18.

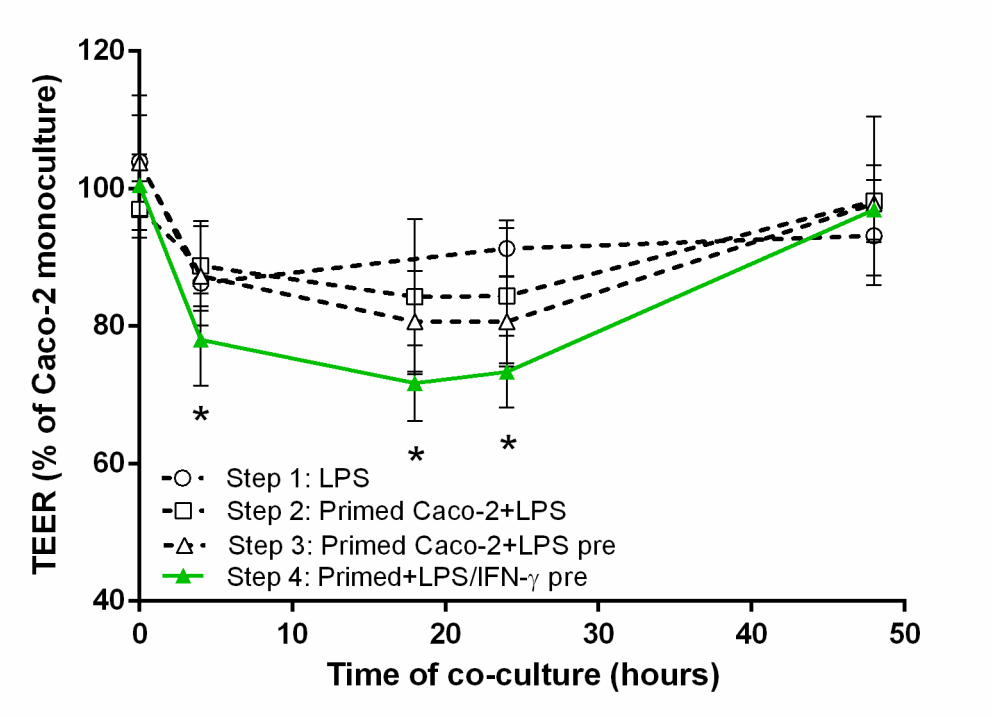

Figure 2.13 Caco-2 barrier integrity measured as TEER over 48h co-culture with differently stimulated 24h-differentiated THP-1 cells

*Step1: LPS (10 ng / mL) addition to the BL compartment at T_0; Step 2: co-culture of IFN-γ-primed Caco-2 barriers and THP-1 cells stimulated with LPS (10 ng / mL) at T_0; Step 3: co-culture of IFN-γ-primed Caco-2 barriers and THP-1 cells pre-stimulated with LPS (10 ng / mL) 4h in advance; Step 4: co-culture of IFN-γ-primed Caco-2 barriers and THP-1 cells pre-stimulated with LPS and IFN-γ (10 ng / mL each) (Average of N≥3 ± StDev; *p≤0.05 compared to Caco-2 monoculture)*

Step 1: LPS-stimulation of THP-1 cells in the BL compartment

At first, 10 ng / mL LPS were added to the BL compartment at the start of the co-culture (T_0) to activate the 24h-differentiated THP-1 cells without altering the stable co-culture set-up (Figure 2.15A). Four hours after initiation of the co-culture, the TEER decreased significantly to ~85 % of the monoculture control (Figure 2.13, white circles). However, the barrier integrity quickly re-established to >90 % after 24h and, hence, did not fulfil the defined requirements.

Step 2: IFN-γ priming of Caco-2 cells and LPS stimulation of THP-1 cells

Since the mere addition of LPS in Step 1 was not sufficient to meet the above defined requirements, IFN-y-priming of Caco-2 cells was introduced as an additional change. As shown in Figure 2.14, the priming with IFN-γ did not induce a reduction in barrier integrity in the Caco-2 monoculture and the unstimulated stable co-culture.

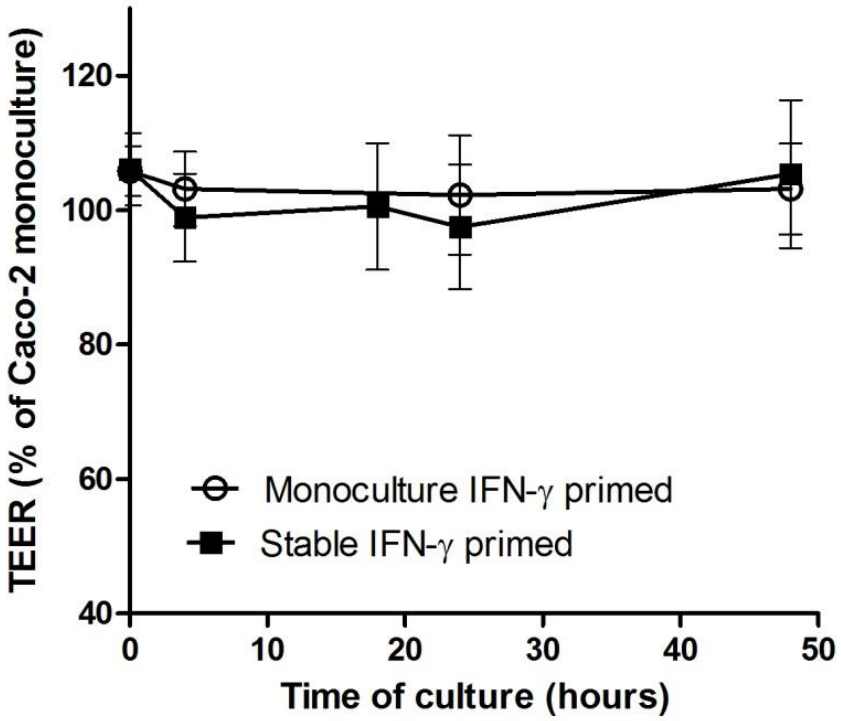

Figure 2.14 Caco-2 barrier integrity measured as TEER after IFN-γ-priming

Caco-2 barriers were primed with 10 ng / mL IFN-γ for 24h and cultured alone or co-cultured with unstimulated 24h-differentiated THP-1 cells for 48h (Average of N=2 ± StDev)

To induce an inflammation-like response, the THP-1 cells were challenged basolaterally with 10 ng / mL LPS. As shown in Figure 2.13 (white squares), the IFN-γ-priming increased the vulnerability of the Caco-2 barrier to the presence of LPS-activated THP-1 cells, which is reflected in the extended duration of the barrier disruption. With a maximum TEER reduction of 15.8 and 15.6 % after 18 and 24h, respectively, the effect was less pronounced than expected and not sufficient to meet the defined requirements.

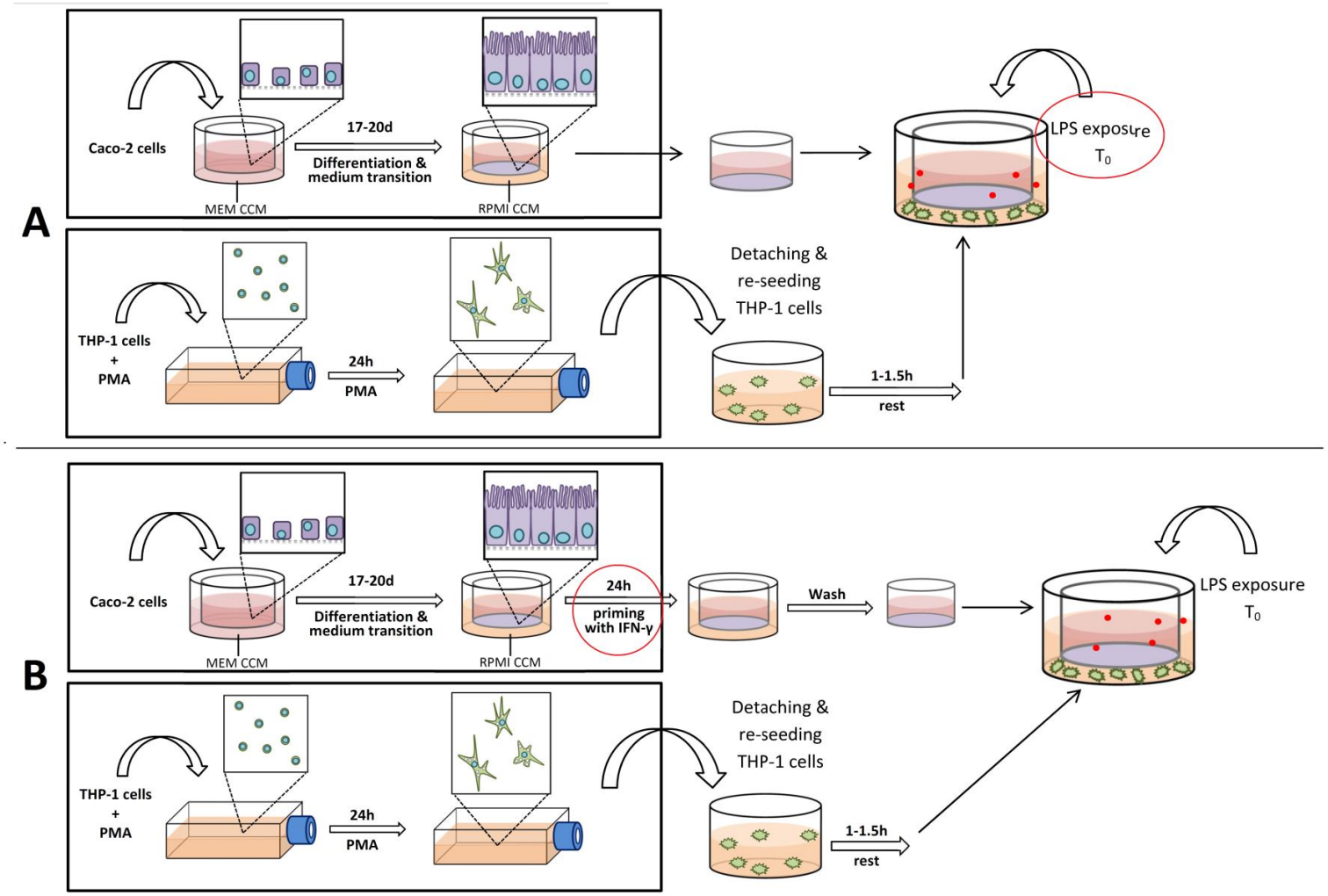

Figure 2.15 Schematic overview: Inflamed co-culture set-ups (A) Step 1 and (B) Step 2

(changes to previous set-ups are marked by red circles)

Based on the LPS-exposure experiments performed in THP-1 monocultures, the release of pro-inflammatory cytokines should be high enough to induce a clear and prolonged barrier disruption, especially in IFN-γ-primed Caco-2 cells (Wang et al., 2005). To investigate why this was not achieved, the BL cytokine contents of LPS-stimulated co-cultures were analysed and compared to cytokine concentrations recovered from stimulated THP-1 monocultures. Interestingly, the release of IL-1β and TNF-α was significantly reduced ($p \leq 0.002$) by around 90 % in LPS-stimulated co-cultures compared to THP-1 monocultures (Figure 2.16). With 23 % reduction compared to LPS-exposed THP-1 monocultures the release of IL-8 was less affected.

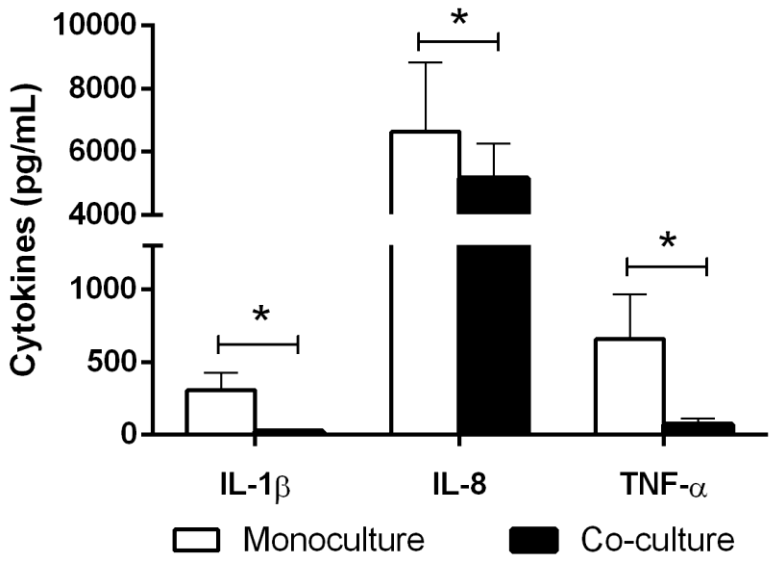

Figure 2.16 Release of IL-1β, IL-8, and TNF-α by LPS-stimulated (10 ng / mL) 24h-differentiated THP-1 cells in monoculture (white bars) or co-culture with Caco-2 cells (black bars)

*(Monoculture: Average of N=4; Co-culture: Average of N=2 ± StDev; *p≤0.05 compared to monoculture)*

A separate experiment was conducted to study the impact of Caco-2 cells on the cytokine response of LPS-stimulated THP-1 cells. For this, THP-1 cells were pre-stimulated with LPS 4h in advance of the co-culture (Figure 2.17A) or as before at the start of the co-culture (Figure 2.17B). Supernatant samples of both conditions were taken at the start of the co-culture (T_0), as well as after 4h of co-culture (T_4).

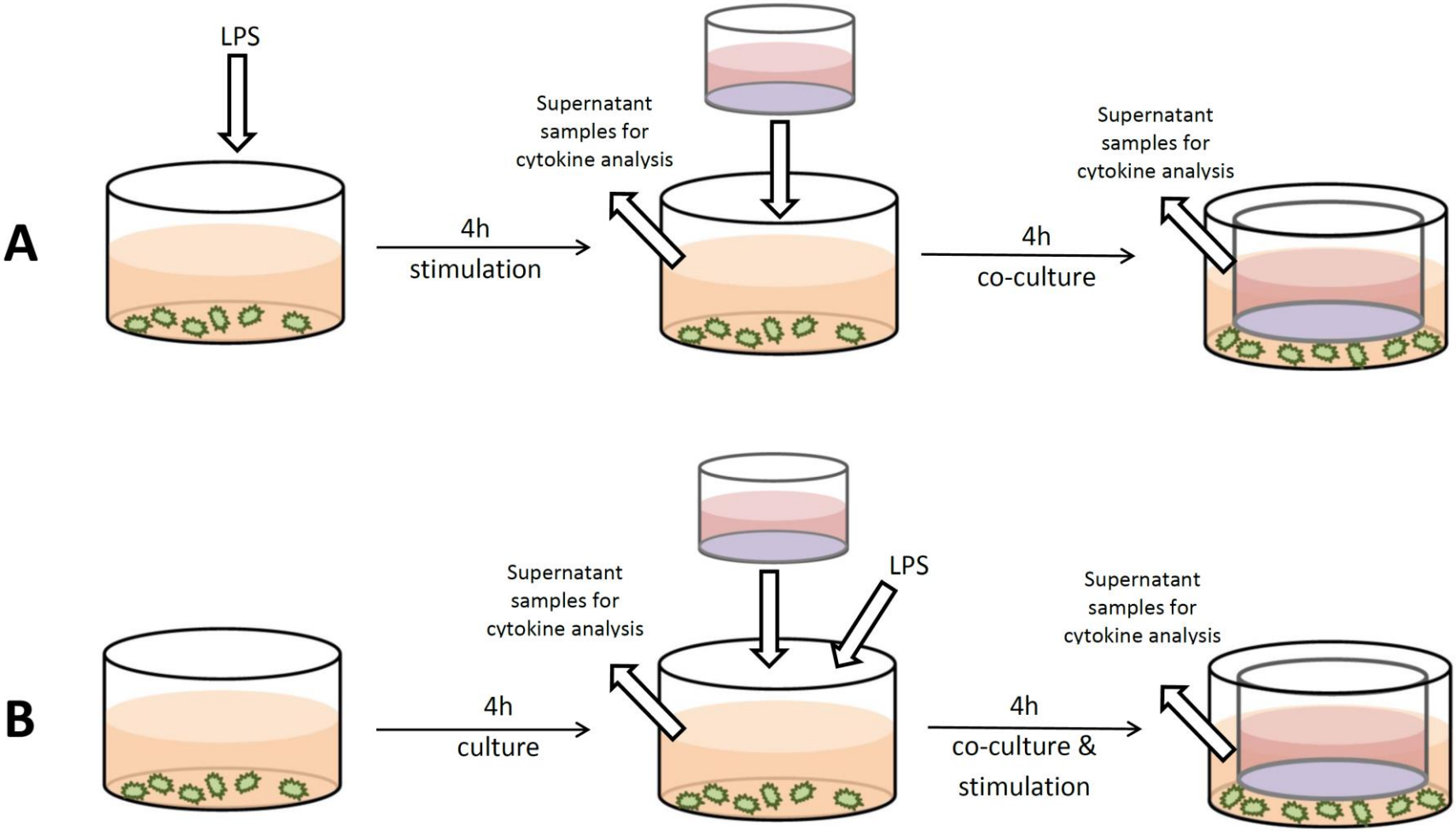

Figure 2.17 Schematic overview: co-culture preparation and LPS exposure to study the down-regulating effect of Caco-2 cell

The following results were obtained: When THP-1 monocultures were stimulated with LPS in advance of the co-culture, high concentrations of pro-inflammatory cytokines were released (Figure S1A). After 4h co-culture with Caco-2 cells the cytokine concentrations were reduced, but still exceeded the release in the unexposed co-culture control (Figure S1B). When exposing the THP-1 cells to LPS at the start of the co-culture, the cytokine release was significantly reduced (Figure S1B). The PMA-differentiation protocol influenced the amount but not the general trend of cytokine release (Figure S2).

Step 3: IFN-γ priming of Caco-2 cells and LPS pre-stimulation of THP-1 cells

To overcome the above described down-regulation of the cytokine response, the THP-1 cells were pre-exposed to LPS for 4h before the start of the co-culture to allow for a period of unrestricted response to the stressor (Figure 2.18A). The increased generation of pro-inflammatory cytokines was expected to overwhelm the IECs at the start of the co-culture so that less or no downregulation of the THP-1 cytokine response could be imposed. As shown in Figure 2.13 (white triangles), the pre-exposure induced a more pronounced and extended reduction in TEER compared to the previous Steps 1 and 2. Subsequent to a moderate decrease by 12.7 % after 4h of co-culture, the TEER reduced further to 80.7 % of the control after 18 and 24h. At 48h of co-culture, the barrier integrity was fully re-established to 97.8 ± 5.5 % of the control.

Altogether, this set-up fulfilled the minimum requirements defined before, but the results were close to lower limit of the criteria. Whereas the barrier integrity decreased on average by 20 %, several individual cultures within one experiment failed to show adequate barrier disruption. Furthermore, the reproducibility of the results heavily dependent on the response of THP-1 cells to the PMA-differentiation. For unknown reasons, the pre-exposure to LPS alone was in several cases not sufficient to disrupt the co-culture.

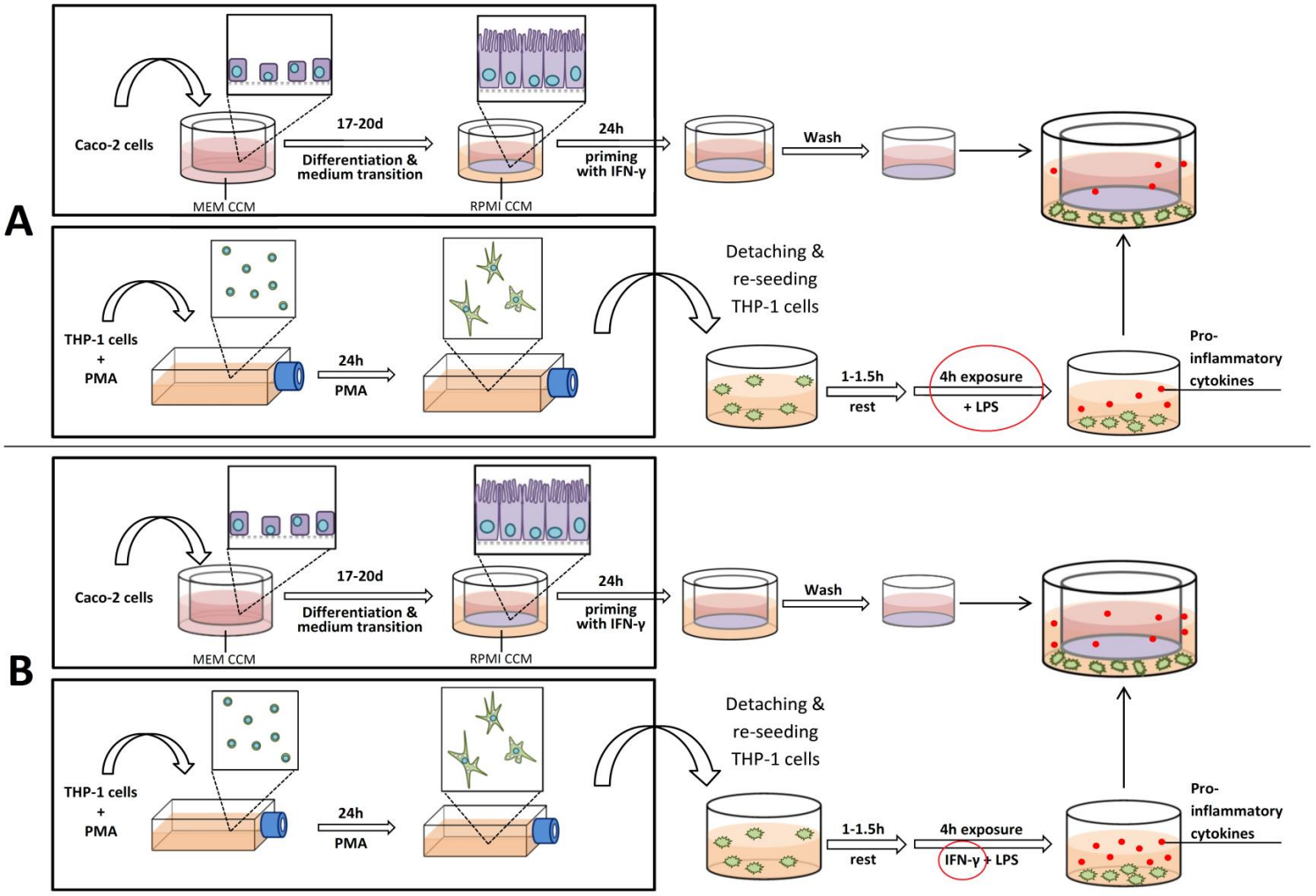

Figure 2.18 Schematic overview: inflamed co-culture set-ups (A) Step 3 and (B) Step 4

(changes to previous set-ups are marked by red circles)

Step 4: IFN-γ priming of Caco-2 cells and pre-stimulation of THP-1 cells LPS & IFN-γ before the co-culture

With regard to the previously observed differences between exposure to LPS alone and combined exposure to LPS and IFN-γ on the THP-1 cytokine response it was decided to introduce IFN-γ as last additional change to the co-culture set-up (Figure 2.18B). To compensate for the diminished impact of LPS alone, 24h-differentiated THP-1 cells were pre-exposed to LPS and IFN-γ (10 ng / mL each) simultaneously in advance of the co-culture. After 4h of pre-exposure, the co-culture was initiated as before.

As presented in Figure 2.13 (green line), the co-stimulation with LPS and IFN-γ had a significant effect on both the magnitude and duration of the induced TEER reduction. Within the first 4h of co-culture (i.e. 8h of LPS + IFN-γ exposure), the TEER decreased significantly ($p \leq 0.001$) to 78 ± 6.7 % of the unexposed Caco-2 monoculture control and further to 71 ±5.5 % and 73 ± 5.2 % after 18 and 24h of co-culture, respectively. After 48h, the TEER had re-established to ~97 % ± 4.3 % of the control without additional manipulation of the system. Altogether, all barrier integrity-related requirements for the inflamed co-culture were met.

2.3 Discussion

The main outcomes of this chapter can be summarised in the following points:

- The differentiation status of the THP-1 cells and the differentiation protocol greatly impact the cytokine response of the cells to stressors like LPS. The cytokine release was significantly reduced after 24h compared to 48h PMA-differentiation, but could be enhanced by co-stimulating the cells with LPS and IFN-γ.
- A stable co-culture can be established with 24h but not 48h PMA-differentiated THP-1 cells.
- The stable co-culture could not simply be turned into an inflamed model by addition of LPS to the BL compartment. To induce an adequate barrier disruption according to the specified criteria the Caco-2 barrier had to be primed with IFN-γ and the THP-1 cells pre-stimulated with both LPS and IFN-γ 4h prior to the co-culture.

2.3.1 Caco-2 and THP-1 monocultures

2.3.1.1 Caco-2 cells

The barrier development of Caco-2 cells comprises two key aspects:

1) The formation of a confluent cell layer containing intact AJs and TJs.
2) The differentiation of Caco-2 cells from a colonic to a small intestinal-like phenotype.

Since the differentiation of Caco-2 cells and expression of differentiation markers has been studied abundantly, we limited our efforts to three easy-to-monitor endpoints: The barrier integrity was measured by TEER and LY passage, the formation of the TJ network with ZO-1, and the indirect estimation of the development of microvillous structures with the detection and quantification of villin.

When monitoring the formation of a cell barrier, the increase in TEER indicates the increasing restriction of the paracellular transport of ions by TJ (Anderson and Van Itallie, 2009). The obtained TEER results were well above the often mentioned minimum barrier integrity of ~150-250 Ω•cm² (Narai et al., 1997; Foraker et al., 2003). Compared to other studies on Caco-2 cells the measured TEER ranks in the middle of reported maximum values, which range between 180 to above 1000 Ω•cm² (Hashimoto and Shimizu, 1993; Ranaldi et al., 2002). Regarding the human intestinal tract, the electrical resistance of the Caco-2 cells is more comparable to the barrier integrity of the colon (300-400 Ω•cm²) than the small intestine (50-100 Ω•cm²) (Fleischer 1999). The maximum TEER at 12 to 15 days post-seeding is in line with the findings of others working with the Caco-2 strain distributed by the German Collection of Microorganisms and Cell Culture (DSMZ) (Steffansen, 2013). For Caco-2 strains obtained from other distributors and some Caco-2 clones, different growth behaviours were described. In those studies the TEER either continued to increase even after 21 days of culture, or a plateau was reached without subsequent reduction in TEER (Ranaldi et al., 2003).

The formation of the TJ network and the, thereby, caused restriction of paracellular passage was additionally monitored with the quantification of LY translocation. The results showed that after 12 days of culture virtually no translocation of LY occurred over 4h of incubation. This confirmed the formation of a continuous functional barrier, which significantly restricted the diffusion of compounds from the AP to BL side. The

P_{app} and the relative barrier crossing of LY at day 21 are in line with the results reported by others (Sandri et al., 2007; Nollevaux et al., 2006).

Both the increase in ZO-1 protein expression and TEER are related to the proliferation of the cells until a dense, continuous cell layer is formed. Upon reaching confluence, cell proliferation reduces and the cells spontaneously start to differentiate from colonic to small intestinal-like cells (Pinto et al., 1983). This differentiation is reflected in the development of a microvillous apical membrane, indicating structural polarisation of the differentiated Caco-2 barrier, and the increase in brush border-associated hydrolases (Chantret et al., 1988; Hilgers et al., 1990). In the GI-tract, villin expression marks the functional border between the gastric and the intestinal parts of the GI-tract (Braunstein et al., 2002). Almost exclusively expressed in the intestinal epithelium, villin is the major actin-associated protein of the intestinal microvilli (Bretscher and Weber, 1979). Hence, the co-localisation of the villin-associated fluorescence signal with F-actin was not the result of unspecific binding but can be explained with the strong co-localisation of the two proteins. It has, however, been shown that many human colon carcinoma cell lines express villin independently of enterocytic differentiation or the formation of a brush border (Chantret et al., 1988). Even though the development of a brush border has been confirmed by Transmission Electron Microscopy (TEM) imaging numerous times before (Kitchens et al., 2007; Giannasca et al., 1996) we can only speculate that the increase in villin-associated FI indicates the development of a microvillous brush border. To support this assumption the development of microvilli on Caco-2 cells should be analysed at different culture time points using TEM.

2.3.1.2 THP-1 cells

THP-1 cells are described as monoblastic cells, which depend on an external stimulus to induce the differentiation to a more mature macrophage-like phenotype (Tsuchiya et al., 1982). The most commonly used differentiation stimuli are 1,25-dihydroxyvitamin D3 (VD_3) and phorbol esters like PMA (Daigneault et al., 2010). In contrast to PMA, the VD_3-mediated differentiation enhances macrophage-associated features, e.g. cell adherence and the release of large cytokine quantities upon stimulation, to a lesser extend (Daigneault et al., 2010). Additionally, PMA is more cost-effective and easier to handle than VD_3. Therefore, PMA was chosen as differentiation stimulus within this project.

The maturation of the THP-1 cells could easily be followed by monitoring the change in adherence and morphology, which are both characteristic for phorbol ester-induced maturation (Tsuchiya et al., 1982). The quantification of the cell surface receptors CD14 and CD68 resulted in ambiguous outcomes. Generally, CD14 was expected to be nearly absent before the PMA-differentiation, since undifferentiated THP-1 cells hardly responded to the exposure to LPS. Hence, the PMA-differentiation was assumed to induce a clear upregulation of CD14, as the cytokine response to LPS was unmistakeably enhanced. It was therefore, surprising to find a clear presence of CD14 on undifferentiated THP-1 cells and a reduction in CD14 expression after PMA-differentiation.

Both receptors are associated with monocytes and macrophages, but are not exclusively expressed by them (Funda et al., 2001; Kunz-Schughart et al., 2003). The presence of the LPS-receptor CD14 is crucial for this project, as it largely determines cellular responsiveness to LPS (Wright et al., 1990). It is involved in the recognition of pathogens and activation of the innate immune system by binding LPS, a PAMP found on the membrane of Gram-negative bacteria, and subsequent activation of immune cells (Komai-Koma et al., 2009). The binding of LPS to CD14 initiates the release of pro-inflammatory cytokines *in vitro*, e.g. TNF-α, IL-1β, and IL-8 (Meng and Lowell, 1997; van der Bruggen et al., 1999; Ngkelo et al., 2012). Whereas CD14 is not essential to induce TNF-α in response to high concentrations of LPS (i.e. >100 ng / mL) it was found to be indispensable for the cytokine's generation after exposure to lower concentrations of LPS (Borzecka et al., 2013). The CD68 receptor was investigated as a potential marker to distinguish THP-1 and Caco-2 cells in the co-culture.

A literature research revealed that reports on the expression and regulation of CD14 in THP-1 cells differ greatly between laboratories (Table 2.3). Whereas some groups observed low to undetectable levels of the receptor in undifferentiated THP-1 cells (Martin et al., 1994; Schwende, 1996; Schilling et al., 2003) others found significant expression on 50 to 90% of control cells (Martin et al., 1994; Ciabattini et al., 2006). Furthermore, many groups saw a strong CD14-upregulating effect of PMA (Zhang et al., 2014; Takashiba et al., 1999). Others noted weak or no impact (Schwende, 1996; Schilling et al., 2003). A hypothesis that these differences might be related to the differing STR profiles of the cells could not be confirmed (Ciabattini et al., 2006; Schilling et al., 2003). Many factors have already been shown to affect the expression and regulation of CD14 in THP-1 cells including the differentiation stimulus, its

concentration, as well as the exposure time (Schwende, 1996; Daigneault et al., 2010; Park et al., 2007). But also less obvious aspects, e.g. cell culture density and resting times, were shown to exert influence (Daigneault et al., 2010; Aldo et al., 2013).

Whereas numerous studies were found describing a PMA-induced increase in CD14 expression, reports on reducing CD14 levels in response to PMA mostly involved peripheral blood monocytes (PMBCs) (Nomura et al., 2001; Kremlev and Phelps, 1997). When exposed to PMA, PBMCs shed the membrane-bound receptor, which was reflected in a parallel increase in soluble $_{(S)}$CD14 (Nomura et al., 2001). A similar observation was made for another human monocytic cell line – Mono Mac (MM)6 (Zarember and Godowski, 2002). Here, exposure to 12-*O*-Tetradecanoylphorbol-13-acetate (TPA) induced a two-fold reduction in membrane $_{(m)}$CD14, but no increase in $_{s}$CD14. Instead of shedding the receptor, the reduction in MM6 cells was related to a downregulation of $_{m}$CD14 mRNA. Only one account could be found describing a reduction of $_{m}$CD14 in THP-1 cells claimed to be caused PMA-induced cleavage of the receptor (Puig-Kroger et al., 2004). Taking into consideration that this report is part of an unpublished under-graduate research project the reliability of this source remains unclear.

Altogether, it is possible that the exposure of THP-1 cells to PMA induced a shedding of $_{m}$CD14. Without additional analyses, however, this hypothesis cannot be verified. For further investigation, the supernatant could be collected after treatment with PMA and analysed by ELISA. Even if this explained the reduction in CD14 it would not elucidate the generally observed differences in CD14 expression on THP-1 cells reported between laboratories (Table 2.3). Since the project essentially depends on the THP-1 responsiveness to LPS these variations might greatly influence the model's establishment and reproducibility in other laboratories.

The high background cytokine levels of unstimulated 48h-differentiated THP-1 cells, which were also observed by other groups, were of more concern. The THP-1 differentiation protocols varied between the common stimuli PMA and VD_3 (Watanabe et al., 2004; Schwende, 1996), or combinations of both with additional stressors like LPS (Xia et al., 2013; Taylor et al., 2014). In the latter cases, the increase in cytokine release is not surprising, since a strongly stimulating compound is used during the differentiation.

Table 2.3 Literature examples for CD14 expression in THP-1 cells with and without exposure to PMA

Source	Distributor	CD14 expression		PMA effect
		Differentiated	PMA-differentiated	
(Fleit and Kobasiuk, 1991)	N/A	-	+	No effect
(Martin, 1994)	ATCC	+	+	No effect
(Schwende, 1996)	DSMZ	-	+	Slight upregulation
(Takashiba et al., 1999)	ATCC	+	N/A	Upregulation
(Nomura et al., 2001)	N/A	+++	N/A	N/A
(Zarember and Godowski, 2002)	ATCC	N/A	+++	Upregulation
(Schilling et al., 2003)	ATCC (TIB202)	+	N/A	Upregulation
(Puig-Kroger et al., 2004)	ATCC	+	+++	Upregulation
(Kohro et al., 2004)	ATCC	N/A	N/A	Upregulation
(Zhou et al., 2005)	ATCC	+	+++	Upregulation (24h exposure needed)
(Ciabattini et al., 2006)	ATCC (TIB202)	+++	N/A	N/A
(Park et al., 2007)	N/A	N/A	N/A	Upregulation (48h exposure needed)
(Chen et al., 2012)	N/A	+/-	++	Upregulation
(Aldo et al., 2013)	N/A	Low cell density: + High cell density: ++	Low: + High: ++	Low: no effect High: upregulation
(Zhang et al., 2014)	ATCC	+	+++	Upregulation

Whereas the PMA-differentiation of THP-1 cells was, undoubtedly, necessary, the increased cytokine release associated with it could negatively affect Caco-2 cell barrier integrity. As Watanabe et al. (2004) observed, the uncontrolled release of high concentrations of cytokines, in that case TNF-α, lead to a severe and permanent disruption of the Caco-2 cell layer. Therefore, a reduction in cytokine release of unstimulated PMA-treated THP-1 cells without having to refrain from differentiating the cells was aimed for. The most obvious approach was to adapt the PMA-differentiation protocol, which is known to have a tremendous impact on the characteristics of THP-1 cells (Daigneault et al., 2010; Aldo et al., 2013; Schwende, 1996). The mere reduction in differentiation time was sufficient to inhibit the synthesis of the most potent inflammation-mediating cytokines (IL-1β and TNF-α) by unstimulated THP-1 cells. The levels of IL-8 strongly reduced, but remained significantly higher compared to untreated THP-1 cells. Since Smythies et al. (2005) observed a similar background level of IL-8 released by iMΦ we did not aim to further reduce the concentrations.

The long term goal of establishing an inflamed co-culture strongly depended on the cells' ability to produce large quantities of pro-inflammatory cytokines. Therefore, the reduced response to LPS after 24h differentiation was critical and had to be compensated. As others reported before, exposing THP-1 cells to LPS and IFN-γ simultaneously could greatly enhance the cells' cytokine response (Tamai et al., 2003).

2.3.2 Stable co-culture set-up

The TEER results showed that Caco-2 cells and 24h-differentiated THP-1 cells could cohabit over a period of 48h without significant effects on the Caco-2 barrier integrity. The results obtained from co-cultures with 48h-differentiated THP-1 cells confirmed that THP-1 cells differentiated according to the initial protocol were not suitable for the establishment of a stable co-culture that fulfils the earlier defined criteria.

For the development of the stable co-culture the increased release of pro-inflammatory cytokines was worrying, as it most likely would have been detrimental to the Cao-2 barrier integrity. Co-cultures of Caco-2 and PMA-differentiated THP-1 cells have already been attempted by other groups with mixed success. In several cases, the co-culture resulted in an uncontrolled cross talk between the cell lines, which ultimately caused severe and permanent barrier disruption in the IEC barrier (Moyes et al., 2010;

Satsu et al., 2006). Studies reporting a reduction in Caco-2 barrier integrity demonstrated the presence of significant concentrations of pro-inflammatory cytokines (Moyes et al., 2010; Satsu et al., 2006 Watanabe et al., 2004). Also in this study the release of cytokines, especially IL-8, has been identified as a potential problem in 48h-differentiated THP-1 cells, which was confirmed in co-culture experiments. With an overall TEER reduction of 15-20 % in these experiments, however, the barrier disruption was rather moderate. In other studies, the TEER was reduced by 70-80 % of the control after 24-48h (Satsu et al., 2006; Moyes et al., 2010).

Interestingly, the PMA-differentiation protocol differed between groups observing a barrier disruption. Whereas both Watanabe et al. (2004) and Satsu et al. (2006) differentiated THP-1 cells with higher PMA concentrations (200 nM) and for a longer period of time (4 days), Moyes and colleagues (2010) applied the very same differentiation protocol as used here. Even more so, the cell strain and source used by Moyes et al. is the same as used in here. Hence, the results might confirm the already discussed heterogeneity of the cell line. It suggests that the variability of the results does not only depend on the source of the cells and the differentiation protocol, but also the handling of the cells within a laboratory. An interlaboratory study using THP-1 cells published by Xia et al (2013) supports this hypothesis. The study outcomes showed a considerable heterogeneity between the participating laboratories, even though the same protocols and materials were applied in all laboratories.

In contrast to this project, Moyes et al. used a slightly higher THP-1 cell density of $1.05x10^5$ cells / cm^2 (vs. $7.8x10^4$ cells / cm^2 well surface). This could indicate that, apart from the heterogeneity of the cell line, the ratio between the cell types of the co-culture is crucial. The importance of the cell type ratio on the behaviour and responses of a system has already been demonstrated in other non-intestinal co-culture set-ups (Bodet et al., 2005; Burguera et al., 2010). It is possible, that an unbalanced ratio of macrophages to IECs induced a disruption in the system. In favour of this explanation are two studies working with similar intestinal co-culture models that did not observe a reduction in barrier integrity. Both Leonard et al. (2010) and Susewind et al. (2016) combined Caco-2 cells with macrophages and DCs, either differentiated from PBMCs or cell lines. Both, however, used significantly lower seeding densities of roughly $9x10^3$ cells / cm^2 of each leukocyte cell type.

Alternatively, the use of undifferentiated THP-1 cells might have been possible, but without prior differentiation the cells hardly responded to stimulation with LPS even though different groups reported otherwise (Detzel et al., 2015; Araujo et al., 2004). Since the ability to stimulate the cells with pathophysiological stresses and the release of pro-inflammatory cytokines was of utmost importance for the development of the inflamed co-culture the use of undifferentiated cells was discarded.

In summary, co-cultures of Caco-2 and 48h-differentiated THP-1 cells failed to meet the defined criteria and could, therefore, not be rated as 'stable'. Based on the barrier integrity results, 24h-differentiated THP-1 cells were found to be suitable for the establishment of a stable co-culture. The term 'stable co-culture', henceforth, refers to a co-culture of 24h-differentiated THP-1 cells with $_{D}$Caco-2 cells.

2.3.3 Development of the inflamed co-culture

To make the stable and inflamed co-culture as comparable as possible, the number and severity of adjustments to the stable co-culture set-up was kept to the necessary minimum. Therefore, a very minor change was introduced first with the mere addition of LPS to the BL compartment (Step 1). Studies have shown that LPS can affect the barrier integrity and lead to significant barrier disruption in Caco-2 cells (Van De Walle et al., 2010; Wells et al., 1993). However, in order to disrupt barrier integrity high concentrations of 10 to 50 µg / mL had to be used (Van De Walle et al., 2010; Yu et al., 2005). In this project, the aim was to induce the barrier disruption through the induction of an inflammation-like response in the THP-1 cells instead of imposing unrealistically high stresses on the IECs. Hence, a low concentration of 10 ng / mL LPS was used, which was not expected to cause any negative effects on the Caco-2 barrier. This assumption was confirmed in a set of control experiments on Caco-2 monocultures presented and discussed in Chapter 3 (Sections 3.3.2 & 3.4.2).

More importantly, such low concentrations of LPS were shown to be sufficient to stimulate macrophages to release high concentrations of pro-inflammatory cytokines (Meng and Lowell, 1997). In experiments on THP-1 monocultures, significant concentrations of IL-1β, IL-8, and TNF-α were detected, which confirmed the stimulation induced by 10 ng / mL LPS. Both IL-1β and TNF-α are known to be able to disrupt intestinal barrier integrity (Van De Walle et al., 2010; Shen, 2012). The concentration of IL-1β released by LPS-stimulated 24h-differentiated THP-1 cells is far

below the amount reported (>10 ng / mL IL-1β) to induce the desired TEER reduction of 20-25 % (Al-Sadi and Ma, 2007).

Therefore, the focus was laid on TNF-α. The cytokine can affect the barrier permeability of Caco-2 cells by itself but only at high concentrations of at least 10 ng / mL (Shen, 2012; Cui et al., 2010). When THP-1 cells were stimulated with LPS at the start of the co-culture, only very low concentrations of TNF-α (~100 pg / mL) were released. This could explain why exposure to LPS alone did not result in a prolonged barrier disruption. The effective dose of TNF-α can be lowered significantly with the addition of IFN-γ (Chen et al., 2012; Wang et al., 2005). As described by Wang and colleagues, the Caco-2 barrier integrity was reduced in case both cytokines are simultaneously present in the BL compartment or the Caco-2 cells were first exposed to IFN-γ and subsequently in contact with TNF-α (Wang et al., 2005). This latter 'priming' effect of IFN-γ induces an up-regulation of TNF-α receptor (TNFR) 1 and 2 in Caco-2 cells, which are located at the BL cell membrane (Wang et al., 2006). Binding of TNF-α to TNFR2 but not TNFR1 leads to an increased expression of MLCK (Blumberg, 2009), which in turn results in amplified phosphorylation of MLC (Zhou et al., 2005). Phosphorylation of MLC, leading to contraction of the actomyosin ring, has been demonstrated to regulate intestinal epithelial permeability by re-organisation of TJ proteins. This re-organisation of TJ protein causes an increased paracellular permeability of the barrier and a strong reduction in TEER (Turner et al., 1997; Wang et al., 2005; Zhou et al., 2005).

In the presence of IFN-γ, the TNF-α concentration necessary to cause a barrier disruption has been shown to be between 1-2.5 ng / mL (Wang et al., 2005). These concentrations can be achieved with stimulated THP-1 cells, as other groups (Park et al., 2007; Szczepanik et al., 2001) and earlier discussed experiments on THP-1 monocultures confirmed. However, the co-culture probably lacked the ability to produce sufficient levels of IFN-γ. Whereas no information could be found for Caco-2 cells, the IFN-γ release of THP-1 cells has been reported to be drastically reduced after PMA-differentiation (Satsu et al., 2006). Also Moyes et al. did not detect any release of IFN-γ in Caco-2 / THP-1 co-cultures (Moyes et al., 2010). Since none of the main sources of IFN-γ, i.e. neutrophils, T-cells and natural killer cells (Lin and Young, 2013) were planned to be introduced in the co-culture the cytokine had to be substituted, which was partially achieved through the IFN-γ-priming of Caco-2 cells (Step 2).

In contrast to the expectations, the priming of Caco-2 cells and LPS-stimulation in the BL compartment did not induce the desired barrier disruption of 20-25 % over 24h. The quantification of cytokine release in BL supernatants revealed a significantly reduced release of all three investigated cytokines compared to LPS-stimulated THP-1 monocultures. These results might reflect a downregulation of the macrophage-driven stress response in presence of Caco-2 cells. IECs are well-known to play an active role in the regulation of homeostasis in healthy intestinal tissue. IECs discriminate between commensal "self" and harmful "non-self" antigens present in the intestinal lumen (Rakoff-Nahoum et al., 2004) and control the responsiveness of immune cells in the lamina propria (Rimoldi, 2005; Parlesak et al., 2004). Without the IEC-mediated downregulation of the immune system the intestine would likely be subject to constant inflammation caused by non-harmful antigens. Whereas the adjustment of macrophage number and PMA-differentiation was crucial to establish the stable co-culture, it greatly complicated the induction of a pro-inflammatory response. On one side, it allows Caco-2 cells to exert control over the immune cells, as shown by the significant downregulation of the THP-1 response to LPS. On the other side, it reduces the LPS-stimulated cytokine release of THP-1 cells, thereby suppressing the evolvement of a pro-inflammatory process. A similar immuno-modulating effect of IEC cell lines had already been reported in combination with primary murine or human mononuclear cells (Parlesak et al., 2004; Nathens et al., 1995), but not for co-cultures of Caco-2 and THP-1 cells.

Why the Caco-2 cells inhibit the THP-1 driven pro-inflammatory response cannot be answered with certainty. A possible explanation might be related to the stress applied to stimulate the cells – LPS. Under certain circumstances, IECs can be activated to initiate an immune response themselves, for instance when binding of a PAMP to Toll-like Receptors (TLR) or nucleotide binding oligomerisation domains (NODs) (Cario and Podolsky, 2000) occurs. Once the cells are activated they respond with the release of pro-inflammatory cytokines and chemokines (Haller, 2000). One of the most studied PAMPs is *E. coli*-derived LPS, which was used in this study. Its ubiquitous presence in the intestinal lumen and known involvement in intestinal inflammation (Guo et al., 2013) made it the most meaningful choice of stimulus to induce an inflammation-like reaction. However, the necessary cell surface receptors for LPS recognition are insufficiently expressed by primary enterocytes (Cario and Podolsky, 2000) and Caco-2 cells (Abreu et al., 2001; Melmed et al., 2003). Hence, whereas LPS readily binds to THP-1 cells it cannot bind and, therefore, should not activate IECs at the low

concentrations used here. This is the reason why the co-cultures were exposed to LPS from the BL instead of the AP side. The lack of LPS recognition by Caco-2 cells might also explain the strict downregulation of the THP-1 stress response: In homeostatic gut tissue, immune cells are closely regulated and do not respond to the encounter of non-harmful antigens. IECs are suspected to be at least partially involved in imposing and maintaining this systemic tolerance (Peterson and Artis, 2014).

Another possible explanation relates to the general de-sensitisation of monocytes in the proximity of the intestinal barrier as described by Smythies et al. (2005). The group observed a TGF-β-mediated downregulation of cytokine release in PBMCs, but only after incubation with stromal cell-conditioned and not epithelial cell-conditioned medium. Since incubating THP-1 cells with Caco-2 cell conditioned medium (cCCM) did not have a noticeable effect on the LPS-stimulated cytokine release (Figure S3) the downregulation is likely not induced by a continuously produced factor. Instead, the Caco-2 cells might actively respond to the presence of THP-1 cells in the co-culture. It remains unclear, whether the downregulation results from the mere presence of the macrophage-like cells or is triggered by an event related to the LPS-stimulation of THP-1 cells.

To induce a barrier disruption through the activation of THP-1 cells, the observed downregulation by Caco-2 cells had to be overcome. The most obvious solution was to pre-expose the THP-1 cells before the co-culture. The hypothesis was that the exposure to LPS prior to the co-culture will allow for an unrestricted response and cytokine synthesis similar to LPS-exposed THP-1 monocultures can be achieved. Furthermore, it was assumed that the increased cytokine concentrations will overwhelm the Caco-2 cells at the start of the co-culture so that no downregulation can be imposed.

As the results of Step 3 showed, the pre-exposure to LPS alone increased the barrier disruption further, but could not always achieve the minimum requirements of the defined criteria. Presumably, exposure to LPS as single stimulant could not induce the release of sufficiently high concentrations of cytokines, as was observed in the THP-1 monoculture experiments. From these monoculture experiments it was known that the co-stimulation of 24h-differentiated THP-1 cells with LPS and IFN-γ significantly increases the release of pro-inflammatory cytokines. This synergistic effect of LPS and IFN-γ is linked to the up-regulation of proteins of the LPS receptor complex and has been demonstrated to influence the release of IL-8 by THP-1 cells (Tamai et al., 2003). After pre-exposing the THP-1 cells to LPS and IFN-γ (Step 4) before the co-culture the

downregulation by Caco-2 cells could eventually be overcome. As will be discussed in Chapter 3, the release of IL-8, IL-1β, and TNF-α was significantly increased after co-stimulation compared to LPS-stimulation alone.

Since all defined criteria were fulfilled and could be reproduced reliably the term 'inflamed co-culture' hereinafter refers to a co-culture according to Step 4: 24h-differentiated THP-1 cells, 4h pre-exposed to LPS and IFN-γ before being brought in co-culture with 24h IFN-γ-primed $_{D}$Caco-2 cells.

2.4 Conclusions

The characterisation of the cell lines in monoculture showed how critical the (PMA)-differentiation protocol and the type of stimuli are for the subsequent cytokine response by THP-1 cells. Without additional stimulation, Caco-2 and THP-1 cells can cohabit in a co-culture model without negatively affecting the Caco-2 barrier integrity confirming the chapter's first hypothesis. Against the second hypothesis, it was not possible to disrupt the barrier integrity of the stable co-culture simply by stimulating the THP-1 cells with a physiologically relevant stressor. Several alterations, e.g. IFN-γ-priming of Caco-2 cells and pre-stimulation prior to the co-culture, had to be introduced to the stable co-culture set-up to induce an inflammation-like response. To achieve the hypothesised barrier disruption the Caco-2-mediated downregulation of the THP-1 pro-inflammatory response to LPS had to be overcome. For this the introduction of IFN-γ as one of the key mediators of inflammation was essential.

3 Characterisation of the stable and inflamed co-culture

3.1 Aims and hypotheses

Throughout the protocol development, the characterisation of the stable and the inflamed co-cultures was limited to the measurement of barrier integrity by means of TEER. Apart from affecting the barrier integrity the induction of an inflammation-like response is expected to result in other significant differences between the co-culture conditions. Therefore, the co-culture models were further investigated regarding the cell viability, the presence of cytokines, and nitrite (NO_2^-), as well as the intactness and integrity of the Caco-2 barrier.

Since the stable co-culture was supposed to be used to study the inflammatory potential of NMs a control was included to investigate whether an inflammation-like response can be induced.

Additional hypotheses regarding the further characterisation of the two co-culture models were:

- The investigated endpoints, i.e. pro-inflammatory cytokine release, LDH levels, and NO_2^- generation, will be similar between the stable co-culture and the Caco-2 monoculture control.
- A pro-inflammatory reaction, marked by the presence of pro-inflammatory cytokines, can be induced in the stable co-culture.
- The outcomes obtained from the inflamed co-culture will be significantly different from the Caco-2 monoculture and the stable co-culture.
- The release of pro-inflammatory cytokines, LDH levels, and NO_2^- generation will be significantly increased in response to LPS / IFN-γ in the inflamed co-culture compared to the Caco-2 monoculture and the stable co-culture.
- The paracellular permeability to LY will be increased in the inflamed co-culture compared to the Caco-2 monoculture and the stable co-culture.

3.2 Materials and Methods

3.2.1 Chemicals

Lithium lactate (L2250), Iodonitrotetrazolium chloride (INT) (I-8377), Phenazine Methosulfate (PMS) (P-9625), β-Nicotinamide Adenine Dinucleotide sodium salt (NAD) (N-0632), Tris-base (T4661), Tris-HCl (T3253), sulfanilamide (SA) (S9251), N-(1-Naphthyl)-ethylenodiamine (NEDA) (222488), and sodium nitrite ($NaNO_2$) (237213) were purchased from Sigma.

3.2.2 Quantification of cytokines using ELISA

The release of IL-1β, IL-8, TNF-α, and in specific cases TGF-1β (R&D, DY240) was quantified in supernatants taken from the BL compartment after 4, 24, and 48h of co-culture. TGF-1β was additionally quantified in AP supernatants. The analysis was performed as described earlier (Section 2.1.8).

3.2.3 Lactate dehydrogenase (LDH) Assay

The LDH assay was used to study the necrotic cell death in Caco-2 monocultures and the co-culture models. To measure the LDH activity, 50 µL of 200 mM TRIS (10.6 mg Tris-base and 22.2 mg Tris-HCl in 1 L H_2O), 50 µL of 50 mM lithium lactate, and 50 µL mix of INT, PMS, and NAD were added to a 96-well plate at concentrations of 1.32 mg / mL, 0.36 mg / mL and 3.44 mg / mL, respectively. To each prepared well, a sample of cell-free supernatant (50 µL) was transferred and incubated for 5 minutes at RT. The optical density was measured spectrophotometrically at 490 nm. A background control in complete CCM was subtracted from the results to account for the absorbance of phenol red and potential LDH activity of FBS. Cells exposed to 0.1 % Triton-X100 for 24h served as positive control.

3.2.4 Detection of NO_2^- with the Griess reaction

The Griess reaction was used to indirectly assess the formation of the radical nitric oxide (NO) through the quantification of its stable metabolite NO_2^-. For the NO_2^- quantification, supernatant samples were taken after 48h of Caco-2 monoculture, stable,

or inflamed co-culture. To each sample (100 µL), SA (stock: 1 mM in MilliQ H_2O), H_3PO_4 (stock: 1.8 M), and NEDA (stock: 1 mM in 95 % EtOH) were added to a final concentration of 100 µM, 170 mM, and 100 µM, respectively. The final volume of each sample was 130 µL. Each step was separated by 30 min incubation time at RT. The background and dye absorbance were measured spectrophotometrically at 548 nm. A calibration curve was prepared in CCM using $NaNO_2$) (0-50 µM) dissolved in H_2O.

3.2.5 Barrier permeability assay and P_{app} calculation

To assess the permeability of Caco-2 cell layers the flux of LY from the AP to the BL compartment was measured in all three culture models. Two different approaches were tested:

1) The culture models were set-up and maintained for 24h to allow their complete establishment. Subsequently, the supernatant was removed and the assay performed as described before (Section 2.1.4). AP and BL supernatants were taken after 0, 2 and 4h.
2) LY was dissolved in MEM-based CCM (5 mg / mL) and added to the AP compartment at the start of the co-culture. The co-culture conditions were maintained for 48h. From both sides, 100 µL samples were taken immediately after addition of LY and after 4 and 18h of incubation / co-culture.

The sample volumes were not replenished in the AP and BL compartments. The measurement of FI and calculation of the P_{app} were performed as described in Section 2.1.5.

3.2.6 Activation of the stable co-culture

To investigate whether the stable co-culture is detect a pro-inflammatory potential of test materials the stable co-culture was exposed to 2.5 mM EDTA on AP and BL side and LPS. LPS was added to the AP compartment at the same mass concentration as used in the pre-exposure of the inflamed co-culture (i.e. 15 ng / well = 30 ng / mL in the AP compartment). The culture was analysed for cytokine release in BL supernatants after 4, 24, and 48h exposure.

3.3 Results

3.3.1 Stable vs. inflamed co-culture

3.3.1.1 TEER

The TEER values of the stable and inflamed co-cultures over a period of 48h are summarised again in Figure 3.1 to underline the differences in barrier integrity between both conditions. The graph combines results already shown and discussed in Sections 2.2.3.2 & 2.2.4.2.

Just 4h after the initiation of the co-culture, the TEER of the inflamed condition (Figure 3.1, green line) was significantly reduced to 78 ± 6.7 % compared to the monoculture (blue line) and stable co-culture (red line). The barrier integrity reduced further to 71 ± 5.4 % after 18h of co-culture. Over the following 6h, the TEER began to increase slightly to 73 ± 5.2 % but remained significantly below the monoculture and stable co-culture. After 48h, the TEER was fully re-established to 96 ± 4.3 % of the monoculture.

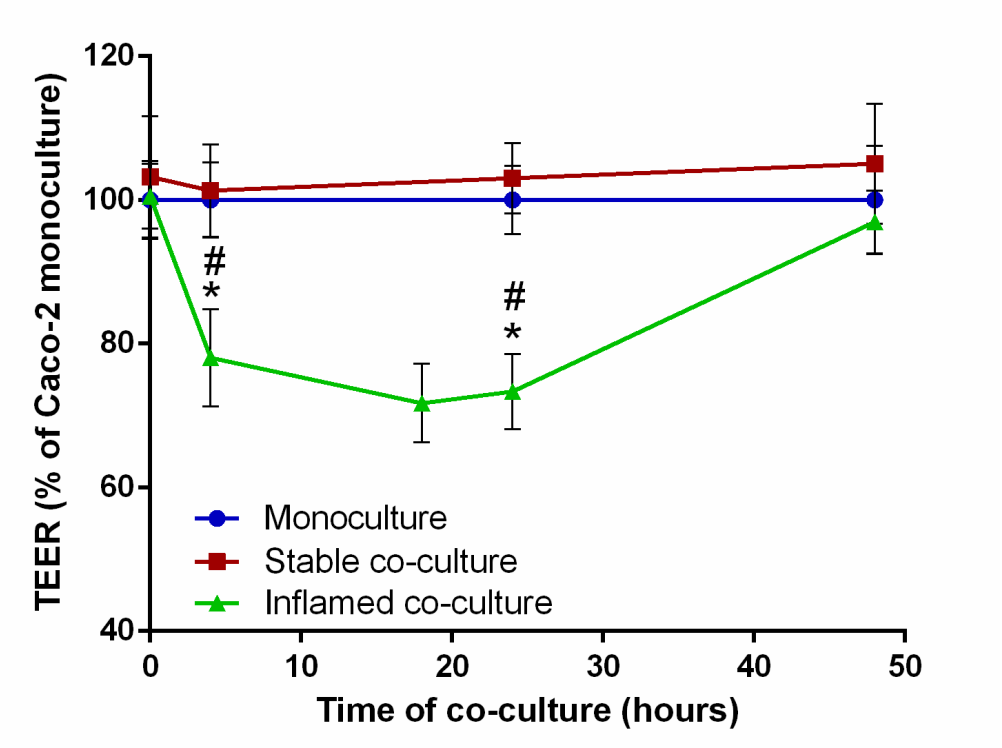

Figure 3.1 Comparison of the barrier integrity measured as TEER over 48h Caco-2 monoculture (blue), stable (red), and inflamed co-culture (green)

*N.B.: the figure was combined from above discussed data presented in Figure 2.12 and 2.13 (Average of N≥3 ± StDev, *p≤0.05 compared to Caco-2 monoculture, #p≤0.05 compared to stable co-culture)*

3.3.1.2 Cytokine release

To study the cytokine release in the three culture models supernatant samples were collected after 4h of culture from the AP (TGF-β1) and BL (IL-1β., IL-8, TNF-α, and TGF-β1) compartment. The results for IL-1β, IL-8, and TNF-α of Caco-2 monocultures, stable, and inflamed co-cultures are summarised in Figure 3.2. TGF-β1 was only expressed at very low concentrations (<10 pg / mL; data not shown) and no differences in expression were observed between the culture models.

In Caco-2 monocultures (Figure 3.2, white bars), IL-8 and TNF-α were expressed at very low concentrations (61 ± 64 and 6.76 ± 18 pg / mL, respectively), whereas IL-1β was below the detection limit (Table 2.2). In the stable co-culture set-up (striped bars), IL-1β was slightly increased to 18 ± 19 pg / mL, but TNF-α remained low to absent with 3.2 ± 7.4 pg / mL. A clear release of ~1,000 pg / mL IL-8 was detected after 4h of stable co-culture. The release of cytokines in the stable co-culture was not significantly higher compared to the THP-1 monoculture (p=0.193, 0.074, and 0.197 for IL-1β, IL-8, and TNF-α, respectively).

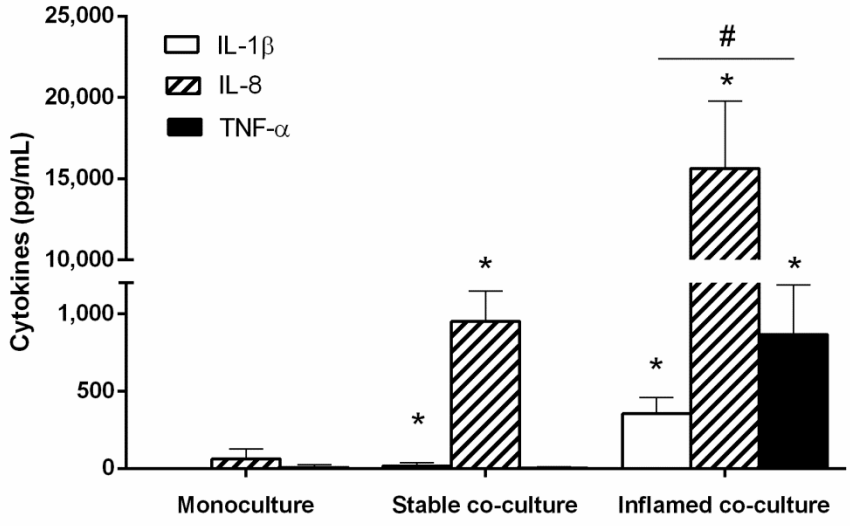

Figure 3.2 Quantification of IL-1β, IL-8 and TNF-a after 4h Caco-2 monoculture, stable, and inflamed co-cultures

*(Average of N≥3 ± StDev; *p≤0.05 compared to the corresponding cytokine release in Caco-2 monoculture, #p≤0.05 compared to the corresponding cytokine release in stable co-culture)*

Compared to the Caco-2 monoculture and stable co-culture, an unambiguous induction of IL-1β, IL-8, and TNF-α was detected in the inflamed condition. Whereas both IL-1β

and TNF-α were nearly absent in the other conditions, strongly increased concentrations of roughly 350 and 860 pg / mL, respectively, were recovered in BL supernatants of the inflamed model. Most striking was the release of IL-8, which increased to >15,000 pg / mL after 4h of co-culture (i.e. 8h of stimulation with LPS and IFN-γ). For IL-8 and TNF-α, the release was significantly higher ($p=0.004$ and $p=0.034$, respectively) compared to LPS/IFN-γ-stimulated THP-1 monocultures.

3.3.1.3 LDH release

The measurement of LDH release was included to assess the occurrence of necrotic cell death in response to the presence of THP-1 cells in the stable co-culture, as well as the impact of THP-1 activation in the inflamed model. The supernatant samples were taken from the AP and BL compartments after 48h of mono- or co-culture.

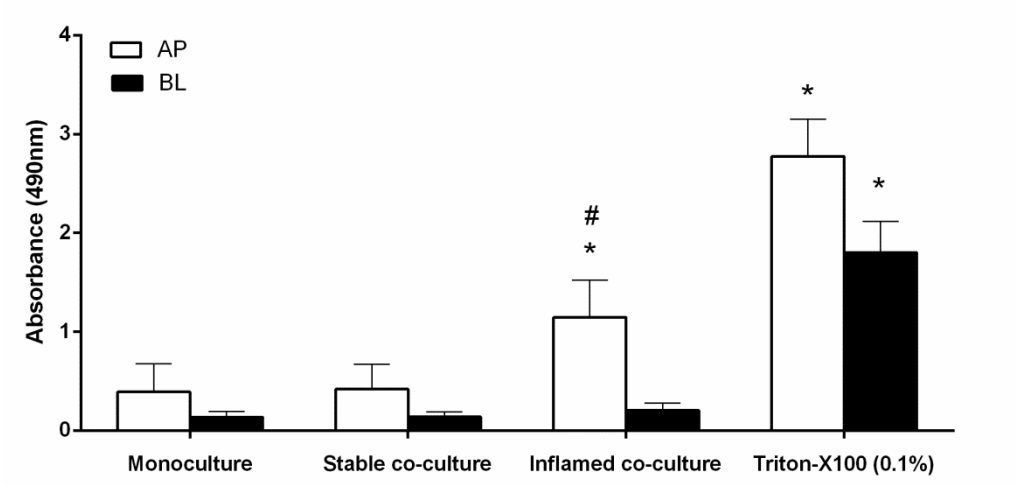

Figure 3.3 LDH release after 48h Caco-2 monoculture, stable, and inflamed co-culture

*Triton-X100 at a concentration of 0.1 % was used as positive control representing 100 % cell lysis (Average of N≥4 ± StDev; *p≤0.05 compared to Caco-2 monoculture; #p≤0.05 compared to stable co-culture)*

The LDH release quantified in Caco-2 monoculture served as baseline. Very low enzymatic activity was detected in both AP and BL compartment of the monoculture (Figure 3.3). No significant increase in LDH was detected in either compartment of the stable co-culture compared to the monoculture. In contrast to the stable co-culture, the analysis of the inflamed co-culture supernatants showed a significant increase ($p\leq0.001$)

in LDH release in the AP compartment (260 % of the control) and a moderate, non-significant increase in the BL compartment (150 % of the control).

3.3.1.4 Quantification of NO_2^-

As summarized in Figure 3.4, the background levels of NO_2^- in Caco-2 monocultures are very low to undetectable. For the correct interpretation of the data it should be mentioned that the reliable detection limit of the Griess reaction is around 3 µM of NO_2^- (Malinski et al., 1996). Hence, results below 3 µM can be regarded as negligible. After 48h of stable co-culture, no change in NO_2^- was detected. In the supernatants of inflamed co-cultures, a significant increase to ~6 µM NO_2^- was quantified in both AP and BL compartment (Figure 3.4).

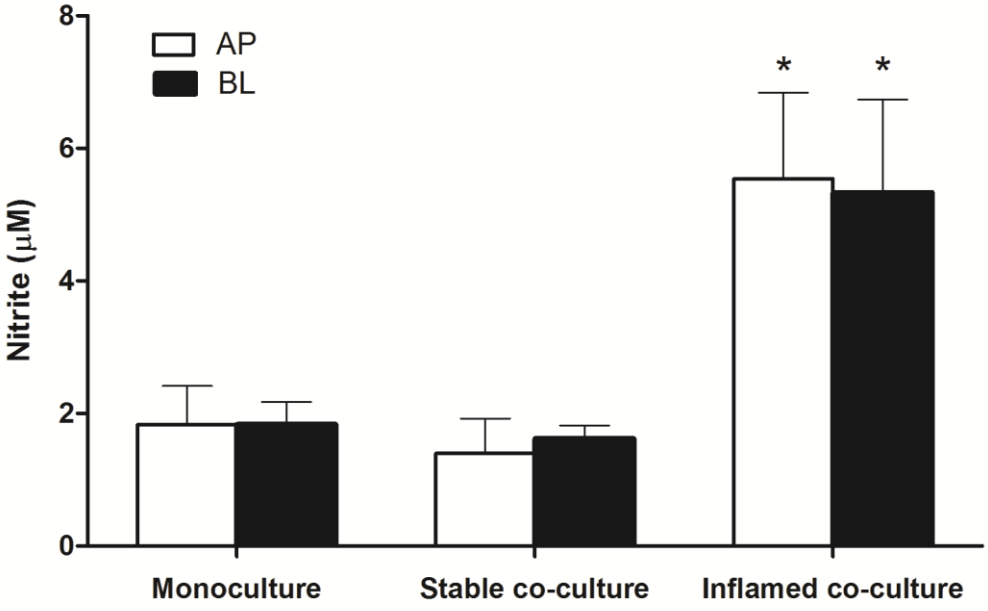

Figure 3.4 Quantification of NO_2^- in AP and BL supernatants after 48h Caco-2 monoculture, stable, and inflamed co-cultures

*(Average of N=3 ± StDev; *p≤0.05 compared to Caco-2 monoculture control)*

3.3.1.5 Integrity of the cytoskeleton and the TJ network

To further investigate barrier integrity in presence of non-stimulated and stimulated THP-1 cells the Caco-2 barrier was microscopically analysed for its cytoskeletal structure and the TJ network. The filters of all three culture models were fixed after 48h and stained for nucleic acid (blue), F-actin (green) and ZO-1 (red) (Figure 3.5).

The Caco-2 monoculture (Figure 3.5A) served as control compared to the Caco-2 barriers after 48h of stable (Figure 3.5B) and inflamed (Figure 3.5C) co-culture. After 23 days of culture, the Caco-2 monoculture formed a dense cell layer occupying the entire growth area of the filter. The layer was heterogeneously organised, with regional multilayers and scattered dome formation. Due to this growth behaviour of Caco-2 cells a quantitative analysis of FI based on the cell number was not possible. Visually, no variation between the stable co-culture barrier (Figure 3.5B) and the monoculture was noted. In the inflamed co-culture barrier (Figure 3.5C), no gaps were observed but the TJ network and cytoskeleton seemed irregular and less organised compared to the monoculture. Furthermore, an occurrence of nuclear fragmentation was observed (red arrows) and the nuclear surface appeared increased compared to the monoculture and stable co-culture (Figure 3.5C).

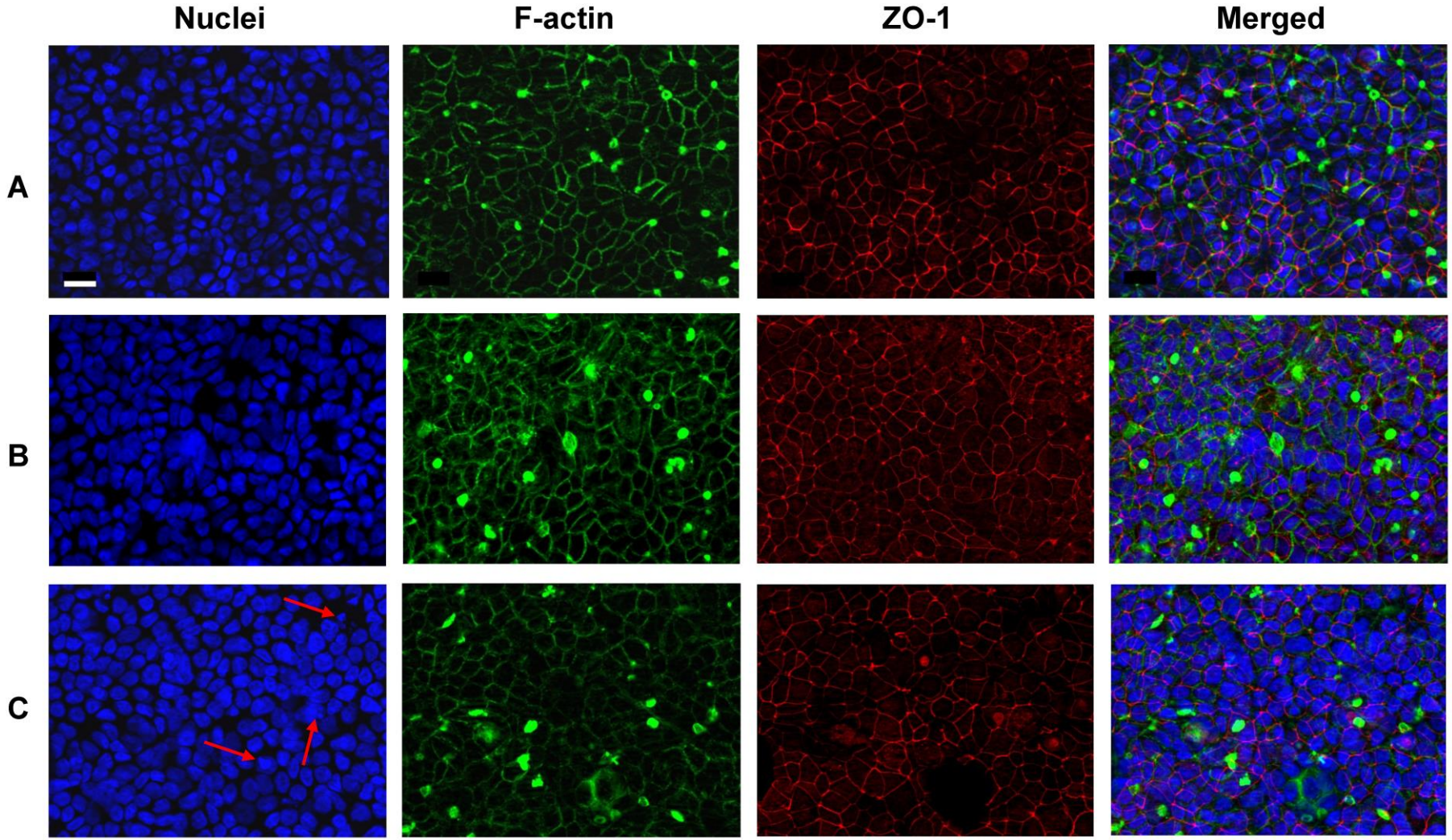

Figure 3.5 Fluorescently labelled nuclei (blue), F-actin (green), and ZO-1 (red) after 48h (A) Caco-2 monoculture, (B) stable, or (C) inflamed co-culture

Images were acquired in Apotome mode at 40x magnification, scale bar: 20 µm, applies to all images

3.1.1 Induction of an inflammation-like response in the stable co-culture

Apart from its reproducibility, the model's applicability to study the pro-inflammatory potential was investigated. To induce a pro-inflammatory response in the stable co-culture, an approach described by Detzel et al. (2015) was adapted. Briefly, they exposed C2BBe1 (a clone of the Caco-2 cell line) cell layers to 0.01 % PPS to increase the TJ permeability and allow for the translocation of apically added LPS. In this project, PPS was replaced by 2.5 mM EDTA, which was added to the AP and BL compartment to reduce cell-to-cell attachment (Meng and Takeichi, 2009) and enable apically added LPS to translocate to the BL compartment. After the addition of EDTA to the stable co-culture at T_0, the TEER rapidly decreased by ~80 % over 4h compared to the unexposed Caco-2 monoculture control (Figure 3.6). After 4h of exposure, the apical CCM was exchanged to counteract the calcium-chelating effect of EDTA. The TEER did, however, not recover before the end of the co-culture at 48h. The long-lasting TEER reduction to ~20 % of the control suggested the cell barrier to be extensively and permanently damaged.

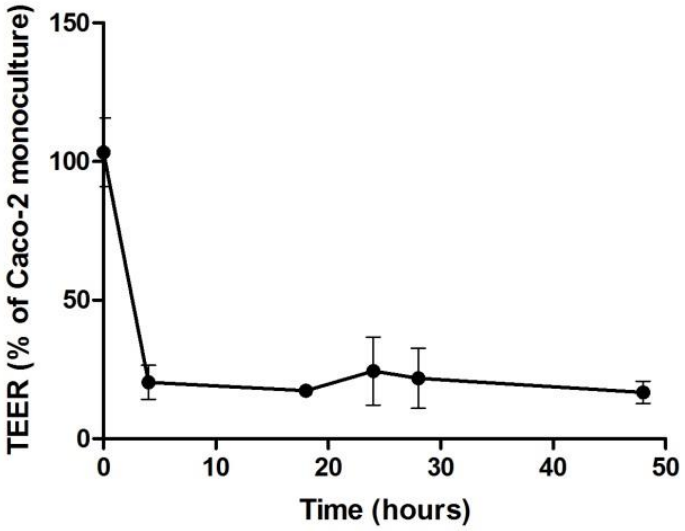

Figure 3.6 Barrier integrity measured as TEER over 48h of stable co-culture exposed to EDTA and LPS

(Average of N≥2 ± StDev)

In Caco-2 monocultures, the exposure to 10 ng / mL LPS in the AP and / or BL compartment did not cause comparable TEER reductions (Figure 3.7A). No TEER reduction was observed in the stable co-culture over 48h apical exposure to LPS or LPS and IFN-γ (10 ng / mL each) (Figure 3.7B).

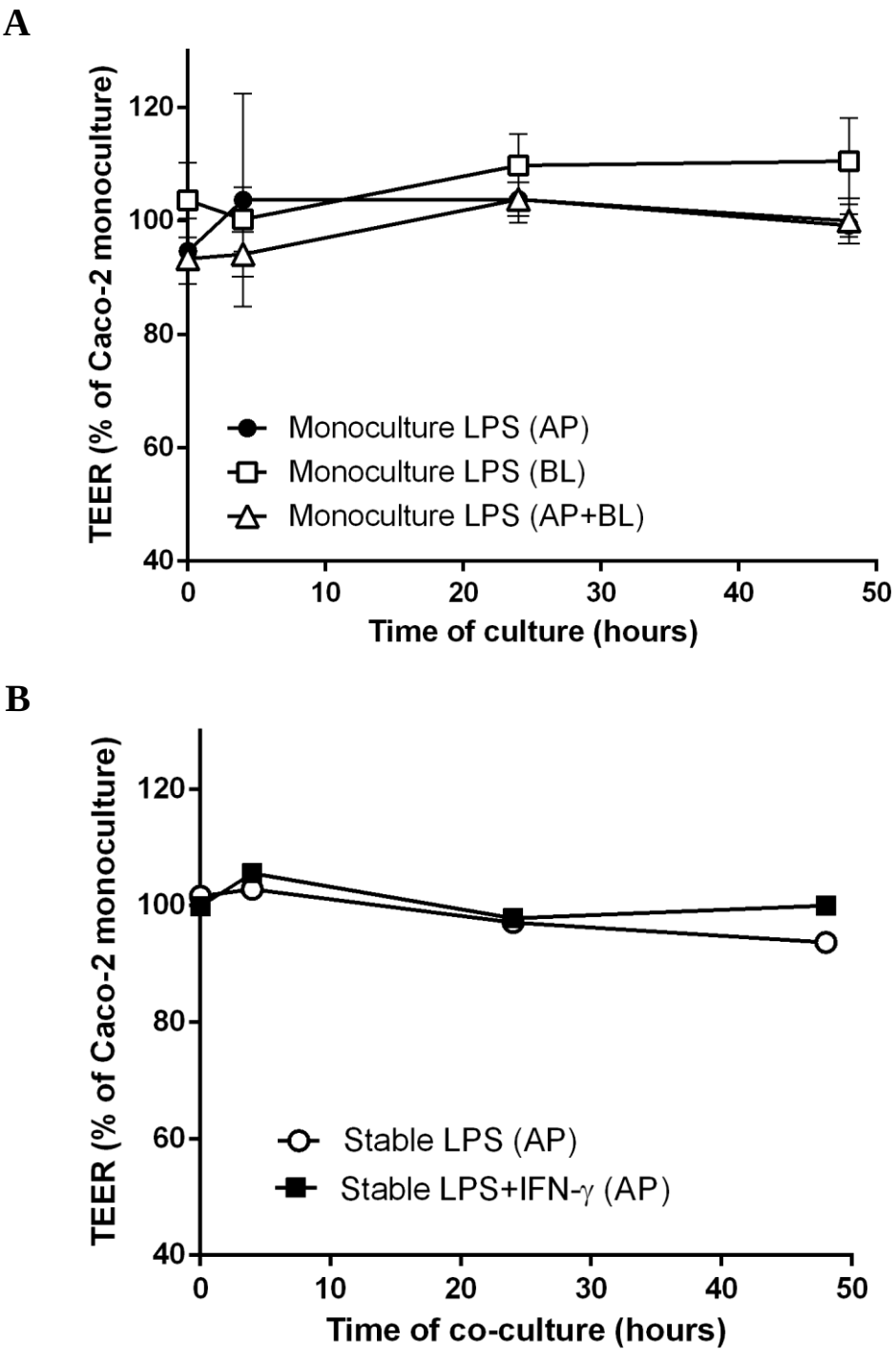

Figure 3.7 Barrier integrity measured as TEER over 48h (A) Caco-2 monoculture with AP and / or BL exposure to LPS (10 ng / mL) and (B) stable co-culture with AP exposure to LPS (10 ng / mL) or LPS + IFN-γ (10 ng / mL each)

(Caco-2 monoculture: Average of N≥2 ± StDev; Stable co-culture: Average of n=3 from one experiment ± StDev)

The magnitude of the barrier disruption was confirmed by analysis of Caco-2 barriers fluorescently labelled for the cytoskeleton and TJ network. As the images show (Figure S4), the majority of the cells had detached from the transwell filters. Both the cytoskeleton and TJ network were discontinuous and scarcely covered the filter. In line with both the TEER measures and the microscopic analysis, the LDH release was significantly increased ($p \leq 0.001$) in the AP and BL compartment of EDTA + LPS-exposed stable co-cultures compared to the stable co-culture control (Figure 3.8). No interference of EDTA with the assay was noted (Figure S5).

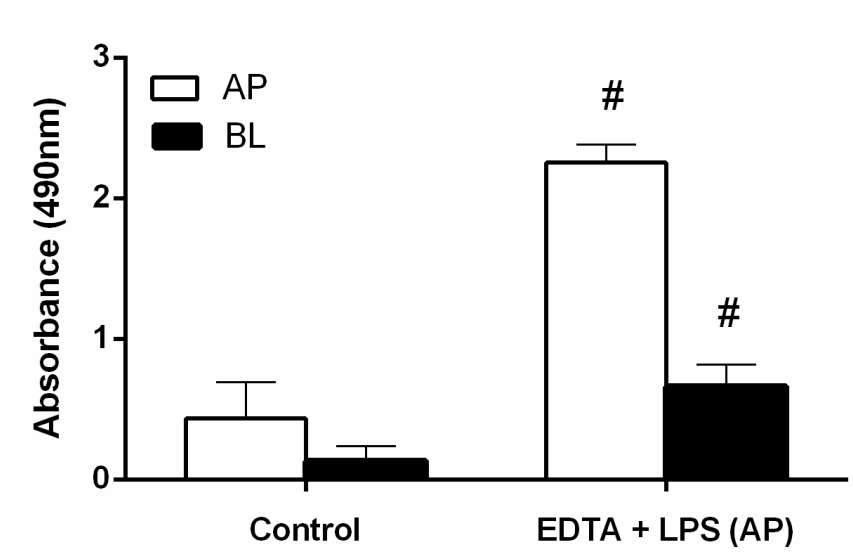

Figure 3.8 LDH activity quantified after 48h stable co-culture with and without exposure to EDTA and LPS

EDTA (2.5 mM) was added to the AP and BL compartment; LPS (30 ng / mL) was added to the AP side (Control = stable co-culture, Average of N=5 ± StDev; EDTA+LPS: Average of N=2 ± StDev; $^{\#}p \leq 0.05$ compared to control)

For cytokine analyses, supernatant samples were taken from the BL compartment after 4, 24, and 48h of exposure and co-culture. The results were compared to the unexposed stable co-culture control. The following conditions were included as controls to exclude the possibility that any observed effect was induced by EDTA or LPS alone: the stable co-culture was apically exposed to LPS without addition of EDTA; Caco-2 monocultures were treated with EDTA and LPS; THP-1 monocultures were exposed to EDTA alone. The results are summarised in Figure 3.9 and Figure 3.10 below.

After 4h stable co-culture, IL-1β and TNF-α were expressed at very low concentrations below 10 pg / mL (Figure 3.9A). Only IL-8 was noticeably released with ~350 pg / mL. At this time point, no significant differences in cytokine release were observed between the EDTA/LPS-exposed and the unexposed stable co-culture control.

With increasing exposure time, the IL-8 concentration increased significantly ($p \leq 0.01$) to >2,000 pg / mL after 24h (Figure 3.9B) and >3,400 pg / mL after 48h (Figure 3.9C). Both IL-1β and TNF-α were slightly but significantly ($p \leq 0.001$ and $p \leq 0.037$, respectively) elevated compared to the stable co-culture control after 24 and 48h exposure.

To analyse the impact of IFN-γ a control was included in which the stable co-culture was exposed to a mix of EDTA, LPS, and IFN-γ (Figure 3.10). The presence of IFN-γ strongly increased the release of all three cytokines compared to stable co-cultures exposed to EDTA and LPS alone after 24h (IL-1β +360 %, IL-8 +430 %, TNF-α +1,800 %) and 48h (IL-1β +360 %, IL-8 +480 %, TNF-α +1,880 %).

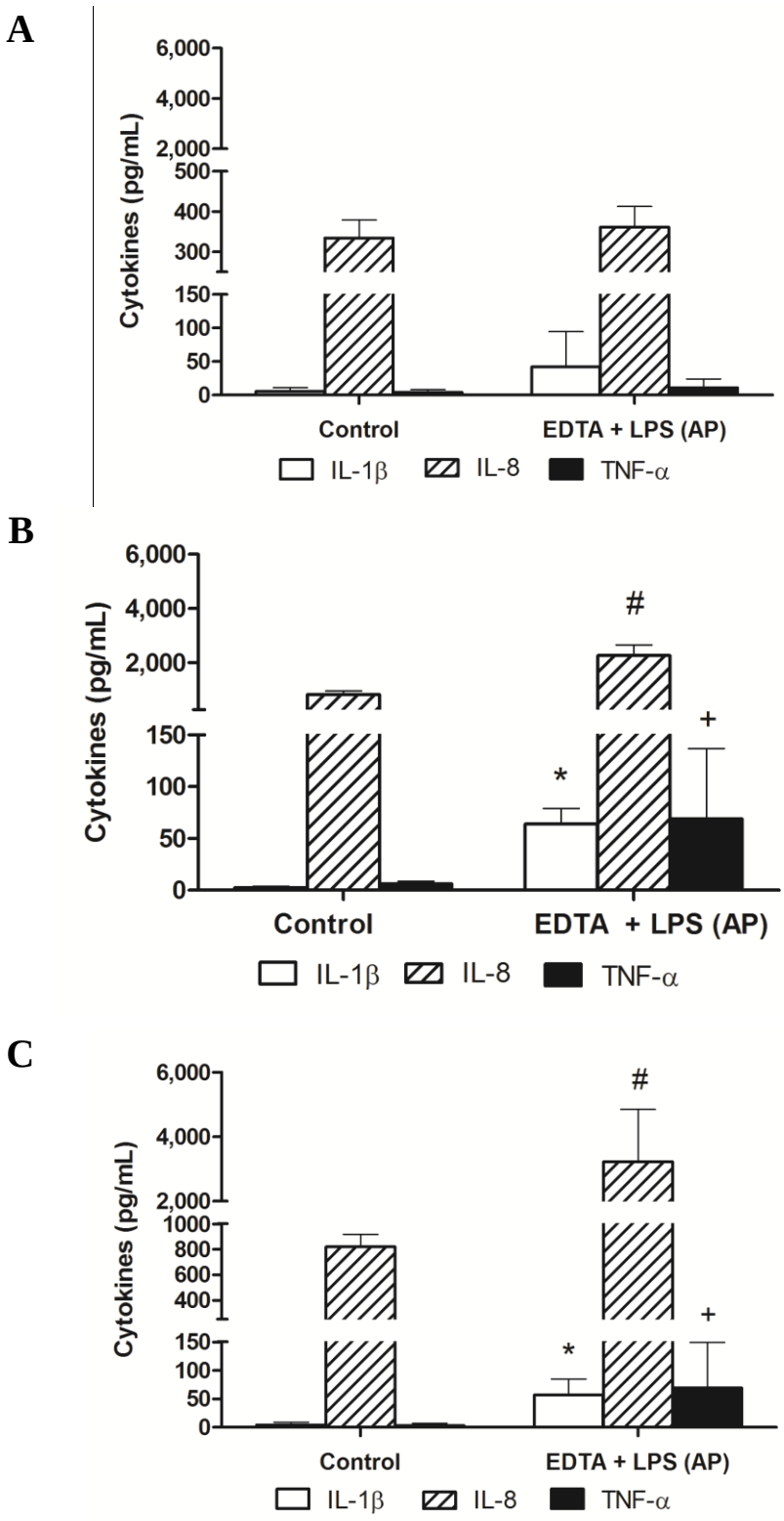

Figure 3.9 Quantification of IL-1β, IL-8, and TNF-a after (A) 4, (B) 24, and (C) 48h stable co-culture with and without exposure to EDTA / LPS

*EDTA (2.5 mM) was added to the AP and BL compartment; LPS (30 ng / mL) was added apically (Control 24h: Average of N=2; Rest: Average of N=3 ± StDev; *p≤0.05 compared to IL-1β in stable co-culture control; $^{\#}$p≤0.05 compared to IL-8 in stable co-culture control; $^{+}$p≤0.05 compared to TNF-α in stable co-culture control)*

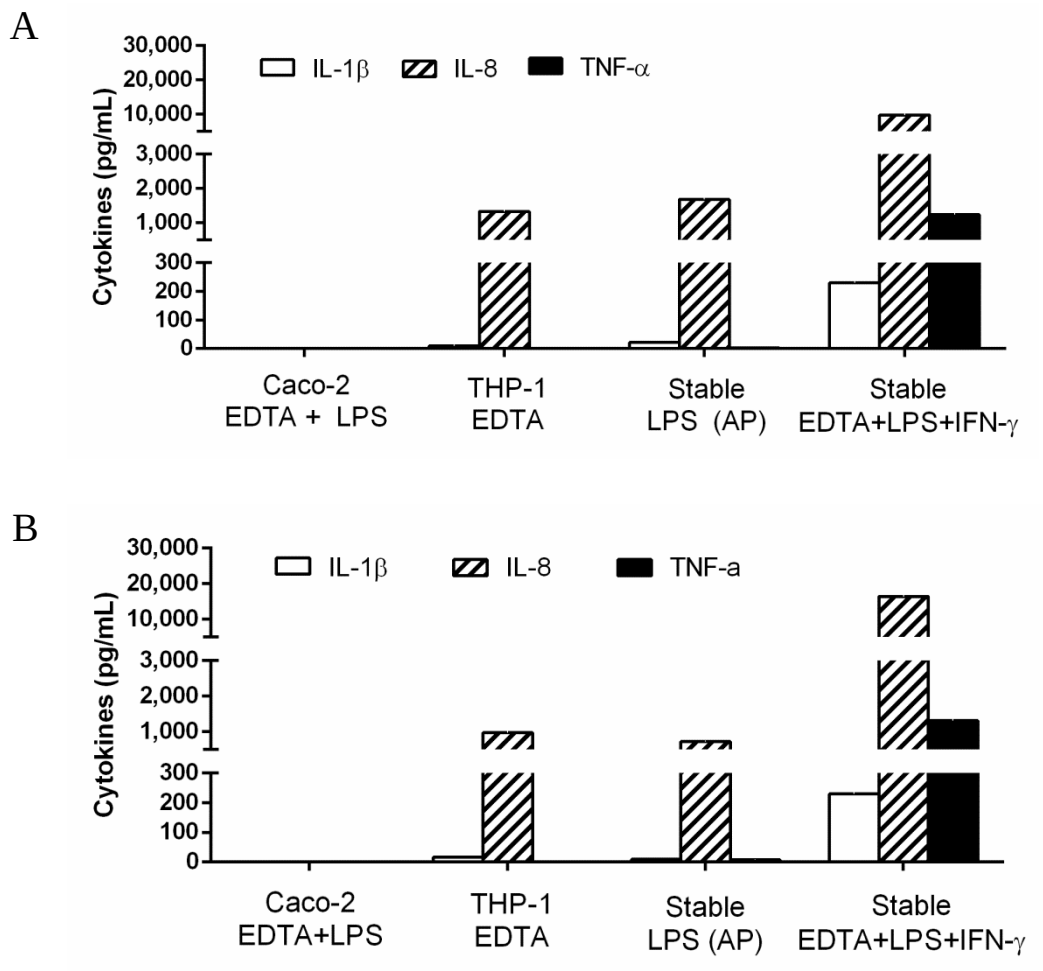

Figure 3.10 Quantification of IL-1β, IL-8, and TNF-α by Caco-2 and THP-1 cells in mono- or stable co-culture

(A) 24h or (B) 48h apical exposure to EDTA (2.5 mM), LPS (30 ng / mL), EDTA and LPS (30 ng / mL), or EDTA+LPS (30 ng / mL)+IFN-γ (30 ng / mL) (Average of n=3 of one experiment ± StDev)

3.3.3 Translocation of LY in the inflamed and stable co-cultures

To compare the barrier permeability between the co-culture models the translocation of LY was studied and expressed as P_{app}. Two different approaches were investigated as described in Section 3.2.5. At first, the co-culture conditions were established and maintained for 24h before the wells were washed and exposed to LY dissolved in $HBSS^{+/+}$ (Figure 3.11, white squares). After the supernatant was exchanged for HBSS+LY the TEER quickly re-established and significantly exceeded the barrier integrity of the Caco-2 monoculture after 28h (116 %) and 48h (151 %) (red squares). Since the exchange of supernatant for $HBSS^{+/+}$ apparently favoured a quick recovery of the Caco-2 barrier integrity, a second approach was tested.

Instead of letting the condition establish before the assay, LY was dissolved in CCM and added to the AP compartment at the start of the co-culture. The inflamed co-culture could be established normally in presence of LY (Figure 3.11, green triangles), reaching a similar reduction in TEER as the inflamed co-culture control (Figure 3.11, black circles). Even though the inflamed co-culture fulfilled the defined requirements regarding the magnitude and duration of the barrier disruption no increased P_{app} for LY was detected after 4 and 18h (Figure 3.12). To exclude potential adverse effects of LY on cell viability or barrier integrity, a control in Caco-2 monoculture and stable co-culture was included (Figure 3.12).

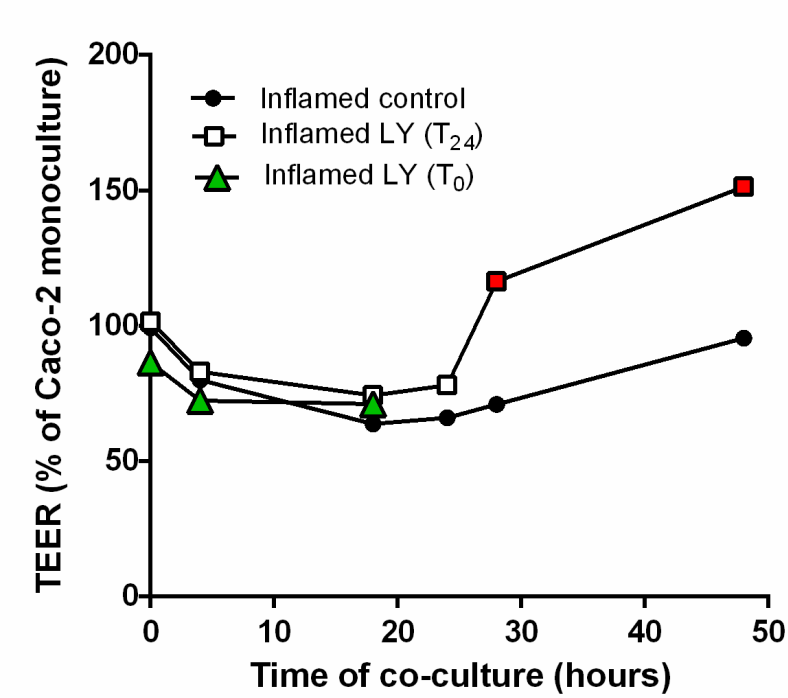

Figure 3.11 Barrier integrity measured as TEER over 48h inflamed co-culture with and without supernatant replacement for LY barrier crossing studies

(Average of n=3 of one experiment ± StDev)

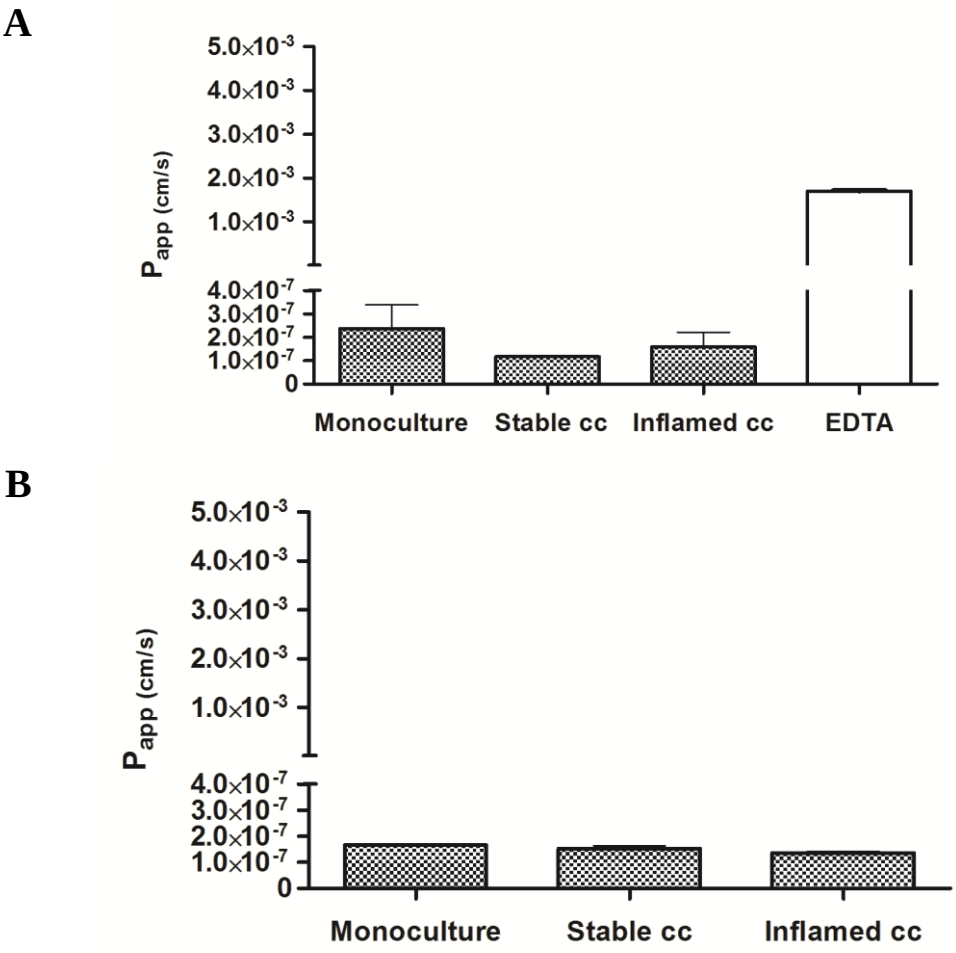

Figure 3.12 P_{app} of Caco-2 monoculture, stable, and inflamed co-culture

(A) 4h treatment with LY starting after 24h of co-culture; (B) after 18h treatment with LY starting at the initiation of the co-culture (Average of n≥3 ± StDev)

3.4 Discussion

3.4.1 Characterisation of the stable and inflamed co-cultures

The characterisation of co-culture models revealed significant differences:

- No increased release of cytokines, NO_2^-, or LDH was detected after co-culture of Caco-2 and unstimulated THP-1 cells, indicating that no activation of the macrophages occurred. The results on the cytoskeleton and TJ network confirmed that unstimulated THP-1 cells did not negatively affect Caco-2 barrier integrity.
- The activation of THP-1 cells with LPS and IFN-γ caused a significant increase in pro-inflammatory cytokines, NO_2^-, and LDH, which underlined the detrimental effect of activated macrophages on Caco-2 cells.

- The positive control using EDTA and LPS confirmed that the stable co-culture can be activated. Additional controls, however, underlined the crucial role of IFN-γ for the induction of inflammation-like processes.
- Even though the barrier integrity was significantly impaired in the inflamed model no increased paracellular permeability for LY was detected.

3.4.1.1 Cytotoxicity

The enzyme LDH is present in virtually all mammalian cells and released after cell damage or necrotic cell death. Therefore, the quantification of the enzymatic activity is a widely accepted method to assess cytotoxicity (Chan et al., 2013). Whereas a significantly increased release of LDH was measured in the AP supernatants of the inflamed co-cultures no change was detected in the stable co-culture compared to the Caco-2 monoculture. Together with the results on TEER and the cytokine release these results support the hypothesis that unstimulated 24h-differentiated THP-1 cells did not exert adverse effects on the Caco-2 barrier over 48h co-culture. The increase in LDH activity in AP supernatants after induction of an inflammation-like process indicates the occurrence of necrosis in the Caco-2 cell layer. Based on the LDH release alone, no estimation can be given on the magnitude of the cell damage. Since the barrier integrity, measured as TEER, is fully re-established after 48h and the immunocytochemical analysis of the cell layer showed a continuous barrier it can be assumed that no excessive necrotic cell death occurred.

Apart from the reduction in barrier integrity intestinal inflammation is strongly associated with the occurrence of cell death in IECs. Even though the majority of the reports concern the observation of apoptotic cell death the occurrence of necrosis in IBD patients has been reported as well (Nunes et al., 2014; Dourmashiin et al., 1983). Several inflammation-related mediators are known to induce necrotic cell death, e.g. TNF-α and NO (Miura et al., 1995; Bonfoco et al., 1995). Both TNF-α and NO were present at significantly higher concentrations in the inflamed model compared to the stable co-cultures and might have induced necrotic processes. In contrast to these results other groups reported an increased release of LDH in presence of THP-1 cells even without additional activation of the macrophages (Watanabe et al., 2004; Satsu et al., 2006). Watanabe et al. nicely demonstrate the correlation of TNF-α and LDH release: In presence of anti-TNF-α Ab the levels of LDH were reduced significantly to

those of the monoculture control (Watanabe et al. , 2004). In contrast to our co-cultures, Satsu and colleagues used almost twice as many THP-1 cells ($3x10^5$) on the same well surface. This underlines the importance of ratios of cell types in the development of co-cultures. As discussed before (Section 2.3.3), intestinal homeostasis greatly depends on the interplay between IECs and the various parts of the GALT. This regulation by IECs, which was observed during the development of the inflamed co-culture, might not be possible in case an overwhelmingly high numbers of immune cells are present.

In contrast to Satsu et al. and Watanabe et al., Susewind and colleagues (2016) did not detected increased LDH levels in either the non-inflamed or inflamed intestinal co-culture of Caco-2, THP-1, and MUTZ-3 cells after challenge with IL-1β. In contrast to TNF-α, IL-1β has been found to induce cell death indirectly through the generation of NO. The exposure to IL-1β caused both apoptotic and necrotic cell death in β-cells of pancreatic islets (Hoorens et al., 2001; Ankarcrona et al., 1994). Several groups reported an adverse effect of IL-1β on the barrier integrity of Caco-2 cells and induction of NO synthesis (Van De Walle et al., 2010; Al-Sadi and Ma, 2007). However, no occurrence of necrotic or apoptotic cell death was observed (Al-Sadi and Ma, 2007). Satsu et al. (2006) even demonstrated that in IL-1β was not responsible for the observed increase in LDH release in the group's co-culture of Caco-2 cells and activated THP-1 cells.

Altogether, these results underline how variations in a culture set-up or the use of different stimuli to evoke the same effect – here an inflammation-like response – can lead to significantly different outcomes in specific endpoints.

3.4.1.2 Cytokine release

Another hallmark of intestinal inflammation is the presence of pro-inflammatory cytokines like TNF-α, IL-8, and IL-1β, which can be released by both immune cells and IECs (Coccia et al., 2012; Mazzucchelli et al., 1994). In the Caco-2 monoculture the concentrations of all three cytokines were close to or below the detection limit (Table 2.2). In contrast, the release of IL-8 was enhanced in the stable co-culture, but did not significantly exceed the levels recovered in unstimulated THP-1 monocultures (Section 2.2.2.2). In the inflamed co-culture, the release of all three investigated cytokines was

markedly increased. Interestingly, TGF-β1 was not detected in any of the culture models.

IL-1β, TNF-α, and IL-8 are well known for their role in the onset and maintenance of inflammatory processes. The absence of cytokine release by unstimulated Caco-2 cells is well in line with the reported findings of other (Kucharzik et al., 1997). Even after the adjusted PMA-differentiation protocol the release of IL-8 was significantly increased in the stable co-culture compared to the Caco-2 monoculture. As mentioned before, it is possible that this release is a typical background level synthesized by the macrophages and does not indicate an activation / stimulation of either cell line (Smythies et al., 2005). This was further supported by the fact that no disruption of the Caco-2 barrier integrity was noted.

The high release of pro-inflammatory cytokines in the inflamed co-culture was both expected and desired. In contrast to LPS exposure at the start of the co-culture (Section 2.2.4.2) the pre-exposure to LPS and IFN-γ induced high levels of cytokines even in presence of Caco-2 cells. The levels for IL-8 and TNF-α were significantly higher in the co-culture compared to LPS/IFN-γ-exposed THP-1 monocultures (Section 2.2.2.2). These results further support the hypothesis that the presence of Caco-2 cells down-regulated the macrophage-mediated cytokine response to LPS in earlier experiments. It is not clear whether the co-culture enhanced the cytokine release by THP-1 cells or Caco-2 cells contributed to the recovered concentrations. Caco-2 cells are able to synthesise several pro-inflammatory cytokines but are mainly associated with the release of IL-8. However, several groups showed no or very low cytokine response in Caco-2 cells after challenge with LPS (Schuerer-Maly et al., 1994) or various non-pathogenic and pathogenic bacterial strains (Parlesak et al., 2004; Haller et al., 2000). In contrast to LPS, already low concentrations of 100 pg / mL of IL-1β induced a significant release of IL-8 of around 2 ng / mL (Schuerer-Maly et al., 1994). Furthermore, higher concentrations of TNF-α (50 ng / mL) were found to induce IL-8 release in Caco-2 cells (Van De Walle et al., 2010). It is, therefore, possible that the cytokines released by activated THP-1 cells stimulated the cytokine synthesis in Caco-2 cells.

The absence of TGF-β1 was surprising as it is known for its immunosuppressive and barrier protective effects in intestinal epithelia (Howe et al., 2005). The cytokine has been shown to be involved in the regulation of cytokine release by other cell types, e.g. endothelial cells, PBMCs, and lamina propria mononuclear cells (Lügering et al., 1998;

Kucharzik et al., 1997). More precisely, it is known to down-regulate the generation of IL-8 in macrophages (Schuerer-Maly et al., 1994). Hence, the absence of TGF-β1 might be involved in the still high releases of IL-8 in the stable co-culture. Furthermore, TGF-β was shown to enhance the barrier integrity of intestinal epithelial cells (Howe et al., 2005), which could have explained the here observed re-establishment of TEER in the inflamed co-culture.

3.4.1.3 Nitrous stress

In the Caco-2 monoculture and stable co-culture the levels of detectable NO_2^- were generally close to or below the lower detection limit of the Griess reaction (~3 µM). It could not be distinguished, whether both cell lines were involved in the NO_2^- generation or the generated NO_2^- translocated from AP to BL compartment or vice versa. Both Caco-2 and THP-1 cells have been demonstrated to express iNOS and release NO_2^- upon stimulation (Vignoli et al., 2001; Chen et al., 1996). It should be noted, though, that the reported results on the NO_2^- release by THP-1 cells vary significantly. Whereas some groups observed the induction of both NO_2^- and the expression of iNOS, others could not detect NO generation upon stimulation (Weinberg, 1998). Also in our laboratory, the NO synthesis of THP-1 cells was variable. Often a significant release of NO_2^- could be triggered by exposing PMA-treated THP-1 cells to LPS (100 ng / mL) (not shown). In some cases, however, the cells did not respond to the stress, independent of the differentiation status and concentration of the stressor. Similar results were obtained throughout the co-culture experiments. Whereas in some cases a clear and significant increase was measured, other experiments failed to cause NO_2^- generation.

After its discovery, most research on the release of NO has been performed using non-human macrophages (Weinberg, 1998). It turned out that even though murine monocytic cells responded to common activating stimuli, e.g. LPS, IFN-γ, and TNF-α, with the release of high concentrations of NO, human primary monocytes and cell lines did not (Pham et al., 2003). It was long questioned, whether human macrophages are capable of generating NO via the iNOS pathway suggesting that reported NO-detections were attributable to *in vitro* artefacts (Schneemann et al., 1997). Interestingly, macrophages isolated from lung transplant patients could be stimulated to synthesise NO *in vitro*, whereas macrophages of healthy controls were largely unresponsive (Fang

and Vazquez-Torres, 2002). In human macrophages the regulation of iNOS and synthesis of NO appears to heavily depend on the type of stimulus. For instance, iNOS was not up-regulated in human monocytes and macrophage cell lines in response to LPS (Pham et al., 2003), whereas they strongly responded to infection with different strains of mycobacteria (Jung et al., 2012) or incubation with serum derived from Kawasaki disease patients (Cheung et al., 2005). Furthermore, the differentiation state of the cells might be important, but also here the reported findings are ambiguous. Daigneault et al. (2010) observed a release of NO by LPS-stimulated monocytes and VD_3-differentiated THP-1 cells, but not in macrophages or PMA-differentiated THP-1 cells. In this case, the variations observed in this project might be related to an incomplete differentiation of the THP-1 cells in some runs. Why the cells would respond differently to PMA between experimental runs remains a separate question. Pham and colleagues (2003) did not note any effect by LPS on monocytes or undifferentiated THP-1 cells. Altogether, it is not fully elucidated yet what determines the NO-induction in macrophages *in vitro* and why large variations persist in the outcomes between laboratories.

In contrast to THP-1 cells, Caco-2 cells have clearly been shown to synthesise NO in response to several pro-inflammatory cytokines, as well as LPS. A combination of IL-1β, TNF-α, IFN-γ, and LPS was demonstrated to act more effectively than the individual compounds alone (Van De Walle et al., 2010). Chen and Kitts (2008) ranked the inducers according to their effectiveness on NO synthesis as follows: IFN-γ > IL-1β > TNF-α > LPS. Even though several known inducers of NO were available in every inflamed co-culture run apical NO_2^- was only detected in some of the experiments. The detection of AP and BL NO_2^- occurred exclusively in parallel. It is unlikely that the NO_2^- in both AP and BL compartment is attributable to the Caco-2 cells alone, as the majority of Caco-2-derived NO_2^- is released to the AP side (Kim et al., 2002). The NO generation in Caco-2 cells has been shown to be influenced by several factors, e.g. passage, culture / differentiation time, and stimulation time (Chen and Kitts, 2008). Whereas the differentiation and stimulation time did not change considerably, the passage number of the cells varied between the experiments. It is possible that a minimum number of passages was necessary to induce NO generation in Caco-2 cells. In many studies observing an NO release the cells were exposed apically to stressors in contrast to this project (Chen and Kitts, 2008; Kim et al., 2002; Eckmann et al., 2000). Others did not observe a significant induction of NO in basolaterally exposed cells (Satake et al., 2001), which suggests a different response to stimuli depending on the

side of encounter. In accordance to this hypothesis, Quadrhiri et al. (1999) reported an interesting observation regarding the impact of IL-6 and IFN-γ on the intracellular growth of *Listeria monocytogenes*. Whereas IL-6 was exclusively beneficial when added on the BL side of Caco-2 cells, IFN-γ was significantly more active on the AP side of the cells. It is possible that a similar effect is observed here. This could also explain the noted variability in NO_2^- detection – at least in Caco-2 cells. As will be discussed later (Chapter 4), IL-6 release occurred in the inflamed co-culture. However, the absolute concentrations varied strongly between the individual runs, whereas the presence of IFN-γ and other NO-inducing cytokines like TNF-α and IL-1β was rather constant.

3.4.2 Activation of THP-1 cells in the stable co-culture

To demonstrate the stable co-culture's ability to react to pro-inflammatory stimuli, an increase in cytokine release induced by the AP exposure to a stressor was documented.

To stimulate the stable co-culture two approaches were initially discussed:

I. Targeting the IEC barrier: stimulating the Caco-2 cells to initiate a pro-inflammatory response.
II. Targeting the THP-1 cells: aiming for a translocation of the stressor from the AP to the BL compartment to stimulate the macrophage-like cells.

In the first approach, the aim would be to stimulate the release of pro-inflammatory cytokines and chemokines from Caco-2 cells to activate the THP-1 cells indirectly. This could be achieved with the exposure to pro-inflammatory chemical compounds (e.g. arsenic species) (Calatayud et al., 2014), the use of enteroinvasive bacterial strains (e.g. *Shigella*, enteroinvasive *Escherichia coli* [EIEC], and pathogenic strains of *Listeria*) (Gaillard, 1987; Jung, 1995) or the exploitation of bacterial enteroinvasive toxins (e.g. Shiga toxin) (Yamasaki, 1999).

For the second approach, targeting the THP-1 cells requires the stressor to penetrate the epithelial barrier to pass from the AP to the BL compartment. Again, pathogenic bacterial strains (e.g. *Salmonella* and *E. coli*) (Finlay, 1990; Philpott et al., 1997), bacterial toxins (e.g. verotoxin-1) (Philpott et al., 1997; Izumikawa et al., 1998), or PAMPs like LPS would be suitable candidates. Some stressors like verotoxin-1 are capable of translocating across the epithelium by themselves (Philpott et al., 1997),

whereas others, e.g. LPS, require the addition of a stressor to target the TJ network or cytoskeletal integrity of the Caco-2 cells to reach the BL side (Detzel et al., 2015; Haller et al., 2000).

Any concept involving the use of live bacterial cultures was overruled, due to the lack of adequate facilities, which left a choice between bacterial toxins and PAMPs. The use of Shiga (-like) toxins would have been the more interesting and elegant solution as it did not require a second stressor to disrupt the Caco-2 barrier. However, its use would have required extensive additional characterisation of the toxin's effects in Caco-2 and THP-1 monocultures, as well as stable and inflamed co-cultures. For reasons of practicality it was, therefore, decided to adapt the approach described by Detzel and colleagues (Detzel et al., 2015) to activate the stable co-culture. A translocation of LPS to the BL compartment was regarded as necessary, since the AP exposure to such low concentrations of LPS does not stimulate Caco-2 cells to release pro-inflammatory cytokines or messenger chemokines like MCP-1 (Schuerer-Maly et al., 1994; Haller et al., 2000).

As the results showed, the AP exposure of the stable co-culture to EDTA induced a rapid and permanent reduction in Caco-2 barrier integrity due to detachment of the cells. After 24 and 48h of exposure the cytokine release was significantly increased compared to the stable co-culture control, indicating an activation of the THP-1 cells. The controls confirmed that neither the exposure to EDTA in THP-1 cells nor the treatment of Caco-2 cells with LPS and EDTA caused an elevated synthesis of pro-inflammatory cytokines. Furthermore, the AP exposure of the stable co-culture with LPS in absence of EDTA failed to induce cytokine release. This confirms that

(1) Caco-2 cells do not respond with the release of IL-8, TNF-α, or IL-1β to the apical presence of LPS.

(2) LPS is not able to translocate across the epithelial barrier without an additional stressor disrupting the barrier integrity.

It can, therefore, be concluded that the cytokine release was caused by LPS after translocation to the BL compartment. Even though the increase of all three cytokines was significant, only IL-8 reached levels comparable to those of the inflamed co-culture, whereas IL-1β and TNF-α remained at levels of questionable biological importance. A control using LPS, EDTA, and IFN-γ resulted in greatly enhanced cytokine concentrations, underlining the importance of IFN-γ for the induction of an

inflammation-like response. This is in line with the crucial role of IFN-y in intestinal inflammation, which has been demonstrated before in IFN-$\gamma^{-/-}$ mice (Ito et al., 2006). In inflammation, IFN-γ is directly involved in the recruitment of immune cells, as well as the induction of chemokines (Su et al., 2015; Ito et al., 2006). Furthermore, IFN-γ can indirectly amplify the effect of other pro-inflammatory mediators, e.g. TNF-α, by up-regulating specific binding sites (Wang et al., 2006). Since the presence of IFN-γ seems to have a pivotal role in the artificial induction of inflammation its lack in the stable co-culture might affect the model's applicability to study the pro-inflammatory potential of NMs.

3.4.3 Translocation of LY

The integrity of the intestinal barrier is a crucial factor to determine its gate function. A reduction in barrier integrity (here primarily measured by means of TEER) is associated with an increased transport of ions and macromolecules from the AP to the BL compartment. One of the distinguishing characteristics of the inflamed co-culture model was the significantly reduced TEER indicating a temporary disruption in barrier integrity. This led us to hypothesise that the barrier's gate function is impaired temporarily, which should allow molecules like LY to pass the inflamed barrier at a higher rate than in the Caco-2 monoculture and stable co-culture. However, the results showed that no increased translocation of LY occurred even though the TEER was reduced by 30-40 %. In the first approach this observation was not surprising, since the barrier integrity re-established promptly after addition of LY in $HBSS^{+/+}$. Probably, the diffusion rate of the dye was slower than the re-establishment of the barrier integrity. Surprisingly, no increased translocation of LY was seen in the second approach either.

These results are in clear contrast to the reports of others showing a significantly increased translocation of molecules in response to cytokine-induced TJ opening. A 30 % reduction in Caco-2 barrier integrity resulted in a 20-fold increase in the paracellular permeability for inulin (5,000 g / mol) (Al-Sadi and Ma, 2007). The exposure to IL-6 reduced barrier integrity up to 40 %, but only increased the translocation rate of very small molecules like urea, and not for mannitol, inulin (5,000 g / mol), or dextran (10,000 g / mol) (Al-Sadi et al., 2014). The barrier disruption in the inflamed co-culture is most likely primarily induced by the synergistic effect of IFN-γ and TNF-α. In Caco-2 barriers individually exposed to either TNF-α or IFN-γ, an increased flux of LY has

been reported (Cui et al., 2010; Koda et al., 2003). The effects of simultaneous exposure have, so far, only been assessed using dextran (3-4 kDa), for which the paracellular transport was clearly increased (Cao et al., 2013; Wang et al., 2005). Since all permeability-enhancing cytokines seem to induce different pathways the results obtained from TNF-α and IFN-γ individually should not be extrapolated to a combined exposure scenario.

In general, LY seems to be an insensitive marker for barrier permeability albeit the low molecular weight. In accordance with this, the dye is mostly used to assess barrier development and cytotoxic effects, but less commonly applied to study TJ functionality (Di and Kerns, 2016). When studying the correlation between TEER and paracellular permeability for two low molecular weight molecules (LY and mannitol) and a higher weight molecule (40-50 kDa dextran) Konsoula and Barile (2005) observed LY translocation in case of heavy reduction in TEER of at least 60 %. It is unlikely that an uptake and subsequent entrapping of LY within the Caco-2 cells causes the lack of translocation (Mashukova et al., 2011). Interestingly, in case the epithelial barrier was substantially disrupted using Ca^{2+} chelators the flux of LY was notably increased and even exceeded the rates obtained with molecules of significantly higher molecular weight (Walczak et al., 2015; Bouwmeester et al., 2011).

Most likely, the nature of the molecules used for transport studies (e.g. molecular weight, hydrodynamic diameter, polarity, and charge) has to be considered in addition to the variations in mechanisms and might explain the apparent discrepancies. In IECs the paracellular pathway was shown to be more permeable to cationic than anionic or neutral molecules (Palm et al., 1999). Apart from its rather large size (12.2 x 9.9 x 2.6 Å), LY is a highly polar molecule with an overall negative charge (Kanaporis et al., 2011). Whereas cytotoxicity causes a complete detachment of the cells most cytokines cause a structural or quantitative change in TJ proteins. Hence, in the former case the size and charge-selective pores are increasingly destroyed, whereas they are still intact in the latter. This further implies that the gate function including the size and charge selectivity (mainly regulated by proteins of the claudin family) is functioning after exposure to cytokines (Chiba et al., 2008). Altogether, this could explain why no increased paracellular permeability is observed for LY albeit the significant reduction in TEER and render the dye an unsuitable probe to study this endpoint.

3.5 Conclusions

For most of the investigated endpoints (LDH, NO, barrier integrity, and TNF-α release) no significant differences were noted between the Caco-2 monoculture and stable co-culture. In contrast to the hypothesis, both IL-1β and IL-8 levels were significantly elevated in the stable co-culture, but no negative effect on the barrier integrity was measured. It was hypothesised that the stable co-culture is suitable to study the pro-inflammatory potential of NMs. Even though the release of pro-inflammatory cytokines could be stimulated this hypothesis could not be fully confirmed due to the observed importance of IFN-γ in inflammation. The stimulation of THP-1 cells with LPS and IFN-γ in the inflamed co-culture caused remarkable differences in barrier integrity, release of pro-inflammatory cytokines, NO formation, and LDH release. Even though the presence of activated THP-1 cells induced necrotic cell death the histochemical analysis of the Caco-2 barrier showed no signs of reduced cell numbers. It can, therefore, be assumed that the observed reduction in TEER is primarily caused by cytokine-induced restructuring of TJ proteins and not cytotoxicity. The inflammation-like process, however, appeared to affect the nuclear integrity of Caco-2 cells, as well as the TJ network and cytoskeletal structure. The cause for the re-establishment of the TEER in the inflamed co-culture after 48h could not be elucidated. The applicability of LY to study the potential increase in paracellular permeability in the inflamed co-culture was questionable. Therefore, it can only be concluded that reduced barrier integrity does not result in an increased translocation of LY but might allow for increased paracellular passage of other substances.

4 Application of the co-culture model to study the effect of AgNPs in homeostatic and inflamed conditions

4.1 Introduction

According to the Consumer Products Inventory (2016), Ag is the most abundantly used NM in consumer products with over 400 registered applications to date. AgNPs are most commonly used in medical devices (Roe et al., 2008; Maneerung et al., 2008), and food contact materials (Llorens et al., 2012), due to their bactericidal activity against both Gram-positive and negative bacteria, including multi-drug resistant strains (Lara et al., 2009; Sondi and Salopek-Sondi, 2004). Due to their broad application in consumer products, a wide public is likely exposed to AgNPs on a regular base. Therefore, assuring their safety for human health is of utmost importance.

4.1.1 *AgNPs exposure effects*

4.1.1.1 Effects of AgNPs exposure in vitro

The effects of AgNP-exposure have been extensively studied in a variety of cell types from human and animal origin, including organ-specific cell types and leukocytes. Most commonly assessed endpoints include cytotoxic (Sambale et al., 2015; Beer et al., 2012), genotoxic (Li et al., 2012; Foldbjerg et al., 2011), and immuno-toxic effects. Depending on the cell type, AgNPs induced effects in a dose- and size-dependent manner either with smaller particles acting more potently than larger sized particles (Gliga et al., 2014; Huk et al., 2014) or vice versa (Kim et al., 2012b).

It is still debated whether AgNPs exert toxicity through the release of Ag ions (Ag^+) or as nano-specific effects related to size and shape of the particles (Kittler et al., 2010). Furthermore, it remains unclear whether the mechanisms differ between species, cell types, or even case by case (Stensberg et al., 2011). Park et al. (2010b) suggested a 'Trojan-horse' type mechanism for AgNP-induced cytotoxicity, meaning that particulate Ag is taken up by the cells and subsequently ionised within. In line with this, a study by Xiu et al. (2012) on *E. coli* observed a strongly reduced cytotoxic potential of AgNPs when the exposure was performed under anaerobic compared to aerobic conditions. The group argued that anaerobic conditions did not allow for the oxidation of Ag(0) to Ag^+ and, therefore, concluded the release of Ag^+ to be the main

cause for toxicity (Xiu et al., 2012). Pratsinis and colleagues (2013) suggested different toxicity mechanisms in relation to the particle size. Whereas the toxicity of AgNPs smaller than 10 nm is supposed to be related to the release of Ag^+, larger AgNPs are proposed to exert effects directly through cell-particle interactions.

4.1.1.2 Effects of AgNPs exposure in IECs and macrophages in vitro

AgNPs can be taken up by IECs in a size-dependent manner (Georgantzopoulou et al., 2016; Miethling-Graff et al., 2014). For intestinal epithelial cell lines, large variations regarding the susceptibility to AgNPs are reported in the literature. Whereas some studies report the induction of cytotoxicity at concentrations as low as 1 µg / mL in HT29 cells (Nguyen et al., 2013), others show remarkable resilience towards concentrations up to 100 µg / mL in Caco-2 cells (Georgantzopoulou et al., 2016). Apart from the exposure concentration and exposure time, AgNP-induced effects were shown to depend on the particle size and surface coating (Nguyen et al., 2013; Sanpui et al., 2011). Next to cytotoxicity, the induction of genotoxicity (Sahu et al., 2014), oxidative stress (Aueviriyavit et al., 2014; Miethling-Graff et al., 2014; Nguyen et al., 2016), cell cycle arrest (Miethling-Graff et al., 2014), and pro-inflammatory responses, e.g. the release of pro-inflammatory cytokines (Abbott Chalew and Schwab, 2013; Georgantzopoulou et al., 2016) have been reported in IECs.

Apart from the particle characteristics the developmental state of the cells influenced the severity of AgNP-induced effects. In proliferating IECs, very low particle concentrations (0.1 µg / cm^2) induced cell cycle arrest and strongly inhibited proliferation, whereas no effects were noted in differentiated, non-proliferating cells (McCracken et al., 2015). These significant variations in susceptibility might be one reason for the large differences in toxic doses reported in the literature.

As in IECs, AgNPs can be taken up by monocytic cell lines (Gnanadhas et al., 2013; Greulich et al., 2011), as well as primary blood monocytes (Krystek et al., 2015). Also in monocytic cells and macrophages the particle characteristics, like surface modifications, coatings and size, affected the toxic potential. When exposed to uncoated AgNPs, a size and dose-dependent induction of cytotoxicity occurred, with smaller particles being more cytotoxic than larger particles at the same mass-volume concentrations (Nguyen et al., 2013). In murine macrophages, the cytotoxic potential

could be reduced by coating the particles with citrate or PVP (Nguyen et al., 2013). In human monocytic cells, however, PVP coated AgNPs of similar size induced necrotic cell death at much lower concentrations, with an EC_{50} of just 2.5 µg / mL compared to no observable cytotoxicity at 50 µg / mL in murine macrophages (Foldbjerg et al., 2009; Nguyen et al., 2013). Peptide-coated particles proved to be less toxic in human monocytic cells with an EC_{50} of around 150 µg / mL (Haase et al., 2011). These results suggest that the effects of particle exposure might not only differ between cell types, but also between cell lines of the same cell type.

In intestinal co-culture models, AgNPs induced less severe adverse effects in IECs compared to the corresponding monoculture controls (Susewind et al., 2016; Georgantzopoulou et al., 2016). Apart from pro-inflammatory and cytotoxic effects, AgNPs impacted the expression of proteins in a manner that was distinguishable from ionic Ag (Georgantzopoulou et al., 2016; Oberemm et al., 2016; Gioria, unpublished results).

Most studies investigating different sizes of AgNPs observed size-dependent exposure effects. However, most authors apply equal mass / volume concentrations for different AgNPs without considering changes in particle number and specific surface area or normalising the results to a comparable characteristic. Hence, the interpretation of the results obtained from differently-sized AgNPs might be misleading. At identical mass/volume concentrations, smaller-sized particles induced stronger effects than larger AgNPs (Haase et al., 2011; Georgantzopoulou et al., 2016). These differences disappeared after normalising the results to the specific surface area of the particles (Haase et al., 2011).

4.1.2 AgNPs exposure effects in vivo

The exposure effects of AgNPs were investigated in numerous *in vivo* studies mostly using rodent species. Since the here developed model aims to study the effects of orally ingested NMs in the intestine the focus was put on oral exposure *in vivo* studies. Thereinafter, a brief overview will be given for *in vivo* studies applying other routes of exposure (dermal, inhalation, and intravenous / intraperitoneal injection).

4.1.2.1 Oral exposure

Numerous *in vivo* studies have investigated the effects of orally ingested AgNPs (10-323 nm) over 14-days (Skalska et al., 2015; Park et al., 2010a), 28-days (van der Zande et al., 2012; Loeschner et al., 2011; Kim et al., 2008; Lee et al., 2013; Park et al., 2010a; Jeong et al., 2010), or 90-days (Kim et al., 2010) repeated exposure. The most commonly studied endpoints included organ distribution, organ toxicity (van der Zande et al., 2012; Loeschner et al., 2011; Kim et al., 2008; Lee et al., 2013; Skalska et al., 2015; Park et al., 2010a), and immunotoxicity (Ebabe Elle et al., 2013; van der Zande et al., 2012; Park et al., 2010a; Lee et al., 2013). Most of the orally administered Ag was excreted with the faeces, hence, probably did not enter the organism at all (van der Zande et al., 2012). In case Ag was detected in organs, serum, or urine it was not clear, whether it was taken up in particulate or ionic state. Notwithstanding the low uptake, Ag could be detected in several organs, including the stomach, intestine, liver, spleen, kidney, testis, and brain (van der Zande et al., 2012; Loeschner et al., 2011). Whereas Ag was rapidly cleared from most organs, it was found to persist surprisingly long in the brain and testes (van der Zande et al., 2012; Lee et al., 2013). A bio-accumulation, and hence, chronic toxic effects cannot be fully excluded. Additionally, Skalska and colleagues (2015) reported the occurrence of nano-sized granules in the brain structures of Wistar rats after oral exposure to AgNPs (10 nm) but not Ag citrate, indicating a nano- rather than an Ag-associated effect. Several groups observed an increase in hepatotoxicity markers (Kim et al., 2010; Kim et al., 2008; Lee et al., 2013; Park et al., 2010a), as well as indications for the induction of an immune response. Reported effects included the infiltration of organs by immune cells (Lee et al., 2013; Park et al., 2010a), increased release of cytokines (Lee et al., 2013; Park et al., 2010a; Ebabe Elle et al., 2013), and increase in oxidative stress markers (Ebabe Elle et al., 2013). Furthermore, pro-longed oral uptake of AgNPs affected the composition of the intestinal microbiota and induced upregulation of genes related to the gut-associated immune response (Williams et al., 2015).

It has to be kept in mind that most *in vivo* studies are not comparable to realistic exposure scenarios regarding the administration (oral gavage) and concentrations. Whereas the average oral daily intake for Ag species (both particulate and ionic) is estimated between 70-90 µg (Böhmert et al., 2014), exposure concentrations of up to 1,000 mg / kg / day were applied. Based on a 28-day and 90-day oral exposure study a NOAEL (no observable adverse effects level) of 30 mg / kg bodyweight and a LOAEL

(lowest observable adverse effect level) of 125 mg / kg bodyweight were established (Kim et al., 2008; Park et al., 2010a).

Recently, a study on AgNP-exposure in human subjects was published (Munger et al., 2014). Munger and colleagues administered an off-the-shelf colloidal Ag solution to a group of healthy volunteers over a period of 14 days. None of the investigated endpoints, including white blood cell count, pro-inflammatory cytokines, and ROS, showed significant changes.

4.1.2.2 Other exposure routes

Dermal: Due to their bactericidal effects, AgNPs are of interest for the application in wound dressing or anti-bacterial ointments. In a study with healthy human volunteers, AgNPs of a commercially available wound dressing were shown to be able to translocate across the epidermis of intact skin but did not reach systemic circulation (George et al., 2014). However, wound dressings and ointments are often in contact with damaged areas of the skin where the barrier function is most likely impaired. It remains unclear, whether AgNPs would be able to enter deeper tissue layers in this case. Studies on mice and guinea pigs indicated that dermally applied AgNPs might cross all layers of the skin and enter the systemic circulation after prolonged exposure (5 days to 13 weeks) to concentrations between 36 and 10,000 µg / mL (Tak et al., 2015; Korani et al., 2013).

Inhalation: Several *in vivo* inhalation studies reported pro-inflammatory reactions in response to short-term (Seiffert et al., 2015; Braakhuis et al., 2014) and long-term (Sung et al., 2008; Roberts et al., 2013) exposure to AgNPs. Most commonly, mixed cell infiltration into the lung tissue was noted in rats after both single-dose and repeated dose exposure (Seiffert et al., 2015; Sung et al., 2008; Braakhuis et al., 2014). AgNPs could translocate across the lung, enter the systemic circulation, and were distributed to other organs, e.g. the liver, kidney, spleen, heart and testes in mice and rats (Kwon et al., 2012; Takenaka et al., 2001). Whereas AgNPs were rapidly cleared from lung tissue, blood, and most organs clearance in the testes was slow (Kwon et al., 2012).

Injection: Intravenous, intramuscular, or subcutaneous exposure might occur after contact with medical equipment containing loosely-bound AgNPs. Most study designs are based on a single exposure and varying periods of recovery time before the animals

were sacrificed (Rahman et al., 2009; Xue et al., 2012). Few studies exposed animals to a repeated dose of particles between 2 and 28 days (Sarhan and Hussein, 2014; Lankveld et al., 2010; De Jong et al., 2013). When mice were exposed intravenously, the particles were rapidly cleared from the blood stream and detected in various organs (Xue et al., 2012). Ag was mainly found in the spleen, liver, and kidneys (Xue et al., 2012; Dziendzikowska et al., 2012; De Jong et al., 2013; Lankveld et al., 2010). In rats exposed to 5 mg / mL AgNPs, an accumulation of Ag-species was noted in the brain with higher deposition concentrations for 20 nm compared to 200 nm particles (Dziendzikowska et al., 2012). Rahman et al. (2009) observed an upregulation of genes associated with oxidative stress in rats exposed to 500-1,000 mg / kg bodyweight. Tang et al. (2008) noted increased levels of Ag in brain tissue of rats exposed to nano- but not micro-sized Ag (both 62.8 mg / kg) as well as structural changes in the brain tissue. After both intravenous and intraperitoneal injection of AgNPs at concentrations as low as 6 mg / kg bodyweight several biomarkers for renal toxicity and hepatotoxicity were increased in rats (Sarhan and Hussein, 2014; De Jong et al., 2013). Apart from organ-specific toxicity, immuno-modulating effects like increased counts of white blood cells (Sarhan and Hussein, 2014), infiltration of immune cells (De Jong et al., 2013), and organ-specific pro-inflammatory processes (Xue et al., 2012) were reported in mice and rats.

4.1.3 Knowledge gaps concerning the exposure to AgNPs

Even though many studies aimed to elucidate the potential health effects of AgNPs and Ag ions, many questions and contradicting results remain. Deleterious effects were often demonstrated *in vitro* and to a lesser extent *in vivo*, but the actual risk of human exposure remains unclear. From the few available human exposure studies no immediate concerns arise. However, these studies did not account for prolonged exposure and potential accumulation of AgNPs, which might induce chronic toxicity. Furthermore, the great majority of *in vitro* and *in vivo* models do not account for impaired health conditions, e.g. IBD. Several studies indicated that the localisation of NMs differs between inflamed and healthy intestinal tissue (Hassani et al., 2009; Schmidt et al., 2013; Lamprecht et al., 2001). Apart from changes in the uptake, impaired tissue might be more susceptible to the exposure to NMs due to the continuous stress induced by pro-inflammatory cytokines, ROS, and RNS. Despite this clear gap in the literature and the need for disease models (Lefebvre et al., 2015), only very few

groups attempted the development of appropriate *in vitro* models. Such models are of utmost importance to study

- potential pro- or anti-inflammatory effects of NMs.
- the influence of the health status at the time of exposure on the effects of NM-exposure.

One of the most disputed effects is the impact of AgNPs on the immune system and inflammatory processes. Several studies observed anti-inflammatory effects both *in vitro* (Parnsamut and Brimson, 2015; Shin et al., 2007) and *in vivo* (Hebeish et al., 2014; Wong et al., 2009). Other studies found AgNPs to act pro-inflammatory, e.g. inducing release of pro-inflammatory cytokines (Yang et al., 2012; Greulich et al., 2011), modulation of immune cell distribution (Park et al., 2010a), induction of ROS (Greulich et al., 2011; Park et al., 2011; Yang et al., 2012) and RNS (Mollick et al., 2015; Singh and Ramarao, 2012).

4.1.4 Aims and hypotheses

The aim was to study the effect of non-toxic exposure concentrations of AgNPs and silver nitrate ($AgNO_3$) (as ion control) in relation to the health status of the *in vitro* model at the time of exposure. The following hypotheses were investigated:

- $AgNO_3$ causes significant cytotoxicity at lower concentrations than AgNPs.
- AgNPs and $AgNO_3$ concentrations that were tested to be sub-toxic in $_{UD}$Caco-2 monocultures can be applied as non-toxic concentration in $_{D}$Caco-2 cells.
- A one-time exposure of the stable co-culture to non-toxic concentrations of AgNPs will affect at least one of the investigated endpoints.
- A one-time exposure of the inflamed co-culture to non-toxic concentrations of AgNPs will affect at least one of the investigated endpoints.
- The exposure to sub-toxic concentrations of $AgNO_3$ will cause different effects than sub-toxic concentrations of AgNPs.
- The effects induced by AgNPs and $AgNO_3$ in the stable co-culture will be different from the effects in the inflamed co-culture.

4.2 Materials & Methods

4.2.1 Chemicals

Citrate, tannic acid (403040), silver nitrate ($AgNO_3$) (209139), Alcian Blue (A5268), and Resazurin sodium salt (R7017) were purchased from Sigma.

4.2.2 AgNPs synthesis

The particles were kindly synthesised by Rita La Spina from the 'Synthesis & Characterisation' (S&C) CG (NBS Unit, JRC, Italy). The synthesis of AgNPs is carried out by reduction of $AgNO_3$ with citrate and tannic acid according to a modified procedure described by Dadosh (2009). For the synthesis, 120 µl of tannic acid ($2x10^{-3}$ M) were added to 6 ml of citrate (28 mM) and stirred at 60°C for 15 min. Subsequently, 6 ml of the solution were added to 94 ml of 0.55 mM $AgNO_3$ in boiling condition and vigorous stirring and kept at 97°C for 40 min. The solution was heated using a microwave synthesis reactor (Discover S, CEM Corporation). The suspension was rapidly cooled down to 40°C and subsequently RT. Every batch of AgNPs was characterised after synthesis to confirm compliance with previous particle characteristics. For dispersant controls, 5 mL of the particle suspension were centrifuged (5,000 rpm, 20 minutes) to sediment the particles. Of the supernatant 90 % were taken from the sample and stored separately at 4°C. This solution primarily contained H_2O and citrate, but also low concentrations of non-reacted tannic acid and $AgNO_3$ could have been present.

The particle stock suspension was analysed for potential endotoxin contamination using a commercially available endotoxin quantitation kit (Thermo Fisher Scientific, 88282) according to the manufacturer's instructions. The analysis was kindly performed by Sabrina Gioria from the IBS CG (NBS Unit, JRC, Italy). No endotoxin contamination was detected.

4.2.3 Characterisation

The AgNPs were characterised in dispersant, as well as after 0, 4, 24, and 48h incubation in MEM-based CCM (Section 2.1.2) at standard culture conditions. All particle suspensions had a concentration of 5 µg / mL.

4.2.3.1 Dynamic Light Scattering (DLS)

The particle size distribution of AgNPs was determined by DLS using a Zetasizer Nano-ZS (Malvern Ltd, UK). Each sample was measured in triplicate at 25°C after an equilibration step of 120 seconds and using an acquisition time of 80 seconds. The hydrodynamic diameter was calculated by the DLS internal software.

4.2.3.2 Centrifugal Liquid Sedimentation (CLS)

CLS was used to determine the particles' hydrodynamic diameter in dispersant and CCM. The disc centrifuge (CPS Instruments, CD24000UHR) was run at 22,000 rpm. A sucrose gradient was established ranging from 8-24 % (w/w) by successively injecting 9 varying ratios of a low density (2 g in 23 g H_2O) and a high density (6 g in 19 g H_2O) sucrose solution and capped with 0.5 mL of dodecane. The gradient was allowed to equilibrate for a minimum of 30 min. The gradient's quality was confirmed with a reference particle analysis (AgNPs 40 nm, Sigma Aldrich, 730807). A PVC calibration standard (0.1 mL) was measured prior to each sample to validate the gradient's stability. Each sample was injected in a volume of 0.1 mL.

4.2.3.3 Spectroscopy using UV-Visible

The AgNPs suspension was analysed with UV-Vis to study the particle size and integrity in dispersant, as well as in CCM. For the measurement, 1 mL of particle suspension was pipetted into clear plastic cuvettes. The baseline was set with water for a wavelength spectrum of 300 to 800 nm. The measurement interval was set to 0.2 nm. Each sample was measured three times. The result is presented as the average of three runs. A background analysis of the appropriate medium was included and subtracted from the AgNP suspension results.

4.2.3.4 TEM analysis

TEM imaging and analysis was kindly performed by Isaac Ojea Jiménez from the S&C CG (NBS Unit, JRC, Italy). For TEM imaging, ultrathin Formvar-coated 200-mesh copper grids (Tedpella Inc.) were coated with Alcian Blue as described by Mast and

Demeestere (2009). The grids were placed onto a drop a particle suspension for 20 min. The particles were visualised using a TEM (JEOL 2100, Japan), at an accelerating voltage of 200 kV. Energy-dispersive X-ray spectroscopic (EDS) analysis was performed with a QUANTAX EDS detector for TEM (Bruker, USA) in automatic acquisition mode and with the same background correction. Samples were stored at 4°C protected from light and analysed within 5 days of sample preparation. The images were subsequently analysed using the software ImageJ.

4.2.4 Cell culture

Caco-2 and THP-1 cells were cultured and maintained as described in Section 2.1.2.

Stable co-culture: For PMA-differentiation, THP-1 cells were seeded in 25 cm^2 culture flasks (3-3.5x10^5 cells in 6 mL CCM) and exposed to 100 nM PMA for 24h. After the differentiation, the adherent cells were washed once with 5 mL pre-warmed PBS. Subsequently, 1 mL pre-warmed Accutase was added to the flask and incubated for 5-10 min at 37°C. The cells were collected and counted in 3 mL fresh pre-warmed CCM. An adequate volume of the cell suspension was transferred to a 12-well plate to achieve a final density of 1.8x10^5 THP-1 cells / well. Additional fresh CCM was added to obtain a final volume of 1 mL / well and the cells were left to re-attach for 1.5 h at standard culture conditions. After exchanging the supernatant with 1.5 mL fresh RPMI-based CCM without mercaptoethanol, a transwell insert with $_D$Caco-2 cells was transferred to each well to start the co-culture. All experiments were performed without mercaptoethanol since Ag is known to form complexes with thiol-groups (Hsiao et al., 2015), which otherwise could have influenced the outcomes.

Inflamed co-culture: Before the start of the co-culture, Caco-2 layers were basolaterally primed for 18-24h with 10 ng / mL IFN-γ as described by Wang et al. (2005). After the priming, the supernatant was discarded and the BL side of the cell layer washed twice with 1 mL pre-warmed PBS. The cells were left to recover for 2 h before starting the co-culture. THP-1 cells were culture, differentiated, detached and plated as described above. After the cells re-attached to the well bottom, the supernatant was exchanged with 1.5 mL fresh CCM containing LPS and IFN-γ (10 ng / mL each). The cells were stimulated for 4h at standard culture conditions before starting the co-culture.

In each exposure experiment an unexposed control of all three culture models (Caco-2 monoculture, stable, and inflamed co-culture) was included. The control co-cultures had to fulfil the criteria defined earlier (Section 2.2.3.1 & 2.2.4.1).

The transwell cultures were monitored with regular measurements of TEER (Section 2.1.4) at the start of the co-culture, as well as after 4, 18, 24, 28 and 48h.

4.2.5 AgNPs and $AgNO_3$ exposure

96-well plate: Caco-2 cells were seeded onto a flat-bottom plate at $1x10^4$ cells / well and maintained for 72h at standard culture conditions. THP-1 cells were seeded at a density of $4x10^4$ cells / well and differentiated with 100 nM PMA for 24h. The AgNPs and $AgNO_3$ exposure suspensions/solutions were prepared freshly before each experiment by diluting the stock suspension (0.5 and 0.55 mM, respectively) to 0.02-20 µg / mL in fresh CCM. For the exposure, the cell supernatant was discarded and replenished with 50 µL fresh CCM / well. By adding 50 µL of the AgNP suspension or the $AgNO_3$ solution the exposure concentrations were diluted 1:2, eventually ranging from 0.01-10 µg / mL. After 24-48h of exposure, the supernatants were collected for the quantification of LDH (Section 3.2.3) before the metabolic activity was measured using the Alamar Blue assay (Section 4.2.6). Subsequently, the cells were used for high content analysis (HCA) using the IN Cell Analyzer (Section 4.2.8).

Transwell plates: For transwell experiments, non-toxic exposure concentrations of AgNPs and $AgNO_3$ were chosen based on the cytotoxicity results in $_{UD}$Caco-2 monocultures. The Caco-2 monoculture and both co-culture models were set up as described before (Section 4.2.4) and allowed to equilibrate for 24h before being exposed to 1 or 10 µg / mL AgNPs or $AgNO_3$ equivalent to 1 µg / mL AgNPs. For AgNPs, the exposure suspension was prepared as described above. Briefly, a suspension containing 2 or 20 µg / mL AgNPs was prepared in fresh CCM. By transferring 250 µL of the suspension to 250 µL CCM in the AP compartment a final exposure concentrations of 1 and 10 µg / mL AgNPs, respectively, were obtained. The $AgNO_3$ (stock: 0.55 mM) was directly added to the CCM in the AP compartment.

The exposed transwell cultures were analysed for various endpoints (Figure 4.1). After 4h of co-culture (T_4) and 4 and 24h of exposure (T_{28} and T_{48}), supernatant samples were taken from the BL compartment for the quantification of pro-inflammatory cytokines

(Section 4.2.9). At the end of the co-culture (T_{48}), both AP and BL supernatants were analysed for LDH release (Section 4.2.7) and NO generation (Section 3.2.4). Subsequently, the cells were fixed in 3.7 % formaldehyde and used for HCA using the IN Cell Analyzer (Section 4.2.8).

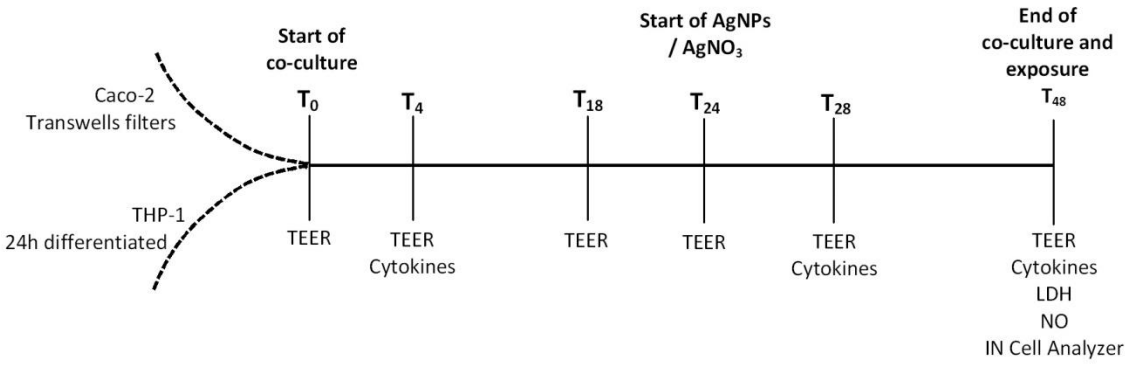

Figure 4.1 Schematic overview of the co-culture and exposure time line

4.2.6 Alamar Blue assay

The Alamar Blue Assay was used to study the cytotoxic effect of AgNPs and $AgNO_3$ $_{UD}$Caco-2 and THP-1 monocultures via the quantification of metabolic activity.

After 24-48h exposure to AgNPs or $AgNO_3$, the cells were washed twice with HBSS. Subsequently, 100 µL fresh CCM containing 100 µM Resazurin was added to each well and the plates incubated for 2h at standard culture conditions. The fluorescence was measured spectrophotometrically at 530 nm emission and 590 nm excitation wavelength. Each experiment included a negative control, a dispersant control, a positive control (20 µM sodium chromate), and a blank in cell-free CCM. The results were corrected for the blank and expressed as metabolic activity in % of the negative control.

4.2.7 LDH assay

The LDH assay was used to study the cytotoxic effect of AgNPs and $AgNO_3$ via the enzymatic activity of LDH after 24-48h exposure. The assay was mainly used for the assessment of cytotoxicity after cellular exposure in transwells. Sample acquisition and analysis was performed as described earlier (Section 3.2.3).

4.2.8 IN Cell Analyzer: Count of DAPI-stained nuclei

To confirm the results obtained from the Alamar Blue and / or LDH assay an automatized cell count was performed based on the imaging and analysis of DAPI-stained nuclei with the IN Cell Analyzer 2200 (GE Healthcare, UK). The image acquisition and analysis was kindly performed by Patricia Urbán from the IBS CG (NBS Unit, JRC, Italy).

After the exposure to AgNPs, $AgNO_3$, and / or at the end of the co-culture, Caco-2 cells were stained as described in Section 2.1.6.

96-well plates: During acquisition, a minimum of 12 fields were imaged per well using a 20x objective. The data analysis was performed on the IN Cell Investigator Software (GE Healthcare, UK) using in-house developed protocols with a minimum of 10,000 cells in the negative control. The cell viability was calculated by determining the percentage of nuclei in the exposure conditions compared to the number of nuclei in the negative control.

Transwell plates: During acquisition, a minimum of 12 fields per filter were imaged using a 60x objective. To obtain a higher resolution, images were acquired as a z-stack of three images (1 µm each), which was eventually converted into a 2D image using the IN Cell Investigator Software. The data analysis was performed on the IN Cell Investigator Software and in-house developed protocols. The analysis protocol was developed using three different targets for the nuclei: seed, nuclei, and bright nuclei. The '*seeds*' were analysed to enable an accurate segmentation of the nuclei, since the filter-grown monolayers contained high numbers of densely packed and partially overlaying cells. The '*nuclei*' target was used to count the total number of cells in each sample. The '*bright nuclei*' target was defined to identify small excessively bright nuclei that were seen in some of the experimental conditions. Using these three targets, the analysis protocol measured in each condition: the number of nuclei, the number of bright nuclei, the total intensity of the nuclei, the intensity of the bright nuclei, the total intensity per cell number, and the percentage of bright nuclei per total number of nuclei.

4.2.9 Cytokine quantification

Apart from the analysis of IL-1β, IL-8, and TNF-α with conventional ELISA (Section 2.1.8), the concentrations of MCP-1, MIP-1α, IFN-γ, IL-4, IL-6, and Granulocyte Macrophage Colony-Stimulating factor (GM-CSF) were quantified using a magnetic bead-based assay analysed with the Bio-Plex MAGPIX Multiplex Reader (Bio-Rad,

171B50-004, 006, 018, 019, 021, 022, 026). For the analysis, supernatant samples were taken from the BL compartment at T_{28} (Figure 4.1).

The magnetic anti-cytokine beads (25x stock) were diluted 12.5-times in Bio-Plex Assay Buffer and a master mix was prepared of all anti-cytokine beads at equal concentrations. To each well, 25 µL of master mix were added and washed 3x with 100 µL washing buffer before addition of samples, standards, or the blank. Of monoculture and stable co-culture supernatants 50 µL were added to each well. The supernatant samples of inflamed co-cultures were first diluted 1:2 in diluent buffer. After addition of the samples, the plate was incubated for 30 min at RT on a shaker. After 3 washing steps, 12.5 µL of the detection antibody master mix (1:25 dilution in antibody diluent) were added to each well and the plate incubated for 30 min at RT on a shaker. After 3 washing steps, the wells were incubated with 25 µL streptavidin-PE (1:100 diluted in Assay Buffer) and incubated for 10 min at RT on a shaker. All wells were washed and the beads re-suspended in 150 µL Assay Buffer for the read-out (Bio-Plex MAGPIX, Bio-Rad). For each plate a standard curve (8 concentrations plated in duplicate), as well as two blanks were included. The results were analysed as 4 parameter logfit. Parts of the sample analysis were kindly performed by Dr. Nilesh Kanase from the Nano-Safety Research Group at Heriot-Watt University (Edinburgh, UK).

4.3 Results

4.3.1 Characterisation of AgNPs

After the synthesis, the AgNPs suspension showed a clear, brown-orange colour without visible particulate matter or sediments. Stored at 4°C and protected from light, the AgNPs suspension remained stable with no visible signs of particle precipitation or sedimentation over the course of 6 months (not shown). The characteristics of AgNPs were studied in dispersant and CCM at relevant cell exposure concentrations and conditions. The results obtained with TEM, CLS, and DLS are summarised in Table 4.1.

Table 4.1 Characterisation of AgNPs in dispersant and cell culture medium

Instrument & parameter		Dispersant	Cell culture medium		
			4h	24h	48h
TEM	Size (nm)	23.04 ± 4.2	23.5 ± 6.1	23.7 ± 7.5	19.1 ± 8.34
	Shape	Spherical, few rods	Increasing number of smaller particles		
CLS	Size (nm)	23.6 ± 1.3	19.7	18.4	18.3
	Half Height Width (nm)	4.1	5	5	4.9
DLS	Size (nm)	37.21 / 2.98	76.92 / 10.63	67.74 / 10.04	83.37 / 10.21
	Z-Average	13.09	38.95	34.74	46.07
	PDI	0.524	0.482	0.445	0.443

Nota bene: CLS and DLS results do not account for decreased density of the particles resulting from protein corona formation.

The quantitative analysis of TEM-acquired images resulted in an average diameter of 23 ± 4.2 nm in dispersant with a low-level occurrence of rod-shaped particles (Figure 4.2). The imaging of AgNP suspensions in CCM and subsequent analysis showed an increasing heterogeneity and particle size changes after extended incubation up to 48h. Whereas the particles were evenly shaped and feature a clear-cut border in dispersant, they appeared to bleb in CCM, resulting in the presence of smaller particles (Figure 4.2A). This formation of smaller 'satellite' particles with a size of 2-5 nm was also notable in the quantitative image analysis of the time points and the resulting average particle size and size distribution (Figure 4.2B). After 48h incubation, the average particle size decreased from 23 nm in dispersant to ~19.1 nm in CCM. The appearance of a second population of smaller particles resulted in an increased StDev (from 4.21 nm for pristine particles to 8.34 nm after 48h in CCM).

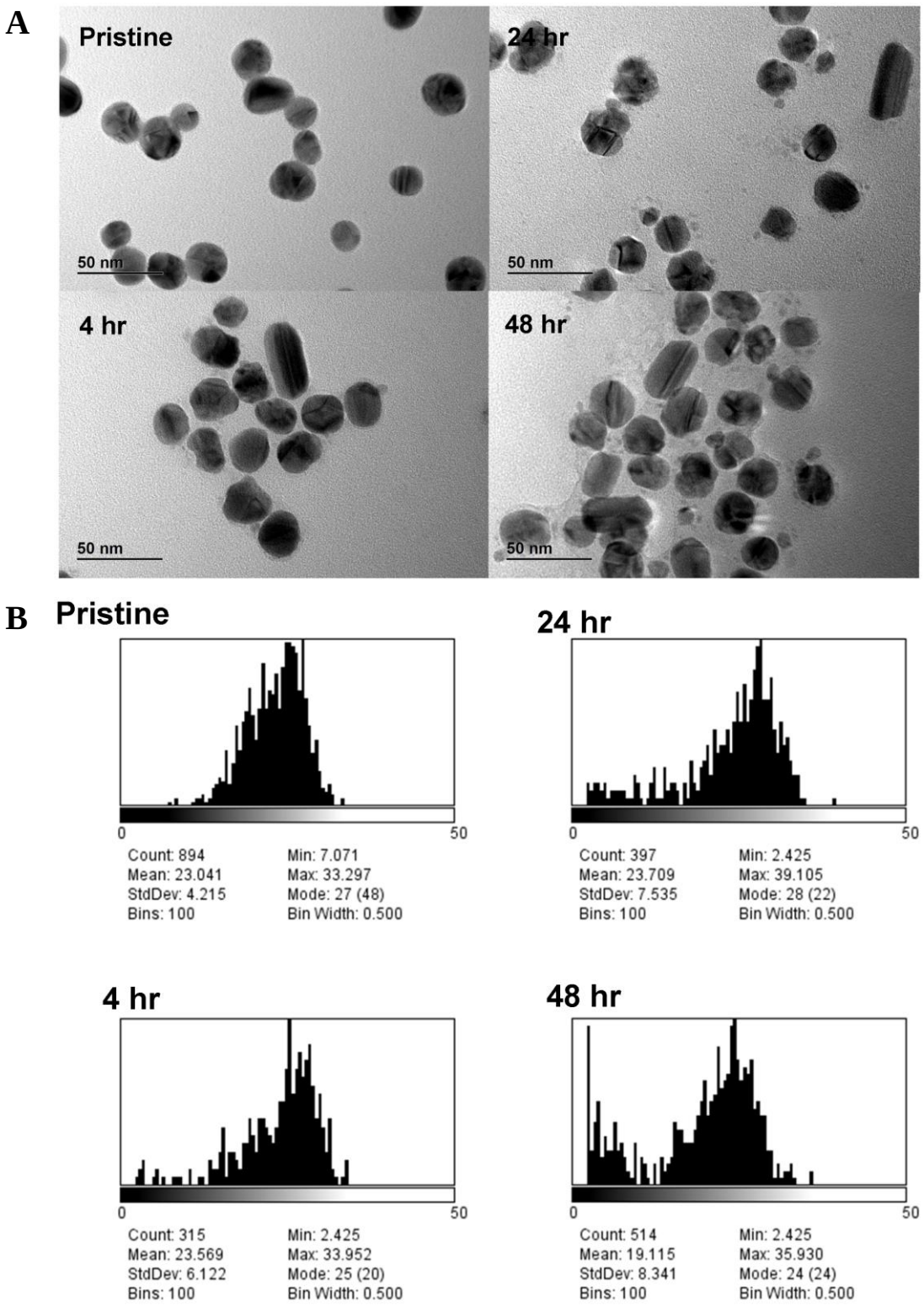

Figure 4.2 TEM imaging of AgNPs in dispersant and CCM and quantitative analysis

(A) Representative TEM images; (B) Quantitative analysis of AgNPs in dispersant (pristine) and after 4, 24, and 48h incubation in CCM at 37°C, 5 % CO_2 (The graphs were kindly provided by Isaac Ojea Jiménez.)

The measurements of hydrodynamic diameter by CLS confirm the observations by TEM. In dispersant, an average hydrodynamic diameter of 23.6 ± 1.3 nm (Figure 4.3A) was measured. The slight shoulder on the left side of the peak (Figure 4.3A) suggested the occurrence of rod-shaped particles in the suspension. When incubated in CCM (Figure 4.3B), the AgNP-associated peak intensity gradually reduced to 57 % of AgNPs in dispersant after 48h. Furthermore, a left-shift of the peak was noted indicating a reduction of the average hydrodynamic diameter to 18.3 nm after 48h.

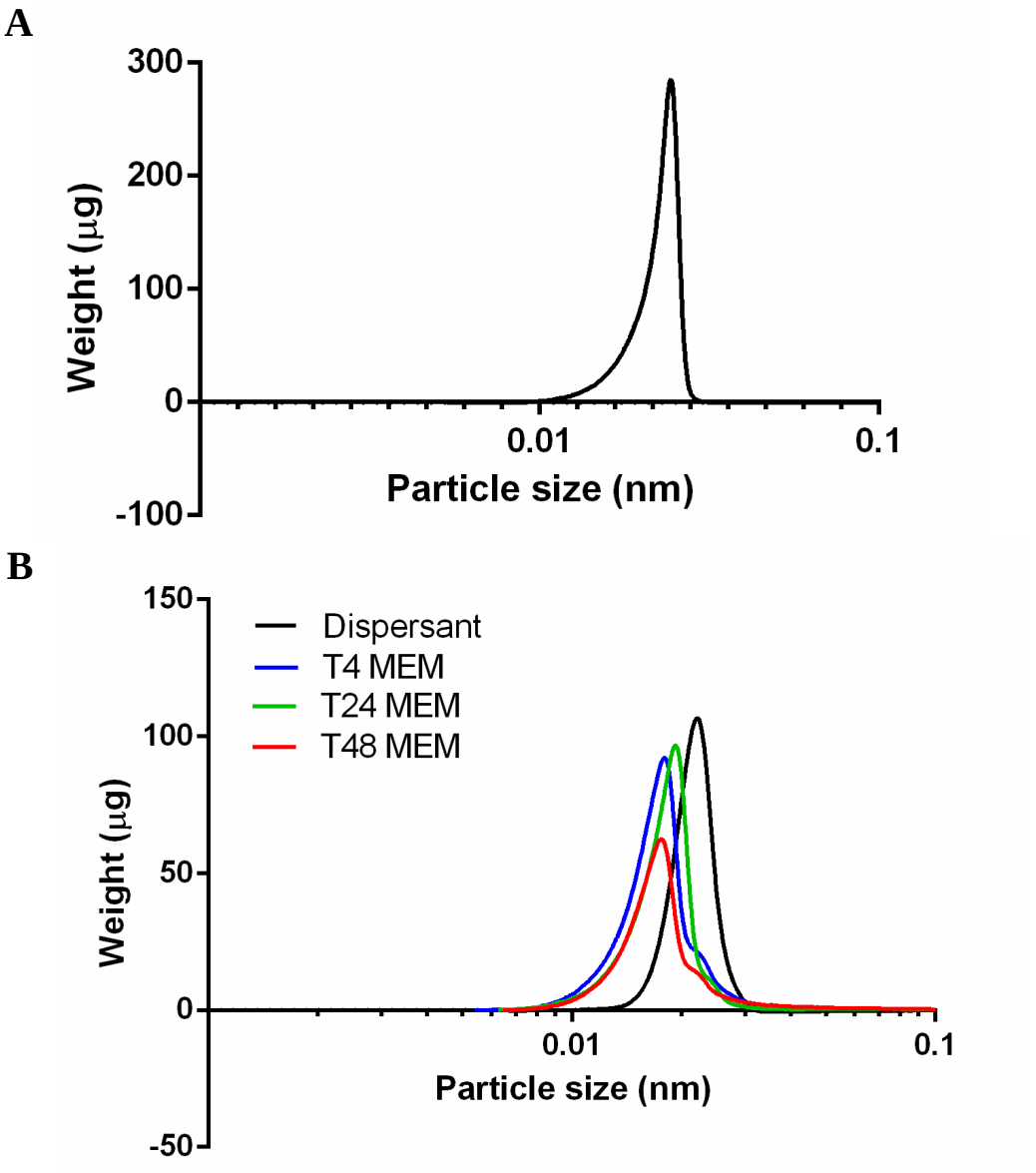

Figure 4.3 Hydrodynamic diameter of AgNPs according to CLS

(A) Stock suspension of AgNPs in dispersant (59 µg / mL); B) AgNPs suspended in dispersant or MEM-based CCM (5 µg / mL) after 4-48h (T4-T48 MEM) incubation at 37°C, 5 % CO_2

The DLS analysis of the particles revealed a high polydispersity index (PDI) in both dispersant and CCM (>0.5 and >0.4, respectively), indicating a substantial heterogeneity of the suspension. The suspected heterogeneity in dispersant was reflected in the occurrence of two peaks in the corresponding DLS graph at 37.21 nm (~72%) and 2.97 nm (~28%) (**Error! Reference source not found.**). In dispersant, the Z-average was 13.09 nm. In CCM, the DLS analysis showed a slightly decreased PDI (0.443-0.482) compared to the measurement in dispersant. After 4h incubation in CCM, the average size of both peaks increased to roughly 77 and 10 nm. Whereas the second population with a size of ~10 nm remained constant throughout the incubation of 48h, the average size of the larger sized population varied reaching an average of 67 nm after 24h and 83 nm after 48h incubation. It is unclear whether the population of small AgNPs is affected by aggregation / agglomeration or the formation of a protein corona after incubation in CCM. Alternatively, the population might not have changed but its signal is overlaid by large quantities of serum protein in the CCM. The latter could explain why the average size of the first peak remains stable at ~10 nm, whereas the average diameter of the second peak changed considerably over a period of 48h.

The UV-Vis spectrum of AgNPs in dispersant (Figure 4.4A) showed a surface plasmon resonance peak at around 400 nm, which is characteristic for nearly-monodisperse 20-30 nm AgNPs (Oldenburg, accessed 2016). Over an incubation time of 24h at standard culture conditions no change in the spectrum was observed. When incubated in CCM, however, the UV-Vis spectrum showed a progressive reduction in AgNP-associated peak intensity, as well as an absorbance shift to higher wavelengths (Figure 4.4B).

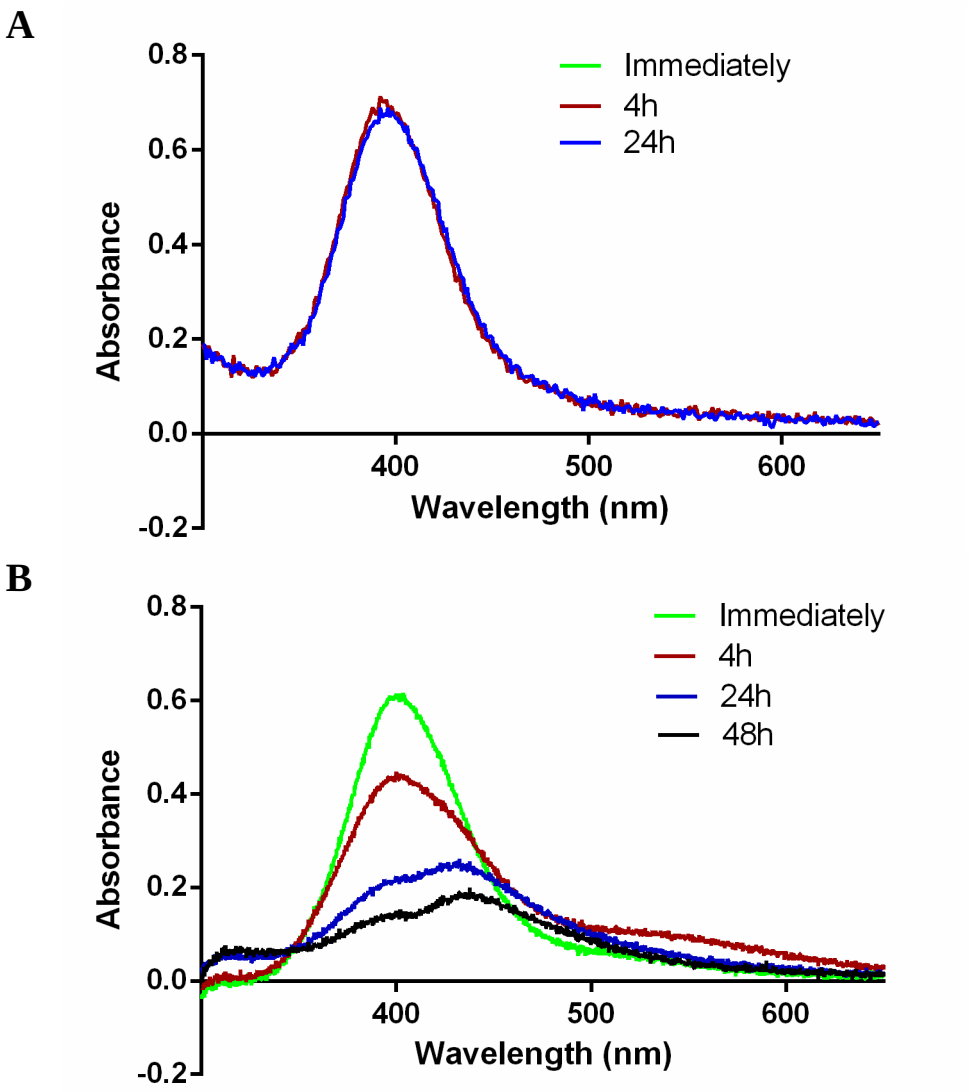

Figure 4.4 Absorbance of AgNPs in (A) dispersant amd (B) CCM as measured by UV-Vis

Absorbance was measured immediately after addition to CCM (green), or after 4h (red), 24h (blue), and 48h (black) incubation in CCM at 37°C, 5 % CO_2

4.3.2 Cytotoxic potential of AgNPs and $AgNO_3$

The cytotoxic potential of AgNPs and $AgNO_3$ was investigated in monocultures of PMA-treated THP-1 cells, non-confluent, and confluent $_{UD}$Caco-2 cells. In Caco-2 cells, cytotoxicity was studied by assessing the metabolic activity with the Alamar Blue assay, LDH release, and number of cells per well by HCA of DAPI-stained nuclei. $AgNO_3$ served as ion control. For THP-1 cells, only the metabolic activity and LDH release were quantified.

Since the transwell cultures will be exposed from the AP side only, Caco-2 cells will most likely be in contact with higher concentrations of AgNPs than the underlying THP-1 cells. Furthermore, studies on the translocation across the intestinal barrier of

NMs so far indicate little to no passage of particles (Schleh et al., 2012; Schmidt et al., 2013). Therefore, higher concentrations were used for the cytotoxicity studies on Caco-2 than for THP-1 cells (1-10 µg / mL vs. 0.01-10 µg / mL, respectively).

Studying the toxicity of AgNPs and $AgNO_3$ in Caco-2 cells was a two-step approach. Firstly, monocultures of $_{UD}$Caco-2 cells were used to establish a range of non-toxic exposure concentrations. Subsequently, these concentrations were used for exposure experiments using the co-culture models and $_{D}$Caco-2 monocultures as controls. Performing the cytotoxicity testing on $_{UD}$Caco-2 cells was decided for several reasons:

1) *Methodological limitations*: Initial experiments on $_{D}$Caco-2 transwell cultures showed that colorimetric assays might not adequately reflect cellular well-being. For instance, whereas the results obtained with the Alamar Blue assay suggested no change in metabolic activity both measurement of TEER and fluorescent imaging of the cells' nuclei showed significant damage of the cell layer (data not shown).
2) As has been shown in the past, Caco-2 cells normally become less sensitive to stressors with increasing confluence and state of differentiation (Gerloff et al., 2013; McCracken et al., 2015). Since this study aimed to investigate the effect of non-toxic concentrations it was decided to establish the exposure dose using the most sensitive (undifferentiated/sub-confluent) and medium sensitive (undifferentiated/confluent) state of the cells. The notion was that any concentration not inducing an effect in these conditions most likely does not induce adverse effects in $_{D}$Caco-2 cultures.
3) *Financial considerations*: The use of transwell cultures is more cost intensive than the application of standard cell culture plates. Firstly, the transwell inserts and compatible well plates need to be purchased. Secondly, the cultures had to be maintained over a period of three weeks, which required larger quantities of serum-containing CCM than a 72h cell culture in 96-well plates.

4.3.2.1 Metabolic activity quantified with the Alamar Blue assay

As presented in Figure 4.5A, concentrations of up to 10 µg / mL of AgNPs did not induce a reduction in metabolic activity after 24-48h of exposure in confluent $_{UD}$Caco-2 cells. It was noted that the confluence of the cells at the time of exposure greatly influenced the cells' vulnerability. Whereas 10 µg / mL AgNPs did not induce any

observable effect in confluent $_{UD}$Caco-2 cells, a significant reduction ($p \leq 0.001$) in metabolic activity by 27 and 30 % after 24h and 48h exposure, respectively, was observed in sub-confluent $_{UD}$Caco-2 cells (Figure 4.5A, 10 SC).

In contrast to AgNPs, the exposure to $AgNO_3$ reduced the metabolic activity in dose-dependent manner starting from concentrations equal to 4 μg / mL AgNPs (Figure 4.5B). No significant differences were observed between 24 and 48h exposed cells.

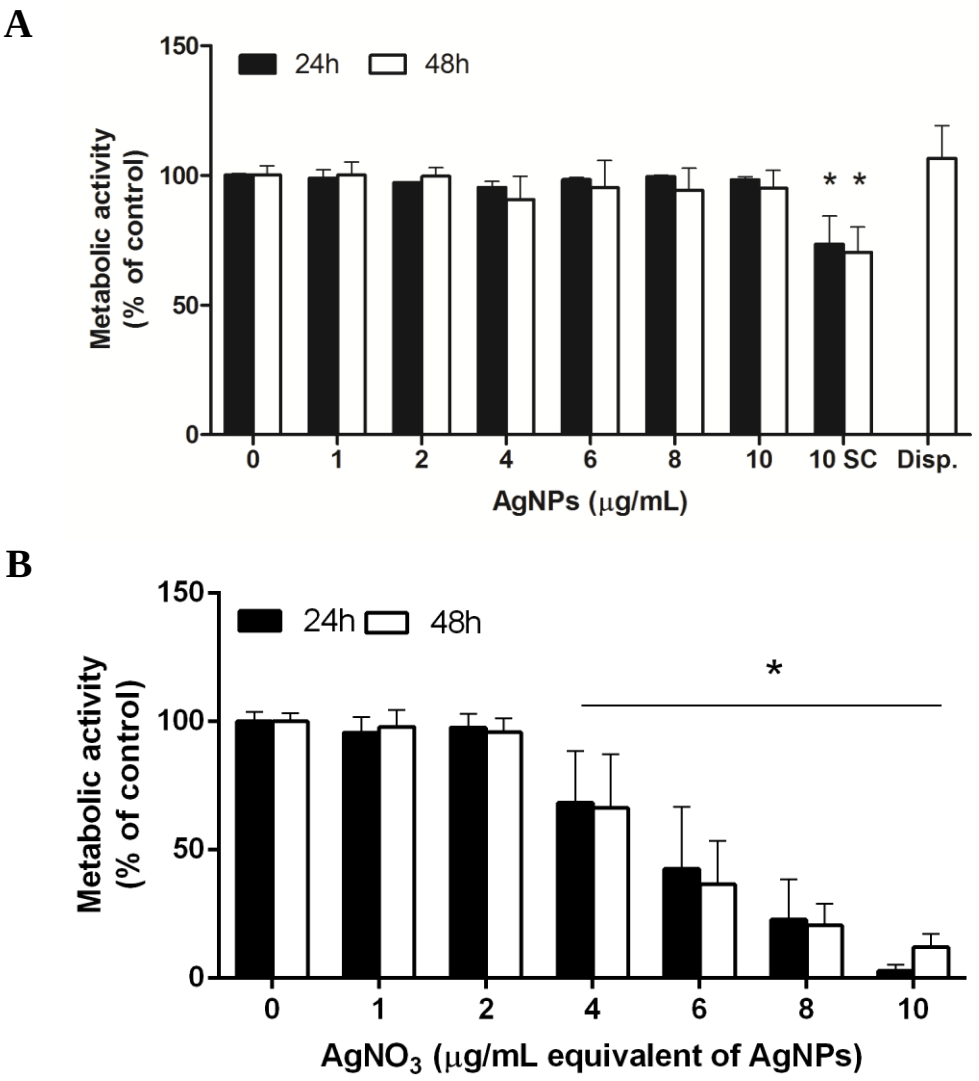

Figure 4.5 Metabolic activity of Caco-2 cells measured with the Alamar Blue assay after 24 and 48h exposure to (A) AgNPs and (B) $AgNO_3$

*(Average of N=3 ± StDev; *p≤0.05 compared to corresponding control)*

The THP-1 cells were expected to be exposed to a much lower concentration of AgNPs, if any at all. Hence, a range including lower exposure concentrations was chosen to assess the cytotoxic potential of AgNPs in PMA-treated THP-1 cells (Figure 4.6). AgNPs concentrations of up to 10 µg / mL did not induce a significant reduction in metabolic activity in PMA-treated THP-1 cells after 48h exposure.

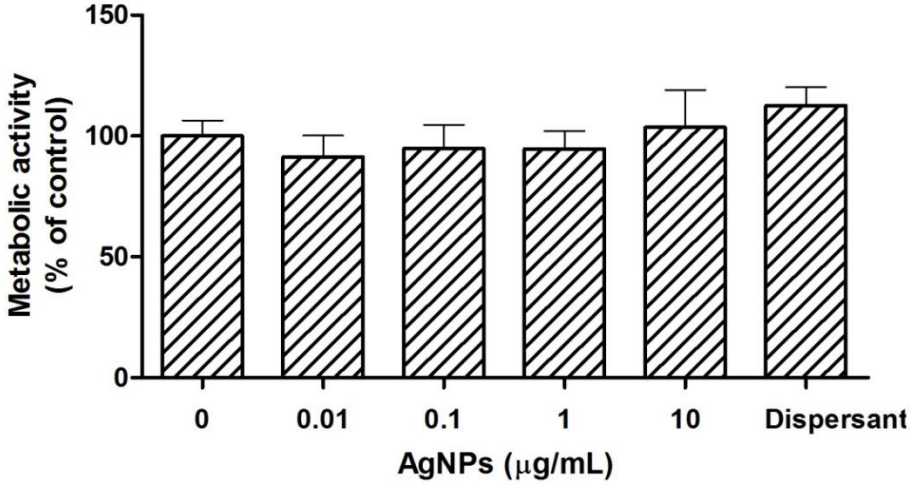

Figure 4.6 Metabolic activity of THP-1 cells measured with the Alamar Blue assay after 48h exposure to AgNPs

(Average of N=3 ± StDev)

Furthermore, $AgNO_3$ exposure concentrations of up to 1 µg / mL did not cause a significant reduction in metabolic activity (not shown).

4.3.2.2 Quantification of LDH release in $_{UD}$Caco-2 cells

As shown in Figure 4.7A, neither 24h nor 48h exposure to AgNPs resulted in an increased release of LDH from $_{UD}$Caco-2 cells at concentrations below 10 µg / mL. After 24h and 48h of exposure to 10 µg / mL, the LDH release was slightly increased compared to the negative control. The changes were not statistically significant ($p=0.741$ and $p=0.097$, respectively).

After 24h exposure to $AgNO_3$ (Figure 4.7B), the levels of LDH were significantly increased in cultures treated with 6 and 8 µg / mL $AgNO_3$. After 48h, a dose-dependent increase in LDH activity was detected at exposure concentrations between 2 and 6 µg / mL $AgNO_3$ (Figure 4.7B). For exposure concentrations between 4 and 6 µg / mL

$AgNO_3$ the increase in LDH release was statistically significant ($p \leq 0.006$). Interestingly, at exposure concentrations ≥8 µg / mL $AgNO_3$ the enzymatic activity increased after 24h exposure, whereas it decreased in samples treated for 48h.

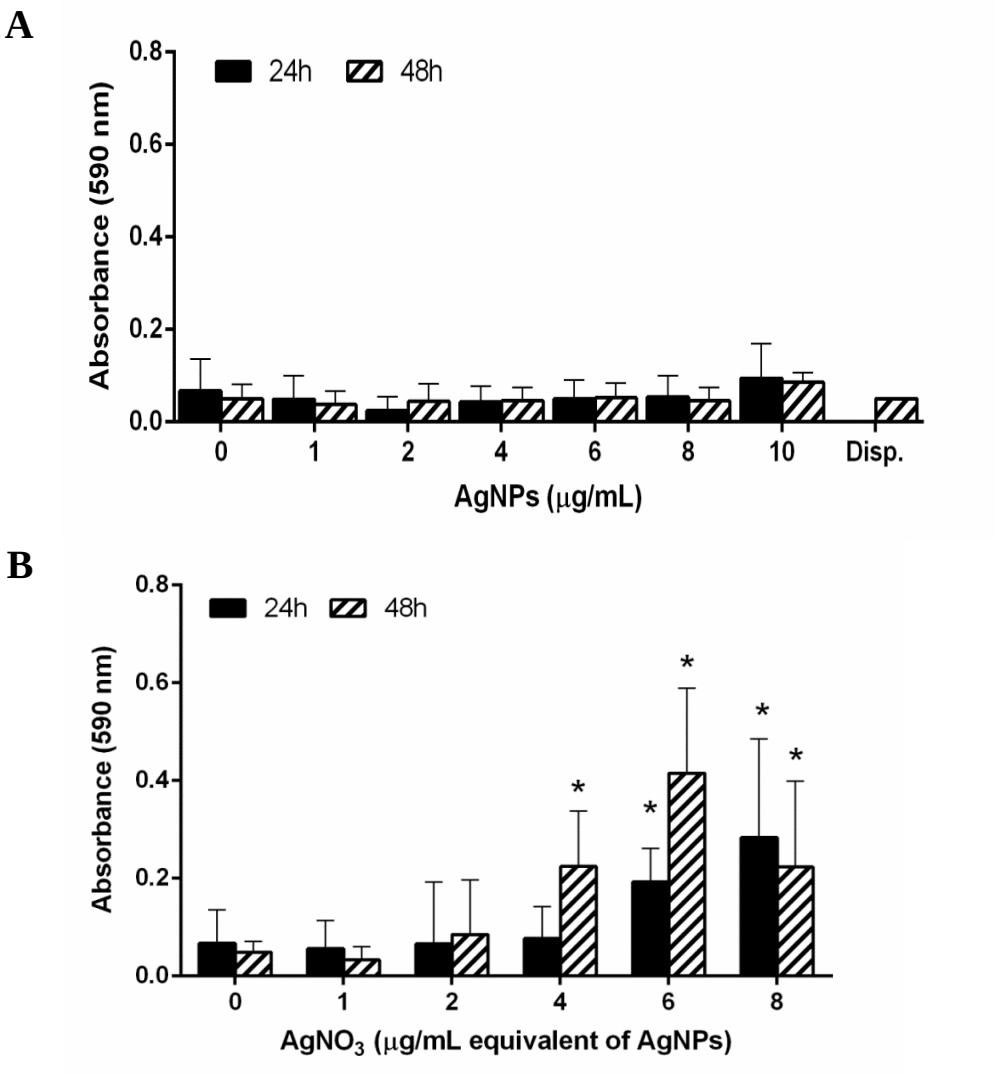

Figure 4.7 LDH release of Caco-2 cells after 24h and 48h exposure to (A) AgNPs and (B) $AgNO_3$

*(Average of N=3 ± StDev; *p≤0.05 compared to corresponding control)*

4.3.2.3 HCA of DAPI-stained Caco-2 nuclei

In addition to the quantification of metabolic activity and LDH release the cytotoxic effect of AgNPs and $AgNO_3$ on $_{UD}$Caco-2 cells was quantified with the analysis of DAPI-stained nuclei using the IN Cell Analyzer (Figure 4.8).

The analysis showed that 24h exposure to up to 10 µg / mL AgNPs did not induce a significant reduction in cell number compared to the negative control (Figure 4.8A). Surprisingly, after 48h exposure the cell numbers were significantly reduced for

exposure concentrations of 4 and 6 µg / mL (p=0.003 and p=0.044, respectively). At lower and higher concentrations of AgNPs no significant differences were detected.

In cultures exposed to $AgNO_3$, the cell numbers reduced drastically in a dose-dependent manner from concentrations as low as 4 µg / mL (Figure 4.8B). The cell numbers were slightly but not significantly lower after 24h compared to 48h exposure. At the highest exposure concentration of 10 µg / mL $AgNO_3$ virtually no cells remained in the wells.

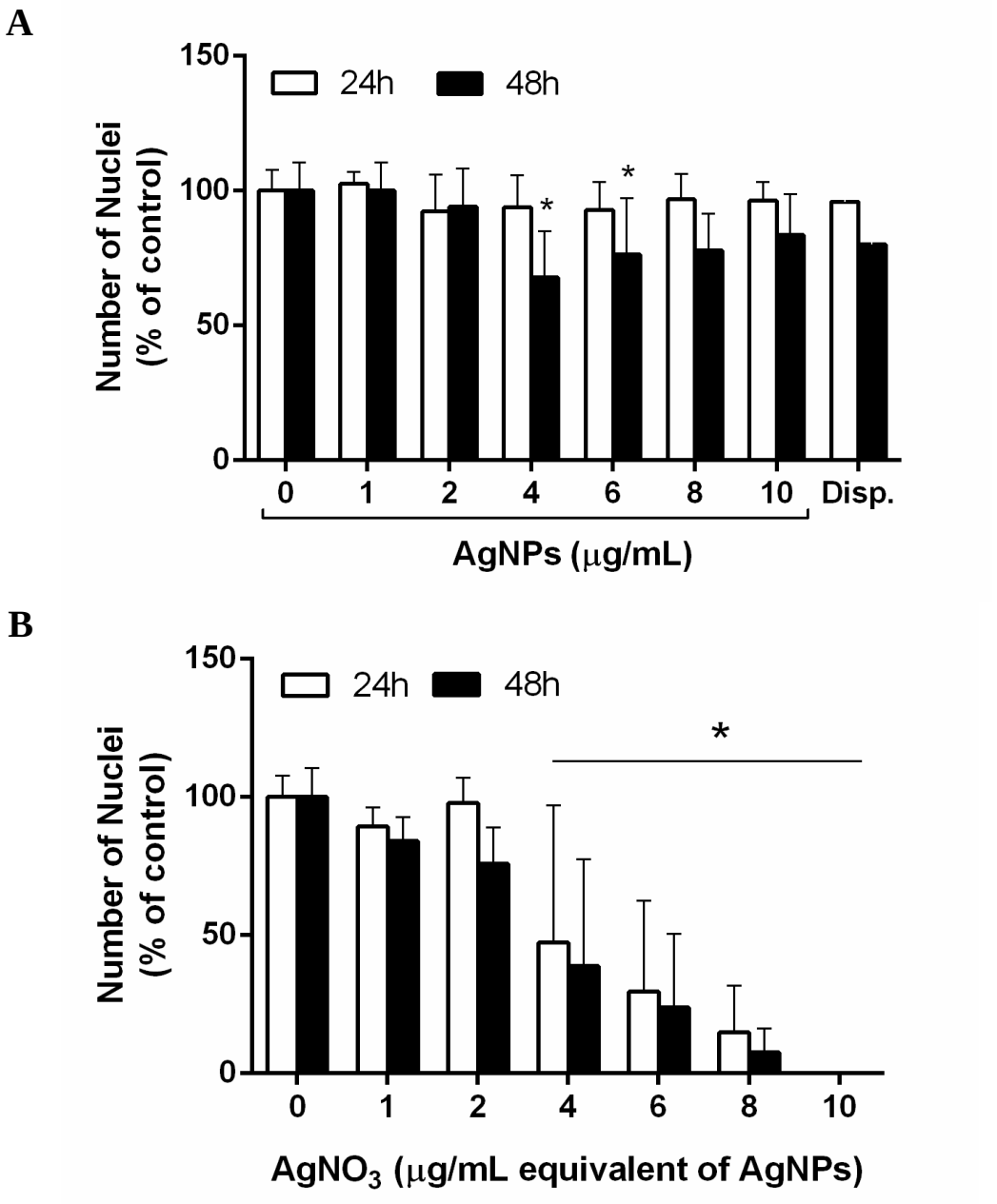

Figure 4.8 Quantification of DAPI-stained nuclei after 24 and 48h exposure to (A) AgNPS and (B) $AgNO_3$

*(Average of N=2, Dispersant and $AgNO_3$ 10 µg / mL: Average of n=3 from one experiment ± StDev; *p≤0.05 compared to corresponding control)*

4.3.3 Exposure of transwell cultures to AgNPs and $AgNO_3$

The Caco-2 monoculture, stable, and inflamed co-cultures were established as described earlier. The cultures were used as unexposed controls or exposed to AgNPs (1 or 10 µg / mL) or $AgNO_3$ (Ag-equivalent to an exposure concentration of 1 µg / mL AgNPs).

4.3.3.1 TEER

To monitor the course of the co-cultures and exposures, the TEER was measured before the start of the co-culture (T_0) as well as after 4, 18, 24, 28 (i.e. 4h after exposure to AgNPs or $AgNO_3$) and 48h (i.e. 24h exposure to AgNPs or $AgNO_3$) of co-culture (Figure 4.1 and Table 4.2). The results are grouped according to the type of exposure (1 or 10 µg / mL AgNPs, and $AgNO_3$) and summarised in Figure 4.9A-C.

Table 4.2 Culture and exposure time points for Caco-2 monoculture, stable, and inflamed co-culture

	T_0	T_4	T_{18}	T_{24}	T_{28}	T_{48}
Co-culture	Start	4h	18h	24h	28h	48h
Exposure	N/A	N/A	N/A	N/A	4h	24h

In the three exposure scenarios, the three culture models (monoculture, stable, and inflamed co-cultures) were directly compared to an unexposed control of each culture model (Figure 4.9, dotted lines). For reasons of practicality only the StDev of the exposed cultures are shown. The StDev of the control conditions were within 3.9-9.2 % (monoculture), 2.8-10.3 % (stable co-culture), and 2.3-7.6 % (inflamed co-culture). The control culture conditions were run additionally in each experiment.

The stable co-culture control was in line with the requirements defined earlier: The TEER did not differ significantly from the monoculture control at any of the investigated time points. In contrast, the TEER of the inflamed co-culture reduced rapidly by ≥25 % compared to the monoculture. From the start (T_0) until 28h of co-culture (T_{28}) the TEER of the inflamed condition was significantly reduced compared to

the monoculture ($p \leq 0.001$) (Figure 4.9A-C; statistical significance not marked). At T_{48}, the TEER of the inflamed co-culture was fully re-established compared to the monoculture control.

As presented in Figure 4.9A, a very low non-toxic concentration of 1 µg / mL AgNPs did not induce a significant effect on the TEER over an exposure period of 24h in any of the three culture models.

When increasing the concentration to 10 µg / mL (Figure 4.9B), the TEER dropped significantly ($p \leq 0.003$) by 8-14 % in all three culture models after 4h of exposure (T_{28}). After 24h of exposure (T_{48}), the TEER of the Caco-2 monoculture and stable co-culture recovered and were equal to the results of the unexposed controls. In the inflamed co-culture, the TEER was significantly increased ($p \leq 0.001$) above the control (127 ± 17.9 %) after 48h of co-culture / 24h of exposure.

To be able to distinguish potential nano-Ag effects from ion effects, $AgNO_3$ was included as ion control (Figure 4.9C). The concentration roughly equals the amount of Ag atoms in an exposure concentration of 1 µg / mL AgNPs. Hence, this dose represents the worst case scenario of a complete dissolution of the particles over an exposure time of 24h. After the first 4h of exposure, no statistically significant differences in TEER were noted in any culture condition. In the inflamed co-culture, 24h exposure to $AgNO_3$ induced a significant ($p \leq 0.001$) increase (133 ± 9.9 %) in TEER compared to the Caco-2 monoculture control. Exposure to $AgNO_3$ also induced a significant ($p \leq 0.003$) TEER increase in the Caco-2 monoculture (120 ± 9.6 %) and stable co-culture (116 ± 8.4 %) after 48h.

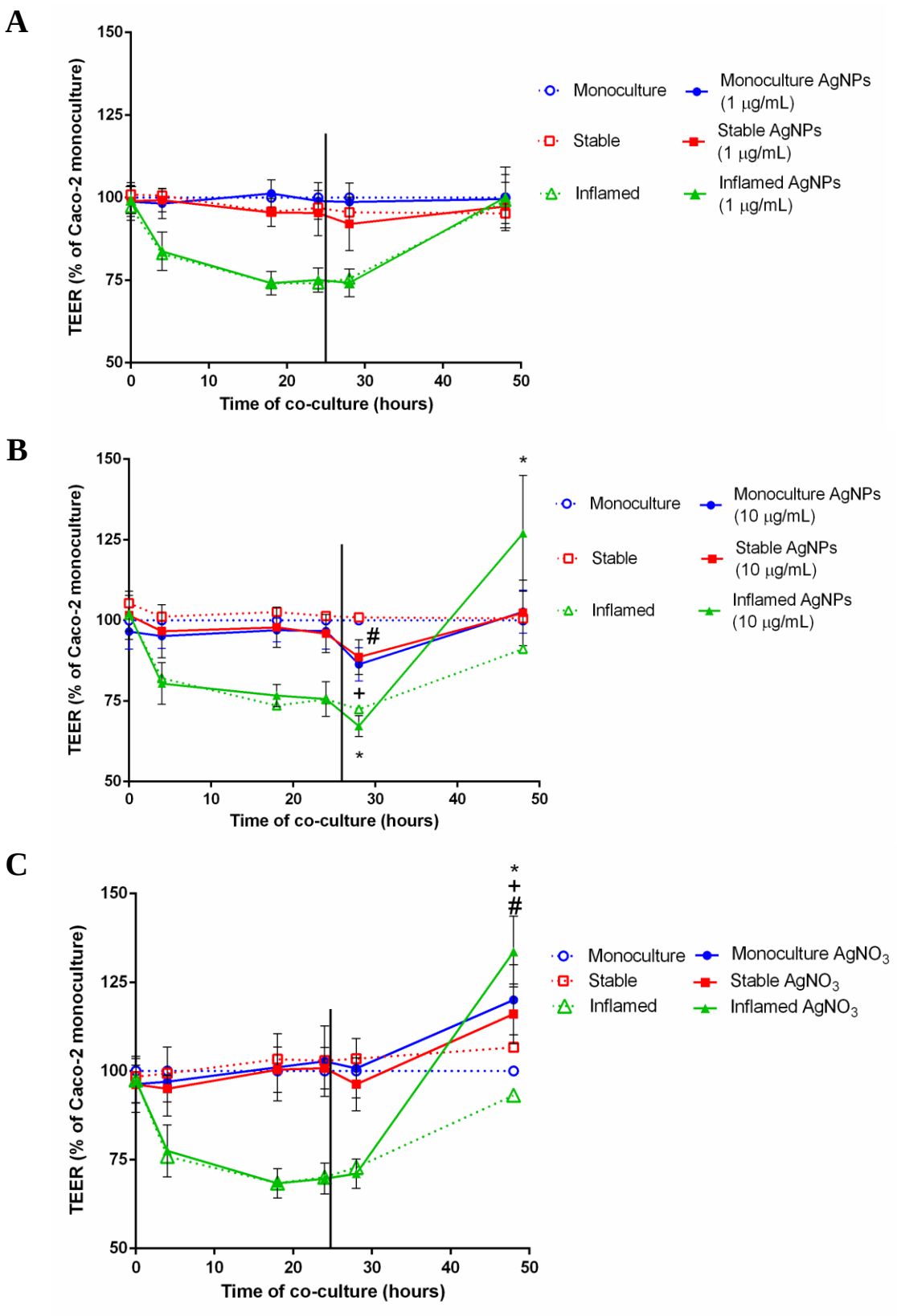

Figure 4.9 Barrier integrity measured as TEER over 48h exposure to (A) 1 µg / mL AgNPs, (B) 10 µg / mL AgNPs or (C) $AgNO_3$ (equivalent to 1 µg/mL AgNPs) in Caco-2 monoculture, stable, and inflamed co-culture

*Black line marks start of exposure (Average of N≥3 ± StDev, *p≤0.05 monoculture compared to corresponding control; $^{\#}$p≤0.05 stable co-culture compared to corresponding control, $^{+}$p≤0.05 inflamed co-culture compared to corresponding control)*

4.3.3.2 LDH release in Caco-2 monoculture, stable, and inflamed co-cultures

The LDH assay was used to quantify potentially occurring necrotic cell death in AgNPs and $AgNO_3$-exposed transwell cultures. As before, the LDH activity was measured in AP and BL supernatants collected at T_{48}.

Similar to earlier results (Section 3.3.1.3), no differences in LDH release were observed in the AP supernatants of the monoculture and stable co-culture (Figure 4.10). In the BL samples of the stable co-culture, a slight non-significant increase in LDH release was noted compared to the Caco-2 monoculture (0.14 ± 0.04 vs. 0.16 ± 0.04). In inflamed co-culture supernatants, the LDH release was significantly increased in both AP and BL compartment.

The exposure to 1 µg / mL AgNPs did not induce an increase in LDH levels compared to the control values in any of the three culture models. The LDH release in the inflamed co-culture control was still significantly higher in the AP and BL compartment compared to the monoculture control ($p \leq 0.001$ and $p=0.004$, respectively), but not different from the inflamed co-culture control ($p=0.646$ and $p=0.528$, respectively). In the AgNP-exposed stable co-culture control, the LDH content of BL supernatants was slightly but significantly ($p=0.03$) decreased compared to the stable co-culture control.

After 24h exposure to 10 µg / mL AgNPs the LDH content of AP supernatants was significantly ($p \leq 0.006$) increased in all three culture models compared to the monoculture control (Figure 4.10). The effect was most pronounced in the inflamed co-culture with a 2.1-fold and 3.7-fold increase compared to the inflamed co-culture control and monoculture control, respectively. In the exposed monoculture and stable co-culture the increase was less clear with 1.12- and 1.14-fold compared to the monoculture control, respectively. In the BL supernatants, no change was noted for the monoculture and stable co-culture. In inflamed co-cultures, the BL LDH release was significantly increased compared to the unexposed Caco-2 monoculture ($p=0.001$), but not compared to the unexposed inflamed co-culture ($p=0.801$).

The exposure to $AgNO_3$ also resulted in higher AP LDH levels in the monoculture and stable co-culture with an increase of 1.29 and 1.57 compared to the corresponding control (Figure 4.10). In the inflamed co-culture, the $AgNO_3$ treatment induced a LDH release which was slightly lower than after exposure to 10 µg / mL AgNPs but still significantly higher compared to the inflamed and monoculture controls ($p \leq 0.001$).

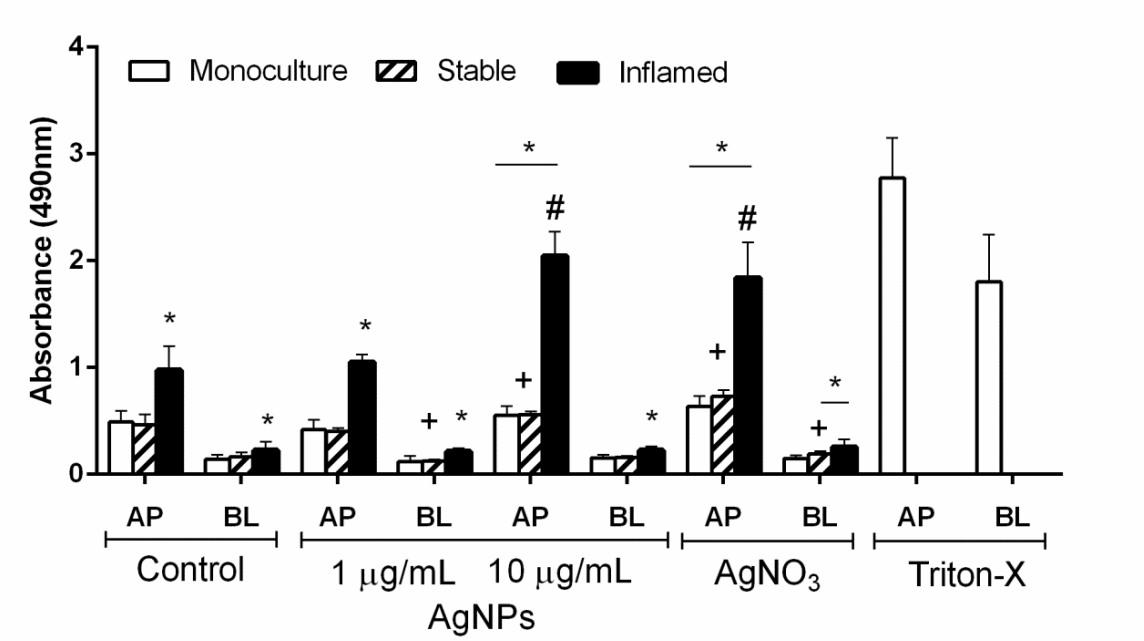

Figure 4.10 LDH release in Caco-2 monoculture, stable, and inflamed co-cultures with and without 24h exposure to AgNPs or $AgNO_3$

*Cultures were exposed to AgNPs (1 or 10 μg / mL) or $AgNO_3$ (equivalent to 1 μg / mL AgNPs) (Average of N≥3 ± StDev; *p≤0.05 compared to monoculture control, $^{+}$p≤0.05 compared to stable co-culture control; $^{\#}$p≤0.05 compared to inflamed co-culture control)*

4.3.3.3 Cytokine release

The cytokine release was investigated in BL supernatants after 4h (T_{28}) and 24h of exposure (T_{48}) to AgNPs (1 or 10 μg/mL) and $AgNO_3$. Supernatants collected after 4h exposure were analysed for TNF-α, IFN-γ, IL-4, IL-6, MIP-1α, MCP-1, and GM-CSF (Figure 4.11 and Figure 4.12). The supernatant samples collected after 24h of exposure were analysed for the presence of TNF-α, IL-8, and IL-1β (Figure 4.13).

4.3.3.3.1 Cytokine release after 4h exposure

For 6 out of the 7 investigated cytokines the results are expressed in pg / mL. For MIP-1α, the concentrations in the inflamed co-culture were above the detection limit (Table 4.3) even after 1:2 dilution of the supernatants. Therefore, the MIP-1α results were expressed as the FI for all three culture models as measured by the Magpix Bioplex instrument.

Table 4.3 Upper and lower limits of detection of the investigated cytokines according to the information made available by the manufacturer

Detection Limit (pg/mL)	TNF-α	IFN-γ	IL-4	IL-6	MIP-1α	MCP-1	GM-CSF
Lower	0.9	2.3	1.2	0.7	0.4	0.3	5.3
Upper	13,878	20,236	4,804	12,000	1,543	4,812	50,000

In the Caco-2 monoculture, most of the investigate cytokines were present at concentrations close to or below the detection limit (Figure 4.11A, white bars). Only GM-CSF and MIP-1α (Figure 4.11B) were released at slightly higher concentrations, however, with high StDev.

In the unexposed stable co-culture, MIP-1α, MCP-1, and GM-CSF were present at concentrations above the detection limit (Figure 4.11, grey bars). Compared to the monoculture, GM-CSF was expressed at slightly lower concentrations (76 ± 96 vs. 124 ± 155 pg / mL). Of MIP-1α and MCP-1 only the levels of the former were significantly higher ($p=0.012$) in the stable co-culture compared to the monoculture.

In contrast to the monoculture and stable co-culture, most of the investigated cytokines were released at high concentrations in the inflamed co-culture control (Figure 4.11, black bars). The levels of TNF-α, IFN-γ, IL-6, MCP-1, and MIP-1α were significantly increased compared to both the monoculture and stable co-culture ($p \leq 0.001$). The concentrations of IL-4 and GM-CSF did not change.

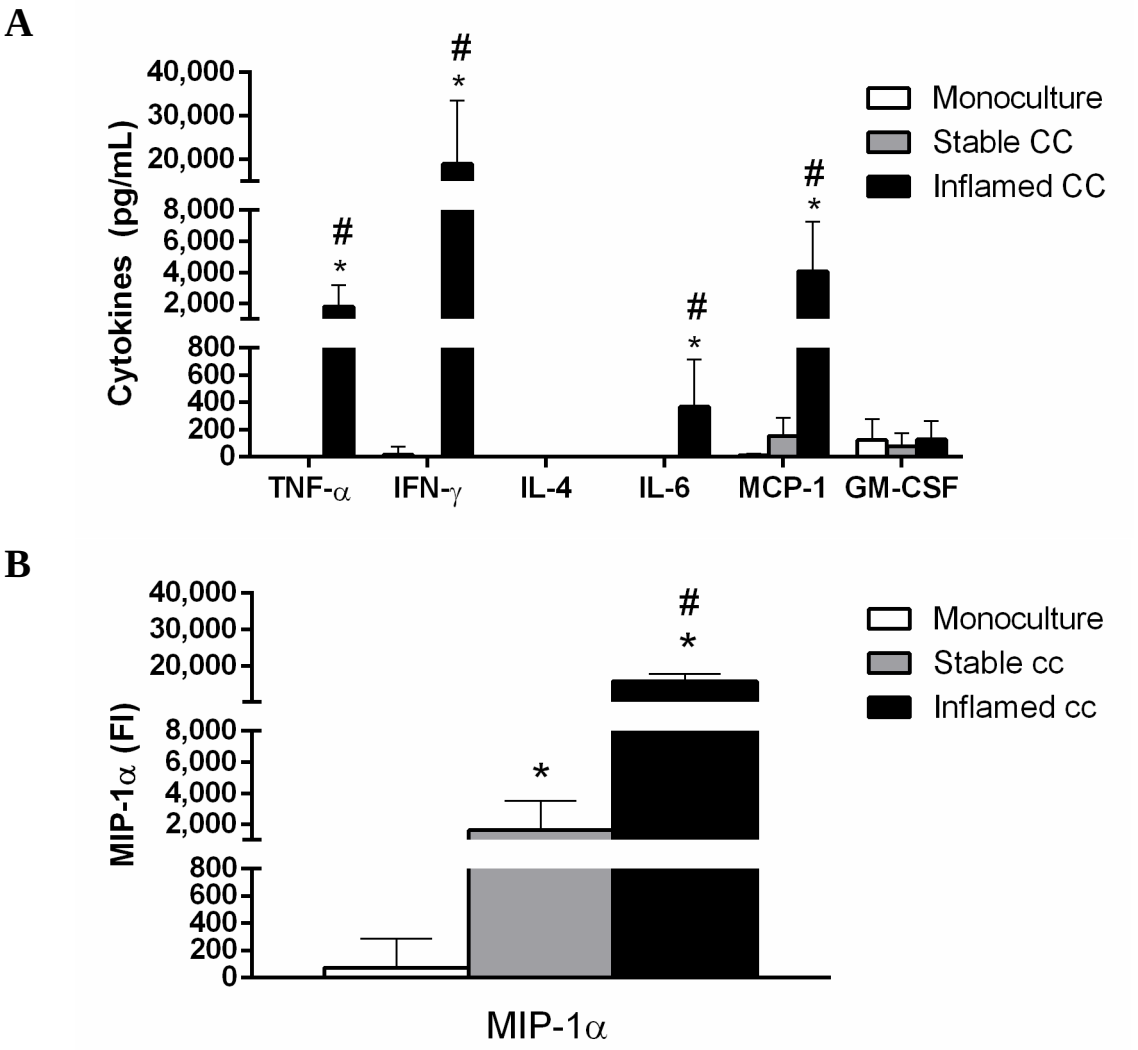

Figure 4.11 Cytokine release after 28h Caco-2 monoculture, stable, or inflamed co-culture

*(A) TNF-a, IFN-γ, IL-4, IL-6, MCP-1 and GM-CSF expressed in pg / mL, (B) MIP-1α expressed as FI (Average of N=6 ± StDev; *p≤0.05 compared to monoculture, #p≤0.05 compared to stable co-culture)*

For some cytokines, the release varied considerably between the individual exposure scenarios. Therefore, the effects of AgNPs and $AgNO_3$ exposure were expressed in % compared to the corresponding control condition (Figure 4.12A-C). GM-CSF concentrations did not change between the culture models and exposure conditions remained close to or below the detection limit. Therefore, the cytokine was excluded from the following graphs.

In the exposed Caco-2 monocultures (Figure 4.12A), TNF-α, IFN-γ, IL-6, and IL-4 remained below the detection limit of the assay. In 2 replicates of the cultures exposed to $AgNO_3$ the release of MIP-1α was greatly increased. In the majority of the samples, however, the concentrations remained comparable to the unexposed control. The

exposure to 1 and 10 µg / mL AgNPs induced a non-significant increase in the levels of MCP-1 to 330 ± 655 and 223 ± 184 % of the control.

In the stable co-culture (Figure 4.12B), TNF-α, IFN-γ, IL-6, and IL-4 were below the detection limit. After the exposure to 10 µg / mL AgNPs, both MIP-1α and MCP-1 were reduced to 21 ± 17 and 44 ± 33 % of the unexposed control. For MCP-1 the reduction was statistically significant ($p=0.033$).

In contrast, all cytokines were detected in the exposed inflamed co-cultures (Figure 4.12C), IL-4 remained close to the detection limit with a maximum of 2.5 pg / mL. Neither the exposure to AgNPs nor $AgNO_3$ caused statistically significant changes in the release of cytokines compared to the inflamed co-culture control.

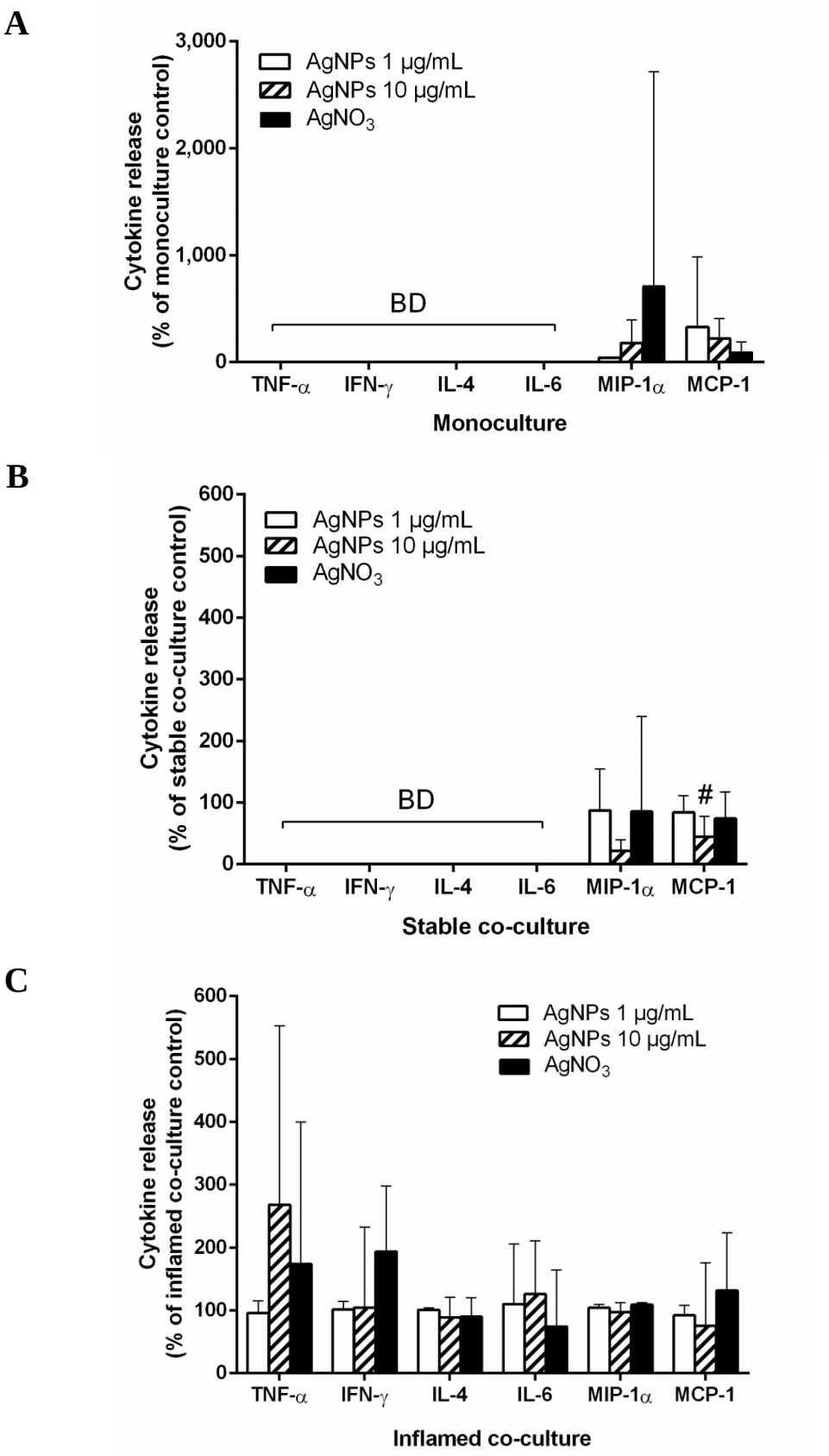

Figure 4.12 Relative change in the release of cytokines after 4h exposure to AgNPs (1 or 10 µg / mL) or $AgNO_3$ (equivalent to 1 µg / mL AgNPs) in (A) Caco-2 monoculture, (B) stable, or (C) inflamed co-culture compared to the corresponding unexposed control

(Average of N=3 ± StDev, $^{\#}p \leq 0.05$ compared to unexposed stable co-culture control; BD = below detection limit)

4.3.3.3.2 Cytokine release after 24h exposure

After 48h of co-culture, a clear difference in the release of IL-1β, IL-8, and TNF-α was detectable between the controls of the three culture models (Figure 4.13A-C). In the Caco-2 monoculture, IL-1β and TNF-α are expressed at concentrations close to or below the assay's detection limit (0.6 ± 1.02 and 3.9 ± 6.4 pg / mL respectively) (Figure 4.13A). IL-8 was detectable in most samples with an average of 123 ± 43.7 pg / mL.

In the stable co-culture, slightly higher concentrations of IL-1β were detected (37.1 pg / mL) (Figure 4.13B). However, considering the overall low release and high StDev of ± 64 pg / mL the amount is negligible. Whereas TNF-α concentrations remained low to undetectable (3.9 ± 4.5 pg / mL) the release of IL-8 was markedly increased to ~3,500 pg / mL. Based on the knowledge that unstimulated PMA-treated THP-1 cells readily release IL-8, this concentration is most likely attributable to the THP-1 rather than the Caco-2 cells.

In contrast to the monoculture and stable co-culture the release of all three cytokines was significantly increased in the inflamed co-culture (IL-1β: 286 ± 254 pg / mL, IL-8: 16,190 ± 5,442 pg / mL, TNF-α: 539 ± 190 pg / mL) (Figure 4.13C).

After the exposure to AgNPs or $AgNO_3$ very few statistically significant differences were observed in the three culture models. In the Caco-2 monoculture, the exposure to $AgNO_3$ resulted in a significant ($p=0.048$) 10-fold increase in IL-1β to 6.09 ± 14.2 pg / mL. In both the stable and inflamed co-culture exposure to $AgNO_3$ did not cause a change in the release of the three investigated cytokines.

The exposure to 10 µg / mL AgNPs induced a slight but significant increase ($p=0.027$) in TNF-α in the stable co-culture (11.1 ± 13.5 pg / mL) and a decrease ($p=0.05$) of IL-1β in the inflamed co-culture (80.1 ± 50.8 pg / mL). Even though these alterations were statistically significant it remains questionable, whether such minimal changes in cytokine release would have a pathophysiological impact.

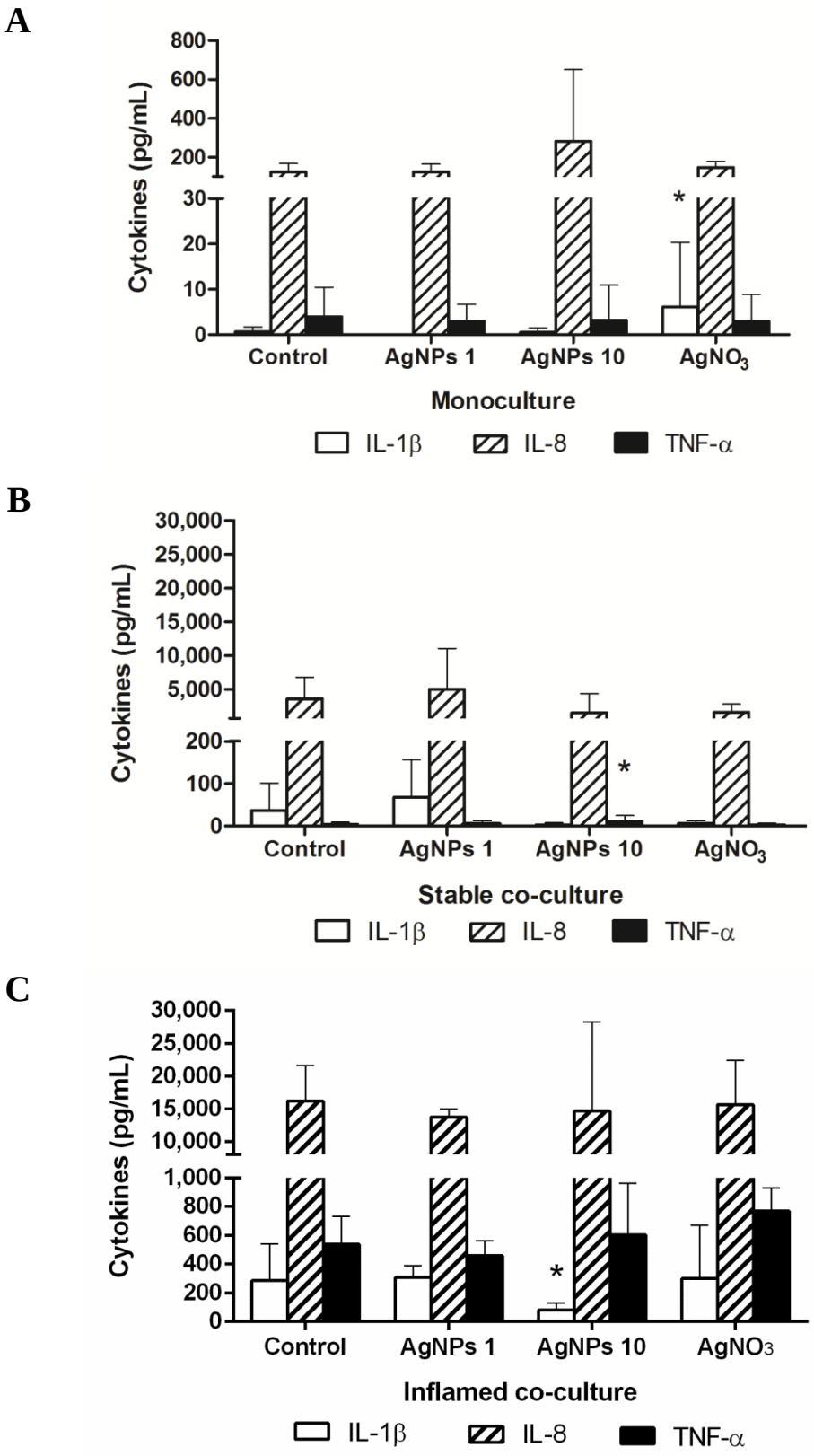

Figure 4.13 Release of IL-1β, IL-8, and TNF-α after 24h exposure to AgNPs (1 or 10 µg / mL) or $AgNO_3$ (equivalent to 1 µg / mL AgNPs) in (A) Caco-2 monoculture, (B) stable co-culture, and (C) inflamed co-culture

*(Average of N≥3 ± StDev; *p≤0.05 compared to corresponding control)*

4.3.3.4 Quantification of NO_2^- release

At T_{48}, cell supernatants from the AP and BL compartment were analysed for the presence of NO_2^- (Figure 4.14). As mentioned earlier (Section 3.4.1.3), the presence of NO_2^- could not always be detected in inflamed co-cultures. Also after the treatment with Ag-species, NO_2^- was not detected in the inflamed co-culture of all experimental runs. Since the inflamed co-culture served as positive control only runs with clearly detectable concentrations of NO_2^- in the inflamed co-culture control were used for the analysis. No valid results could be generated from co-cultures exposed to 10 µg / mL AgNPs.

In Caco-2 monocultures, very low concentrations below 3 µM NO_2^- were detected in both AP and BL compartments (Figure 4.14, white bars). In the inflamed co-culture the detectable concentration of NO_2^- was significantly increased in both AP and BL compartments compared to the monoculture (250 and 270 %, respectively) and stable co-culture (290 and 270 % respectively) control. After exposure to 1 µg / mL AgNPs and $AgNO_3$, the release of NO_2^- decreased in both the AP (43 and 35 %) and BL (16 and 53 %) compartment of Caco-2 monocultures. These changes were, however, not statistically significant. In contrast, treatment with 1 µg / mL AgNPs elevated the NO_2^- concentration in the stable co-culture by 130 and 180 % in the AP ($p=0.41$) and BL ($p=0.004$) compartment, respectively. In samples from inflamed co-cultures exposed to AgNPs or $AgNO_3$ the levels of NO_2^- significantly exceeded the concentrations measured in exposed monocultures and stable co-cultures (not marked), but were not significantly different from the inflamed co-culture control.

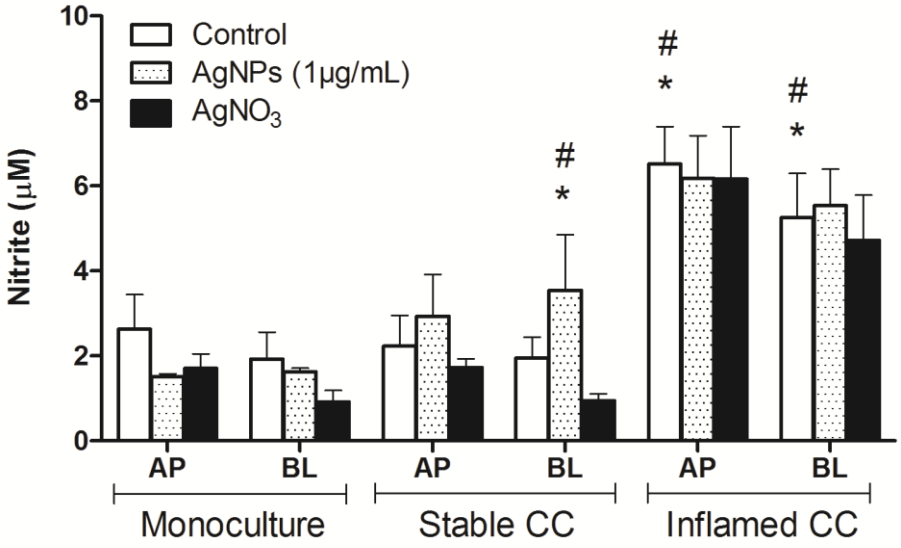

Figure 4.14 Quantification of NO_2^- in AP and BL supernatants after 48h Caco-2 monoculture, stable, or inflamed co-culture (CC) with and without 24h exposure to AgNPs (1 µg / mL) or $AgNO_3$

*(Control: Average of N=3 ± StDev; AgNPs Monoculture: Average of n=3 ± StDev from one experiments; Stable and inflamed co-culture: Average of N=2 ± StDev, $AgNO_3$: Average of N=2 ± StDev; *p≤0.05 compared to Monoculture control, #p≤0.05 compared to stable co-culture control)*

4.3.3.5 Quantification of Caco-2 nuclei and nuclear fragmentation

At T_{48}, Caco-2 cell layers of all culture models and exposure conditions were stained for nucleic acid and subsequently imaged using the IN Cell Analyzer. In total, 12 conditions were analysed: Caco-2 monocultures, stable, and inflamed co-cultures as unexposed controls or after 24h exposure to AgNPs (1 and 10 µg / mL) or $AgNO_3$. Example images of all conditions are summarised in Figure 4.15. The results of the quantitative image analysis are presented in Figure 4.16.

In the control conditions of all three culture models the Caco-2 cells form a dense and continuous barrier (Figure 4.15A, E, and I). In the inflamed co-culture control (Figure 4.15I) a number of fragmented nuclei are visible, which are absent in both the Caco-2 monoculture (Figure 4.15A) and stable co-culture control (Figure 4.15E).

No change in total nuclei number was noted after 24h exposure to $AgNO_3$. However, an increased rate of nuclear fragmentation was observed in the monoculture (Figure 4.15B) and inflamed co-culture (Figure 4.15J).

Exposure effects of AgNPs were depending on the concentration and culture model. In the Caco-2 monoculture and stable co-culture no changes were noted after exposure to 1 µg / mL (Figure 4.15C and F). In the inflamed co-culture (Figure 4.15K) the surface area of the nuclei appeared enlarged. In inflamed co-cultures treated with 10 µg / mL AgNPs (Figure 4.15L) a reduction in nuclei and clear increase in nuclear fragmentation was observed compared to the inflamed co-culture control. In the monoculture (Figure 4.15D) and stable co-culture control (Figure 4.15H) no or very low effects were observed after exposure to AgNPs.

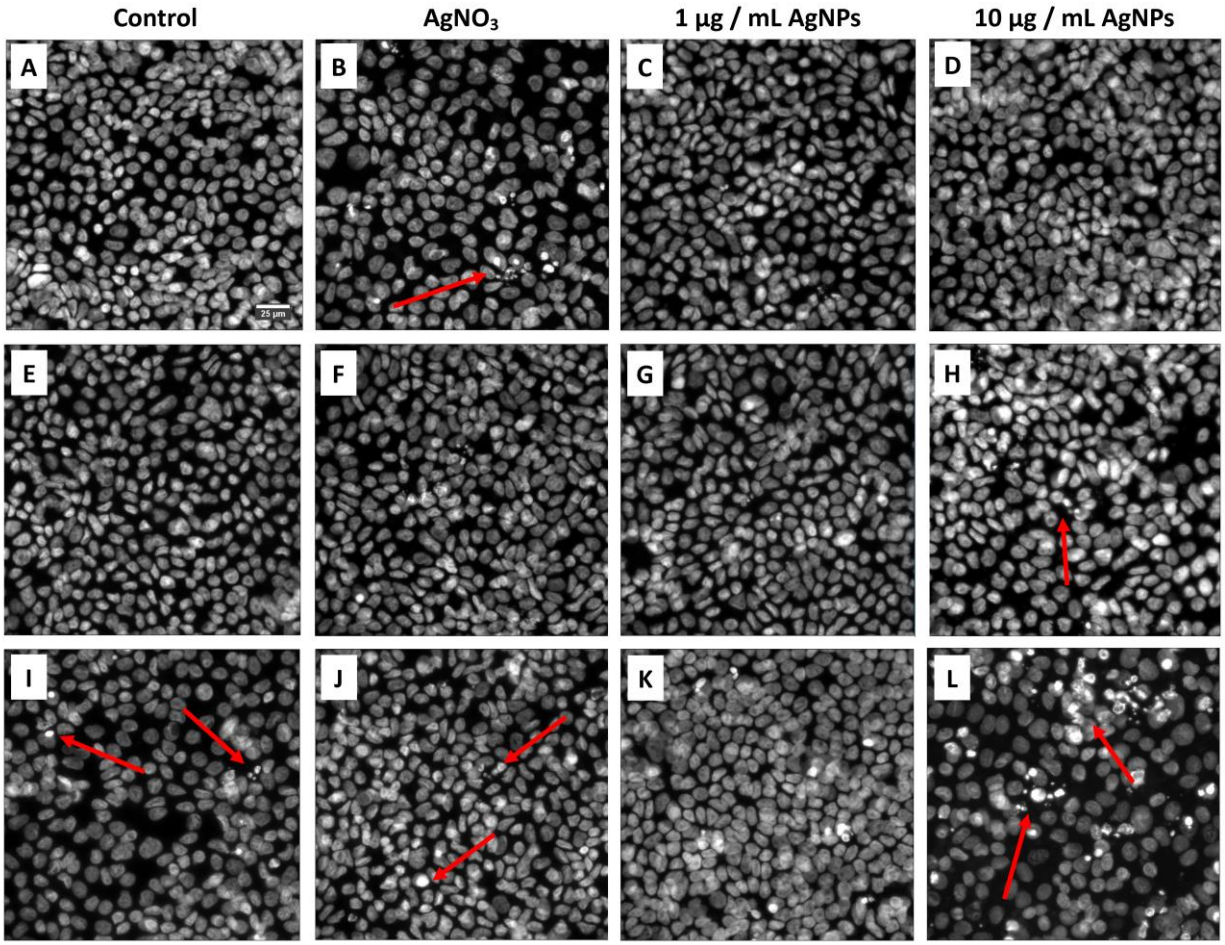

Figure 4.15 DAPI stained nuclei after 48h (A-D) Caco-2 monoculture, (E-H) stable co-culture, and (I-L) inflamed co-culture with or without 24h exposure to AgNPs or $AgNO_3$

Cell cultures were apically exposed to AgNPs (1 or 10 µg / mL) or $AgNO_3$ (equivalent to 1 µg / mL AgNPs) after 24h of mono- or co-culture (imaged with IN Cell Analyzer, 60x magnification, scale bar=25 µm)

The images were analysed quantitatively based on the nuclear staining. The total number of nuclei and 'bright nuclei' were investigated as individual parameters (Figure 4.16A). Since the total number of nuclei varied between the samples, the number of bright nuclei was expressed per 1,000 counted nuclei (Figure 4.16B). The graphs are based on a very limited amount of samples. Therefore, no statistical analysis was performed.

As summarised in in Figure 4.16A, no major differences in the total number of nuclei were noted between the monoculture and stable co-culture control. In the inflamed co-culture the total number of nuclei was slightly decreased compared to the monoculture control (Figure 4.16A). More interestingly, the number of bright nuclei increased from 19 / 1,000 nuclei in the monoculture to 92 / 1,000 in the inflamed co-culture (Figure 4.16A&B).

After exposure to $AgNO_3$, the total number of nuclei was drastically reduced in the monoculture sample (5,902 ± 1,354 vs. 2,907 nuclei). This might change if more samples were analysed. No change was noted in the stable and inflamed co-culture compared to the corresponding control conditions. The number of bright nuclei increased in all three models after $AgNO_3$-exposureto 84, 50, and 159 / 1,000 nuclei in the monoculture, stable, and inflamed co-culture, respectively.

In response to 1 µg / mL AgNPs, the total number of nuclei increased slightly in all three models (Figure 4.16A). Whereas the number of bright nuclei rose marginally in the monoculture and inflamed co-culture it decreased in the stable co-culture compared to the corresponding control (21 vs. 44 / 1,000 nuclei, respectively) (Figure 4.16B). After treatment with 10 µg / mL AgNPs, the number of nuclei decreased in all three culture models compared to the corresponding control (Figure 4.16A), whereas the number of bright nuclei increased clearly. The increase in bright nuclei was most pronounced in the monoculture and inflamed co-culture with 3.6 and 2.8-fold to 66 and 261 / 1,000 nuclei, respectively. In the stable co-culture the number rose moderately (1.8-fold) to 84 / 1,000 nuclei (Figure 4.16B).

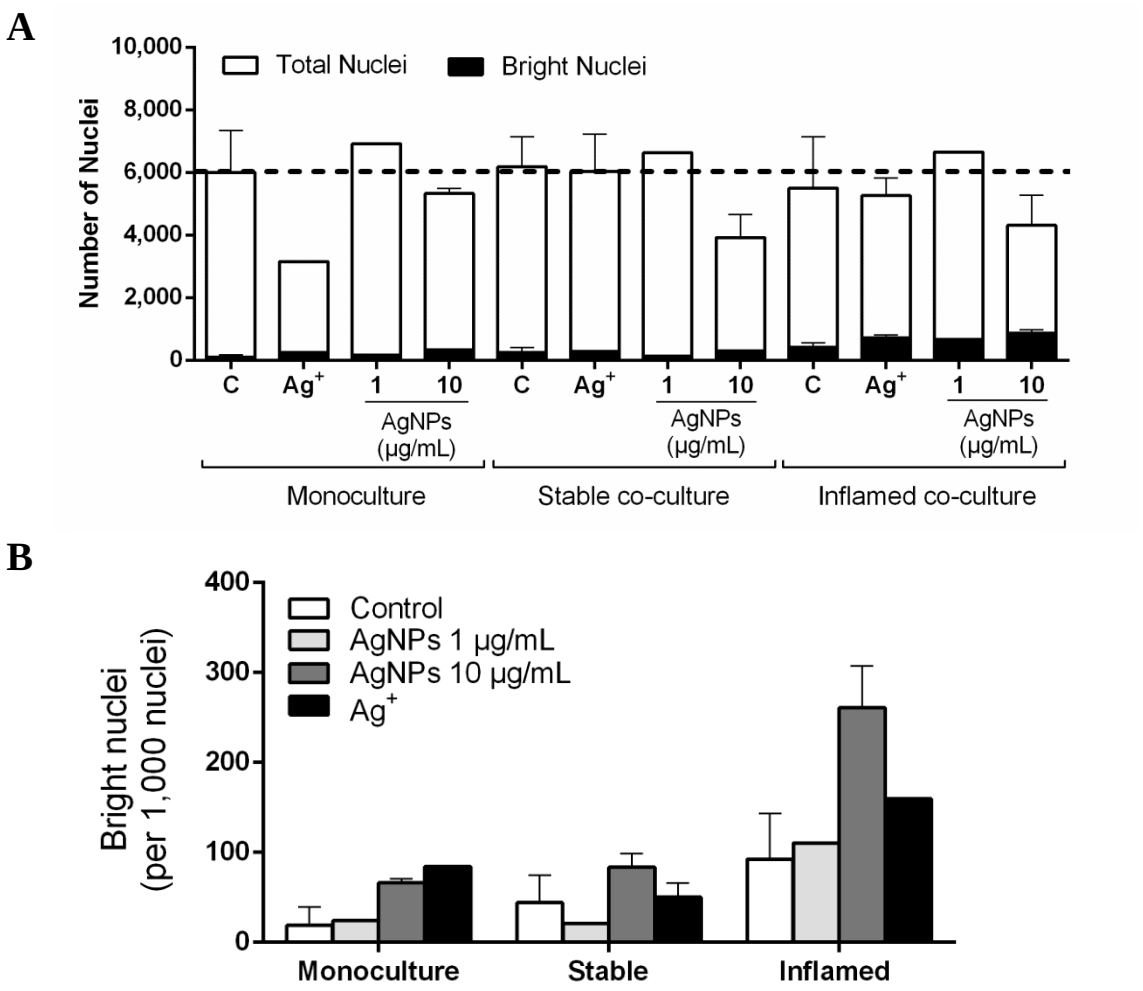

Figure 4.16 Quantitative analysis of images acquired of DAPI-stained nuclei of Caco-2 monoculture, stable, and inflamed co-culture barriers after exposure to AgNPs or $AgNO_3$

(A) Total counts of nuclei and bright nuclei and (B) number of bright nuclei per 1,000 counted nuclei in Caco-2 monoculture, stable, and inflamed co-culture (CC) without exposure (control) and after 24h exposure to $AgNO_3$ or AgNPs (1 or 10 µg / mL) (Controls: Average of n=3 of N=3 ± StDev; $AgNO_3$ monoculture: n=1 of N=1; $AgNO_3$ rest: Average of n=2 of N=2 ± StDev; 1 µg / mL AgNPs monoculture: n=1 of N=1, rest: Average of n=2 of N=2 ± StDev; 10 µg / m AgNPs: Average of n=2 of N=2 ± StDev)

4.4 Discussion

The most important findings of this chapter can be summarised in the following points:

- AgNPs slowly dissolved in CCM at standard culture conditions. Hence, cells are likely not only exposed to 23 nm AgNPs, but also increasing numbers of smaller particles and ionic Ag.
- $AgNO_3$ was more toxic to Caco-2 cells than AgNPs. Whereas concentrations of up to 10 µg / mL AgNPs did not induce a reduction in cell viability $AgNO_3$ concentrations equivalent to ≥4 µg / mL AgNPs damaged Caco-2 cells significantly.
- AgNPs and $AgNO_3$ induced differential effects in the three culture models: Whereas low concentrations of AgNPs did not affect the Caco-2 barrier integrity higher concentrations significantly increased the TEER of the inflamed co-culture. The exposure to $AgNO_3$ markedly increased the barrier integrity in all three culture models.
- The exposure to high concentrations of AgNPs and $AgNO_3$ caused an increased LDH release in all three culture models. Treatment with AgNPs caused a clear increase in the occurrence of fragmented nuclei in the monoculture, stable, and inflamed co-culture, whereas effects of $AgNO_3$ were only detected in the Caco-2 monoculture and inflamed co-culture.
- Neither the exposure to AgNPs nor to $AgNO_3$ caused an effect on the release of cytokines or the formation of NO.

4.4.1 Characterisation of AgNPs

The here used AgNPs showed a homogenous and narrow size distribution in dispersant with an average size of 23 nm. The great majority of particles was of spherical shape with a low level occurrence of rod-shaped particles. After extended incubation in CCM at standard culture conditions the particles appeared to slowly dissolve, which resulted in the formation of a separate population of smaller particles of around 5 nm.

The stability of the particle suspension and the integrity of the particles throughout the exposure are important points to consider for cell-based experiments. The composition of the surrounding matrix, e.g. the presence of proteins and salts, as well as the time of storage and temperature conditions can greatly alter the characteristics of NMs

(Teeguarden et al., 2007). The particles might aggregate or agglomerate, which ultimately impacts the particle size distribution, as well as the sedimentation behaviour (Halamoda-Kenzaoui et al., 2015). In the context of metallic NMs, the dissolution of NMs results in the generation of metal ions, which often have distinct effects on biological systems.

With regard to AgNPs, biological media were demonstrated to negatively affect the integrity, especially of non-stabilised particles (Sharma et al., 2014; Stebounova et al., 2011). The particles used in this study were charge-stabilised by citrate, but not surface modified. In comparison with other capping agents, e.g. polyethylene glycol or polyvinylpyrrolidone, citrate stabilisation was shown to be less effective (Tejamaya et al., 2012). Apart from biological media, the extended storage of particles in the dispersant itself was shown to result in increasing concentrations of Ag^{+}, which lead to a considerable rise in toxicity (Kittler et al., 2010).

The incubation in protein-containing solutions usually leads to the formation of a protein corona. The protein corona greatly determines the 'biological identity' of NMs and can have a significant impact on cellular uptake and NP-induced toxicity (Cheng et al., 2015; Docter et al., 2014). The formation of the protein corona can drastically increase the hydrodynamic diameter, which is measured by both DLS and CLS. Whereas the size-calculation by CLS is based on the light scattering of a particle and the time a particle requires to travel across the sucrose gradient, DLS measurements solely rely on optical properties of the tested material. Since changes in light scattering caused by the protein corona cannot easily be taken into account it can greatly influence the results calculated by DLS. Hence, the results obtained by DLS might not be accurately reflecting the state of the AgNPs. In this study, the measurements performed with CLS generated more reliable results. However, also here, care has to be taken regarding the interpretations. The protein corona reduces the particles' density compared to the density of the uncoated, pristine material. Since the size calculations are based on the original density, an underestimation of the particle diameter is possible.

Depending on the particle characteristics and the type of protein, the incubation of AgNPs with proteins can have beneficial or unbeneficial effects. Whereas both human serum albumin and BSA had a stabilising effect, incubation with high density lipoproteins was shown to even enhance the dissolution (Shannahan et al., 2015). In this project, the incubation in serum-containing biological media affected AgNP-stability negatively. With TEM, the appearance of a population of smaller sized NPs

was demonstrated and the particles' clear-cut border became blurry. It is not clear, how the fraction of small AgNPs developed. The small AgNPs could be remains of dissolving 23 nm particles. Alternatively, they could have originated from Ag^+ released from 23 nm AgNPs, which subsequently precipitated with chloride ions (Groh et al., 2015).

Also the absorbance results obtained with UV-Vis require careful interpretation. The reduction in peak intensity and simultaneous shift of the absorbance maximum from 400 to ~430 nm could indicate a time-dependent aggregation or agglomeration of AgNPs in CCM. Whereas an absorbance maximum at 400 nm is characteristic for AgNPs between 10 and 30 nm, the increase in absorbance maximum and reduction in peak intensity are associated with larger particles of 60-100 nm (Oldenburg and Saunders, accessed 2016; Evanoff and Chumanov, 2005). However, the combination of peak intensity and maximum absorbance at 430 nm is uncharacteristic for larger AgNPs. Furthermore, such a conclusion would contradict the results obtained from TEM and CLS, which pointed towards a size reduction. Based on Mogensen and Kneipp (2014), the decreasing peak intensity and blue-shift in the absorbance spectrum can also indicate a decrease in particle size.

Altogether, the characterisation of AgNPs in dispersant showed an evenly dispersed particle suspension with an average diameter of 23 nm. The great majority of particles were of spherical shape with a low occurrence of rod-shaped particles. Based on the analysis in CCM using TEM, CLS, and UV-Vis, the AgNPs probably dissolve partially over time. Therefore, exposed cells are in contact with metallic, particulate Ag with an average diameter of 23 nm, but will likely also face increasing concentrations of smaller particles (2-5 nm), as well as ionic Ag.

4.4.2 AgNPs-induced cytotoxicity in Caco-2 and THP-1 monocultures

When the $_{UD}$Caco-2 cells were grown to confluence before the exposure, they proved to be more resilient to the exposure to AgNPs. Whereas the viability of sub-confluent $_{UD}$Caco-2 cells was negatively affected by the exposure to 10 µg / mL AgNPs, no significant effect was detected in confluent cells in any of the three cytotoxicity endpoints. In contrast to AgNPs, all cytotoxicity assays confirmed the detrimental effect of $AgNO_3$ exposure. Even at very low concentrations equivalent to 4 µg / mL

AgNPs a significant reduction in metabolic activity, number of nuclei, and increase in LDH release were detected.

Induction of cytotoxicity is one of the most commonly reported exposure effects of AgNPs. However, large variations regarding the minimum effective dose were reported in relation to the cell type and the differentiation status of cells. For $_{UD}$Caco-2 cells, concentrations of 15 and 25 µg / mL were reported to reduce cell viability by 50 and 80 %, respectively (Aueviriyavit et al., 2014; Böhmert et al., 2014). In this context, the here presented results suggest that not only the differentiation state but also the confluence are important determinants for the cells' sensitivity. Caco-2 cells begin to differentiate into enterocyte-like cells upon reaching confluence (Pinto et al., 1983). In general, a period of 20-30 days of culture is accepted to regard Caco-2 cells as fully differentiated. Even though some differentiation markers might be enhanced after 3 days treatment with growth supplements, a culture period of just 72h is generally not sufficient for Caco-2 cells to differentiate (Ferruzza et al., 2012). Hence, the cells used for the initial cytotoxicity tests represent undifferentiated cells.

The higher cytotoxicity of $AgNO_3$ compared to AgNPs was in line with the findings reported by other groups (Oberemm et al., 2016). Since the ion release from AgNPs could not be quantified in this project, an $AgNO_3$ exposure concentration equivalent to 1 µg / mL AgNPs was chosen as ion control. This concentration represents the worst case scenario of 100 % AgNPs dissolution. Neither we nor others observed any cytotoxic effects in $_{UD}$Caco-2 cells at such low concentrations of $AgNO_3$ (Nguyen et al., 2013).

In comparison to the metabolic activity, the LDH release was more variable after the exposure to AgNPs and $AgNO_3$, indicated by large standard deviations. The variations might partially be caused by an interference of Ag-species with the assay similar to the observations by Han et al. (2011). The group demonstrated that copper (Cu) NPs can interfere with the LDH assay through the inactivation of the enzyme. Another group observed that citrate-capped and bare AgNPs can interfere with the assay by adsorbing LDH onto the particle surface (Oh et al., 2014). This could give an explanation for both the generally lower LDH results after 48h compared to 24h exposures and the strongly reduced LDH release after 48h exposure to 8 µg / mL $AgNO_3$. It is not clear at what concentrations AgNPs and / or Ag^+ start to interfere with the accuracy of the assay. It is possible, that Ag-induced cellular damage resulted in LDH releases below the detection limit of the assay. Another possible explanation might be that exposure to Ag species

also induced apoptotic processes. In that case, a reduction in metabolic activity would not be paralleled by an increase in LDH release.

Altogether, concentrations of 1-10 µg / mL AgNPs and an $AgNO_3$ concentration equivalent to 1 µg / mL AgNPs were found to not induce cytotoxic effects in confluent $_{UD}$Caco-2 cells. Since the vulnerability of Caco-2 and other adenocarcinoma cell lines is known to be inversely related to the state of confluence and differentiation status (Pelletier et al., 1990; Böhmert et al., 2014) these concentrations were used as 'non-toxic' in the subsequent co-culture exposure studies.

4.4.3 Effects of AgNPs and $AgNO_3$ in the co-culture conditions

4.4.3.1 TEER

The effect of AgNPs on the culture models was dependent on the exposure concentration. Low concentrations of 1 µg / mL did not affect the TEER in any of the three models. Higher concentrations of 10 µg / mL, however, caused a significant increase in TEER in the inflamed co-culture, but did not affect the Caco-2 monoculture or stable co-culture. A similar effect was observed after treatment with the $AgNO_3$ ion control equivalent to the Ag content of 1 µg / mL AgNPs. Whereas the barrier integrity did not change after short-term exposure (4h) a significant increase in TEER was noted after 24h in all three culture models. It is unlikely that this increase in TEER was caused by the physical properties of Ag. In this case, the effect should have become apparent immediately after the exposure and in all culture models equally.

Based on the reported cytotoxic and barrier disruptive potential of AgNPs and Ag^+ (Martirosyan et al., 2014; Susewind et al., 2016) the significant increase in TEER was surprising. When monitoring the formation of a cell barrier, the increase in TEER corresponds to the cell density and the increasing restriction of the paracellular ion transport by TJ (Anderson and Van Itallie, 2009). An increase in TEER might, therefore, indicate a tightening of the barrier, e.g. due to increased cell numbers or a reduction of intra- and intercellular space as a result of cell swelling. Also others measured a transient increase in electrical resistance in Caco-2 barriers after exposure to NMs. These measures were obtained by means of impedance monitoring and showed an increase in resistance before a drastic decrease in resistance as a result of cell death (Böhmert et al., 2012; Sperber et al., 2015). Increases in impedance have been

associated with expanding cell size (e.g. due to cell swelling) and, in parallel, decreasing extra-cellular volume (Olsson et al., 2006). Cell swelling can be a sign of necrotic cell death (Bonfoco et al., 1995), as was also observed in our group: after the exposure to AgNPs, the analysis of A549 cell surface using the IN Cell Analyzer revealed a substantial increase in the surface area at cytotoxic exposure concentrations (Urbán, unpublished). It was therefore hypothesised that in the present study a significant level of necrotic cell death is induced by the exposure to very low concentrations of $AgNO_3$ in all three conditions and by 10 µg / mL AgNPs in the inflamed co-culture.

Other groups studying the effect of AgNPs in intestinal co-culture models obtained highly different outcomes on cytotoxicity and IEC barrier integrity. Susewind et al. (2016) worked with a model of Caco-2, THP-1, and MUTZ-6 cells in non-inflamed or inflamed state. In contrast to us, the group observed the highest sensitivity to AgNPs in the Caco-2 monoculture with a significant TEER reduction (~20 %) after exposure to concentrations equal to or higher than 78.1 µg / cm². Both the non-inflamed and inflamed co-cultures were more resilient with barrier disruption starting at exposure concentrations of 312.5 and 156.25 µg / cm², respectively (Susewind et al., 2016). Georgantzopoulou and colleagues (2016) studied the effects of AgNPs and $AgNO_3$ in a co-culture of Caco-2 and HT29-MTX cells without involvement of immune cells. The group did not observe any effect on the barrier integrity in cell monocultures or the co-culture for either AgNPs or $AgNO_3$ (Georgantzopoulou et al., 2016). Interestingly, Bouwmeester et al. (2011) observed a similar increase in in barrier resistance after the exposure of Caco-2 cells to AgNPs and $AgNO_3$. Even though the TEER increased to 120-130 % of the control the group did not investigate or discuss this increase further.

4.4.3.2 LDH release

The quantification of LDH activity in AP and BL supernatants confirmed that both $AgNO_3$ and 10 µg / mL AgNPs induced significant cytotoxicity even though both were found to be non-toxic in $_{UD}$Caco-2 cultures. Again, the effect was most pronounced in the inflamed co-culture, supporting the hypothesis that a stressed Caco-2 barrier is more susceptible to the exposure.

The LDH results obtained from $AgNO_3$- and AgNP-exposed $_D$Caco-2 cells clearly contradict the results from numerous studies, which usually showed an increased resilience of Caco-2 cells after differentiation (Gerloff et al., 2013; McCracken et al., 2015). However, a similar observation was reported by Thit et al. (2013) and the exposure of epithelial cells to Cu oxide (CuO) NPs. Differentiated, non-dividing cells were significantly more affected by the exposure to CuO NPs than dividing cells. As a result of the differentiation process of cells, many genes and pathways are up-regulated (Tadjali et al., 2002). It is possible that certain pathways protecting undifferentiated cells against Ag-induced effects are not active anymore after differentiation. Likewise, the differentiation might lead to the formation of additional apical membrane receptors that allow for an increased and / or easier uptake of $AgNO_3$ but not AgNPs (Thit et al., 2013). It is puzzling, though, that this effect has not been observed by other groups.

The results obtained from $_D$Caco-2 monocultures and the co-culture models are in clear contrast to the findings reported by Susewind et al. (2016) and Georgantzopoulou et al. (2016). Both groups observed the Caco-2 monoculture to be more sensitive to the exposure to AgNPs than co-cultures with goblet cells (Georgantzopoulou et al., 2016) or immune cells (Susewind et al., 2016). Furthermore, no adverse effects were noted after exposure to similar concentrations of AgNPs as used in this project. Also the exposure to similar concentrations of $AgNO_3$ was not found to induce cytotoxicity by other groups (Oberemm et al., 2016; Georgantzopoulou et al., 2016). Interestingly, Susewind and colleagues obtained very different results in their inflamed model. The induction of inflammation did not result in increased levels of LDH, indicating that the cell viability was not affected. Furthermore, hardly any difference in response to AgNPs exposure was noted between the non-inflamed and inflamed co-culture. In the here presented experiments, however, the inflamed co-culture reacted significantly more sensitive to the exposure to AgNPs and $AgNO_3$ compared to the stable co-culture, which was reflected in a drastic increase in LDH release.

The induction of necrotic cell death and the associated cellular swelling could explain the TEER increase in the inflamed co-culture (treated with $AgNO_3$ and AgNPs), as well as in Caco-2 monocultures and stable co-cultures (treated with $AgNO_3$). It remains unclear why no increase in TEER was observed in Caco-2 monoculture and stable co-cultures after exposure to 10 µg / mL AgNPs. This is unexpected since the exposure induced similar levels of cytotoxicity according to the LDH results.

4.4.3.3 Quantification of nuclei and nuclear fragmentation

With the HCA of DAPI-stained nuclei we intended to confirm the occurrence of necrotic cell death in response to the exposure to $AgNO_3$ and 10 µg / mL AgNPs. In the monoculture and stable co-culture a very low rate of condensed or fragmented nuclei was found. The induction of inflammation-like processes, however, resulted in increased nuclear fragmentation and reduced number of nuclei. The fragmentation was further increased after exposure to $AgNO_3$ and 10 µg / mL AgNPs. Interestingly, higher concentrations of AgNPs also elevated the occurrence of fragmented nuclei in the monoculture and stable co-culture, but no effect was noted for lower concentrations. Whereas $AgNO_3$ increased the occurrence of bright nuclei in the monoculture and inflamed co-culture it did not induce obvious changes in the stable co-culture.

Whereas the LDH outcomes showed the same trend for all three culture models, the results on the number of nuclei in the different exposure conditions were inconclusive. For instance, the exposure to $AgNO_3$ reduced the number of nuclei in the monoculture but not in either of the co-culture models. In the monoculture and the inflamed co-culture, $AgNO_3$ increased the occurrence of fragmented nuclei. In the stable co-culture virtually no effects were noted even though the LDH release and TEER were clearly increased. In contrast, 10 µg / mL AgNPs clearly reduced the total number of nuclei and increased the rate of bright nuclei in all three models. This is in line with the LDH release, which showed a significant increase in all models, but in contrast to the TEER results, which were only significantly increased in the inflamed co-culture.

The FI, as well as the mean size of the nucleus are important indicators for cellular health and integrity. The binding of DAPI is related to the condensation state of chromatin in the nucleus (Mascetti et al., 2001). The condensation of chromatin and nuclear fragmentation are late events in apoptotic cell death (Tounekti et al., 1995; Collins et al., 1997). Hence, the FI and mean nuclear size can be used for the identification of apoptotic events.

Apoptosis can be induced through various mechanisms, which makes pinpointing the exact route of induction challenging. On the one hand, it could have originated from the IFN-γ-priming of Caco-2 cells before the start of the co-culture. The extended exposure of Caco-2 cells to IFN-γ has been demonstrated to induce apoptosis and to decrease cell proliferation (Nava et al., 2010). On the other hand, the cell damage might be directly linked to co-culture with stimulated THP-1 cells. TNF-α is known for its ability to

induce apoptotic mechanisms (Miura et al., 1995), whereas NO can be involved in both apoptotic and necrotic cell death (Liu et al., 2003; Bonfoco et al., 1995).

Also AgNPs have been shown to induce apoptosis in various cell types (Lee et al., 2011; Xue et al., 2016). For Caco-2 cells, however, no apoptotic effect of AgNP-exposure has been observed in either differentiated or undifferentiated state (Böhmert et al., 2015; Georgantzopoulou et al., 2016; Böhmert et al., 2012). In contrast to AgNPs, $AgNO_3$ was found to slightly induce several apoptosis-associated proteins, but most increases were not statistically significant (Georgantzopoulou et al., 2016).

The induction of apoptosis does not explain the elevated LDH activity measured earlier (Chan et al., 2013), but necrosis does not feature the condensation of chromatin (Vanden Berghe et al., 2010) as was observed here. However, other necrosis-related mechanisms might have been triggered, which could explain the observed combination of the LDH release and chromatin condensation / nuclear fragmentation. The exposure to AgNPs and $AgNO_3$ might have induced of a highly regulated type of necrosis termed necroptosis (Chan et al., 2013; Rayamajhi et al., 2013), which has been reported to occur in the intestinal epithelium (Negroni et al., 2015). Necroptosis can be induced by TNF-α and seems to occur in case the apoptotic cascade is blocked (Günther et al., 2011; Pasparakis and Vandenabeele, 2015). However, necroptosis causes only moderate chromatin condensation and the nucleus remains largely intact (Pasparakis and Vandenabeele, 2015), which is in contrast to the results presented here.

In the inflamed co-culture two other sub-types of programmed necrotic processes – *pyronecrosis* and *pyroptosis* – might be involved in the observed cytotoxicity (Pasparakis and Vandenabeele, 2015). Pyroptosis shares several characteristics with apoptosis, e.g. nuclear condensation and DNA fragmentation, but also displays features associated with necrosis, like cell lysis, cell swelling, and LDH release (Labbé and Saleh, 2011). The induction of pyroptosis is linked to the activation of caspase-1 (Labbé and Saleh, 2011; Rayamajhi et al., 2013). However, in some cell types, e.g. epithelial cells, the activation of caspase-1 does not trigger pyroptosis but rather initiates cell protective mechanisms (Yang et al., 2015). In contrast to pyroptosis, pyronecrosis is characterised by the activation of a protein of the NOD-like receptor (NLRs) family – NLRP3 (Satoh et al., 2013). The activation of NLRP3 in the intestinal epithelium is associated with protection against pathogens, whereas its reduced expression is linked to increased susceptibility to Crohn's disease (Song-Zhao et al., 2014). AgNPs were shown to activate NLRP3 in THP-1 cells (Simard et al., 2015). Both pyroptosis and

pyronecrosis are associated with moderate chromatin condensation and might, therefore, not be involved in the here observed effects (Pasparakis and Vandenabeele, 2015).

A more likely explanation is the occurrence of apoptosis-induced secondary necrosis, which occurs when the normal scavenging capacities of phagocytising cells are overwhelmed or impaired (Silva et al., 2008). In contrast to primary necrosis, secondary necrosis features nuclear shrinkage and severe fragmentation of the nucleus, as well as cytoplasmic swelling (Silva, 2010). As mentioned above, pro-inflammatory cytokines and NO can induce apoptosis in IECs, whereas the low level of LDH release could have been caused by TNF-α-mediated necrotic processes. In the inflamed co-culture, the exposure to stressors, e.g. AgNPs and $AgNO_3$, could have resulted in additional induction of apoptotic processes. Apart from its role in apoptosis and necrosis, TNF-α has been demonstrated to be essential for 'apoptosis-induced-apoptosis'. Apoptosis-induced-apoptosis describes a process of non-autonomous apoptosis that can occur within a tissue (Perez-Garijo et al., 2013). Even though IECs are capable of engulfing apoptotic neighbouring cells their capacity might have been exceeded by this additional increase in apoptosis. Eventually, the cells underwent secondary necrosis, which could explain the significant increase in LDH after exposure to AgNPs and $AgNO_3$. In contrast to this hypothesis, Böhmert et al. (2012) did not observe induction of apoptosis by AgNPs. However, the already stressed state of the cells in the inflamed model could have increased their susceptibility.

The occurrence of secondary necrosis could, furthermore, elucidate the increases in TEER discussed earlier (Sections 4.3.2.1 & 4.4.3.1). Like primary necrosis, secondary necrosis is characterised by cell swelling, which can cause an increase in TEER. A significant increase in TEER was only observed in Caco-2 monocultures and stable co-cultures exposed to $AgNO_3$ but not after exposure to 10 µg / mL AgNPs, even though the levels of LDH release were similar. It is possible, that the cytotoxic mechanisms induced by 10 µg / mL AgNPs were different from those caused by $AgNO_3$ or, simply, not sufficient to cause secondary necrosis.

4.5 Conclusions

The cytotoxicity studies in THP-1 and $_{UD}$Caco-2 monocultures confirmed that $AgNO_3$ exerts toxic effects at significantly lower concentrations than AgNPs. Surprisingly, concentrations of both ionic and particulate Ag that were found to be non-toxic in monocultures of $_{UD}$Caco-2 cells caused significant cytotoxicity in $_{D}$Caco-2 cells, clearly disproving the corresponding hypothesis. Confirming the initial hypothesis, the presented results showed distinct effects of AgNPs and $AgNO_3$ depending on the health status of the *in vitro* model at the time of exposure. Whereas lower concentrations of AgNPs did not cause any effects regardless of the condition, higher concentrations of AgNPs induced a significant increase in barrier integrity in the inflamed but not in the stable co-culture. In contrast to this, the exposure to non-toxic concentrations of $AgNO_3$ resulted in elevated TEER in both co-cultures and the Caco-2 monoculture. In both co-culture models, AgNPs and $AgNO_3$ caused a significant increase in cell death, which was likely caused by a combination of apoptosis, secondary necrosis, and apoptosis-induced-apoptosis. The occurrence of secondary necrosis might be involved in the observed increase in TEER above the unexposed Caco-2 monoculture control. Like the general re-establishment of barrier integrity in the inflamed co-culture the cause for the TEER increase could not be conclusively explained. The observed effects were significantly more pronounced in the inflamed model than in the stable co-culture. The exposure to AgNPs and $AgNO_3$ did not induce a pro-inflammatory reaction in the stable co-culture and did not affect the cytokine release or NO synthesis in the inflamed co-culture.

5. Application of the co-culture model in homeostatic and inflamed state to study the effect of exposure to CuO NPs

5.1 Introduction

Due to their very favourable thermo-physical properties (Bondarenko et al., 2013), CuO NPs are used in the manufacture of electronics and technologies, e.g. semiconductors (Rahnama and Gharagozlou, 2012), electro chips, or conductivity-enhancing nano-fluids (Chang et al., 2011). Even though CuO NPs exert strong antimicrobial effects (Borkow et al., 2009; Ren et al., 2009), this function only accounts for around 4 % of the material's applications (Bondarenko et al., 2013).

In contrast to Ag, Cu is an essential trace element needed by the great majority of cell types (Bondarenko et al., 2013), where it is involved in electron transfer reactions, neurotransmission, and antioxidant defence mechanisms, e.g. CuZn superoxide dismutase (SOD) (Bo et al., 2008). The average dietary intake of Cu for adults is estimated between 0.6-1.6 mg / d (Tapiero et al., 2003). The absorption of Cu is inversely related to the dietary intake: the more Cu is ingested, the less is absorbed (van den Berghe and Klomp, 2009). Reliable data on the daily exposure of particulate Cu through ingestion, inhalation, or skin contact are not available.

5.1.1 Toxicity mechanism

As a trace element, Cu is necessary for a number of vital processes, but an oversupply can have deleterious effects. One example is the ability to replace other metal cofactors from their ligand, e.g. in receptors or enzymes (Tapiero et al., 2003). Even though it is not their required material, most proteins favour Cu over the designated metallic cofactor (Foster et al., 2014). These 'mismetallations' can render proteins transcriptionally and functionally inactive (Predki and Sarkar, 1994; Foster et al., 2014). To prevent Cu from replacing other metals, its intracellular concentration has to be closely controlled using specialised cellular uptake pathways and regulation mechanisms (Foster et al., 2014). Since organisms have historically received the required Cu in ionic state as Cu^{+} or Cu^{2+} the regulating uptake mechanisms are likely specialised on ionic but not particulate Cu. As other NMs, CuO NPs are expected to be taken up by the cell through endocytic mechanisms (Thit et al., 2013). In this context, a 'Trojan Horse'-type toxicity process has been suggested, meaning the uptake of the

particles and subsequent induction of toxic effects through Cu ions generated by the lysosomal degradation of the particles. The acidic environment of the lysosome favours the dissolution of CuO NPs, resulting in the generation of uncontrolled concentrations of Cu^{+} and Cu^{2+} within the cell (Studer et al., 2010; Bondarenko et al., 2013).

If ionic and particulate Cu species are taken up through individual mechanisms, differences in the toxicity should be observed. Supporting this, CuO NPs were found to be more cytotoxic than ionic Cu in a non-human kidney epithelial (A6) and a human lung epithelial cell line (A549) (Thit et al., 2013; Wang et al., 2012). Karlsson et al. (2008) demonstrated in A549 cells that CuO NP-induced cyto- and genotoxicity were independent of the release of ionic Cu. Furthermore, Wang and colleagues (2012) observed that the intracellular Cu levels in A549 cells increased more strongly after exposure to CuO NPs than equal mass concentrations of Cu^{2+}, supporting the hypothesis of different uptake and control mechanisms. Whereas the uptake of CuO NPs into the cells could be reduced by endocytosis inhibitors, the uptake of Cu^{2+} was unaffected (Wang et al., 2012).

5.1.2 Cu in inflammatory conditions

Various studies in humans and animals have investigated the levels of Cu in unimpaired health and in presence of ongoing inflammatory processes. In children with IBD, the analysis of serum Cu concentrations at presentation at the hospital showed significantly increased levels in those diagnosed with Crohn's disease but not Ulcerative Colitis (Ojuawo and Keith, 2002). In adult IBD patients, the type of nutrition appeared to influence serum Cu levels. In patients receiving an uncontrolled diet the serum concentrations were increased compared to healthy controls (Fernández-Banares et al., 1990), whereas no significant differences were detected in patients on a controlled enteral or parenteral nutrition (Johtatsu et al., 2007; Kobayashi et al., 2012). A study using rats showed that the inflammation-related increase in serum Cu levels is not exclusive to conditions of intestinal inflammation. In a pulmonary inflammation model, elevated Cu levels were found in serum and liver tissue, which the authors suggested to indicate an increased Cu-demand in the organism (Milanino et al., 1986). A study by DiSilvestro and Marten (1990) proposed the increased Cu-demand to be linked to the elevated activity of Cu-dependent antioxidant mechanisms like CuZn SOD. The authors demonstrated that the enzyme's activity in the liver and blood depended on the

availability of sufficient concentrations of dietary Cu by feeding rats a diet containing adequate, marginal, or insufficient levels of the trace element.

5.1.3 Toxic effects in vitro

In cell culture experiments, CuO NPs were found to be highly toxic, for instance in different airway epithelial cell lines (Fahmy and Cormier, 2009; Karlsson et al., 2008; Edelmann et al., 2014), keratinocytes (Alarifi et al., 2013), hepatocytes (Cuillel et al., 2014), and cardiac endothelial cells (Sun et al., 2011). Whereas cytotoxicity was generally observed, the sensitivity to CuO NPs-induced effects varied between cell types (Jing et al., 2015).

Exposure to CuO NPs caused generation of ROS and depleted levels of intracellular antioxidants (Fahmy and Cormier, 2009; Karlsson et al., 2008). Further effects include DNA damage (Karlsson et al., 2008), mitochondrial depolarisation (Wang et al., 2012), as well as induction of pro-inflammatory cytokines (Jing et al., 2015). Many of the effects, including cytotoxicity, seem to be linked to the formation of ROS. Co-exposure or pre-incubation of cells with antioxidants was able to increase cell viability, prevented the depletion of glutathione, and decreased the formation of ROS (Niska et al., 2015; Siddiqui et al., 2013; Jing et al., 2015). Additionally, CuO NPs were found to cause cell death through the induction of autophagy in A549 cells (Sun et al., 2012). Proteomic analysis of BEAS-2B cells exposed to very low concentrations of CuO NPs (0.01 µg / cm^2, 24h) revealed distorting effects on the actin cytoskeleton, as well as on protein ubiquitination (Edelmann et al., 2014).

5.1.4 Toxicity in IECs and macrophages

In IECs, Piret et al. (2012b) noted significant cytotoxic effects in response to the exposure to both CuO NPs and ionic Cu. The exposure resulted in barrier destruction, which was reflected in strong TEER reduction and increased passage of LY (Piret et al., 2012b). As observed in other cell types, the exposure to particulate Cu was more detrimental than ionic Cu. The toxicity of CuO NPs mainly depended on the specific surface area of the particles (Piret et al., 2012b). Chen et al. (2015a) demonstrated the uptake of CuO NPs by Caco-2 cells through energy-dependent endocytic mechanisms. The groups' quantification of Cu recovered from the BL side of the cell culture

suggested a transport and exocytosis of CuO NPs across the cell layer. The transport rate of nano-sized CuO particles (60%) was significantly higher compared to equal Cu concentrations in ionic (40 %) and microparticulate state (11 %) (Chen et al., 2015a). In contrast to ionic Cu and CuO MPs, no obvious saturation was observed for the uptake and transfer of CuO NPs (Chen et al., 2015a).

In macrophages, the exposure to CuO NPs induced strong cytotoxic effects with an EC_{50} between 5 and 10 µg / mL (Lanone et al., 2009). Khatri et al. (2013) observed an upregulation in the gene expression and protein levels of pro-inflammatory cytokines in THP-1 cells in response to CuO NPs. Treatment with CuO NPs resulted in the formation of ROS, which seemed to be largely responsible for the observed cytotoxicity, as co-incubation with antioxidants increased cell viability significantly (Rotoli et al., 2012). Contradicting results were reported regarding the cytotoxic effects of ionic and particulate Cu in macrophages. Whereas Rotoli et al. (2012) did not observed significant differences in murine RAW264.7 macrophages, Triboulet and colleagues (2015) reported higher toxicity for the exposure to CuO NPs compared to Cu ions in murine J774A1 macrophages.

5.1.5 Toxicity in vivo

In contrast to other metal and metallo-oxide NMs, very few *in vivo* studies in mammals were conducted to investigate the effects of CuO NPs. Therefore, also studies on Cu NPs will be considered, which might help to estimate the potential effects of CuO NPs.

In rats, the inhalation of a single dose of 1 or 5 mg / kg bodyweight CuO NPs resulted in a dose-dependent cell damage and lasting infiltration of leukocytes detected in the broncho-alveolar lavage fluid at 1 and 7 days post-exposure (Rani et al., 2013). The CuO-induced cell damage lead to increased levels of LDH in lung lavage fluid and histopathological changes in the lung tissue (Rani et al., 2013; Kim et al., 2011). Exposure chamber experiments in mice using Cu NPs (surface phase: CuO) revealed a higher rate of leukocyte infiltration, as well as cell damage after chronic exposure (2 weeks, 5 days / week, 3.68 mg / m^3 per treatment) compared to an acute single dose (6.23 mg / m^3) (Pettibone et al., 2009). Furthermore, the levels of pro-inflammatory cytokines and chemokines, e.g. TNF-α, IL-6, GM-CSF, MIP-1α, and MCP-1, were significantly increased in chronically exposed animals that were sacrificed one day after the last exposure. Many cytokines returned to the control levels after a recovery period

of 3 weeks (Pettibone et al., 2009). Interestingly, Kim and colleagues (2011) found that both sub-acute inhalation (2 weeks, 5 days / week, ~32 µg / mouse) and single-dose instillation (3-100 µg / mouse) exposure to Cu NPs significantly impaired the clearance of bacteria from the lung.

After one-time intraperitoneal injection of 1 or 3 mg CuO NPs in mice, indications for a genotoxic effects were found in red blood cells. Together with an increased occurrence of micronucleated reticulocytes, elevated markers of oxidative DNA damage were detected in the bone marrow and liver at 1 to 3 days post-exposure, respectively (Song et al., 2012). Sub-chronic exposure of rats to intraperitoneally injected CuO NPs resulted in an accumulation in several organs, primarily in the kidneys and liver tissue. Furthermore, neurotoxic changes were noted in parts of the brain, as well as significant DNA fragmentation in the liver and spleen after sub-chronic exposure to 2 mg / rat / exposure (3 times / week, up to 6 weeks) (Privalova et al., 2014).

The oral exposure route has scarcely been investigated to date, and no *in vivo* studies addressing CuO NPs were found. An oral *in vivo* exposure study is currently conducted within the 'Sustainable Nanotechnologies (SUN) Project', but final results were not yet available. However, few studies on Cu NPs were found. Meng et al. (2007) exposed mice to a single dose of 70 mg / kg bodyweight Cu NPs by oral gavage. Most interestingly, the authors described a striking morphological change in the stomach of Cu NP-exposed mice 24h after the gavage. The organ swelled and displayed an unnatural cyan colour, which was exclusive to the exposure to nano-sized Cu and not observed after treatment with proportional concentrations of micro-sized or ionic Cu. Meng et al. (2007) argued that Cu NPs were retained in the stomach longer than Cu MPs, where the continuous dissolution of Cu in the acidic environment caused an acid-base imbalance. A strong deposition of Cu was found in the kidneys, accompanied by necrotic changes in the renal tubules (Meng et al., 2007). Another study investigated the acute toxicity of Cu NPs in mice by administering single doses between 108 and 1,080 mg / kg bodyweight via oral gavage (Chen et al., 2006). After 48h, the group observed pathological changes in the liver, spleen, and kidneys at exposure concentrations ≥341 mg / kg bodyweight. In a study using rats, the animals were exposed sub-chronically to 50-200 mg / kg bodyweight for 5 days via oral gavage. The most overt hepatotoxic and nephrotoxic results were observed in the high-dose group (Lei et al., 2008).

5.1.6 Aims and hypotheses

The assessment of CuO NP-exposure in the stable and inflamed co-culture was performed as part of Aim III – the application of the model to study the effects of orally ingested NMs. The oral uptake of noticeable concentrations of CuO is rather unlikely. However, the material offered the interesting possibility to investigate an essential trace element, which might interact differently with cells than non-essential metals like Ag. Furthermore, the pH-sensitive nature of the material allowed us to assess the influence of artificial digestion on CuO-induced toxicity. This study aimed to investigate the induction of cytotoxicity in relation to the health status of the co-culture, as well as potential inflammatory effects after the exposure to non-toxic concentrations of digested and undigested CuO NPs.

The following hypotheses were tested:

- Digested CuO NPs are less toxic than undigested CuO NPs.
- CuO NP concentrations that are non-toxic in $_{UD}$Caco-2 monocultures can be applied as non-toxic concentration in $_{D}$Caco-2 cells.
- A one-time exposure of the stable co-culture with non-toxic concentrations of digested and undigested CuO NPs will affect at least one of the investigated endpoints.
- The exposure to non-toxic concentrations of undigested and digested CuO NPs will induce the same effects in the stable co-culture.
- A one-time exposure of the inflamed co-culture with non-toxic concentrations of undigested and digested CuO NPs will affect at least one of the investigated endpoints.
- The exposure to non-toxic concentrations of undigested and digested CuO NPs will induce the same effects in the inflamed co-culture.
- The effects induced in the stable co-culture will be different from the effects in the inflamed co-culture.

5.2 Materials & Methods

5.2.1 CuO NPs

The CuO NPs were received from a commercial source (PlasmaChem GmbH, Berlin, Germany). The primary particle size is between 15-20 nm with a specific surface area of 47 m^2 / g (Gosens et al. 2016). The particles were used by the partners of the Sustainable Nanotechnologies (SUN) project and kindly made available by Prof. Vicki Stone from Heriot-Watt University (Edinburgh, UK). The particles were received as brown-blackish powder and freshly dispersed before each experiment:

A particle suspension of 1 mg / mL CuO NPs was prepared in H_2O containing 2 % FBS. For experimental digestions, the particles were re-suspended at a higher concentration of 10 mg / mL in 2 % FBS / H_2O. After vortexing the suspension for 30 seconds, the vial was sonicated using a waterbath sonicator for 16 min. Subsequently, the suspension was kept on ice until further use. Just before use, the vial was briefly vortexed again to re-disperse sedimented particles.

5.2.2 Artificial digestion of CuO NPs

To account for the environmental changes throughout the GI-passage, the CuO NPs were subject to a very simple artificial digestion. An artificial gastric fluid was prepared in a bijou vial by adding 0.2 % w/v NaCl and 0.7 % v/v HCl to 8 mL distilled H_2O. The pH was measured and adjusted to ~1.5-1.7 using HCl (0.4 M) (an explanation of why the pH was reduced below the physiological pH of the gastric environment will be given in Section 5.3.1.). Of this, 4 mL were transferred to a second bijou vial and served as digestive fluid control. To the other vial, 1 mL of the 10 mg / mL CuO NPs suspension was added and incubated at standard culture conditions for 2h. After 2h, the pH was measured and adjusted in both vials to ~6.8 using NaOH (1 M). The vials were then incubated again for 1.5h at standard culture conditions. After the incubation time, the suspension was used directly for the exposure of the cultures or to prepare a dilution range in CCM.

5.2.3 Characterisation of CuO NPs

Both undigested and digested CuO NPs were analysed using CLS. The analysis was performed on the pristine particles in dispersant and the artificial digestive fluid, as well as after dilution in CCM (100 µg / mL) and incubation at standard culture conditions for 4, 24, and 48h.

For the analysis, the CPS instrument was prepared and operated as described before (Section 4.2.3.2). Due to expected large size of the particles the rotational speed was reduced from 22,000 to 12,000 rpm.

5.2.4 Cell cultures

For the experiments, monocultures of Caco-2 and THP-1 cells, as well as stable and inflamed co-cultures were used. The culture and maintenance of the cells, as well as the preparation of the co-culture models were done as described before (Sections 2.1.2 & 4.2.3).

5.2.5 Alamar Blue assay

The Alamar Blue assay was used to estimate the cytotoxic effects induced by CuO NPs. For the exposure, THP-1 cells and Caco-2 cells were grown and treated as described earlier (Section 4.2.4) and the assay run as described in Section 4.2.6. Undigested and digested CuO NPs were prepared freshly according to the protocols above. A range of 7 concentrations (from 1.6 to 100 µg / mL) was prepared as 1:2 dilutions in fresh CCM and the cells exposed for 24 or 48h. In each experiment a negative control, as well as a dispersant or digestion control were included.

5.2.6 IN Cell Analyzer: Count of DAPI-stained nuclei

A second measurement of cytotoxicity in Caco-2 cells was provided by quantification of DAPI-stained nuclei (IN Cell Analyzer) using the cell cultures of the Alamar Blue assay. The cells were washed 2x with 200 µL PBS and fixed with 3.7 % formaldehyde for 13 min at RT. The cells were permeabilised and stained as described in Section 2.1.6 and imaged and analysed as before (Section 4.2.8). The imaging and image analysis was kindly performed by Patricia Urbán.

TEER measurements (Section 2.1.4), measurements of cytokine release using ELISA (Section 2.1.8), and the Griess reaction (Section 3.2.4) were performed as described before.

5.3 Results

5.3.1 Characterisation

After suspending the CuO NPs in dispersant the occurrence of two fractions was noticeable by the naked eye: one fraction remained in a relatively stable dispersion, while a second fraction of presumably larger particles sedimented quickly. Due to this rapid sedimentation the use of DLS was not applicable and it was decided to limit the characterisation to CLS.

The CLS analysis revealed a considerable heterogeneity between individual dispersions (Figure 5.1A), which were all prepared according to the described protocol. Whereas in some dispersions (Figure 5.1A, black and red line), a population of nano-sized CuO particles with an average diameter of 90 nm could be detected, particles in this size range were entirely absent in others (green line). Likewise, the average diameter of the major particle population was either between 1.2-1.4 µm (red and green line) or greatly exceeded a size of 2 µm. After an incubation time of 24h in dispersant at 4°C and without re-suspending the sample before measurement, nearly 100 % of the CuO particles were sedimented to the bottom of the vial (not shown) and no signal was recovered by CLS (Figure 5.1A, striped line).

After addition to MEM-based CCM (Figure 5.1B, black line), the signal intensity measured by CLS strongly decreased. The maximum peak remained at >1 µm particle diameter. A second very small peak was visible at ~70 nm.

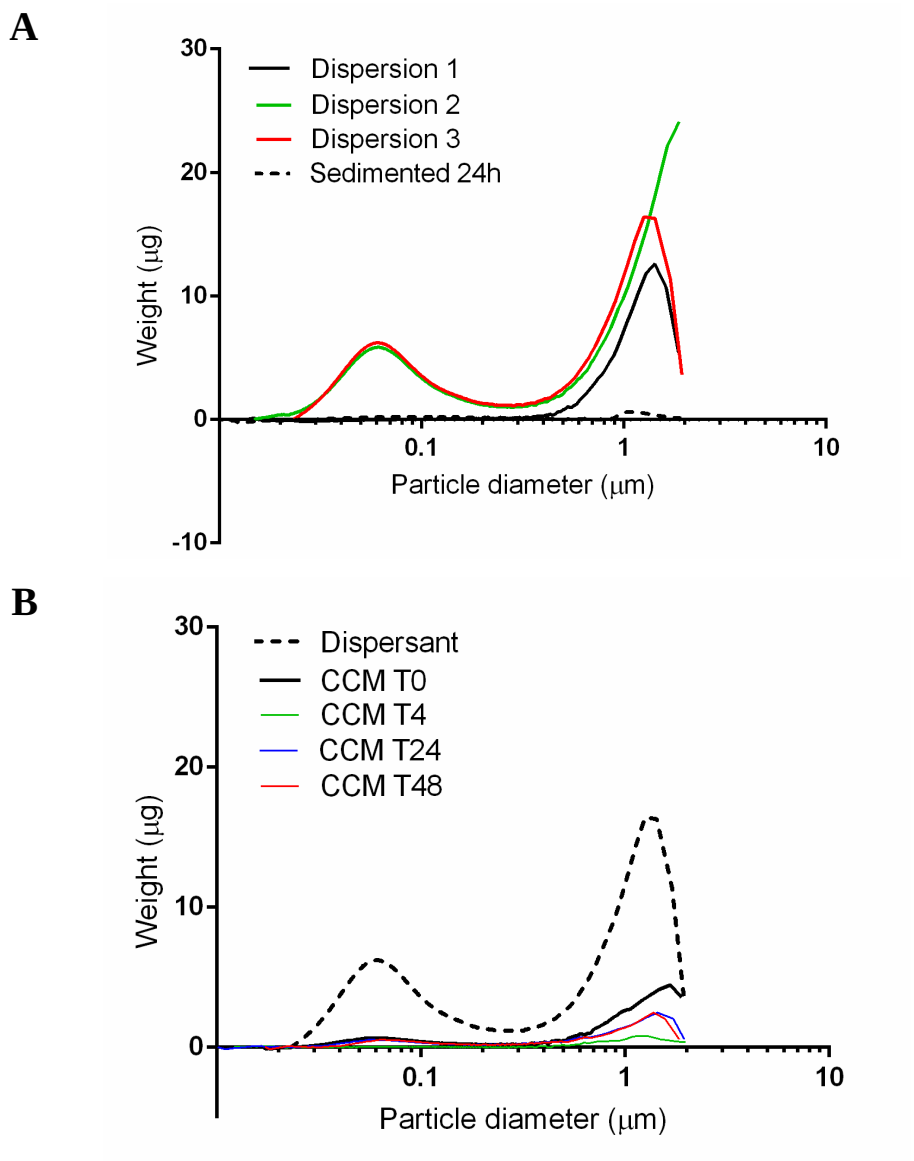

Figure 5.1 Hydrodynamic diameter of CuO NPs (100 µg / mL) in dispersant and CCM measured by CLS

(A) Measurements of 3 independent dispersions of CuO NPs in dispersant (Dispersion 1-3) and after 24h storage at 4°C; (B) CuO NPs in dispersant and after 0, 4, 24, and 48h incubation in MEM-based CCM (CCM T0-T48) at 37°C, 5 % CO_2.

After incubation in gastric fluid, the dark brown particle suspension turned transparent. At this stage, no particulate matter could be observed by the naked eye and / or CLS (data not shown). Interestingly, when the pH was adjusted to a physiologically more relevant value of ~2.2 the CuO particles were not fully dissolved after 2h incubation. When measuring the pH it was found to have increased from 2.2 to >5.

After incubation in acidic conditions, the pH was increased to roughly 6.8 using NaOH and a light blue, particulate fallout formed (Figure 5.2A). When allowing the suspension to rest for 2-3 minutes, the blue particles sedimented quickly to the bottom of the bijou vial (Figure 5.2B). The particles could be re-suspended easily and, as the repeated CLS analysis of a digested CuO batch confirmed, did not change over several days of storage at 4°C (data not shown).

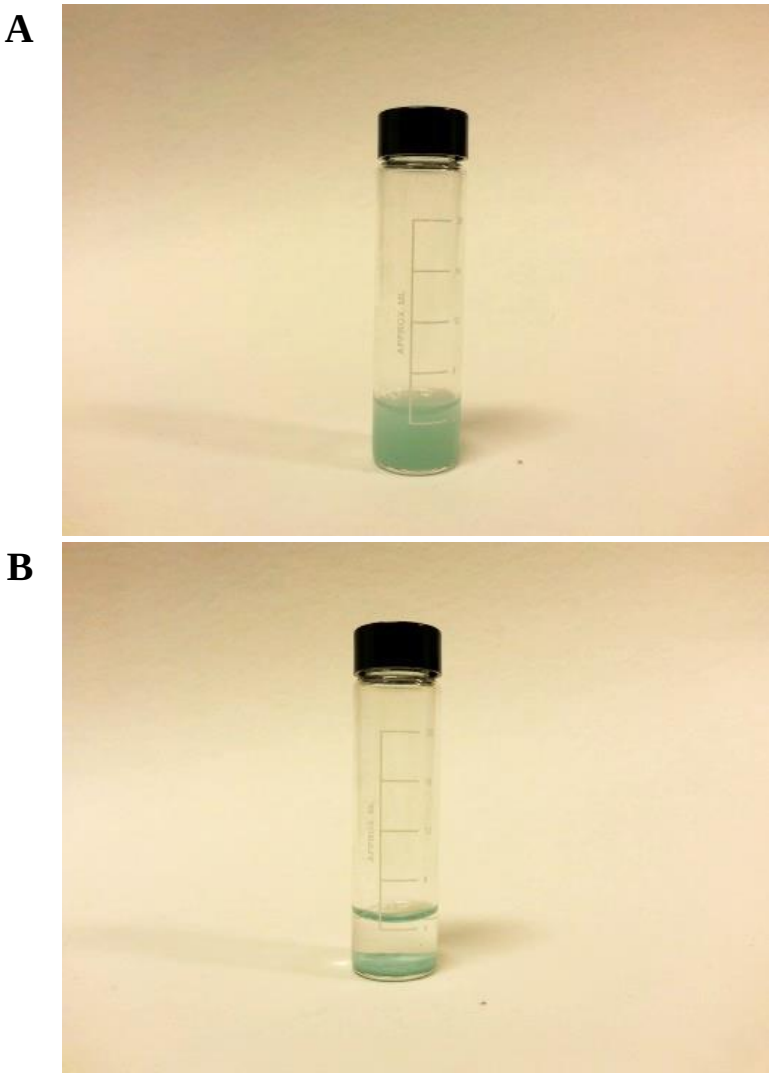

Figure 5.2 CuO NPs after increasing the pH from acidic (pH 1.7) to near-neutral (pH 6.8)

(A) vortexed digested CuO NPs, (B) sedimented digested CuO NPs after 10 min

After the artificial digestion, the blue fallout could be detected by CLS using the same protocol as for the analysis of the CuO NPs (Figure 5.3, dotted line). Compared to the undigested CuO NPs in dispersant the peak intensity was clearly decreased. Whereas before the digestion two differently sized populations were detectable, only one peak was measured after the digestion at around 750 nm. Immediately after the addition to MEM-based CCM, the peak intensity decreased and the average particle diameter slightly increased to ~810 nm (Figure 5.3, black line). When the artificially digested CuO NPs were incubated in CCM at standard culture conditions for 48h, no particulate matter could be detected anymore between 0.01 and 2 µm.

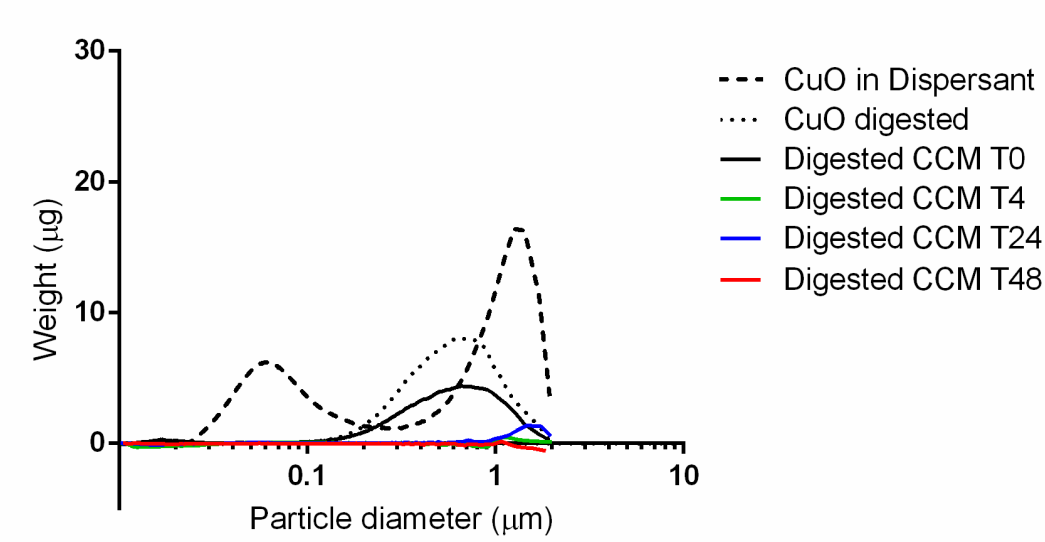

Figure 5.3 Hydrodynamic diameter of artificially digested CuO NPs (100 µg / mL) measured by CLS

CuO NPs were measured before digestion (CuO in Dispersant), after digestion in dispersant (CuO digested), after digestion and addition to CCM after incubation at 37°C, 5 % CO_2 (Digested CCM T0-T48)

5.3.2 Cytotoxicity in Caco-2 and THP-1 monoculture

To ensure the use of non-toxic exposure concentrations in the co-culture experiments, the cytotoxicity of digested and undigested CuO NPs was investigated in monocultures of confluent $_{UD}$Caco-2 cells and 24h PMA-differentiated THP-1 cells. The toxicity was quantified via the measurement of metabolic activity with the Alamar Blue assay. In Caco-2 cells the quantification of DAPI-stained nuclei using the IN Cell Analyzer was performed additionally.

5.3.2.1 Quantification of metabolic activity

In monocultures of $_{UD}$Caco-2 cells, the exposure to undigested CuO NPs of up to 12.5 µg / mL did not reduce metabolic activity noticeably after 24 and 48h (Figure 5.4A). At concentrations higher than 25 µg / mL a dose-dependent decrease in metabolic activity was detected, which was more pronounced after 48h compared to 24h of exposure. The exposure to 100 µg / mL resulted in 100 % reduction in metabolic activity after 24h and 48h. No adverse effect was observed in the dispersant control corresponding to the highest CuO exposure concentration at either time point.

The exposure effects of undigested and digested CuO NPs were largely comparable. Up to a concentration of 12.5 µg / mL no reduction in metabolic activity was detected (Figure 5.4B). At concentrations higher than 12.5 µg / mL, a dose dependent decrease in cell viability occurred. After 48h, the metabolic activity was significantly lower ($p \leq 0.001$) in cells exposed to 25 µg / mL digested CuO NPs (40 % of the control) compared to the same concentration of undigested CuO NPs (28 %). The observed reduction in cell viability is not linked to the components of the digestive fluid, since the digestion control (DC) did not induce significant effects over 48h (Figure 5.4B).

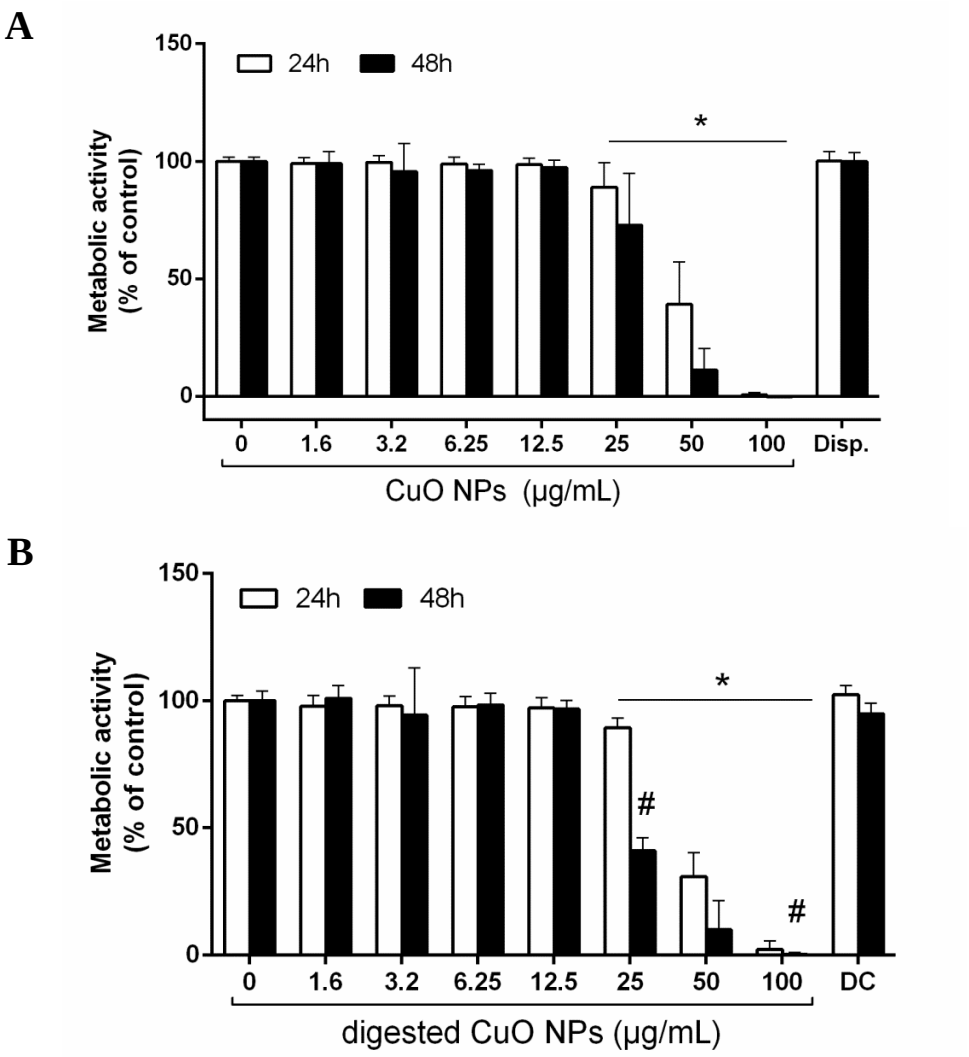

Figure 5.4 Metabolic activity of $_{UD}$Caco-2 cells after 24 and 48h exposure to CuO NPs

*The Alamar Blue assay was performed after exposure to (A) undigested CuO NPs or (B) digested CuO NPs; Disp.= Dispersant control, DC= Digestion control (Average of N≥3 ± StDev, *p≤0.05 compared to corresponding negative control; $^{\#}$p≤0.05 compared to corresponding concentration of undigested CuO NPs)*

In PMA-differentiated THP-1 cells, undigested CuO NPs at concentrations of up to 6.25 µg / mL did not affect the metabolic activity significantly (Figure 5.5A). Concentrations of undigested CuO NPs equal to or higher than 12.5 µg / mL induced significant cytotoxicity (Figure 5.5A). After 24h, the metabolic activity was reduced to 74 ± 14 %, whereas it was slightly higher after 48h with 82 ± 21 %. Again, the CuO-associated cytotoxicity was induced in a dose- and time-dependent manner for concentrations equal to or higher than 12.5 µg / mL.

Interestingly, digested CuO NPs were less toxic than undigested CuO NPs in PMA-differentiated THP-1 cells. Only at concentrations ≥25 µg / mL a statistically significant reduction in cell viability was detected (Figure 5.5B). After 48h, lower concentrations of digested CuO NPs between 1.6 and 12.5 µg / mL caused a non-significant increase in metabolic activity by 11-16 % compared to the control. A similar non-significant increase in metabolic rate was observed after the exposure to the digestion control (112 and 119 % compared to the negative control after 24h and 48h, respectively).

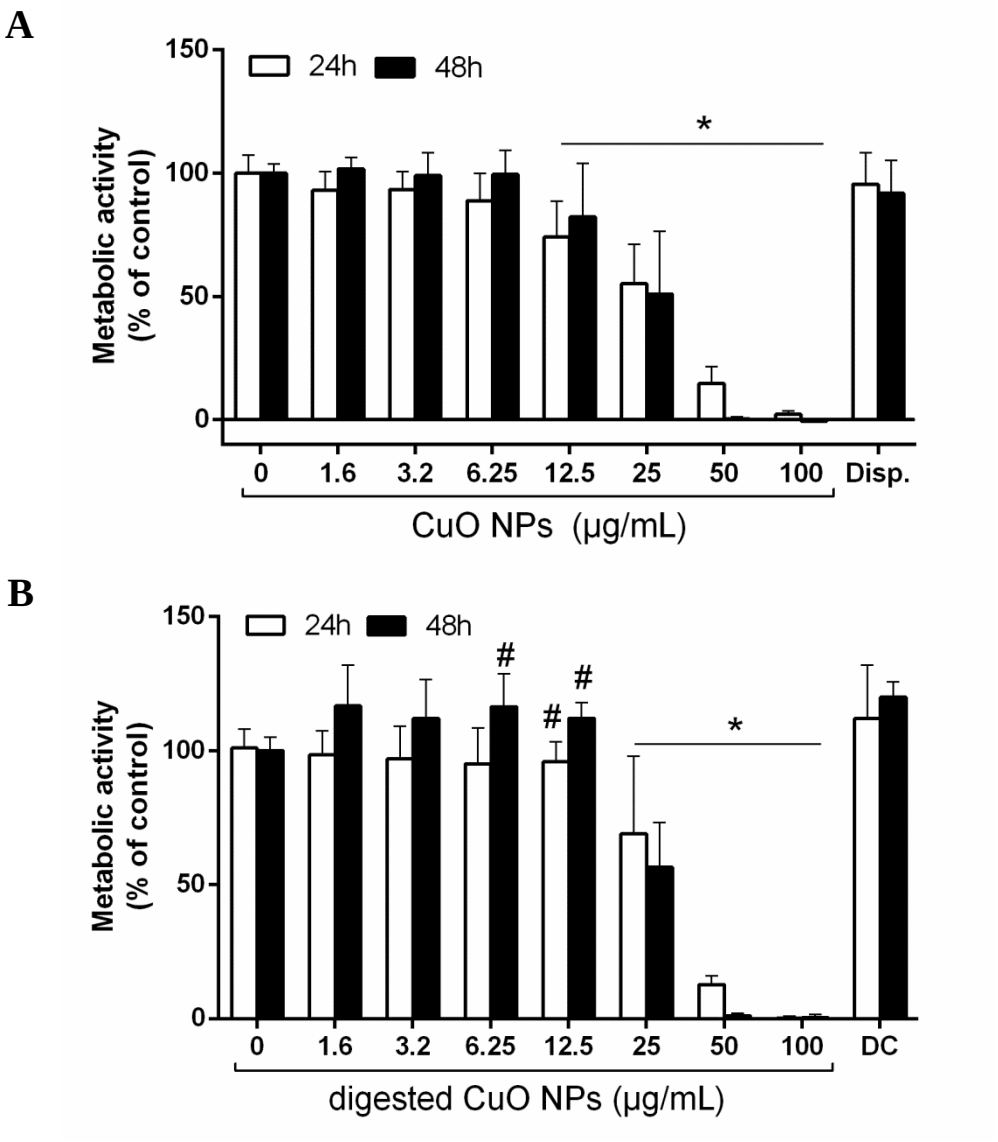

Figure 5.5 Metabolic activity of PMA-differentiated THP-1 cells after 24 or 48h exposure to CuO NPs

*The Alamar Blue assay was performed after exposure to (A) undigested CuO NPs or (B) digested CuO NPs; Disp.= Dispersant control, DC= Digestion control (undigested CuO NPs: Average of N=3 ± StDev; Digested CuO NPs: Average of N=2 ± StDev, *p≤0.05 compared to corresponding negative control, #p≤0.05 compared to corresponding concentration of undigested CuO NPs)*

5.3.2.2 Quantification of DAPI-stained nuclei of Caco-2 cells using HCA

For Caco-2 cells, the CuO NP-induced cytotoxicity was additionally quantified by HCA of DAPI-stained nuclei. After exposing the cells to undigested CuO NPs for up to 48h, no significant reduction in the number of nuclei was detected for concentrations equal to or below 12.5 µg / mL (Figure 5.6A). The exposure to 25 µg / mL induced moderate but significant cytotoxic effects, reducing the total number of nuclei by 25 and 14 % after 24h and 48h, respectively. At an exposure concentration of 50 µg / mL, the cytotoxicity drastically increased. Compared to the control, the number of nuclei was reduced by 95 % after 24h and >99 % after 48h of exposure. No reduction in cell number was detected in cells exposed to the dispersant control.

Also the exposure to digested CuO NPs induced significant cytotoxicity at concentrations equal to or higher than 25 µg / mL (Figure 5.6B). In contrast to the undigested particles, 25 µg / mL digested CuO NPs induced a drastic decrease in the number of nuclei after 24 and 48h (55 and 93 %, respectively). The exposure to the digestion control did not result in noticeable adverse effects.

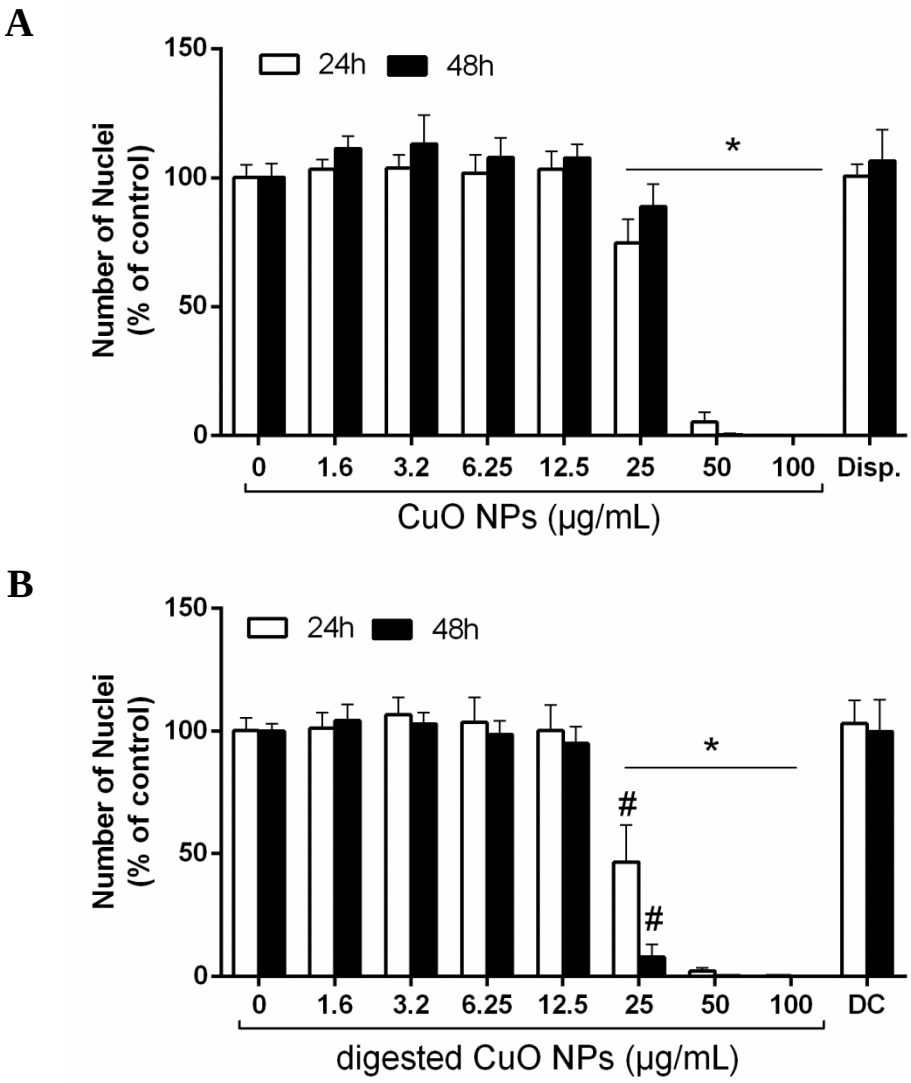

Figure 5.6 Number of DAPI-stained Caco-2 nuclei after 24 and 48h exposure to CuO NPs

*Nuclei were stained and counted (In Cell Analyzer) after exposure to (A) undigested or (B) digested CuO NPs; Disp.= Dispersant control, DC= Digestive control (DC 48h: Average of N=2, rest: Average of N≥3 ± StDev; *p≤0.05 compared to corresponding negative control, #p≤0.05 compared to corresponding concentration of undigested CuO NPs)*

5.3.3 Co-culture exposure to CuO NPs

Based on the cytotoxicity results, a concentration of 12.5 µg / mL digested and undigested CuO NPs was chosen for the co-culture experiments. The stable and inflamed co-cultures were established as described before (Section 4.2.4) and maintained for 24h before the exposure. After 24h of co-culture, 12.5 µg / mL digested CuO NPs, undigested CuO NPs, or the equivalent volume of the digestive fluid as digestion control were added to the AP compartment.

5.3.3.1 Caco-2 barrier integrity

The first TEER measurement was taken just before the start of the co-culture (T_0), as well as after 4, 18, 24, 28, and 48h. The exposure to digested and undigested CuO NPs or the digestion control started after 24h of (co-)culture and continued for another 24h. Hence, the time points T_{28} and T_{48} correspond to 4h and 24h of exposure (Table 4.2).

For all three culture models an unexposed control was included in each experiment. The Caco-2 barrier integrity in stable and inflamed co-cultures was comparable to earlier results. Both conditions met all earlier defined requirements (Sections 2.2.3.1 & 2.2.4.1). To enhance the clearness of the graphs (Figure 5.7A-C) the StDev of the control conditions were not included. For all time points the StDev was within a range of 5.1-7.9 %, 5.2-9.0 %, and 5.8-11.9 % for the monoculture, stable, and inflamed co-culture, respectively.

In the Caco-2 monoculture (Figure 5.7A), no statistically significant differences were measured between the control and the cultures designated for the exposure conditions before the start of the co-culture, except for the designated digestion control at T_0 ($p=0.012$) (Figure 5.7A, green line). Since no significant differences were observed at the subsequent pre-exposure time points (T_4, T_{18}, and T_{24}) this should not affect the credibility of the results. Any differences in TEER observed at T_{28} and T_{48} can in all probability be linked to the exposure to undigested CuO NPs, digested CuO NPs, or the digestion control. After 4h of exposure (T_{28}), digested CuO NPs (red line) and the digestion control (green line) induced a slight but not significant increase in TEER by 2 and 4 %, respectively. No changes were observed in response to undigested CuO NPs (blue line). At T_{48}, the TEER of the digestion control was identical to the unexposed control. Treatment with both undigested and digested CuO NPs induced a reduction in TEER compared to the control by 13 ± 16 and 8 ± 5 %, respectively. For undigested CuO NPs this reduction was statistically significant ($p=0.002$).

In the stable co-culture (Figure 5.7B), no significant differences in TEER were noted between the barriers before the exposure T_{24}. From T_{24} to T_{28}, a slight but not significant reduction in TEER was noted in co-cultures exposed to undigested (blue line) and digested (red line) CuO NPs. No change was observed in stable co-cultures treated with the digestion control. At T_{48}, the TEER of digestion control-exposed stable co-cultures was equal to the corresponding control and the Caco-2 monoculture control (100.2 ± 2.6 %). The TEER of stable co-cultures exposed to undigested CuO NPs was

significantly reduced ($p \leq 0.001$) to 80 ± 8.9 % of the monoculture control. In contrast, the TEER of co-cultures exposed to digested CuO NPs was slightly but not significantly ($p=0.216$) reduced (94 ± 8.6 %).

In the inflamed co-culture (Figure 5.7C), the TEER of the unexposed inflamed control (dotted line) was significantly reduced ($p \leq 0.001$) over the first 28h compared to the Caco-2 monoculture control (Figure 5.7 A, dotted line). After 48h, the TEER of the inflamed co-culture control was re-established to 97.6 ± 11.9 % of the monoculture control. Before the exposure to CuO NPs (red line), digested CuO NPs (blue line), or the digestion control (green line) the TEER of the designated inflamed co-cultures were not significantly different from the inflamed co-culture control (Figure 5.7C, dotted line). After 4h of exposure, no significant changes in TEER were observed. At T_{48}, the barrier integrity of digestion control-exposed inflamed co-cultures was fully recovered with a TEER of 95.9 ± 12.6 % of the monoculture control. In contrast, the TEER of cultures treated with undigested and digested CuO NPs remained reduced compared to the Caco-2 monoculture control by 14.4 % ± 18.6 and 22.3 % ± 17.7, respectively. For cultures exposed to digested CuO NPs the TEER reduction was statistically significant compared to both the Caco-2 monoculture ($p=0.002$) and inflamed co-culture control ($p=0.016$).

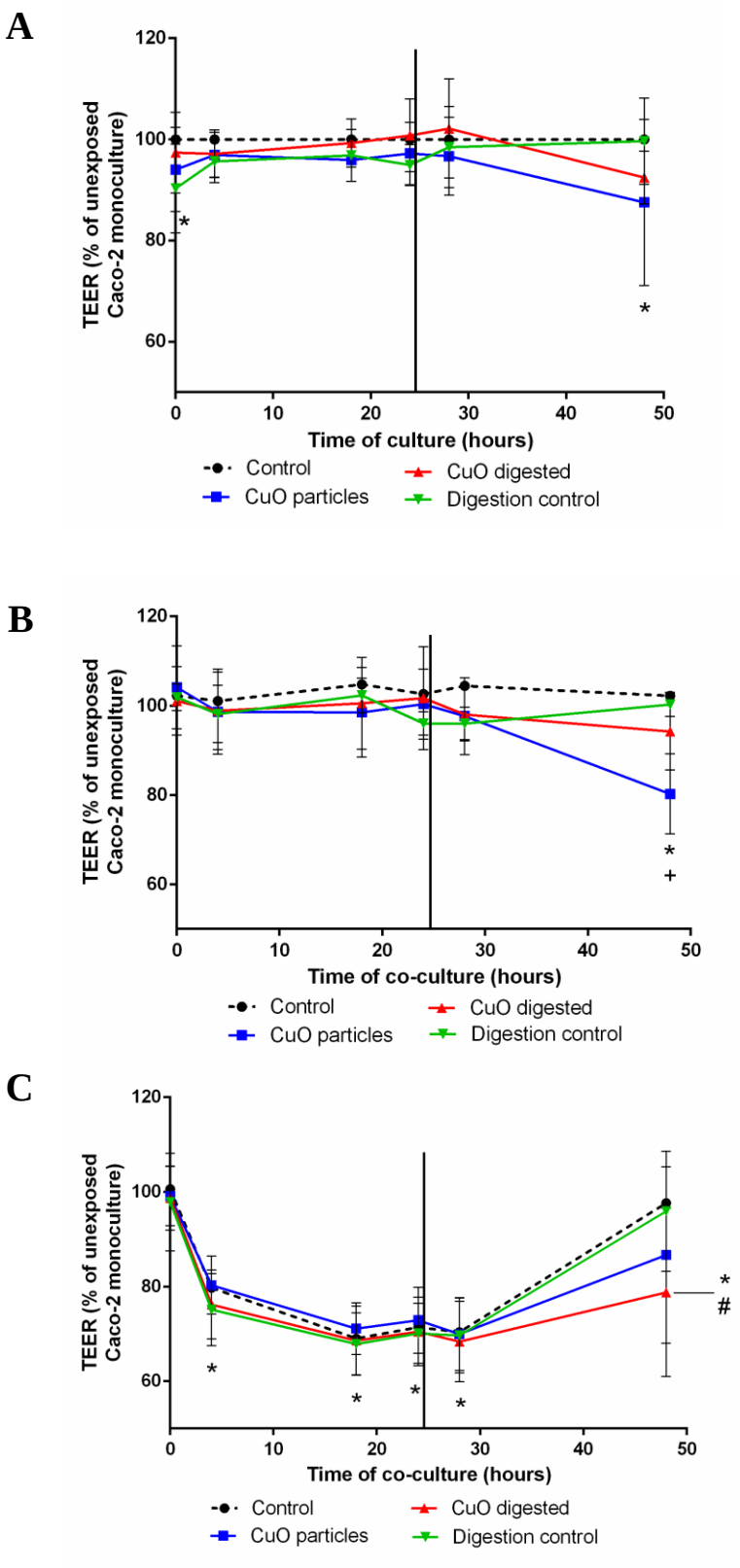

Figure 5.7 Barrier integrity measured as TEER over 48h (A) Caco-2 monoculture, (B) stable, and (C) inflamed co-culture with and without exposure (24h) to 12.5 µg / mL CuO NPs, 12.5 µg / mL digested CuO NPs, or the digestion control

*Black line marks the start of the exposure (Average of N≥3 ± StDev, *p≤0.05 compared to monoculture control; $^{+}$p≤0.05 compared to stable co-culture control; $^{\#}$p≤0.05 compared to inflamed co-culture control)*

5.3.3.2 Cytokine release

The release of IL-1β, IL-8, and TNF-α was quantified in BL supernatants of Caco-2 monocultures, stable, and inflamed co-cultures after 24h exposure to undigested CuO NPs, digested CuO NPs, or the digestion control (Figure 5.8A-C).

In the Caco-2 monoculture (Figure 5.8A), all three cytokines were released at very low concentrations. In both the control and the three exposure conditions, IL-1β and TNF-α remained at concentrations below the detection limit (Table 2.2). The release of IL-8 was generally higher compared to IL-1β and TNF-α. However, large variations between the independent runs resulted in high a StDev. In unexposed controls, 47 ± 35 pg / mL IL-8 were detected. Whereas the concentration of IL-8 remained similar after treatment with the digestive fluids (53 ± 33 pg / mL), it slightly but not significantly increased in response to undigested and digested CuO NPs to 65 ± 78 and 104 ± 142 pg / mL, respectively.

Also in the stable co-culture the release of IL-1β remained at concentrations close to the detection limit of the assay (Figure 5.8B). In contrast to the Caco-2 monoculture, low concentrations of TNF-α could be detected in the stable co-culture control (23 ± 45 pg / mL). However, the release of TNF-α was subject to considerable variations between the independent runs causing a large StDev in the control and all exposure conditions. Even though the TNF-α concentration was slightly increased after the exposure to undigested CuO NPs (34 ± 54 pg / mL), digested CuO NPs (61 ± 117 pg / mL), and the digestion control (109 ± 165 pg / mL), the effect was not found to be statistically significant compared to the stable co-culture control. The release of IL-8 was clearly increased in the stable co-culture control (1,051 ± 545 pg / mL) compared to the monoculture. After 24h exposure to undigested CuO NPs, the level of IL-8 remained similar to the untreated control (1,092 ± 441 pg / mL). Slightly higher but not significantly increased amounts were detected after exposure to digested CuO particles (1,376 ± 680) and the digestion control (1,473 ± 769 pg / mL).

In the unexposed inflamed co-culture (Figure 5.8C, Control), all three cytokines were detected at significantly increased ($p \leq 0.001$) concentrations (IL-1β: 359 ± 362 pg / mL; IL-8: 12,120 ± 4,031 pg / mL; TNF-α: 826 ± 421 pg / mL) compared to the Caco-2 monoculture and stable co-culture control. In the different exposure conditions, the release of IL-1β, IL-8, and TNF-α remained similar to the inflamed co-culture control (Figure 5.8C). No statistically significant differences were observed.

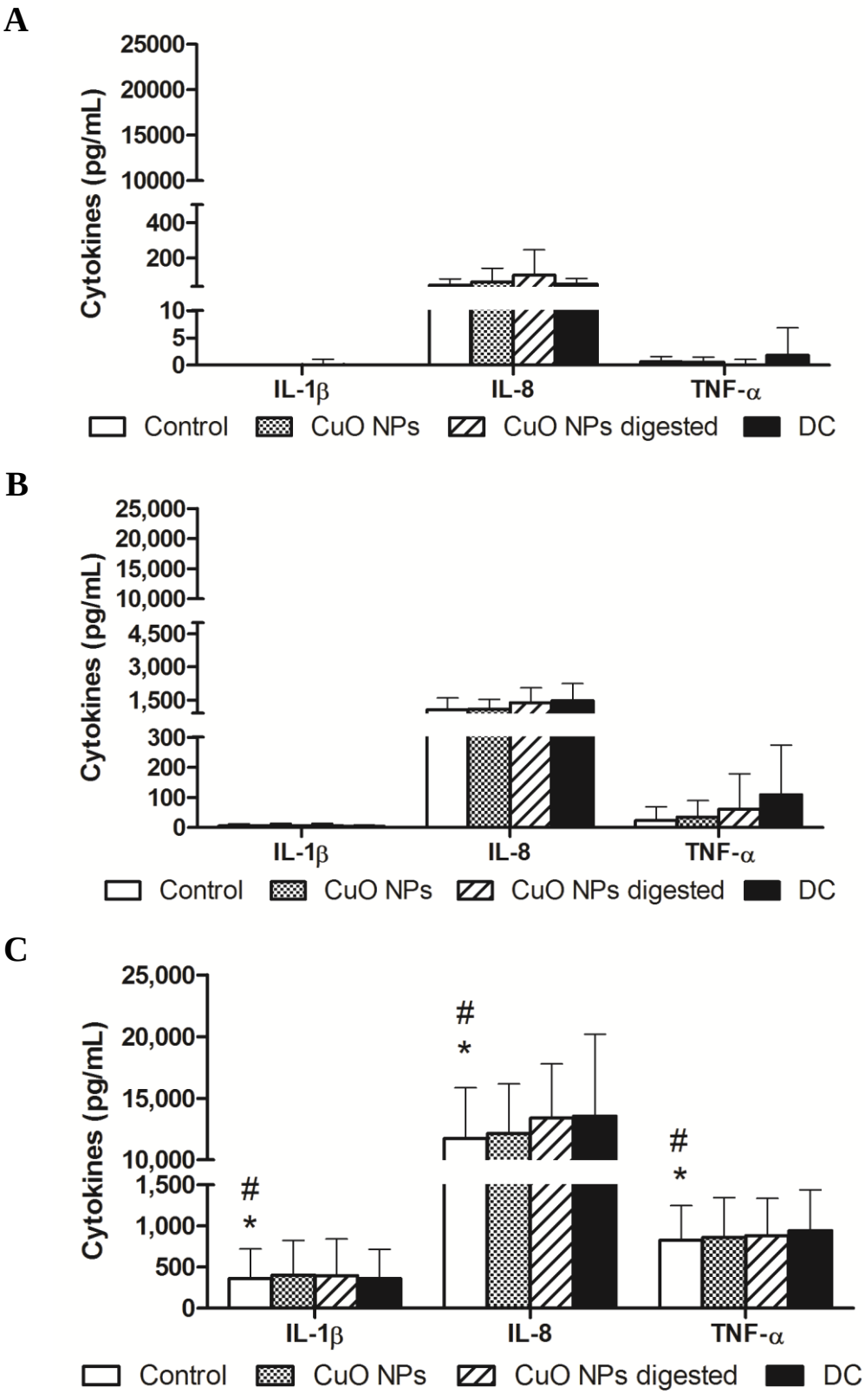

Figure 5.8 Release of IL-1β, IL-8, and TNF-α in (A) Caco-2 monoculture, (B) stable co-culture, and (C) inflamed co-culture with and without exposure to 12.5 µg / mL CuO NPs, 12.5 µg / mL digested CuO NPs, or the equivalent volume of the digestion control (DC)

*(Average of N=3 ± StDev; *p≤0.05 compared to corresponding monoculture control, #p≤0.05 compared to corresponding stable co-culture control)*

5.3.3.3 Quantification of NO_2^-

The formation NO in response to the exposure to CuO NPs or the digestion control was indirectly determined by measurement of NO_2^-. Here, the inflamed co-culture control also acted as positive control for the formation of NO. If no increased concentrations of NO_2^- were detected in the inflamed co-culture control, the run was not considered further for the analysis.

After 48h of Caco-2 monoculture (Figure 5.9A), the levels of NO_2^- in both AP and BL compartment were very low (1.8 and 1.3 µM, respectively). Neither the exposure to CuO NPs nor the digestion control induced a noticeable change in the release of NO_2^-. In the stable co-culture condition the concentration of NO_2^- was not significantly different from the monoculture in both AP and BL compartment (Figure 5.9B). Also after the exposure to digested and undigested CuO NPs, as well as the digestion control the levels remained close to the detection limit of the assay. In the inflamed co-culture, the release of NO_2^- increased significantly 3.8-fold in the AP and 4.5-fold in the BL compartment compared to the monoculture control to 6.9 and 5.9 µM, respectively (Figure 5.9C). Also in the inflamed model the exposure to digested and undigested CuO NPs and the digestion control did not results in significantly changes.

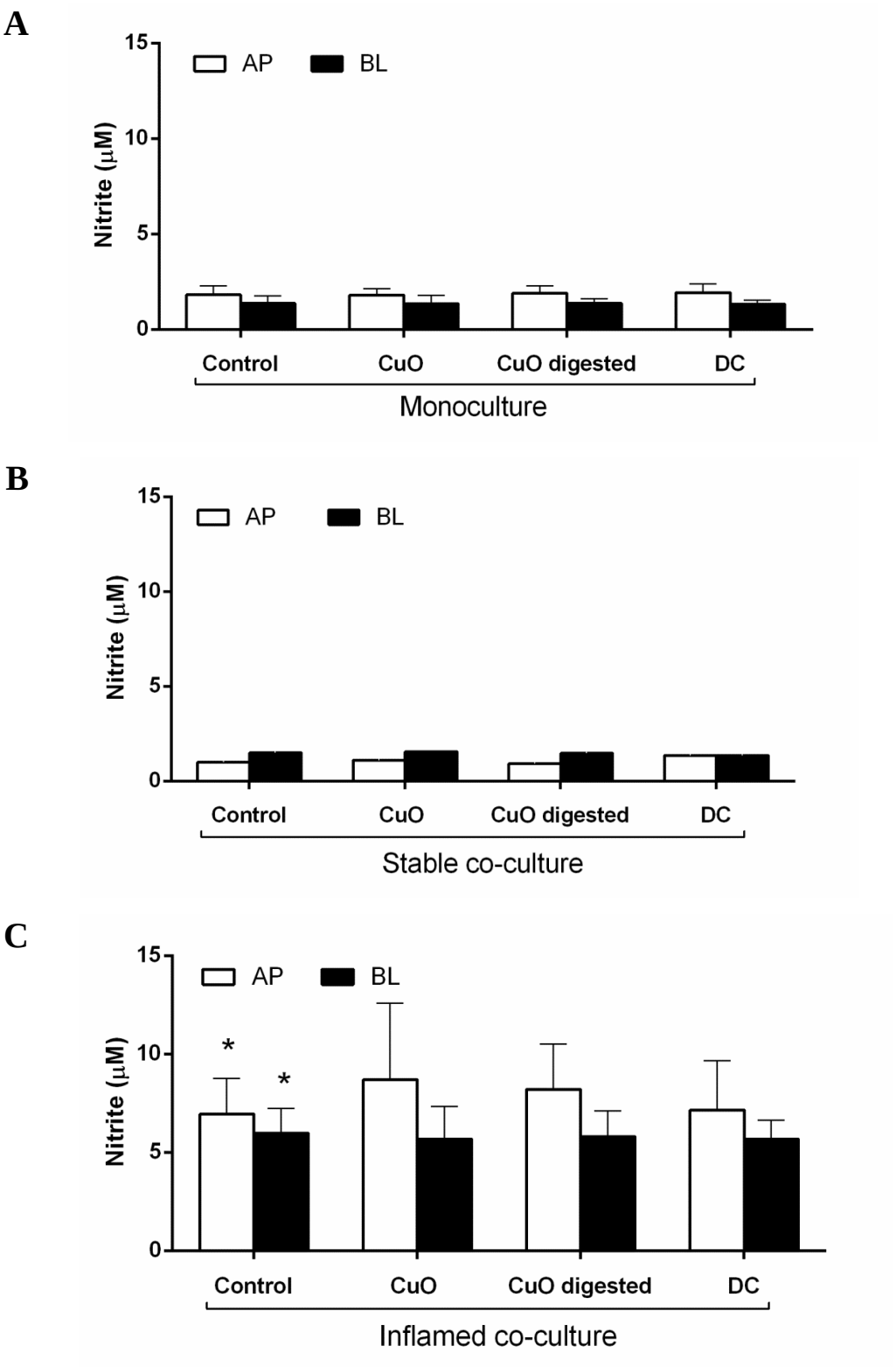

***Fi*gure 5.9 Quantification of NO_2^- after 48h (A) Caco-2 monoculture, (B) stable, or (C) inflamed co-culture with and without 24h exposure to 12.5 µg / mL CuO NPs, 12.5 µg / mL digested CuO NPs, or an equivalent volume of the digestion fluids as control (DC)**

*(Caco-2 monoculture and inflamed co-culture: Average of N=2 ± StDev; Stable co-culture: Average of n=3 from one experiment; *p≤0.05 compared to Caco-2 monoculture control)*

5.4 Discussion

In the present study, the stable and inflamed co-culture models were used to study the effects of CuO NPs. The main findings can be summarised in the following points:

- The CuO NPs rapidly dissolved in CCM so that the cells were likely exposed to increasing concentrations of ionic Cu instead of particulate CuO.
- THP-1 cells were more sensitive to the exposure to undigested CuO NPs than Caco-2 cells, but less vulnerable to digested CuO NPs, as indicated by changes in metabolic activity.
- The exposure to undigested CuO NPs significantly reduced the Caco-2 barrier integrity in the monoculture and stable co-culture. In the inflamed co-culture, the exposure to digested CuO NPs significantly inhibited the re-establishment of barrier integrity.
- The exposure to undigested and digested CuO NPs did not affect the release of IL-1β, TNF-α, and IL-8 or the generation of NO in any of the three culture models.

5.4.1 CuO NPs characterisation

The characterisation of the CuO NPs with CLS confirmed the presence of a substantial amount of micron-sized CuO particles, agglomerates, or aggregates next to a second fraction of nanoparticulate CuO. The observed rapid sedimentation was, therefore, not surprising. For a short period of time, the cellular dose of the particles can be expected to be equal to the exposure concentration. When incubated in CCM at standard culture conditions the particles sedimented rapidly but also dissolved over time. From the CLS curves it can be assumed that the dissolution occurred mainly throughout the first 4h and reached equilibrium at longer incubation times. Therefore, treated cells were likely exposed to nano- and micron-sized CuO particles, but also to an increasing concentration of ionic Cu.

As discussed previously (Section 4.4.1), the particle size and stability greatly influence the cellular dose, i.e. the concentration of sedimented NMs the cells are eventually exposed to in contrast to the total exposure concentration (Hinderliter et al., 2010). Apart from the media density and viscosity, the particle size and density are important

characteristics to determine a particle's deposition, as they define its diffusion and sedimentation behaviour (Hinderliter et al., 2010).

In line with the here presented results, a similar dissolution behaviour of CuO NPs was described by Misra and colleagues (2014). The group observed that ~80 % of both spherical and rod-shaped CuO NPs rapidly dissolved over the first 4h of incubation in CCM without further changes over the subsequent 20h (Misra et al., 2014). Interestingly, we observed an increase in peak intensity in the CLS measurements between 4 and 24h of incubation, which cannot be clearly explained. It is possible that a precipitation of solubilised Cu ions occurred, as has been observed for AgNPs (van der Zande et al., 2012). Otherwise, the lower peak intensity after 4h compared to 24 and 48h of incubation might have been caused by insufficient re-suspension of sedimented particles before the CLS sample was taken. Taking into account the general heterogeneity of the particle stock suspension, the differences in peak intensity could reflect variations in the subsequently prepared samples.

Due to the rapid sedimentation rate, the exposed cells likely encounter intact CuO NPs or particle aggregates before they dissolve. Since cells are able to engulf particles of up to 5 µm by macropinocytosis (Odzak et al., 2014) an uptake of these large CuO particles or complexes is generally possible (Lim and Gleeson, 2011). Since the average size of the particles varied considerably between different stock suspensions the average particle size and specific surface area that cells were getting in contact with probably differed between the experiments.

After the artificial digestion of the particles, probably no or little particulate CuO remained in the stock suspension. Indeed, both *in vivo* and *in vitro*, the dissolution of Cu and CuO NPs has been shown to be strongly influenced by the pH of the environment (Meng et al., 2007; Odzak et al., 2014). Interestingly, we noted a pH-increasing effect of CuO NPs in artificial gastric fluid at physiologically relevant pH. A similar effect was observed earlier by Meng et al. who demonstrated nicely how nano-Cu but not micro-Cu particles consumed significant amounts of H^+ in strongly acidic environment (pH<2) and, thereby, induced an increase in pH to above 5. As a basic oxide, CuO dissolves in mineral acids. In HCl, the dissolution results in the formation of copper chloride ($CuCl_2$) and H_2O (Equation 5.1). As a consequence of the continuous oxidation of the particles, H^+ is consumed. This explains why in our conditions the initial pH of ~2.2 increased over the incubation time with CuO NPs. Therefore, we decided to decrease the pH of the gastric phase further, even though it

does not perfectly represent a physiological condition. We assumed that in a realistic exposure condition *in vivo* the organism would likely react with an increased synthesis of gastric fluid to compensate for the H^+ scavenging. In a study conducted in mice, however, Meng et al. (2007) found severe swelling and green discoloration of the gastric tissue after exposure to Cu NPs. The group suggested that nano but not micro-sized Cu particles are retained in the stomach and continue to react in the acidic environment generating considerable amount of Cu ions.

When the pH was subsequently increased to ~6.8 to reflect the conditions in the small intestine, the Cu ions reacted with NaOH to form copper (II) hydroxide ($Cu(OH)_2$) (Equation 5.2). Hence, cells exposed to digested CuO NPs probably encountered only very low concentrations of solid particles if any at all. Instead, the cells were likely exposed to Cu compounds like $CuCl_2$ and $Cu(OH)_2$.

$$CuO_{(S)} + 2HCl \rightarrow CuCl_2 + H_2O \qquad \textbf{(5.1)}$$

$$CuCl_2 + 2NaOH \rightarrow Cu(OH)_2 + 2NaCl \qquad \textbf{(5.2)}$$

In retrospective, a more elaborate digestive process or at least use of $NaHCO_3$ instead of NaOH should have been favoured, as it is more representative of the physiological processes within the GI-tract (Säfsten, 1993). In presence of $NaHCO_3$, $CuCl_2$ would have likely reacted to Cu carbonate ($CuCO_3$) instead of $Cu(OH)_2$. The implication of these differences for the downstream effects of exposure to digested CuO NPs is not clear. Cu^{2+} is generally regarded as the main form to cause toxicity, whereas $CuCO_3$ appears to be less or non-toxic. The potential of $Cu(OH)_2$ is less clear but has also been shown to exert a certain level of cytotoxicity. At a pH of 6.5-7 the Cu complexes might dissolve over time to ionic Cu^{2+} regardless of the composition (Grosell, 2012).

It remains debateable, whether the particulate fallout formed after addition of NaOH acts on the cells like particulate or ionic Cu. Since the calculation by the instrument's internal software is based on the molecular weight and density of CuO the average size of the particles as measured by CLS is probably distorted. The molecular weight of $Cu(OH)_2$ is slightly higher with 97.5 compared to 79.5 g / mol.

5.4.2 Cytotoxic effects of undigested and digested CuO NPs in cell monocultures

Undigested CuO NPs induced a dose–dependent decrease in cell viability in both $_{UD}$Caco-2 and PMA-differentiated THP-1 cells. The more detailed cytotoxicity assessment, however, revealed considerable differences between Caco-2 and THP-1 cells, as well as between undigested and digested CuO NPs. In contrast to Caco-2 cells, the viability of PMA-differentiated THP-1 cells was already significantly reduced at exposure concentrations of 12.5 µg / mL undigested CuO NPs. Similar observations were made by other groups, for both CuO NPs and other NMs. In an interlaboratory study investigating the toxicity of 24 NMs, Lanone et al. (2009) reported significant differences in the sensitivity between an epithelial cell line (A549) and monocytes (THP-1). Whereas rather low concentrations of just 3 µg / mL were sufficient to reduce THP-1 viability by 50 %, 26.5 µg / mL CuO NPs were necessary to induce the same effect in A549 cells (Lanone et al., 2009). In contrast, Soto and colleagues (2007) observed a slightly higher sensitivity to the exposure to NMs in A549 cells compared to human macrophages. What seems like a contradiction at first might be related to the proliferation rate of the cells. It was suggested that the cytotoxic effect of NMs also depends on the metabolic activity of the cells, with slower proliferation times increasing the susceptibility (Chang et al., 2007). In contrast to Soto et al., Lanone and colleagues and this project used PMA-differentiated THP-1 cells. One of the effects of PMA exposure is the drastically reduced or even inhibited proliferation of the cells. Instead, the $_{UD}$Caco-2 cells are likely in a phase of rapid growth and a high proliferation rate (Singh et al., 1996), which might explain the reduced vulnerability compared to the macrophages.

Another potential reason for the higher cytotoxicity of CuO NPs in the macrophages is the cells' phagocytic activity, which is increased in response to PMA-differentiation (Tsuchiya et al., 1982). Furthermore, the uptake of particles by PMA-differentiated THP-1 cells has been shown to be almost exclusive to macropinocytosis, a mechanism which is essentially required for the uptake of very large particles (Lunov et al., 2011) as used here.

Several groups have studied the influence of artificial digestion on exposure effects of NMs, for instance induction of cytotoxicity. The impact of digestion seems to heavily depend on the type of investigated NM. Both Böhmert et al. (2014) and Gerloff et al. (2013) did not find a significant influence of digestion of the toxic potentials of either

AgNPs or SiO_2 NPs in Caco-2 cell cultures. A study using PEG-coated CdSe quantum dots on Caco-2 cells showed a drastically increased cytotoxicity after incubating the particles in acidic pH (Wang et al., 2008a). As mentioned earlier (Section 5.1.1), different groups noted a lower level of cytotoxicity induced by ionic Cu compared to CuO particles (Thit et al., 2013; Piret et al., 2012b). The artificial digestion caused the complete dissolution of the CuO NPs and the cells were most likely exposed to ionic Cu compounds instead of particulate CuO. Based on the assumption that cells have better regulated uptake mechanisms for ionic than particulate Cu we expected to see a less potent induction of cytotoxicity by digested compared to undigested CuO NPs. This was, however, only the case for THP-1 cells. In Caco-2 cells, digested CuO NPs were slightly more toxic after 48h of exposure than undigested CuO NPs. In contrast to other groups, we investigated the cytotoxicity in confluent $_{UD}$Caco-2 cells. As was discussed before (Section 4.4.3.2), the differentiation of the cells might lead to the induction or resting of pathways or proteins, e.g. receptors, which might be essential for the uptake of ionic Cu. Whereas the uptake of Cu ions is strictly regulated in differentiated enterocytes it might be controlled less rigidly before and throughout the differentiation.

5.4.3 The effect of CuO NPs exposure in the (co-)culture models

The monoculture and both co-culture conditions were used to study the cytotoxic and pro-inflammatory potential of non-toxic concentrations of CuO NPs, as well as the impact of the health status on the exposure effects. However, quantifying cytotoxic effects in the context of the health status was challenging, as neither the Alamar Blue nor the LDH assay could be applied. Hence, the analysis of a representative number of cells of the Caco-2 cell layer using the IN Cell Analyzer was the only feasible alternative. Due to the complexity of the image acquisition and analysis, these results could not be generated on time. Therefore, no information on the potentially increased susceptibility of differentiated compared to $_{UD}$Caco-2 cells and inflamed compared to stable co-cultures are available.

In the experiments presented here, CuO NPs did not induce a cytokine release or NO generation in the Caco-2 monoculture and the stable co-culture. In contrast to this, Piret et al. (2012b) found a clear upregulation of IL-8 synthesis in monocultures of $_{D}$Caco-2 cells. However, Piret and colleagues applied much higher exposure concentrations of 25 µg / mL which in our cell cultures reduce the viability significantly. Furthermore, in

the study by Piret et al. (2012b) the noticeable induction of IL-8 release required an exposure time of at least 48h. It is possible that an exposure period of 24h was not sufficient to observe changes in the cells' cytokine profile. In other cell lines, e.g. the lung epithelial cell line A549, a 24h treatment has been reported to be sufficient to induce IL-8 at even lower concentrations of around 10 µg / mL (Cho et al., 2011). At high concentrations of 100 µg / mL, an exposure time as short as 3h caused a significant release of pro-inflammatory cytokine in lung epithelial cells (Moschini et al., 2013).

Another important point to consider is the translocation rate of apically added CuO NPs or Cu ions across the Caco-2 barrier. In this study it is not clear what concentrations of CuO particles and Cu ions passed the Caco-2 barrier to directly interact with the THP-1 cells in the BL compartment. Moreover, as shown by the CLS results, the average particle size can vary considerably between different batches of stock dispersion. It can be assumed that the dissolution of the particles in the CCM differs depending on the initial ratio of MPs to NPs in the suspension. In this context, it is difficult to estimate the composition of the supernatant including the ratio of ionic to nano- to micro-sized Cu throughout the exposure period. This information is, however, crucial since large variations in Cu uptake are likely between particulate and ionic Cu, as well as between nano- and micro-sized CuO. According to *in vitro* experiments in Caco-2 cells and *in vivo* research in chicken the absorption rate is highest for CuO NPs (60 and 51 % respectively) and lowest for CuO microparticles (MPs) (12 and 14 %, respectively) (Chen et al., 2015a). The transfer rate of ionic Cu has been measured to be ~40 % (Chen et al., 2015a; Bauerly et al., 2004).

Additionally, the effect of CuO exposure seems to vary considerably between cell types and even within the same cell type of different origin. When the same particles and exposure concentrations were used, CuO particles induced the generation of IL-8 in alveolar epithelial cells, but not in bronchial epithelial cells (Cho et al., 2013a). Whereas CuO NPs could induce the release of IL-1β in alveolar macrophages, no increase in either TNF-α or IL-1β was observed in both differentiated PBMCs and PMA-differentiated THP-1 cells (Cho et al., 2013a). Even though this study found digested and undigested CuO NPs to exert strong cytotoxic effects in THP-1 cultures it is possible that the cells generally do not react to the exposure with the release of pro-inflammatory cytokines.

Instead of inducing an inflammation in the co-culture it is possible that CuO affected the system differently if the exposure occurs during an ongoing inflammatory condition. As mentioned in the introduction, studies suggest that ongoing inflammatory processes lead to a dysregulation of the otherwise well-controlled uptake of Cu ions (Fernández-Banares et al., 1990; DiSilvestro and Marten, 1990). However, no worsening or amelioration of the ongoing inflammation was observed in this project. In contrast, Triboulet et al. (2013) observed a reduction in RNS as well as the release of IL-6 but not TNF-α in LPS-stimulated murine macrophages after 26h exposure to different concentrations (5 and 20 µg / mL) of CuO NPs. Based on the earlier mentioned differences between different cell types and cell lines it is possible that this effect does not occur in THP-1 but only J774 cells.

Even though no effects were noted in the cytokine release and induction of nitrous stress the exposure to CuO NPs had an impact on the barrier integrity in all three conditions. In the Caco-2 monoculture and stable co-culture the exposure to undigested CuO NPs induced a significant reduction in TEER indicating a disruption of the barrier function. Whether this barrier disruption was based on an effect on the TJ network or the Caco-2 cell viability cannot be answered. Based on the cytotoxicity data generated in $_{UD}$Caco-2 cells the exposure concentrations should not have induced cytotoxicity. It might, however, confirm the discussed susceptibility of cells in relation to their metabolic activity (Section 5.4.2). Whereas $_{UD}$Caco-2 cells were in rapid growth phase after 3 days of culture their proliferation was likely strongly reduced or halted after a culture period of 13 days (Singh et al., 1996). If a reduced proliferation rate renders the cells more susceptible it is possible that 12.5 µg / mL CuO NPs negatively affected $_{D}$Caco-2 cells, even though no effect was noted in $_{UD}$Caco-2 cells. Similar results were obtained by Thit et al. (2013) after exposing kidney cells (aquatic toad *Xenopus laevis*) to CuO particles. The group reported increased vulnerability of differentiated compared to dividing cells to both ionic Cu and CuO NPs. Interestingly, in the experiments presented here the effect on the barrier integrity of $_{D}$Caco-2 cells was limited to undigested CuO particles in both the monoculture and stable co-culture. This was in line with the findings of other groups showing that ionic Cu induces less severe effects than Cu or CuO particles (Piret et al., 2012a; Wang et al., 2012).

In contrast, the opposite effect was observed in the inflamed co-culture. Here, the exposure to digested CuO NPs interfered more strongly with the re-establishment of the barrier integrity than undigested CuO NPs. So far, the results were discussed assuming

that the uptake of ionic Cu is well controlled and regulated and, therefore, causes less damage than particulate CuO. As research showed, patients suffering from chronic inflammation of the intestine display significantly higher serum Cu levels than healthy controls (Fernández-Banares et al., 1990; Ojuawo and Keith, 2002). This suggests that the uptake of dietary Cu and the systemic balance of the trace element are distorted in inflamed conditions. It is possible that we observed a similar effect in the inflamed co-culture. Whereas the undigested CuO NPs affected the barrier to a similar extent as in the monoculture and stable co-culture, the Cu ions of the digested CuO NPs could possibly exert a stronger effect due to an increased / distorted uptake in stressed Caco-2 cells. Even though the exposure did not influence the release of pro-inflammatory cytokines and NO, digested CuO NPs might interfere with the re-establishment of barrier integrity in intestinal inflammation. A decreased integrity of the intestinal wall impairs the gate function of the intestinal barrier (Suzuki et al., 2011; Al-Sadi and Ma, 2007; Gerova et al., 2011), which in turn might result in the increase translocation of potentially harmful antigens. Therefore, the interference of CuO NPs with the barrier re-establishment *in vivo* might cause a prolongation or even worsening of an existing medical condition.

5.5 Conclusions

The aim of this study was to apply the developed stable and inflamed co-cultures to study the cytotoxic and inflammatory effects of non-toxic concentrations of undigested and digested CuO NPs. The results generated in cell monocultures showed that the cytotoxic potential of digested CuO NPs is not generally lower compared to undigested CuO NPs but depends on the studied cell type, which clearly disproved the chapter's first hypothesis. Due to the lack of available methods to study the cell viability in transwells the CuO-induced cytotoxicity could not be addressed sufficiently in the transwell cultures. An indirect assumption regarding the CuO-induced toxicity could be made based on the CuO-mediated reduction in TEER. This indication is, however, very vague since a reduction in TEER does not necessarily reflect a reduction in cell viability. Whether non-toxic CuO NP-concentrations remain non-toxic in $_{D}$Caco-2 cells could not be answered. Interestingly, digested and undigested CuO NPs affected the exposed co-cultures differently. On the one hand, this disproved the hypotheses that the digestion will not affect the effects in the stable or inflamed co-culture. On the other hand, these results confirmed the hypothesis that digested and undigested CuO NPs will

induce different effects the stable compared to the inflamed co-culture. This was clearly proven as undigested but not digested CuO NPs negatively affected the barrier integrity in the stable co-culture, whereas effects in the inflamed co-culture were only significant in response to digested CuO NPs. No pro- or anti-inflammatory effects were noted in either co-culture model.

6 Application of the co-culture models to study the barrier crossing of radio-labelled [^{195}Au]AuNPs

6.1 Introduction

For many years, nanotoxicological research has focused on studying the effects of NMs with the investigation of fixed endpoints, like cytotoxicity, genotoxicity, or induction of inflammation. Therefrom, a considerable amount of knowledge has been generated regarding the toxicity mechanisms of NMs in biological systems. However, the understanding of the biokinetics of NMs (i.e. absorption, systemic bioavailability, tissue distribution, accumulation / excretion) has been insufficiently covered to date. Understanding the uptake and distribution kinetics of NMs in biological systems is crucial to determine the concentrations effectively crossing biological barriers, e.g. the intestine (Lee et al., 2014). The effective uptake and subsequent distribution are important pieces of information for a thorough risk assessment of NMs (Bouwmeester et al., 2009).

Also with regard to the developing field of nanomedicine knowledge on the biokinetics of NMs is of utmost importance. Firstly, oral administration of drugs still is the preferred and often only feasible route of drug administration, e.g. in case of insufficient health care infrastructure (Sastry Venkateswara et al., 2000). Furthermore, several developments in the medical field like cancer research and cell-based therapies depend on the availability of reliable and safe real-time *in vivo* detection/imaging solutions to determine systemic availability and tissue distribution of nano-sized objects (Taylor et al., 2012). However, the tracing, and quantification of unlabelled NMs is problematic and often unprecise (Holzwarth et al., 2014). Therefore, the labelling of NMs has received increasing interest over the last years, with radioactive isotopes having emerged as one of the most sensitive methods to quantify and visualise the location of NMs *in vivo* and *in vitro* (Holzwarth et al., 2014).

6.1.1 Application of radio-labelled NMs to study intestinal availability

The labelling of NMs with radionuclides can be effected by different means. It can either be performed on a material before the synthesis of the desired nano-object (Yang et al., 2013) or follow post-synthesis on the final object (Holzwarth et al., 2014). For post-synthesis labelling, the radio-label can be introduced into the structure of the NM

(e.g. by proton irradiation of NPs that causes transmutation in a small fraction of their atoms into radionuclides) or attached onto its surface (Abbas et al., 2009; Gibson et al., 2011; Holzwarth et al., 2014). In contrast to surface-labelling, which is an important determinant for the behaviour of NMs in biological systems, the introduction of radio-isotopes in the internal structure seems to hardly, if at all, alter the surface chemistry of NMs (Lee et al., 2014; Abbas et al., 2009; Holzwarth et al., 2014). Several research groups have successfully labelled various types of NMs, e.g. ZnO, SiO_2, and polymers, and subsequently applied for kinetic studies and nanomedical applications, or a combination of both. Radio-labelled polylactic acid NPs were used to demonstrate the impact of polyethylene glycol surface coverage on mucus penetration and absorption of NMs (Ensign et al., 2012). Both Lee et al. (2012) and Bimbo et al. (2010) used ^{18}F-labelling to study the bio-compatibility and -distribution of ZnO and SiO_2 NPs in rats. The application of SiO_2 NPs was further developed as potential drug delivery system to increase the oral bioavailability of drugs (Sarparanta et al., 2012). However, not all NMs are suitable for oral exposure applications due to colloidal instability, dissolution, and hence, release of ions (Bergin and Witzmann, 2013). For example, CdSe quantum dots (QD) did not induce a cytotoxic effect *in vitro* when dispersed in CCM unless they were subject to an artificial gastric digestion, which drastically increased their toxic potential (Wang et al., 2008).

6.1.2 Use of AuNPs for radio-tracer studies

Even though several materials have been investigated and used for radio-labelling and -tracing studies, Au has received special attention because of its biocompatibility, easy handling of surface modification, and high colloidal stability under physiological conditions (de Barros et al., 2012; Chanana et al., 2013). AuNPs are generally reported to be non-cytotoxic even at high exposure concentrations of 500-1000 µM (Freese et al., 2012; Lin et al., 2011), but potentially induce the release of pro-inflammatory cytokines. In mesenchymal stem cells, for instance, the exposure to AuNPs caused an increased release of IL-8 and IL-6 (Mahl et al., 2010). In macrophages the reported effects are more diverse. Some groups noted more detrimental effects of AuNP-exposure with a reduction in cell viability and upregulation of pro-inflammatory cytokines like IL-6 and TNF-α (Yen et al., 2009). Others observed a similarly high resilience to AuNPs as in epithelial and endothelial cells and no indications for pro-inflammatory processes (Shukla et al., 2005; Bancos et al., 2015). All studies using

macrophages uniformly described an uptake of AuNPs, though the uptake efficiency seemed to heavily depend on the particle characteristics like geometry, surface modification, and protein corona (Arnida et al., 2011).

6.1.3 Aims and hypotheses

Several studies have investigated the intestinal uptake of AuNPs *in vivo* (Schleh et al., 2012; Hillyer and Albrecht, 2001) and *in vitro* (Lin et al., 2011). To our knowledge, the effect of an inflammation-like process on the uptake / translocation of AuNPs has not been addressed to date. With radio-actively labelled [^{195}Au]AuNPs we aimed to study the paracellular translocation across the Caco-2 epithelial barrier and the potential uptake by the THP-1 cells in the BL compartment in relation to the health status of the co-culture at the time of exposure, as well as the particle size.

The investigation was based on the following hypotheses:

- In the Caco-2 monoculture and stable co-culture the translocation of [^{195}Au]AuNPs to the BL compartment is minimal to absent.
- In the inflamed co-culture the loosened TJ network allows for a significantly increased translocation of [^{195}Au]AuNPs to the BL side compared to exposed Caco-2 monocultures and stable co-cultures.
- The rate of translocation is higher for smaller [^{195}Au]AuNPs.
- [^{195}Au]AuNPs passing into the BL compartment are taken up by THP-1 cells.

6.2 Materials & Methods

6.2.1 Au irradiation

The irradiation was kindly performed by Neil Gibson and Uwe Holzwarth from the Radiotracers CG (NBS Unit, JRC, Italy).

The radionuclide ^{195}Au was produced by irradiating Au foil (99.99 %, 0.25 mm thick, 25x25 mm, Sigma Aldrich) with protons of 29.8 MeV energy. During the proton irradiation the foil was immersed in a cooling water flow to ensure simultaneous cooling from the front (oriented towards the incoming proton beam) and the rear side. The collimated proton beam had a circular shape with a diameter of 10 mm. Hence, only a circular central part of the foil with a diameter of 10 mm was irradiated and

contained the desired radionuclide. Only this irradiated part – hereinafter ^{195}Au or 'hot' Au – was used for the subsequent synthesis.

The activity $A(t)$ of a radionuclide after proton irradiation of a target for a duration t can be calculated as

$$A(t) = N_{\mathrm{V}}\dot{\Phi}\left(1-e^{-\lambda t}\right)\int_{E_{\min}}^{E_{\max}}\sigma\left(\frac{\mathrm{d}E_{\mathrm{p}}}{\mathrm{d}x}\right)^{-1}\mathrm{d}E_{\mathrm{p}}\,, \tag{6.1}$$

where N_{V} denotes the number density of target atoms in the irradiated volume and $\dot{\Phi}$ the flux of protons through the irradiated volume per second. The irradiation conditions were selected to exceed an activity concentration of 1 MBq / mg of Au in the irradiated area. A total proton dose of 400 μA.h was applied.

6.2.2 Quantitative γ-ray spectrometry

Quantitative γ-ray spectrometry was applied to quantify the ^{195}Au activity in the different experimental fractions and to determine the mass of AuNPs from the activity concentration of the irradiated Au foils used for the synthesis of the NPs back to end of proton bombardment as time reference. Quantitative γ-ray spectrometry was performed with ultrahigh-purity germanium (HPGe) detectors from CANBERRA (USA) and EG&G Ortec (USA) calibrated in energy and efficiency with certified standard calibration sources (uncertainty: 1-1.5 %) for each standard geometry (DAMRI and CERCA, France; ENEA, Italy; the Czech Metrological Institute, Czech Republic).

Standardised geometrical conditions were defined for measuring the activity of the irradiation capsule, Au foils, [^{195}Au]-$HAuCl_4$ x H_2O solution (0.01 M), as-synthesised [^{195}Au]AuNPs (5 nm) and [^{195}Au]Au core-shell NPs (30 nm), washing liquids and all samples from the intestinal barrier model exposed to the NPs for each time point. The γ-ray spectra were analysed using the spectrometry analysis software packages of Canberra (Genie 2000 software) and EG&G Ortec (Gamma Vision Software). In order to correct for radioactive decay during the experiments all activity values were calculated back to end of bombardment as reference time t=0 or back to the end of synthesis of the radiolabelled AuNPs.

6.2.3 [^{195}Au]AuNPs synthesis

The particles were synthesised by Isaac Ojea Jiménez and Elena Bellido of the Radiotracers CG (NBS unit, JRC, Italy).

6.2.3.1 Preparation of the radioactive precursor - ^{195}Au-labelled gold(III) chloride hydrate

The precursor for the NP synthesis [^{195}Au]-$HAuCl_4 \cdot x\ H_2O$ was prepared by the dissolution of hot Au foil in a stoichiometric appropriate volume of freshly prepared aqua regia and subsequent evaporation of the liquid at boiling temperature. All solutions were freshly prepared and glassware was cleaned before use with aqua regia and MilliQ water.

6.2.3.2 Synthesis of 5 nm [^{195}Au]AuNPs

After dissolving 63.8 mg Au contained in dried $HAuCl_4$ in MilliQ H_2O and subsequent filtration (0.22 µm pore size), 76% of the starting activity were recovered in the filtered solution. Hence, the NP-synthesis started from 48.5 mg Au in 10 mL aqueous solution, which corresponds to a concentration of 25 mM.

Of this 25 mM Au(III)-salt solution 1 mL was added to 100 mL of 0.25 mM sodium citrate solution under permanent stirring. The synthesis of particles was initiated by adding 1 mL of 0.1 M chilled sodium borohydride ($NaBH_4$) solution under immediate stirring, which resulted in a dark red solution. Stirring was continued for 20 min at RT. A sample was taken for DLS analysis and γ-ray spectrometry. The remaining [^{195}Au]AuNPs suspension was stored at 4°C protected from light. For the batch used in these experiments an initial activity concentration of 286 ± 18 kBq / mg was calculated.

6.2.3.3 Synthesis of 30 nm core-shell [^{195}Au]AuNPs

Citrate-stabilized 30 nm [^{195}Au]Au core-shell NPs were synthesized by seeding growth from non-radioactive Au seeds. Small non-radioactive AuNPs (12 nm by TEM, data not shown) were used as seeds for growing a [^{195}Au]Au-labelled shell. The process results in the synthesis of cold Au core hot Au shell NPs (Figure 6.1). In a typical

synthesis, trisodium citrate dihydrate solution (5.6 mL, 0.1 M) and sodium hydroxide solution (0.8 mL, 0.2 M) were added to MilliQ H_2O (184 mL) while stirring and heated up to 65°C in a silicone oil bath. Then the 12 nm cold Au seeds (5.2 mL, 0.5 mM) were added to the solution under continued stirring. Finally, a solution of [^{195}Au]-$HAuCl_4 \cdot x\ H_2O$ (4.4 mL, 0.01 M) was added to the mixture and the reaction was allowed to continue under stirring at 65°C for 48h. Subsequently, the reaction solution was cooled to RT.

For example the following activity was calculated for one batch: the synthesis resulted in a total mass of 9.18 mg [^{195}Au]Au-NPs with a total activity of 4.07 MBq. Therefore, an activity concentration of 444 ± 28 kBq / mg was obtained.

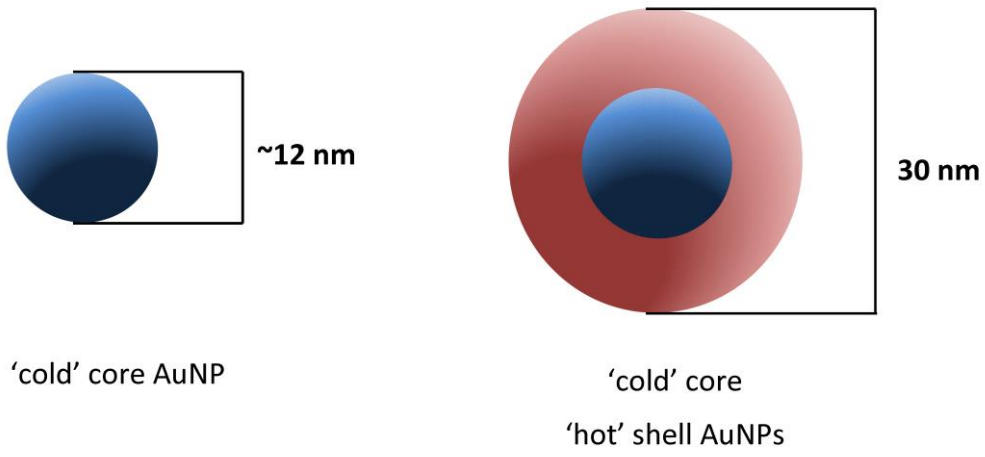

Figure 6.1 Structural composition of 30 nm core-shell AuNPs

6.2.3.4 Determination of the radiochemical yield after NP synthesis

The radiochemical yield was determined from the liquid phase after filtration using 10 kDa Amicon centrifugal filters (Merck). The centrifugation was carried out at 2,415 x*g* for a total of 45 minutes at 4°C. The centrifugation recovered a fraction of $^{195}Au^+$ ions with a total activity of 0.030 ± 0.013 Bq / mL. Based on the total activity of irradiated Au foil the recovered ion-associated activity accounted for less than 0.01 % of the material used for the synthesis. Hence, a reaction yield of 99.9 % was achieved.

6.2.3.5 Evaluation of ^{195}Au release from [^{195}Au]AuNPs in CCM

To evaluate the integrity of the two sizes of [^{195}Au]AuNPs throughout the *in vitro* experiments, leaching tests were performed in MilliQ H_2O and CCM at standard culture conditions. 35 mL of the nanoparticle suspensions (100 μM) in CCM and MilliQ water were kept in Falcon tubes under standard culture conditions. At different time points (0, 6, 24, and 96h), the tube contents were mixed by inverting the tubes. Three aliquots of 2.5 mL each were collected from which the [^{195}Au]AuNPs were removed by filtration (10 kDa Amicon filters at 3,460 x*g* for 20 min). Finally, the presence of ^{195}Au radioisotopes was determined in the filtrate by γ-ray spectrometry.

6.2.3.6 Preparation of NP suspensions for biological experiments

For cell exposure experiments, the original NP suspension was concentrated 20x from 0.25 mM to 5 mM (stock) using 10 kDa Amicon centrifugal filters. The particle suspension was centrifuged at 2,415 x*g* at 4°C in several stages of up to 50 min each until the desired volume was obtained.

To prepare the working stock concentration (100 μM), 1 mL of the 5 mM stock suspension was diluted 1:50 in fresh pre-warmed MEM-based CCM. To obtain a homogenous distribution, the NPs suspension in CCM was vortexed for 30 sec and used within 30 min.

6.2.4 Characterisation of [^{195}Au]AuNPs

The characterisation of 5 and 30 nm AuNPs was kindly performed by Patricia Urbán, Carine Drewes (IBS CG, NBS Unit, JRC, Italy), Isaac Ojea Jiménez, and Uwe Holzwarth. The radio-labelled [^{195}Au]AuNPs of both sizes were characterised by DLS and TEM as described earlier (Sections 4.2.2.1 & 4.2.2.4). The particles were analysed in dispersant, as well as at different time points after incubation in CCM. A cold batch of small AuNPs was investigated using CLS (Section 4.2.3.2) and UV-Vis (Section 4.2.3.3). Since the visual inspection of the samples collected after incubation with cells indicated a potential for aggregation/agglomeration, the batch of cold 5 nm AuNPs was used to study the particle size distribution after incubation with Caco-2 monocultures. For this, Caco-2 cells were seeded onto transwell filter inserts and maintained as

described in Section 6.2.5.1. At day 21, the cells were apically exposed to 100 µM of 5 nm [^{195}Au]AuNPs. After 0, 4, 24, and 48h the AP supernatants containing [^{195}Au]AuNPs were collected and analysed using CLS and TEM.

6.2.5 Exposure experiments

6.2.5.1 Cell culture and co-culture set-up

The cell culture, IFN-γ-priming of Caco-2 cells, PMA-differentiation and activation of THP-1 cells was done by Angela Kämpfer. The co-culture establishment and exposure, as well as subsequent sample collection and TEER measurements were performed by Agnieszka Kinsner-Ovaskainen (IBS CG, NBS Unit, JRC, Italy) under oversight and instruction of Angela Kämpfer.

Caco-2 and THP-1 cells were cultured and maintained as described before (Section 2.1.2). For co-culture experiments, the Caco-2 cells were seeded onto 6-well PET-transwell filter inserts with a pore size of 1 µm (Falcon, 353102) at a density of $1.8x10^5$ cells / cm². The THP-1 cells were differentiated using PMA (100 nM, 24h). Before the start of the co-culture, the THP-1 cells were seeded onto transwell-suitable 6-well plates at a density of $6.7x10^5$ cells / well in 3 mL RPMI-based CCM without ME. Compared to the 12-well based co-cultures the THP-1 cell density increased 3.7 fold, whereas the BL volume doubled. Therefore, the exposure concentrations for both LPS and IFN-γ were increased to 20 ng / mL. The stable and inflamed co-cultures were started as described earlier (Section 4.2.4). For all conditions and time points, cell cultures were prepared in triplicates.

6.2.5.2 Exposure to [^{195}Au]AuNPs and sample collection

The AP and BL medium was discarded from the wells. For the Caco-2 monocultures, the BL medium was replenished with fresh RPMI-based CCM. For the co-cultures, the designated transwell filters were directly transferred to the corresponding well plates containing unstimulated or stimulated THP-1 cells. Subsequently, 2 mL of the [^{195}Au]AuNPs suspension in CCM (100 µM, Section 6.2.3.6) were transferred to the AP compartment. In each experiment, an unexposed Caco-2 monoculture was included,

which served as the negative control for the analysis of barrier integrity as measured by TEER.

The sedimentation behaviour of the particles and their kinetics of passage through cell-free filter inserts were evaluated separately. The cell-free filter inserts were treated with [^{195}Au]AuNPs using the same protocol as for the cell cultures.

All exposed cultures were incubated for 24 or 48h at 37°C, 5 % CO_2. After 24 or 48h of incubation, each Caco-2 monoculture and cell-free transwell generated 4 individual samples:

1. A: AP supernatant
2. B: BL supernatant
3. C: Wash of the AP compartment / transwell filter ('filter wash')
4. D: Transwell filter insert

The stable and inflamed co-cultures generated a 5th sample:

5. E: Accutase-detached THP-1 cells.

The AP and BL supernatants were collected in 15 mL Falcon tubes. The AP compartment and filter were washed once with 2 mL PBS, which was collected in 15 mL Falcons. After washing the filter inserts were collected in zip-lock bags. To the BL compartments of the stable and inflamed co-culture conditions 1 mL Accutase was added to detach the THP-1 cells. After 10 min incubation, the cells were collected with 2 mL PBS in a separate 15 mL Falcon tubes and activity measured as described in Section 6.2.2.

6.2.5.3 Monitoring barrier integrity

Before the start of the co-cultures and after 18, 24, and 48h of exposure the barrier integrity of the Caco-2 monocultures and co-cultures was measured as TEER as described in Section 2.1.4. The TEER was monitored to confirm the compliance of the co-cultures with the earlier defined criteria, as well as to study potential cytotoxic effects of [^{195}Au]AuNPs.

6.3 Results

6.3.1 Characterisation of [^{195}Au]AuNPs

6.3.1.1 Characterisation of 5 nm [^{195}Au]AuNPs

The characterisation results for 5nm [^{195}Au]AuNPs in dispersant and CCM are summarised in Table 6.1.

Table 6.1 Summary of TEM, CLS and DLS measurements of 5 nm AuNPs performed in water and MEM-based CCM

Instrument	Parameter	Dispersant	MEM-based CCM		
			1h	24h	48h
TEM	Size (nm)	4.5 ± 0.693	N/A		
	Shape	spherical			
DLS	Z-average	*	*		
	Peak				
	PDI				
	ζ-potential	-46	-11		
CLS	Size (nm)	5.5	6.3	6.5	31.8
	HHW	2	8	7	N/A

** no meaningful results could be generated; PDI: poly-dispersity index; HHW: half-height width of the measured size distribution*

The 5 nm [^{195}Au]AuNPs were found to be homogenously dispersed with an average diameter of 4.5 ± 0.7 nm according to TEM analysis (Figure 6.2). No change in colloidal stability was noted after incubating the particles in fresh CCM for a minimum of 48h (Figure 6.3).

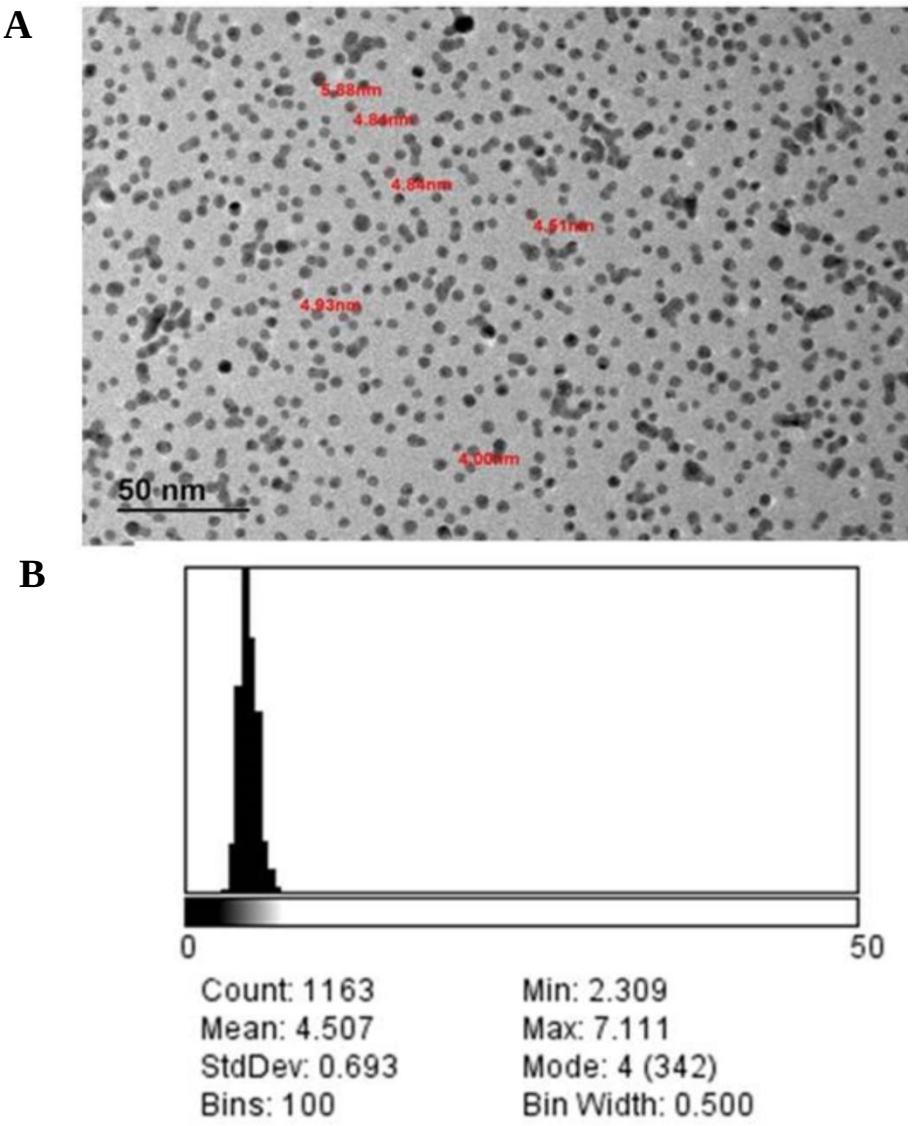

Figure 6.2 TEM imaging of 5 nm [^{195}Au]AuNPs and quantitative analysis

(A) Representative image of AuNPs suspension in dispersant acquired by TEM, (B) particle size distribution of AuNPs in dispersant based on the quantitative analysis of TEM images (The graph was kindly provided by Isaac Ojea Jiménez)

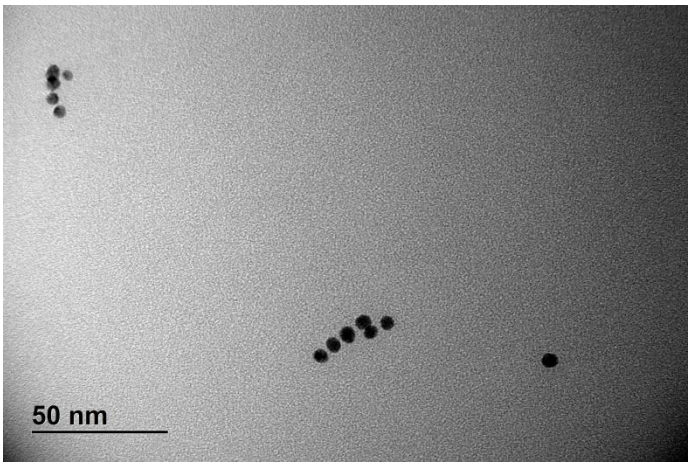

Figure 6.3 TEM image of 5 nm [^{195}Au]AuNPs after 48h+ incubation in fresh CCM at 37°C, 5 % CO_2

The significance of results generated by DLS was limited (Figure 6.4). In dispersant, various batches of [^{195}Au]AuNPs showed a hydrodynamic diameter at around 6 nm. The results obtained for Batch 4 (Figure 6.4A, yellow line) were clearly different from the other 4 batches tested, with an increase in hydrodynamic diameter to roughly 10 nm. Therefore, the batch was discarded. After incubation in CCM for 0, 6, 24, or 48h the size distribution changed considerably (Figure 6.4B). After 6h incubation, the DLS-derived graph showed 3 peaks at 10 nm, 200 nm, and > 5 µm. The size distribution developed two further peaks after 24h incubation at ~40 and 300 nm. Between 24 and 48h of incubation the AuNPs size did not change significantly anymore.

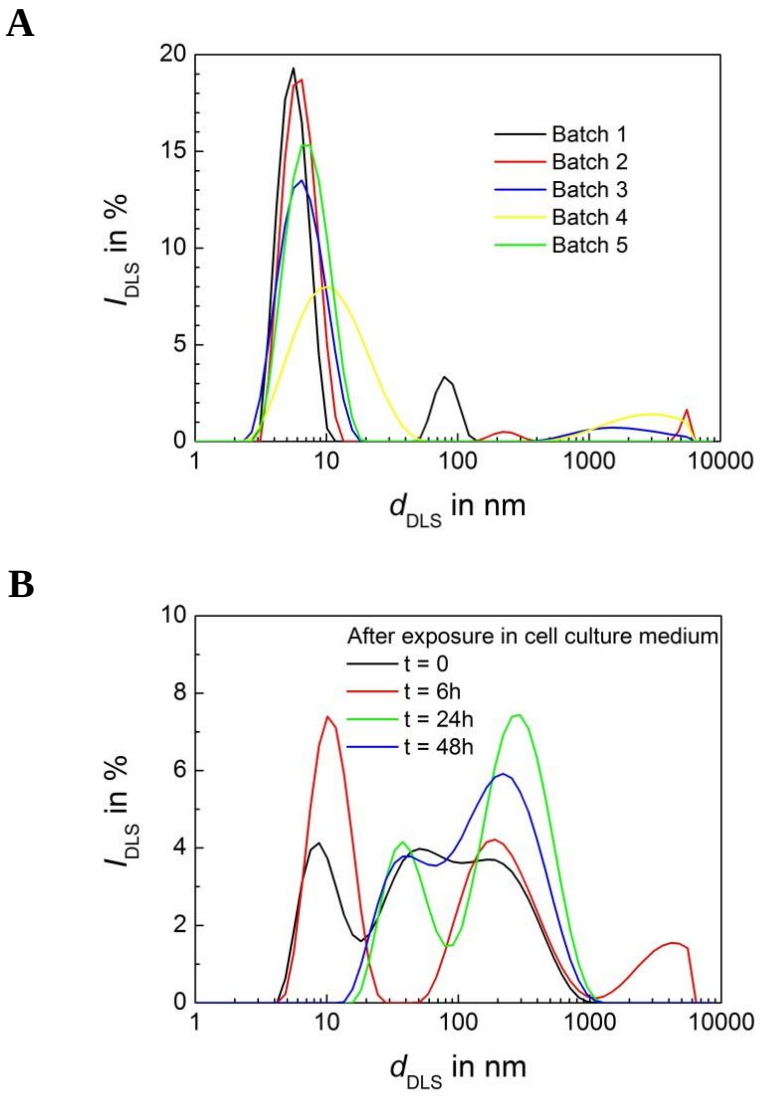

Figure 6.4 Hydrodynamic diameter of 5 nm [^{195}Au]AuNPs measured by DLS

(A) Various batches of AuNPs in dispersant, (B) AuNPs after incubation in MEM-based cell culture medium at 37°C, 5 % CO_2 (The graphs were kindly provided by Uwe Holzwarth.)

More reliable results could be obtained using CLS (Figure 6.5). The hydrodynamic diameter of 5 nm [^{195}Au]AuNPs dispersed in CCM measured by CLS was slightly higher than in TEM with 5.5 nm (Figure 6.5). After incubation in fresh CCM the hydrodynamic diameter increased to 6.3 and 6.5 nm after 1 and 24h, respectively. After 48h, an increase to around 32 nm was noted.

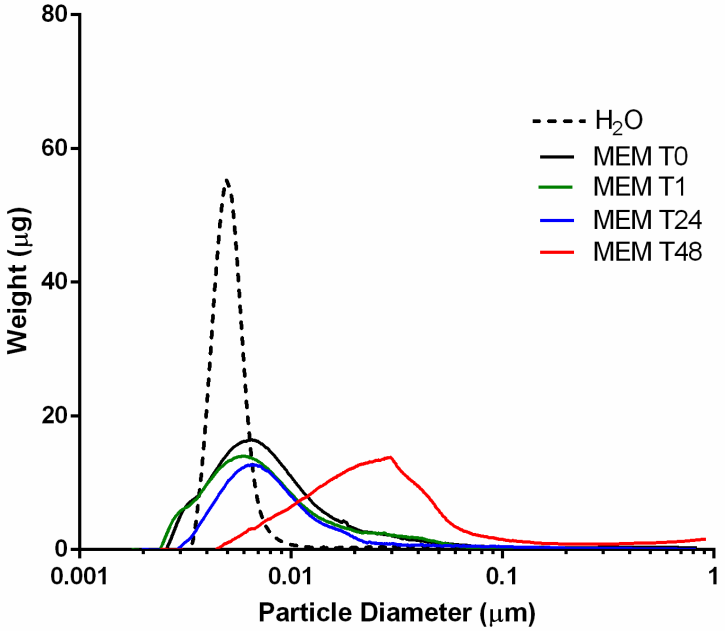

Figure 6.5 Hydrodynamic diameter of 5 nm AuNPs incubated in fresh complete MEM-based CCM measured by CLS

Measured by CLS after 0, 1, 24, and 48h (T0-T48) incubation in CCM at 37°C, 5 % CO_2

The spectroscopic analysis of 5 nm AuNPs using UV-Vis showed a maximum absorbance at around 520 nm after the addition to fresh CCM (Figure 6.6, black line). After 1h incubation in CCM, the maximum absorbance remained at 520 nm and the peak intensity reduced minimally. After 24 and 48h (Figure 6.6, blue and red line, respectively) a slight right-shift to roughly 528 nm was observed.

Summing up, the 5 nm [^{195}Au]AuNPs were homogenously dispersed in both water and fresh CCM. The presence of serum proteins in CCM did not affect the AuNPs size distribution significantly over 24h of incubation. After extended incubation times some agglomeration or aggregation might occur.

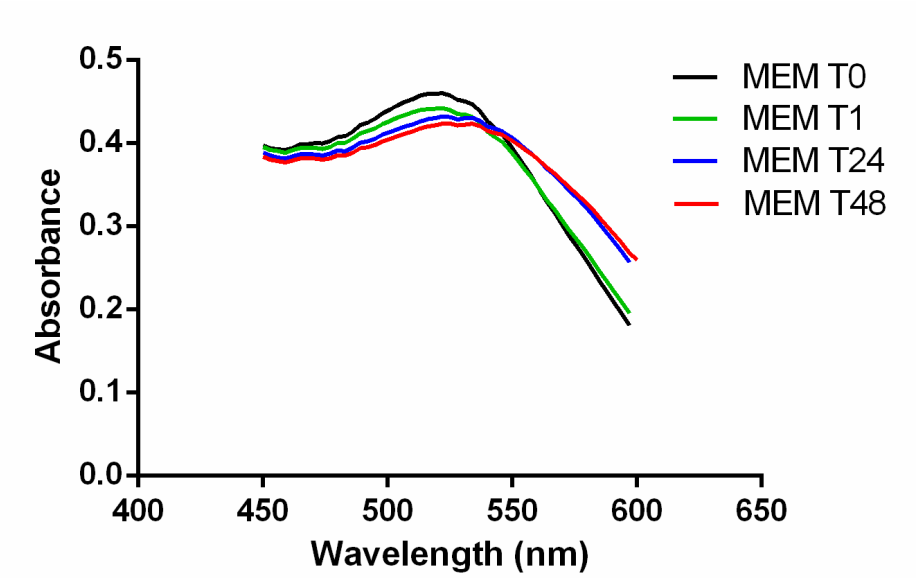

Figure 6.6 UV-Vis spectra of 5 nm AuNPs after incubation in fresh MEM-based CCM

Measurements were taken after 0, 1, 24, and 48h (T0-T48) incubation at 37°C, 5 % CO_2 (The graph was kindly provided by Carine Drewes.)

6.3.1.2 Characterisation of 30 nm [^{195}Au]AuNPs

The characterisation results for 30 nm [^{195}Au]AuNPs are summarised in Table 6.2.

Table 6.2 Summary of TEM and DLS measurements of 30 nm [^{195}Au]AuNPs performed in water and CCM

Instrument	Parameter	Dispersant	MEM-based CCM
TEM	Size (nm)	31.8 ± 6.5	
	Shape	spherical	
DLS	Z-average	54.4 ± 5.7	48.8 ± 3.2
	Peak	73.0 ± 9.4	80.0 ± 8.0
	PDI	0.358 ± 0.043	0.367 ± 0.063
	ζ-potential (mV)	-44	-10

The TEM analysis of the 30 nm core-shell [^{195}Au]AuNPs in dispersant showed a homogenous distribution of single particles with an infrequent occurrence of agglomerates (Figure 6.7A). A small fraction of smaller particles (15-20 nm) was observed. The quantitative analysis of the TEM images resulted in an average particle diameter of 31.8 ± 6.5 nm.

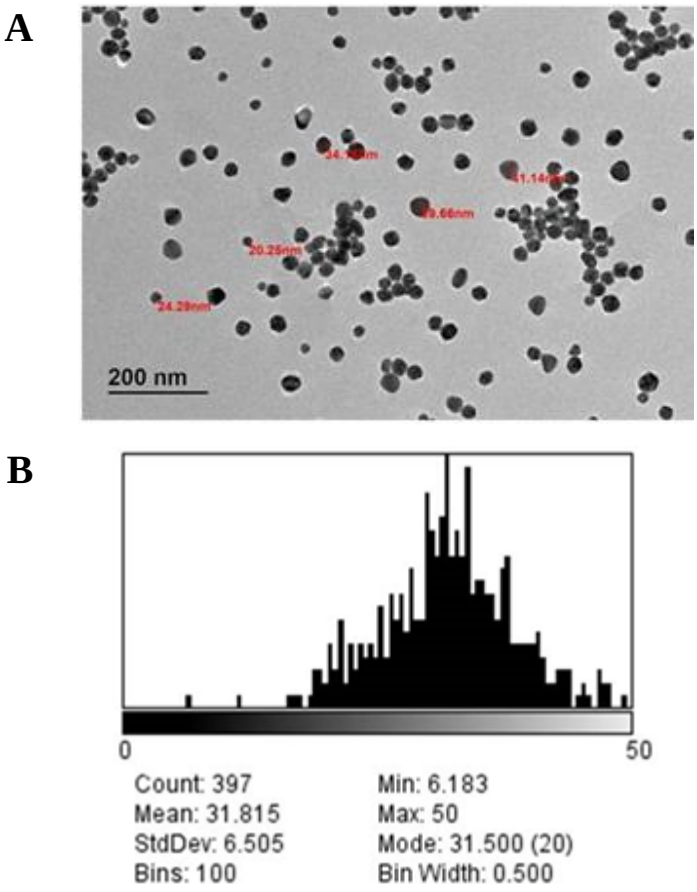

Figure 6.7 TEM imaging of 30 nm [^{195}Au]AuNPs and quantitative analysis

(A) Representative image of AuNPs in dispersant acquired by TEM, (B) Particle size distribution of AuNPs in dispersant based on the quantitative analysis of TEM images (The graph was kindly provided by Isaac Ojea Jiménez.)

The hydrodynamic diameter measured with DLS was clearly larger in both dispersant and fresh CCM. In dispersant, the Z-average was 54.4 ± 5.7 nm with the primary peak at 73 ± 9.4 nm (Figure 6.8A). In most batches a small fraction of very large particles was detected in the range of >5 µm. This second peak disappeared after incubating the particles in fresh CCM (Figure 6.8B). In CCM, another peak appeared at 10 nm, which was probably caused by the large amount of serum proteins. Hence, the Z-average

decreased slightly to 48.8 ± 3.2 nm, even though the main peak shifted to 80 ± 8 nm. The PDI remained similar with 0.358 and 0.367 in dispersant and CCM, respectively.

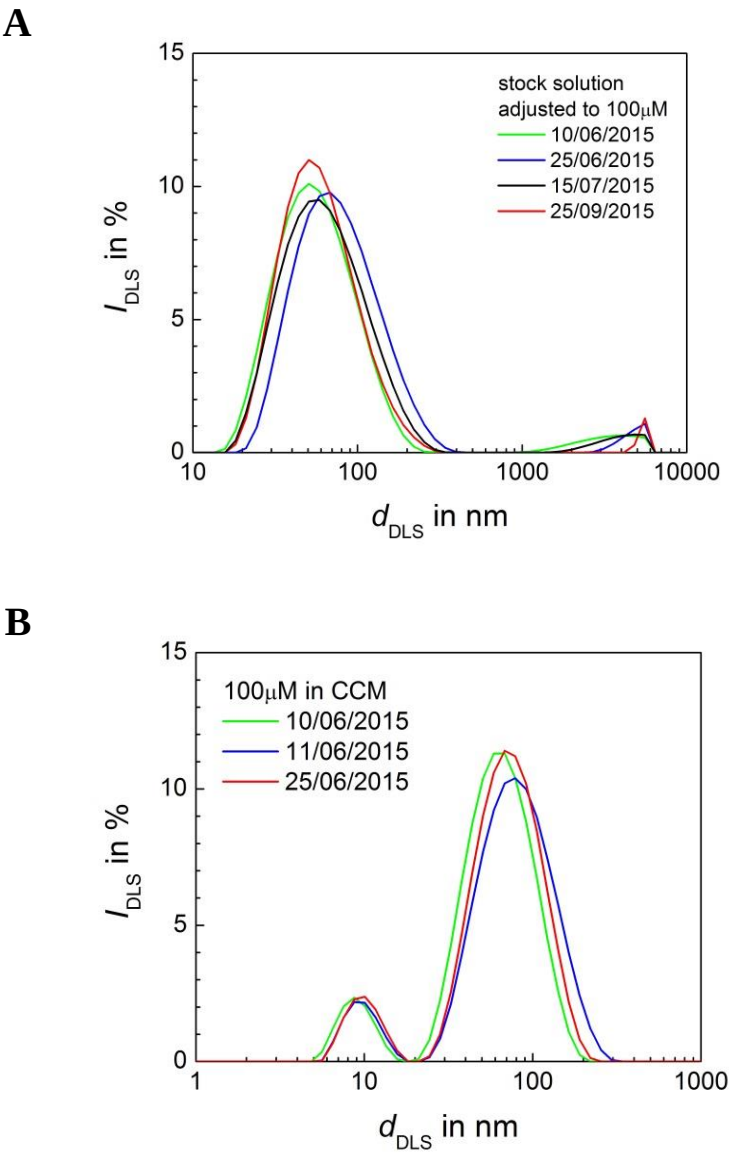

Figure 6.8 Hydrodynamic diameter of 30 nm [^{195}Au]AuNPs in dispersant and CCM measured by DLS

(A) 30 nm AuNPs in dispersant; (B) 30 nm AuNPs after incubation in CCM at 37°C, 5 % CO_2 (The graphs were kindly provided by Uwe Holzwarth.)

6.3.2 ^{195}Au release from [^{195}Au]AuNPs in CCM

During *in vitro* experiment to study NP-translocation it was important to guarantee that the measured activity of ^{195}Au-radioisotopes can be related to the presence of AuNPs and not free ^{195}Au released into the medium due to a partial dissolution of the NPs. Free ^{195}Au might easily pass thorough the cell barriers and mistakenly be considered as the signature of NP-translocation. In our experiments we did not detect any activity of ^{195}Au radioisotopes in the filtered solutions of AuNPs incubated both in MilliQ H_2O and in CCM for up to 48 hours (not shown). Thus, the release of free ^{195}Au was below the detection limit, which indicated that no significant disintegration of 5 nm and 30 nm [^{195}Au]AuNPs occurred under the experimental conditions.

6.3.3 Passage of [^{195}Au]AuNPs across cell-free filters

The passage of [^{195}Au]AuNPs across cell-free filter inserts was investigated for two reasons. Firstly, to ensure that the NPs can cross the 1 µm filter and translocate to BL compartment of the transwell. Secondly, studying the passage of the NPs across cell-free filters gave a general indication of their sedimentation behaviour, which is an important parameter to estimate the cellular exposure concentration.

To study the passage of [^{195}Au]AuNPs, 2 mL of the working stock suspension in CCM (100 µM) was added to the AP compartment of a cell-free transwell insert and placed onto a transwell-suitable 6-well plate containing 3 mL RPMI-based CCM. The plates were incubated a standard culture conditions and the samples taken as described in Section 6.2.5.2.

6.3.3.1 Passage of 5 nm [^{195}Au]AuNPs across cell-free transwell filters

After 24h incubation, 70.5 % of the total activity was measured in the AP supernatants (sample A) (Figure 6.9). Of the remaining 29.5 %, 28 % were recovered in the BL supernatants (sample B). The other 1.5 % were distributed over the filter (C) and the filter insert (D). After 48h incubation, 37.5 % of the total activity was measured in the BL compartment, whereas 61 % remained on the AP side. The activity recovered in the filter wash increased slightly to 0.83 %. The activity retained in the filter insert decreased to 0.64 %.

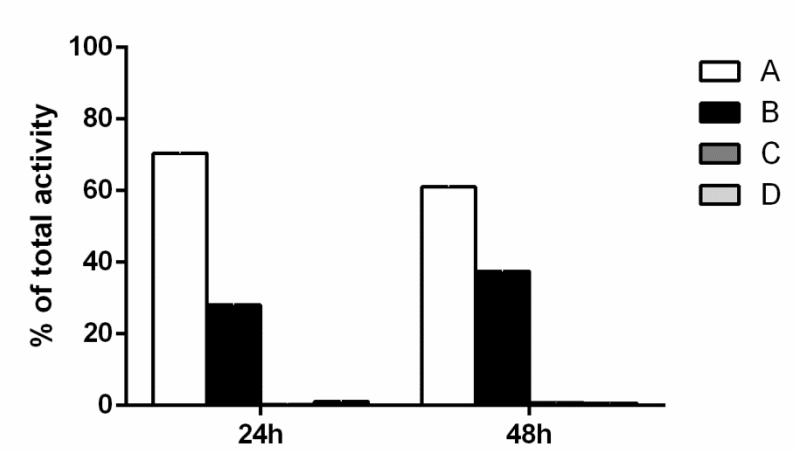

Figure 6.9 Sedimentation and passage of 5 nm [^{195}Au]AuNPs across cell-free transwell filter inserts over 24 and 48h

[^{195}Au]-associated activity in the AP (A) and BL (B) compartment, the filter wash (C) and the filter insert (D) after incubation at 37°C, 5 % CO_2 (Average of n=3 of one experiment ± StDev)

6.3.3.2 Passage of 30 nm [^{195}Au]AuNPs across cell-free transwell filters

After 24h incubation, 55 % of the total activity was detected in the AP supernatants (sample A) (Figure 6.10). One third of the total activity was recovered from the BL side (sample B). The remaining 10 % were allocated over the filter wash and the filter insert with 4.2 and 6.4 %, respectively. After 48h incubation, the activity measurements of the AP and BL compartment were almost identical with 46 % each. The activities recovered from the filter wash and filter samples decreased slightly to 2.9 and 4.6 %, respectively.

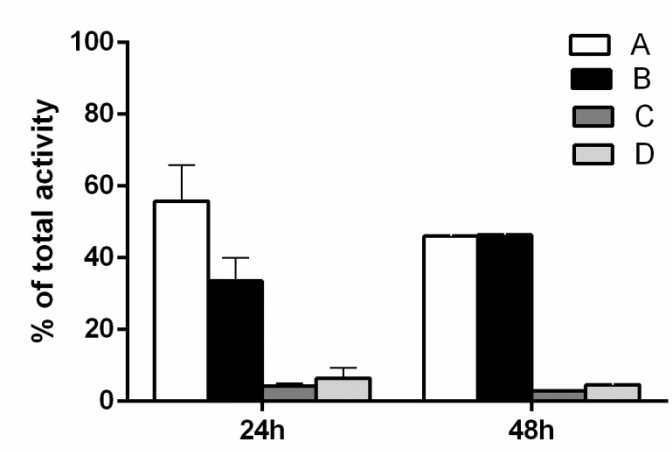

Figure 6.10 Sedimentation and passage of 30 nm [^{195}Au]AuNPs across cell-free transwell filter inserts over 24 and 48h

[^{195}Au]-associated activity in the AP (A) and BL (B) compartment, the filter wash (C) and the filter insert (D) after incubation at 37°C, 5 % CO_2 (24h: Average of N=2 ± StDev, 48h: Average of n=3 of one experiment ± StDev)

6.3.4 The effect of [^{195}Au]AuNPs exposure on the barrier integrity

Throughout the exposure to 5 and 30 nm [^{195}Au]AuNPs the TEER was measured in all culture models at the start of the exposure (T_0), as well as after 18, 24, and 48h.

Before exposure to 5 nm [^{195}Au]AuNPs (Figure 6.11A, T_0), the TEER of the designated exposure filters for the monoculture (blue line) and stable co-culture conditions (red line) were not statistically different from the control barrier (striped line). The IFN-γ-primed barriers for the inflamed co-culture had a significantly increased ($p=0.003$) TEER compared to the control.

In exposed Caco-2 monocultures no significant changes in TEER were observed over the exposure time of 48h. Also in the stable co-cultures the exposure to 5 nm [^{195}Au]AuNPs did not cause changes in the TEER over the first 24h. After 48h, the TEER was significantly increased ($p=0.013$) to 115 ± 13 %.

The TEER of the inflamed co-culture (green line) was strongly reduced compared to the untreated monoculture control over the first 24h of exposure (Figure 6.11A). The reduction was only statistically significant ($p\leq0.001$) at T_{24} with 66 ± 13 % compared to the unexposed monoculture control. Subsequently, the barrier integrity was re-established and no significant difference was measured at T_{48}.

Before the exposure to 30 nm [^{195}Au]AuNPs (Figure 6.11B, T_0), no statistically significant difference in TEER were measured between the Caco-2 barriers. The TEER of the exposed Caco-2 monoculture (blue line) and stable co-culture (red line) were not significantly different from the unexposed control at T_{18} and T_{24}. At T_{48}, the TEER of the exposed monoculture and stable co-culture were significantly increased compared to the unexposed monoculture control to 120 ± 7.8 % ($p\leq0.001$) and 112 ± 10 % ($p=0.006$), respectively.

The TEER of the inflamed co-culture (green line) was significantly decreased ($p\leq0.001$) at T_{18} and T_{24} compared to the unexposed monoculture control to 72 ± 4 and 74 ± 7 %, respectively. At T_{48}, the barrier integrity of the inflamed co-culture was completely re-established to 100 ± 4.4 % compared to the unexposed monoculture control.

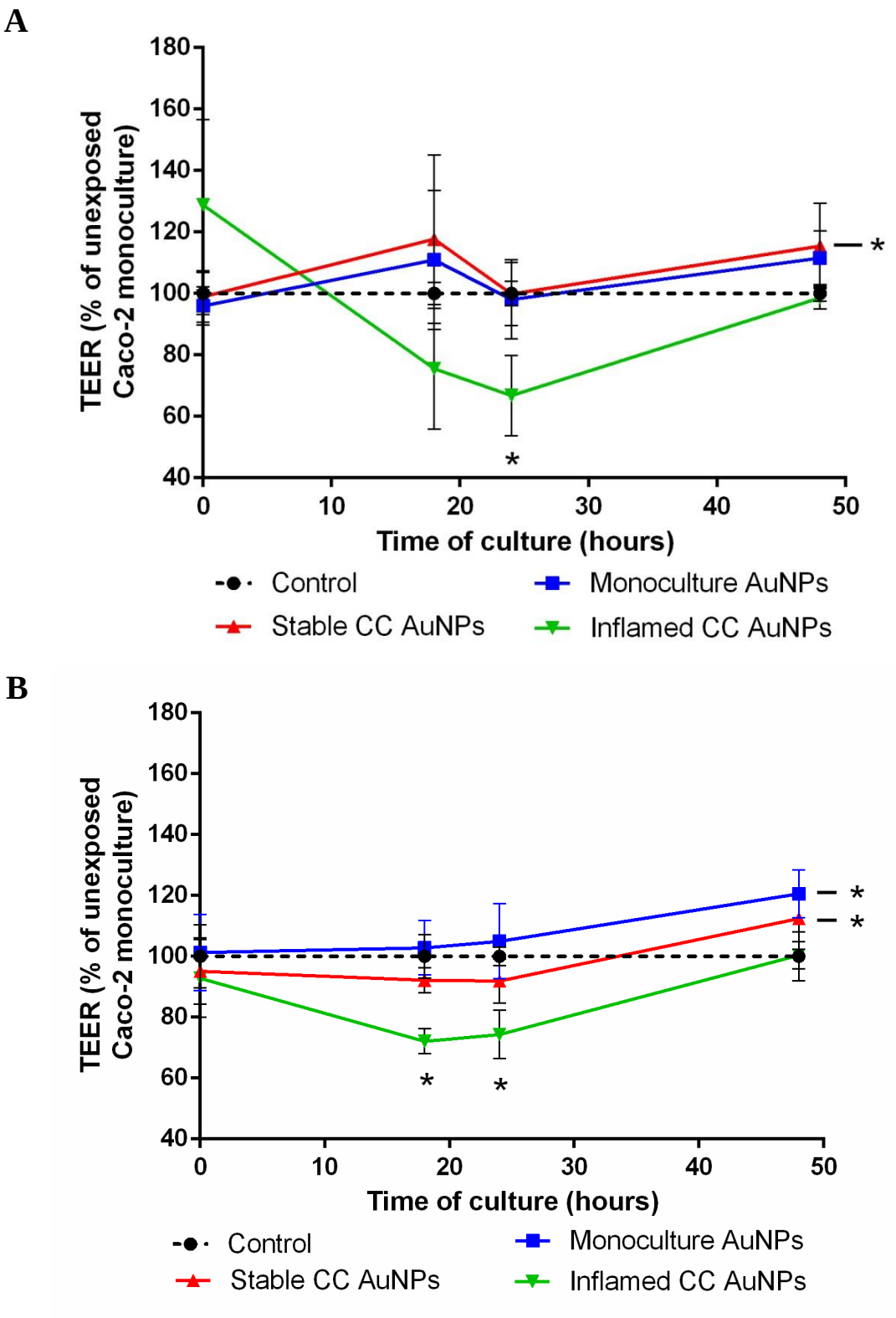

Figure 6.11 Barrier integrity measured as TEER in Caco-2 monoculture, stable, and inflamed co-cultures after exposure to [^{195}Au]AuNPs

*(A) over 48h exposure to 5 nm [^{195}Au]AuNPs; (B) over 48h exposure to 30 nm [^{195}Au]AuNPs (5 nm: Average of N=2 ± StDev; 30 nm: Average of N=3 ± StDev, T_{18}: N=2 ± StDev; *p≤0.05 compared to corresponding unexposed Caco-2 monoculture (control))*

6.3.5 *Colloidal stability of 5nm [^{195}Au]AuNPs suspension in presence of Caco-2 cells*

After 24h incubation with cells no effect on the colloidal stability of the particle suspension was noted (Figure 6.12A). Two interesting observations were made, however, after an increased incubation time of 48h. Firstly, significant differences in the colour of the CCM were visible between the Caco-2 monoculture and the inflamed co-culture. As this was also observed in unexposed cultures (not shown) the colour differences cannot be attributed to the presence of the [^{195}Au]AuNPs. Secondly, sedimented dark material accumulated at the bottom of the vials after sample collection.

When comparing the particle suspension after 48h incubation in a cell-free environment to samples taken from exposed cell cultures a clear difference in the suspension stability is visible (Figure 6.12B). Whereas dark particulate material sedimented to the bottom of the vial in the cell culture sample no sedimentation occurred in cell-free transwells.

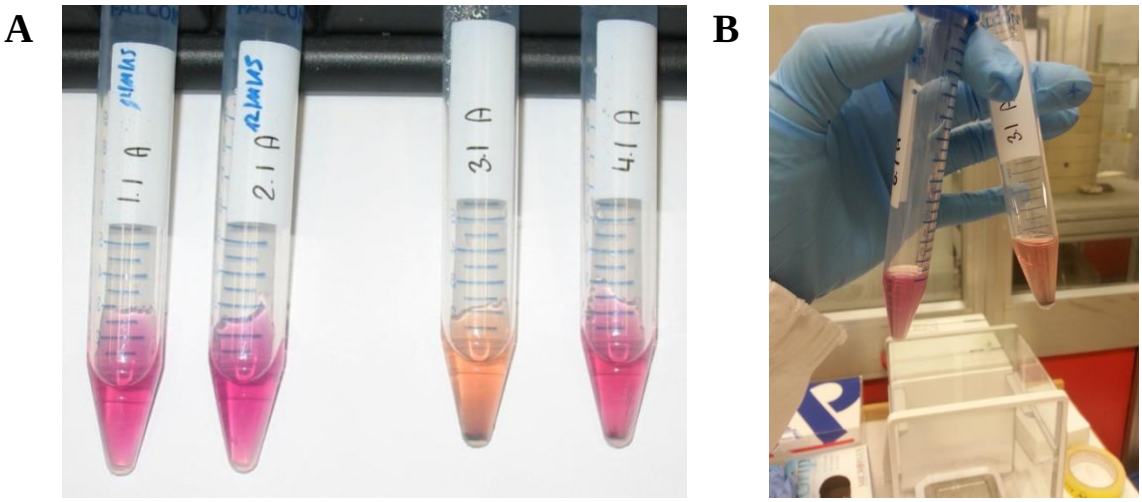

Figure 6.12 Colloidal stability of 5nm [^{195}Au]AuNPs in presence and absence of cells

(A) Particle suspensions of the AP compartment after 24h incubation and 48h incubation at 37°C, 5 % CO_2 in the Caco-2 monoculture (24h: 1.1A; 48h: 4.1A) and inflamed co-culture (24h: 2.1.A; 48h:3.1A); (B) particle suspensions of the AP compartment after 48h incubation at 37°C, 5 % CO_2 in cell-free environment (left vial) or in the inflamed co-culture (right vial)

To further investigate the impact of cells on the colloidal stability of the particles a batch of cold 5nm AuNPs was analysed using CLS and TEM after incubation with Caco-2 monocultures. Interestingly, the exposure of Caco-2 monocultures resulted in a significantly larger hydrodynamic diameter (Figure 6.13) starting from 4h of incubation compared to fresh CCM (Figure 6.5B). After 48h, the average hydrodynamic diameter was increased 5-fold to 27.7 nm.

Table 6.3 Hydrodynamic diameter of 5 nm [^{195}Au]AuNPs measured by CLS after incubation with Caco-2 monocultures

	Cell-exposure in CCM		
	4h	**24h**	**48h**
CLS Size (nm)	9.8	20.7	27.7

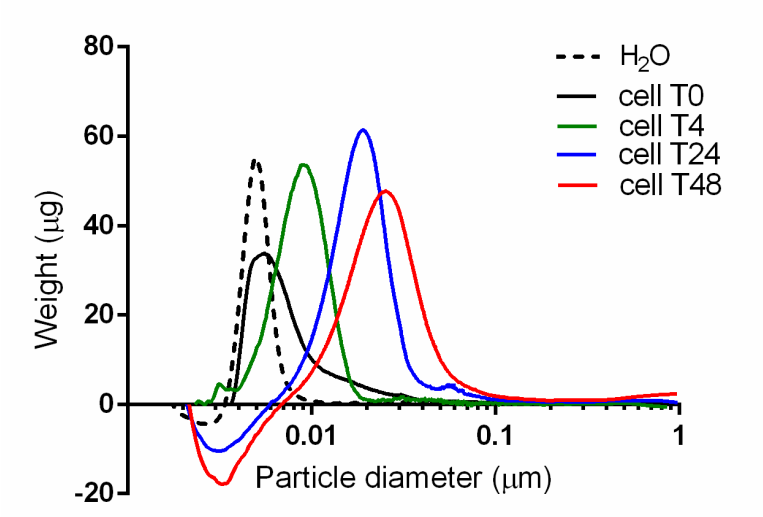

Figure 6.13 Hydrodynamic diameter of 5nm AuNPs in presence of cells measured by CLS

Measured in H_2O and after 0, 4, 24, and 48h (T0-T48) incubation with Caco-2 monocultures in MEM-based CCM at 37°C, 5% CO_2

The analysis with TEM confirmed the occurrence of considerable agglomeration or aggregation in presence of Caco-2 cells (Figure 6.14A-D). Whereas the particles were homogenously distributed directly after addition to the cell cultures (Figure 6.14A) small agglomerates of around 10 particles were visible after 4h of incubation (B). The size of the agglomerates steadily increased which resulted in the formation of large clusters after 24 (C) and 48h of incubation (D).

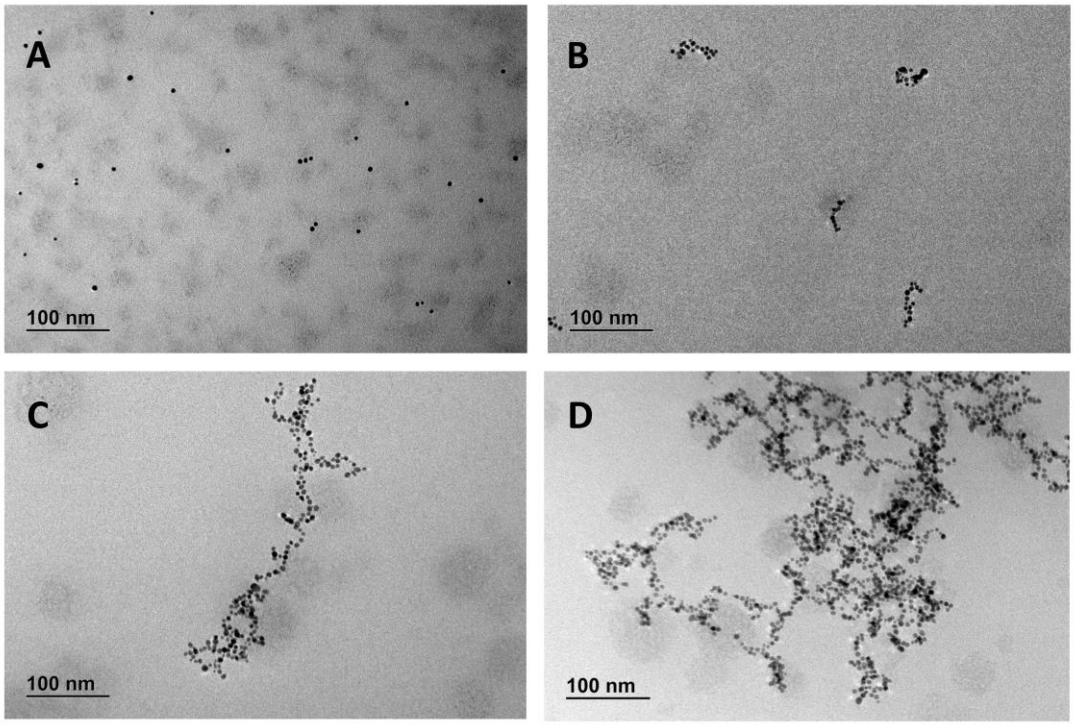

Figure 6.14 TEM images of 5 nm AuNPs incubated with Caco-2 monocultures

Samples of 5nm AuNPs (100 µM) were prepared after (A) 0h, (B) 4h, (C) 24h, (D) 48h incubation with Caco-2 monocultures at 37°C, 5% CO_2

6.3.6 Measurement of radioactivity in the collected transwell samples

6.3.6.1 Exposure to 5 nm [^{195}Au]AuNPs

The results for Caco-2 monocultures and both co-culture models exposed to 5 nm [^{195}Au]AuNPs are summarised in Figure 6.15.

After 24h exposure to [^{195}Au]AuNPs (Figure 6.15a) more than 97 % of the total activity remained in the AP supernatants (A) in all three culture models. Virtually no activity could be measured in the BL supernatants (B) (0.039 ± 0.055 %, 0.007 ± 0.004, and 0.044 ± 0.047 % for the monoculture, stable co-culture, and inflamed co-culture, respectively). Between the individual replicates large variations in activity were observed ranging from <1 to ~30 Bq for 5 nm [^{195}Au]AuNPs (not shown). The remaining 2.2-2.3 % of activity were recovered in almost equal parts in the filter wash (C) and filter inserts (D). No statistically significant differences were observed between the cultures.

In the Caco-2 monoculture (Figure 6.15b, white bars), the [^{195}Au]AuNPs-associated activity in the AP compartment was slightly but significantly reduced compared to the activity recovered after 24h to 96.8 ($p=0.015$) after 48h incubation. The decrease in AP activity did not result in an increase in BL activity. The activity in the filter wash (C) and the filter insert (D) remained similar to the results after 24h with 1.8 ± 0.45 and 1.3 ± 0.19 %, respectively.

Also in the stable co-culture (Figure 6.15b, striped bars), the AP activity reduced significantly after 48h compared to 24h of incubation ($p=0.022$) to 95.7 %. As in the monoculture, no increase in BL activity was measured. The filter wash recovered slightly higher results with 2.4 ± 0.83 %. The activity measured in the filter of the stable co-cultures after 48h was significantly increased compared to the monoculture ($p=0.003$) but not compared to the stable co-culture filter results after 24h exposure.

In the inflamed co-culture (Figure 6.15b, black bars), the AP activity was significantly lower ($p\leq0.001$) after 48h compared to the corresponding 24h results with 92.8 %. The AP activity of the inflamed co-culture was significantly lower ($p\leq0.001$) compared to the 48h results of the monoculture and stable co-culture. Also in the inflamed co-culture, no increase in BL activity was noted after 48h. Most interestingly, the activity detected in the filter wash and filter was significantly increased ($p\leq0.003$) compared to corresponding 24h results, as well as compared to the monoculture and stable co-culture after 48h. Together, the activity in samples C and D accounted for roughly 7 % of the total activity (3.2 ± .053 % in the filter wash, 3.9 ± .071 % in the filter).

Neither in the inflamed nor in the stable co-culture ^{195}Au-related activity was recovered in the THP-1 cells after 24 or 48h exposure.

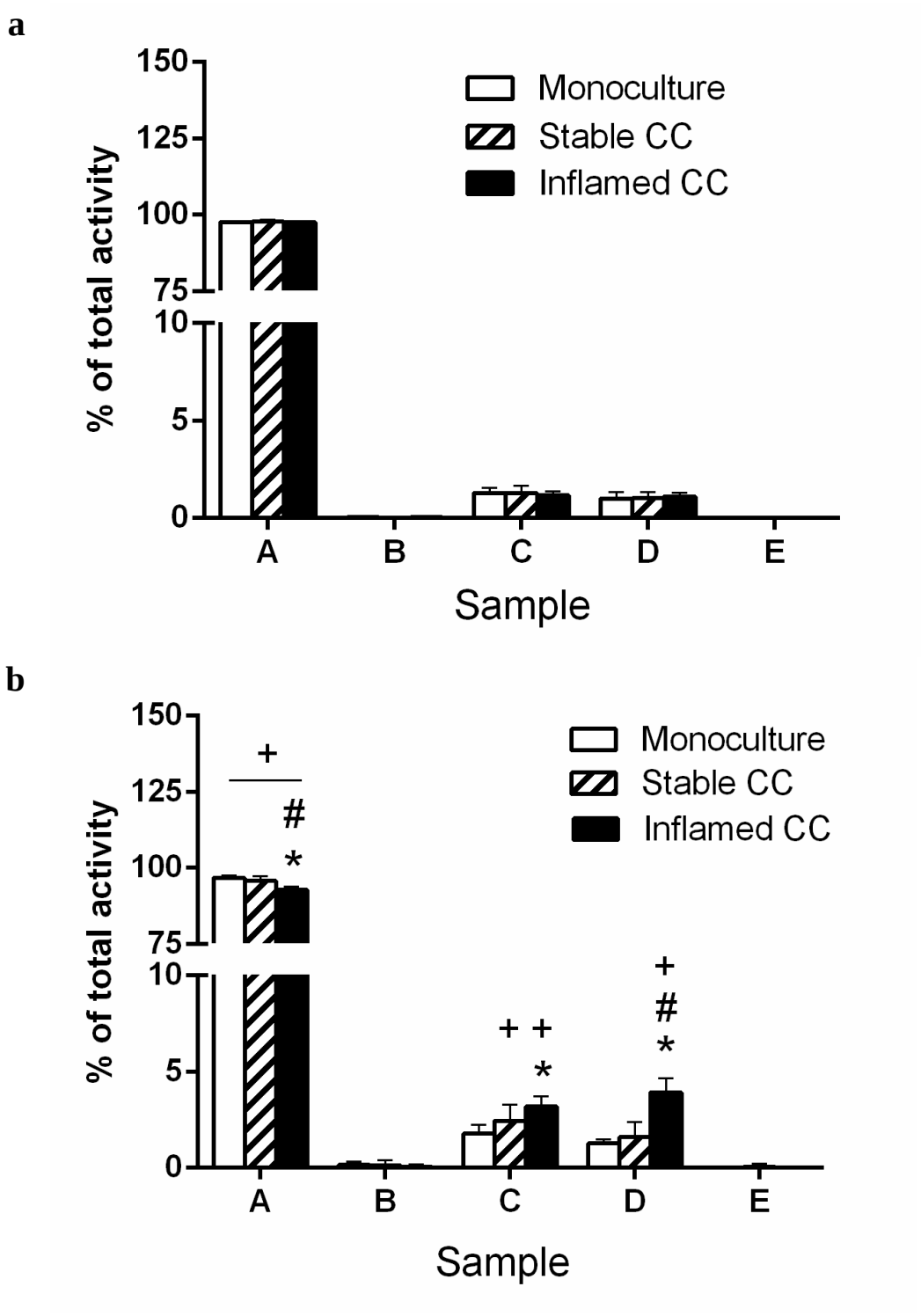

Figure 6.15 Distribution of ^{195}Au-associated activity in Caco-2 monocultures, stable, and inflamed co-cultures after exposure to 100 µM 5nm [^{195}Au]AuNPs

*The ^{195}Au-associated activity was measured in AP (A) and BL (B) supernatants, the filter wash (C), the filter insert (D), and if applicable the THP-1 cells (E) in Caco-2 monocultures, stable, and inflamed co-cultures (CC) after (a) 24h exposure and (b) 48h exposure (Average of N=2 ± StDev, *p≤0.05 compared to corresponding monoculture, $^{\#}$p≤0.05 compared to corresponding stable co-culture; $^{+}$p≤0.05 compared to corresponding 24h sample)*

6.3.6.2 Exposure to 30 nm [^{195}Au]AuNPs

After 24h exposure to 30 nm [^{195}Au]AuNPs (Figure 16a), ~96.5-96.6 % of the activity was measured in the AP supernatants of all three culture models. Of the remaining 4 %, 1.3-1.5 % was detected in the filter wash (C) and 2 % in the filter insert (D). Virtually no activity was measured in the BL supernatants of all culture models or the THP-1 cells of the stable and inflamed co-cultures. The differences between the culture models were not statistically significant for any of the 5 samples.

After 48h exposure (Figure 6.16b), the activity of AP supernatants remained at 96 % in the Caco-2 monoculture (white bars). The activity in the filter wash significantly ($p=0.046$) increased compared to the corresponding 24h results to 1.8 %. No change in activity was measured in the BL supernatants and the filter insert.

In the stable co-culture (Figure 6.16b, striped bars), the activity in AP supernatants decreased significantly ($p=0.019$) between 24 and 48h of exposure to 95.6 %. However, no statistically significant increase in activity was measured in samples B-E after 48h.

Also in the inflamed co-culture (Figure 6.16b, black bars), the activity in AP supernatants decreased significantly ($p=0.003$) to 95 % after 48 compared to 24h of exposure. In accordance, the activity in the filter wash and filter insert increased significantly after 48h to 1.9 and 3.0 %, respectively.

No activity was detected in samples B and E in any of the culture models.

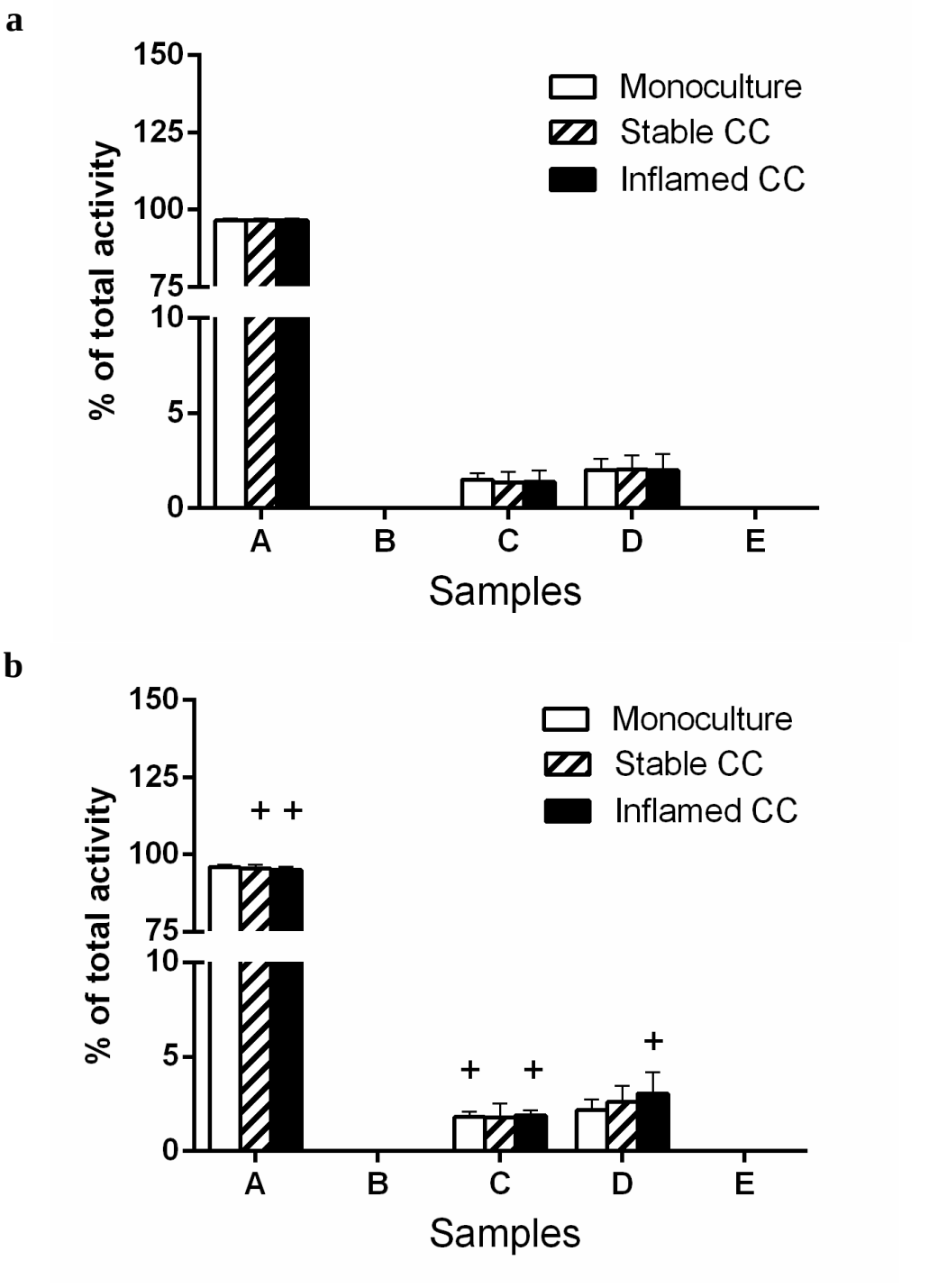

Figure 6.16 Distribution of measured ^{195}Au-associated activity in Caco-2 monocultures, stable, and inflamed co-cultures after exposure to 100 µM 30 nm [^{195}Au]AuNPs

The ^{195}Au-assoicated activity was measured in the AP (A) and BL (B) supernatants, the filter wash (C), the filter insert (D), and if applicable the THP-1 cells (E) in Caco-2 monocultures, stable, and inflamed co-cultures (CC) after (a) 24h and (b) 48h exposure (Average of N=3 ± StDev; $^{+}p \leq 0.05$ compared to corresponding 24h sample)

6.4 Discussion

With the use of radio-labelled [^{195}Au]AuNPs this study aimed to investigate the barrier passage of NMs across a Caco-2 cell layer, and to detect a potential increase in particle translocation during an ongoing inflammation-like process. The results discussed hereinafter, can be summarised in the following points:

- The environment greatly influenced the characteristics of the [^{195}Au]AuNPs. In contrast to fresh CCM, the presence of cells caused significant agglomeration or aggregation of the 5 nm particles, which most likely accelerated the particles' sedimentation.
- In fresh CCM, 30 nm [^{195}Au]AuNPs sedimented faster across cell-free filters than 5nm [^{195}Au]AuNPs.
- The 48h exposure to 30 nm [^{195}Au]AuNPs caused a significant increase in TEER in the Caco-2 monoculture and stable co-culture, whereas the exposure to 5 nm [^{195}Au]AuNPs significantly increased the TEER in the stable co-culture only.
- No barrier integrity-related effects were observed for either size of [^{195}Au]AuNPs in the inflamed model.
- For 5 nm [^{195}Au]AuNPs an increased accumulation of ^{195}Au-associated activity was found in the filter insert of the inflamed co-culture.
- The induction of an artificial inflammation-like process did not cause an increased translocation of [^{195}Au]AuNPs over 48h.

6.4.1 Characterisation and stability of ([^{195}Au])AuNPs

The characterisation of 5 and 30 nm [^{195}Au]AuNPs in dispersant showed a homogenous and narrow size distribution. Whereas the hydrodynamic diameter of the larger 30 nm particles increased significantly in fresh CCM, the 5 nm [^{195}Au]AuNPs were very stable over an incubation period of 24h, but increased to a size of 30 nm after 48h. This increase in hydrodynamic diameter was not reflected in the TEM analysis of 5nm particles. The 5 nm [^{195}Au]AuNPs behaved differently in fresh CCM compared to CCM in the presence of cells. In cell-free CCM no agglomerates, aggregates, or deposition of 5 nm [^{195}Au]AuNPs were visible by the naked eye after 48h incubation. In cell exposure experiments on the other hand, a clear deposition at the bottom of the AP compartment was noted after 48h. Whereas the deposition suggested the presence

of very large particle complexes only a 6-fold increase in hydrodynamic diameter from 5 to ~30 nm was measured. TEM imaging of 5nm AuNPs incubated with Caco-2 cells, however, confirmed a gradual formation of large agglomerates.

The effect of salts and proteins on the stability of NMs has received increasing attention over the last years. Several groups demonstrated a significant impact of the dispersant composition on the characteristics of NMs. Ji et al. (2010) systematically analysed how the combination of the basic culture medium together with the type and concentration of protein influences the colloidal stability of TiO_2 NPs. The group demonstrated a striking impact of the dispersant but not the agglomeration state on the sedimentation behaviour of the particles. Whereas the agglomeration behaviour of TiO_2 NPs was largely unaffected by the type and concentrations of protein the sedimentation varied between 7 and 94 % (Ji et al., 2010). In case of AuNPs the addition of proteins to CCM was shown to prevent rather than cause agglomeration independent of the type of protein used (Mahl et al., 2010; Luby et al., 2015). Probably also in our case such a stabilising effect took place when dispersing the 30 nm [^{195}Au]AuNPs stock suspension in CCM. Whereas a small fraction of very large structures in the micrometre range was detected in dispersant the signal disappeared immediately after diluting the stock in CCM. The availability of large quantities of proteins in the CCM and, therefore, formation of a protein corona around the particles possibly led to a dissociation of formerly present agglomerates.

The composition of the protein corona seems to play an important role in determining the colloidal stability of NPs in CCM (Ji et al., 2010; Halamoda-Kenzaoui et al., 2015). It has to be noted that the protein corona is not only influenced by the type of protein added to the CCM but also by compounds released by the cells (Albanese et al., 2014). This might explain the different stability we observed for 5 nm AuNPs in fresh CCM compared to the stability in cell exposure experiments. As Tenzer et al. (2013) showed elegantly, the protein corona composition depends less on the size or surface charge of NPs, but is influenced by the type of material (e.g. Au, Ag, SiO_2,…). Hence, even though it was not explicitly studied within this project an effect of the presence of cells on the stability of the 30 nm [^{195}Au]AuNPs is likely to occur in a comparable fashion to our observations for 5 nm [^{195}Au]AuNPs.

6.4.2 Sedimentation and passage of [^{195}Au]AuNPs across cell-free filters

Disregarding the colloidal stability, both 5 and 30 nm [^{195}Au]AuNPs sedimented and passed into the BL compartment at significant concentrations, as indicated by the results obtained in cell-free filter inserts. The passage of 30 nm particles was higher compared to 5 nm particles, indicating that the sedimentation of the smaller particles was slower.

Indeed, the transport of NPs in the *in vitro* conditions is mainly driven by diffusion and gravitational sedimentation (Hinderliter et al., 2010; Teeguarden et al., 2007). The diffusion rate is a function of the surrounding liquid properties (temperature, medium viscosity) and of the NP diameter, while the gravitational velocity depends on the mass density of the NPs and the medium. Therefore, the NP diameter and mass density have a major impact on the transport of NPs. The velocity of sedimentation is proportional to the square of the NP diameter (Hinderliter et al., 2010), which explains the faster passage of larger 30 nm [^{195}Au]AuNPs across cell-free filters.

6.4.3 Effect of [^{195}Au]AuNPs exposure on the barrier integrity in the culture models

The exposure to 5 and 30 nm [^{195}Au]AuNPs did not induce a reduction in barrier integrity in the Caco-2 monoculture and stable co-culture. Furthermore, the exposure did not affect the barrier disruption or the re-establishment of barrier integrity in the inflamed co-culture. Interestingly, both sizes of [^{195}Au]AuNPs increased the TEER of the monoculture and stable co-culture after 48h of exposure but not in the inflamed co-culture.

These results suggest that [^{195}Au]AuNPs did not negatively affect the TJ network or the Caco-2 cell viability. This is in line with the majority of published findings of other groups. To date, most studies agree that AuNPs do not exert cytotoxic effects unless functionalised with cationic surface charge or administered at very high concentrations (500-1000 µM) (Boisselier and Astruc, 2009; Freese et al., 2012). Even highly sensitive cytotoxicity assays, like the study of colony forming efficiency, did not show adverse effects of 5 and 30 nm AuNPs in Caco-2 cells (Bajak et al., 2015). As mentioned earlier, results of *in vitro* experiments using macrophages are in disagreement. Whereas some groups observed significant cytotoxicity at rather low concentrations (10 µg / mL) and induction of pro-inflammatory cytokines (Yen et al., 2009), others did not note any adverse effects (Shukla et al., 2005; Bancos et al., 2015). Since it is unlikely that

AuNPs cross the intact Caco-2 barrier at sufficiently high numbers to reach potentially cytotoxic concentrations, no adverse effects on the THP-1 cells were expected.

Some studies challenge the generally assumed harmlessness of AuNPs. Lin et al. (2011) reported a significant reduction in TEER in Caco-2 cells after 3h exposure to 45 µg / mL AuNPs. All AuNPs tested by Lin and colleagues were modified with various polymer chains to provide negative, neutral, or positive surface charges. A clear reduction in barrier integrity was noted for all tested AuNPs independent of their size and surface charge, and was accompanied by an increase in the translocation of mannitol (Lin et al., 2011). A study using 13 nm PEG-coated AuNPs in mice resulted in the induction of apoptosis in the liver, as well as elevation of inflammatory mediators (Cho et al., 2009).

The [^{195}Au]AuNPs in our study were not further functionalised or surface modified. The surface properties of NPs can greatly influence the composition of the protein corona (Safi et al., 2011). It is, therefore, possible that the surface modifications unbeneficially influenced the protein corona and, hence, the biological identity of the AuNPs, whereas the pristine surface in our project enabled the formation of a more favourable protein corona composition.

6.4.4 [^{195}Au]AuNPs translocation in the different culture models

In the Caco-2 monoculture, virtually no ^{195}Au-associated activity was measured in the BL supernatants, indicating that no significant translocation of 5 or 30 nm [^{195}Au]AuNPs across the IEC barrier occurred. Even after a prolonged exposure period of 48h more than 95 % of the activity remained in the AP supernatant. Furthermore, no statistically significant differences were found between the Caco-2 monoculture and stable co-culture, supporting the statement that the presence of unstimulated THP-1 cells does not negatively affect the Caco-2 barrier. Interestingly, in the inflamed co-culture exposed to 5 nm [^{195}Au]AuNPs the measured activity in the AP supernatants was significantly reduced compared to both the monoculture and stable co-culture after 48h. In parallel, an increased activity was measured in the filter wash and the transwell inserts. A similar trend was observed for 30 nm [^{195}Au]AuNPs, but these results failed to be statistically significant. However, no increase in the translocation of [^{195}Au]AuNPs to the BL side of the transwell was detected for both particle sizes.

Neither the BL supernatant samples nor the separately investigated THP-1 macrophages revealed an increased ^{195}Au-associated activity after 48h of exposure.

These results suggest that the [^{195}Au]AuNPs were deposited and potentially taken up by the Caco-2 cells at a higher rate in the inflamed model compared to the monoculture or stable co-culture. They, furthermore, indicate that the effect was more pronounced for the smaller 5 nm particles compared to 30 nm [^{195}Au]AuNPs, even though the sedimentation studies in fresh CCM showed a higher sedimentation rate for 30 nm than 5 nm [^{195}Au]AuNPs. Here the discussed effect of cells on the colloidal stability might be of importance. In presence of cells, 5 nm AuNPs formed large agglomerates, which did not occur in fresh CCM. Most likely, the sedimentation of these large agglomerates was accelerated compared to single 5 nm particles. In contrast, the presence of cells might have had the opposite effect on the 30 nm [^{195}Au]AuNPs. Instead of accelerating the sedimentation, it might have rather led to an increased colloidal stability, slowing down sedimentation.

Even though an increased ^{195}Au-associated activity was measured in the filters the exact location of the [^{195}Au]AuNPs could not be determined. The particles might be attached to the apical side of the cells, located within the cells after uptake, or between the basolateral cell membrane and the filter after exocytosis. In all exposure conditions and culture models, however, the translocation to the BL compartment and uptake by THP-1 cells was negligible or absent.

Based on the current literature, an increased accumulation of [^{195}Au]AuNPs in IECs of the inflamed compared to the stable model is not surprising. A localisation of NMs at inflamed lesions has already been reported *in vivo* and *in vitro*. Biodegradable polystyrene NPs and SiO_2 NPs were primarily detected at inflamed sites in rodent colitis models (Lamprecht et al., 2001; Moulari et al., 2008). Moulari et al. (2008) clearly demonstrated an increased accumulation of SiO_2 NPs at inflamed tissues compared to healthy and non-inflamed areas. The deposition of NPs at inflamed lesions might depend on specific characteristics like the particle size as was shown for polystyrene NPs in a triple co-culture model of the intestine. Whereas 50 nm particles adhered significantly more to the Caco-2 cell layer of inflamed co-cultures compared to the control cells no differences were measured for larger particles between 100-500 nm (Leonard et al., 2010). In contrast to this, Schmidt et al. (2013) found a statistically increased accumulation of micro- but not nano-sized PLGA particles, as well as an

elevated translocation from the mucosal to the serosal side of nano- but not micro-sized particles.

The translocation of NPs at inflamed areas of the intestine has been suggested to be related to the increased synthesis of mucus at these sites (Lamprecht et al., 2001). The elevated synthesis of mucus has also been demonstrated in Caco-2 cells after the induction of an inflammation-like response using IL-1β (Leonard et al., 2010). The formation of a mucus layer has not been studied within this project; however, based on other groups' findings it is possible that the THP-1-mediated inflammation-like process caused a similar effect here. Concerning the interaction of NMs with mucus, the particles' surface charge and hydrophilicity appear to be crucial determinants. Mucus carries an overall negative charge and is characterised by the presence of numerous hydrophobic domains (Lai et al., 2009). The 5 and 30 nm [^{195}Au]AuNPs used here had a strong negative surface charge in dispersant (-46 and -44 mV respectively), which increased closer to neutral charge in fresh CCM (-11 and -10 mV, respectively). An increased formation of mucus on the Caco-2 cells and subsequent entrapment of particles could explain the increased recovery on the filter in the inflamed condition, but also the increased activity measured in the wash. It has been shown that particles with an overall negative charge penetrate mucus more easily than positively charged particles, which became entrapped and immobilised within (Crater and Carrier, 2010; Wang et al., 2008b). In line with this, several groups reported increased cellular penetration and barrier crossing of negatively and neutrally charged compared to positively charged NPs. Schleh and colleagues (2012) observed a significantly increased intestinal uptake of carboxylated compared to amine-modified AuNPs in orally exposed rats. Also Jo and colleagues (2015) reported an uptake of slightly negatively charged AuNPs (5-15 nm diameter) in orally exposed rats. Whereas the translocation rate *in vivo* was below 2 % a surprisingly high barrier crossing rate of up to 20 % was observed *in vitro* for neutrally charged AuNPs and 10 % for negatively charged particles in Caco-2 cells (Lin et al., 2011; Lin et al., 2012). The increased barrier crossing might have been caused by the strong reduction in barrier integrity (30-50 %) in response to the exposure (Lin et al., 2011). Even though we measured a similar reduction in TEER in the inflamed co-culture model we could not detect an increased translocation of either 5 or 30 nm [^{195}Au]AuNPs to the BL compartment. One might assume that the reduction in barrier integrity observed by Lin et al. was caused by cytotoxicity rather than an effect on the TJs as in the inflamed model of this project. However, the rapid recovery of barrier integrity after elimination of AuNPs, as well as a

separately conducted cytotoxicity assay strongly suggested that no cell death occurred (Lin et al., 2011). This supports the idea that NPs might pass an epithelial barrier through disrupted TJs. However, Leonard et al. (2010) did not find a co-localisation of NPs with ZO-1, suggesting that they were not transported in the paracellular space but penetrated the Caco-2 cells directly.

6.5 Conclusions

Neither 5 nm nor 30 nm [^{195}Au]AuNPs crossed the Caco-2 barrier at significant numbers in the Caco-2 monoculture confirming the corresponding hypothesis. However, also in the inflamed co-culture no increased translocation of either size [^{195}Au]AuNPs was noted, which disproved our initial hypothesis. Hence, the loosening of the TJs and reduction in barrier integrity by 40-50 % after induction of an inflammation-like response was not sufficient to cause a paracellular passage of the particles. No increased levels of ^{195}Au-associated activity were detected in the BL supernatants or the separately investigated THP-1 cells. The ongoing inflammatory process did, however, result in an elevated retention of 5 nm [^{195}Au]AuNPs on the filter insert. The results, furthermore, underlined the importance of a thorough characterisation of NMs not only in fresh CCM but also in presence of cells, as even smallest variations in the dispersant's composition can greatly influence the colloidal stability of the particle suspension.

7. Discussion of the project

7.1 Reconciliation of the project's aims and the findings

The following paragraphs will reflect on the aims and general hypotheses of the project laid out in Section 1.5 and discuss whether they can be accepted or rejected. A summary of the specific hypotheses is listed in tabular form and attached in the Annex (Table S1).

The goal of the project was the establishment of an *in vitro* cell line-based co-culture model of the human intestine using Caco-2 and THP-1 cells for nanosafety research. The establishment was divided into the development of a co-culture mimicking the homeostatic ('stable') intestine (Aim I), and its advancement to resemble the intestine in diseased ('inflamed') state after exposure to a pathophysiological stressor (Aim II).

Altogether, the overarching goal of developing this 3D co-culture model with its two conditions was achieved, as presented and discussed in Chapter 2. Throughout the process, however, several challenges were encountered. As has been shown before (Daigneault et al, 2010; Aldo et al, 2013), the characterisation of the THP-1 cell line in monoculture once again demonstrated how critical the (PMA)-differentiation protocol and the type of stimuli are for the subsequent (cytokine) response of the cells. When the adequate PMA-differentiation protocol was established, the two cell lines could exist in a co-culture model without negatively affecting each other. This conclusion was based on the findings that no statistically significant differences in the barrier integrity, viability, release of pro-inflammatory cytokines (except IL-1β and IL-8), and generation of NO were detected in the stable co-culture compared to the Caco-2 monoculture. Even though the release of IL-1β and IL-8 was higher in the stable co-culture than the monoculture it did not exceed the levels found in THP-1 monocultures. It can, therefore, be argued that the levels are attributable to the typical release by THP-1 cells and do not indicate an activation of the macrophages. Hence, the first hypothesis the project was based on ('Caco-2 and THP-1 cells can cohabit in a paracrine co-culture system to mimic the intestine in homeostatic state.') was confirmed.

The second step of inducing an inflammation-like response with LPS as pathophysiological stressor turned out to be unworkable without changing some details of the co-culture set-up and cell treatment. Whereas the cohabitation of Caco-2 and THP-1 cells was necessary for the establishment of the stable co-culture it greatly complicated the development of the diseased model. It is highly likely that the

macrophage-mediated pro-inflammatory response to LPS was suppressed by the Caco-2 cells. The 'immuno-shaping' role of IECs in the homeostatic intestine has become increasingly clear over the past years (Miron and Cristea, 2012) and was demonstrated to occur *in vitro* in presence of PBMCs (Parlesak et al., 2004). On the one hand, this confirmed the applicability of the stable model as representative of the healthy intestine. On the other hand, it made further changes to the co-culture protocol necessary to achieve an inflammation-like response. To overcome the downregulation of the inflammatory response in THP-1 cells, the Caco-2 barriers were primed with IFN-γ and the THP-1 cells were pre-stimulated with LPS and IFN-γ in advance of the co-culture. Therefore, the second general hypothesis of the project ('An inflammation-like response displaying hallmarks of intestinal inflammation can be induced in the homeostatic co-culture through the stimulation of the THP-1 cells.') was partially but not fully accepted. The induction of an inflammation-like response required more than the stimulation of THP-1 cells with LPS. Treatment of the Caco-2 cells (IFN-γ-priming) did not cause inflammation-like effects by itself but only in combination with pre-stimulated THP-1 cells (Section 2.2.4.2).

Co-cultures treated according to the adapted protocol (Step 4) displayed several hallmarks of intestinal inflammation, e.g. a significant reduction in TEER, increased cytotoxicity in the IEC barrier, high levels of pro-inflammatory cytokines and generation of NO. Nevertheless, the reduction in TEER, which can indicate both a destruction of the barrier through cell death or a loosening of the TJs, did not result in an increased translocation of LY. However, the permeability of the barrier to LY is not necessarily a proof for TJ integrity but instead requires careful evaluation. Even though few groups reported an increased LY translocation in response to cytokine-induced barrier disruption, the dye seems to be rather suitable to assess barrier destruction caused by cytotoxic effects rather than the integrity of TJs (Section 3.4.3). Hence, the choice for LY to study the initial Caco-2 barrier development was adequate, but a different molecule, e.g. dextran, should have been applied to investigate the TJ integrity throughout the inflamed co-culture.

Another issue was encountered when studying the possibility to activate the stable co-culture with EDTA and LPS. The exposure to EDTA and LPS confirmed that significant release of pro-inflammatory cytokines can be triggered in the stable co-culture (Section 3.4.2). For IL-1β and TNF-α, two essential cytokines for the induction and maintenance of inflammation, the release remained very low, albeit significantly

higher compared to the control. The additional control experiment including IFN-γ in the apical exposure, however, resulted in a significantly increased cytokine response compared to EDTA/LPS exposure alone. This confirmed the importance of IFN-γ for the synthesis of IL-1β and TNF-α, which has also been demonstrated *in vivo* (Shinozawa et al., 2002). These results imply that the ability of the stable co-culture to react to a pro-inflammatory stimulus in the absence of IFN-γ is limited. This, furthermore, leads to obvious questions regarding the applicability of the stable co-culture to study the pro-inflammatory potential of NMs. A possible solution to enhance the model's validity could be the introduction of IFN-γ into the set-up of the stable co-culture. Segura et al. (2002) reported a priming effect of IFN-γ on THP-1 cells, which caused only minimally increased background levels of pro-inflammatory cytokines. Upon stimulation with LPS, Segura et al. (2002) observed a higher cytokine response in primed vs. non-primed THP-1 cells. Taking into account the mentioned diversity in THP-1 responses to differentiation stimuli and stressors (Section 2.3.1.2) it cannot be guaranteed that the priming would cause the same effects here. This consideration is supported by the observation of Sanceau et al. (1991), who did not note a priming effect of IFN-γ but only a synergistic effect of IFN-γ and TNF-α.

Based on the results of the inflamed co-culture presented in Chapters 2 and 3 we concluded that the IEC barrier is not permanently destroyed and the inflammation-mediated barrier disruption resolved itself. The decisive factors for these statements were the increase in TEER at the end of the co-culture (Section 2.2.4.2), as well as the immunocytochemical staining of the corresponding barriers showing no gaps in the Caco-2 cell layer (Section 3.3.1.5). In this context, the increased levels of LDH were interpreted as result of necrotic cell death within the first 24h of co-culture, when the TEER is clearly reduced. Taking into account the observations in Chapter 4, however, the conclusion of a self-resolving inflammatory response might have been hasty. The reduction in TEER is most likely attributable to the known synergistic effect of IFN-γ and TNF-α on the TJ proteins claudin 2 and 4 (Capaldo et al., 2014). In contrast to other groups (Bruewer et al., 2003; Wang et al., 2005; Susewind et al., 2016), the barrier integrity in the inflamed model of this study was restored after 48h without any additional interference, e.g. medium change or addition of Ab. The initial criterion for the inflamed co-culture of inducing a self-resolving inflammation-like process was not achieved. Instead, TNF-α and IL-1β remained constant over 48h. Furthermore, the turning point for the barrier re-establishment was between 18 and 24h of co-culture. At this time point, the levels of both IFN-γ and TNF-α were remarkably high (Section

4.3.3.3). The next possible explanation was based on the paracrine nature of the model, which allowed a dynamic co-culture of and communication between the IECs and macrophages. It is possible that the inflammation like response also induced anti-inflammatory, barrier-protecting mechanisms to counteract the barrier disruption which were not measured.

Another possible explanation is that the increase in TEER can be traced back to cellular swelling. Since no increase in TEER was observed in the Caco-2 monoculture and stable co-culture control the swelling might have been caused by the occurrence of secondary necrosis resulting from cytokine-induced apoptosis (Silva, 2010). It may also explain the strong increases in barrier integrity in the inflamed co-culture after exposure to $AgNO_3$ and AgNPs, as well as in the Caco-2 monoculture and stable culture in response to $AgNO_3$ (Sections 4.3.3.1 & 4.4.3). This explanation, however, challenges the initial interpretation of the 're-establishment' of TEER, which we initially attributed to the restoration of the TJ network. Instead, the increase in TEER might have originated from a reduction in intercellular space caused by cellular swelling as part of necrotic cell death.

The third aim of the project was to use the developed co-culture models to study the effects of NMs in relation to the health status at the time of exposure. The main hypothesis was that different effects of AgNPs can be observed in the two different co-culture conditions. When studying CuO NPs, several hypotheses aimed to show differences in the exposure effects between digested and undigested CuO NPs. We hypothesised that, overall, the exposure to digested CuO would cause less pronounced effects in the co-culture conditions compared to the undigested particles.

Even though no pro- or anti-inflammatory effects were noted for AgNPs several interesting observations were made on the cytotoxic potential of both AgNPs and $AgNO_3$ (Section 4.3.2). The results clearly showed an increased sensitivity to ionic Ag in $_{D}$Caco-2 compared to $_{UD}$Caco-2 cells underlining the importance of the differentiation status for the outcomes. Furthermore, the model revealed a dramatically enhanced susceptibility of the inflamed co-culture to Ag species compared to the stable set-up.

The results obtained from the co-culture exposure to CuO NPs were, overall, less dramatic. Again, no effect on the cytokine release of NO generation was observed in any of the culture models. Interestingly, digested and undigested CuO NPs had distinct effects on the barrier integrity in the stable and inflamed co-culture conditions.

Whereas only the exposure to undigested CuO NPs significantly reduced the TEER of the stable co-culture, significant effects in the inflamed co-culture were limited to the exposure to digested CuO NPs. Hence as before, the two models were able to show distinct effects of NMs in relation to the health status of the co-culture. In contrast to the study of Ag-species no clearly increased susceptibility of the inflamed co-culture was noted in case of CuO NPs. The use of CuO NPs also rendered a limitation of the model visible regarding the detection of NM-induced cytotoxicity. As we observed earlier, assays quantifying the metabolic activity are not suitable to sensitively assess cell viability in the transwell cultures. Therefore, the LDH assay was used for AgNPs and $AgNO_3$ exposure experiments. Cu ions however, interfere with LDH and make it unavailable for the detection of enzymatic activity in the LDH assay. Hence, in case NMs interfere with cytotoxicity assays the cell viability has to be assessed using cell count methods, e.g. based on nuclear counts. Automated systems like the IN Cell Analyzer are highly suitable for these situations, but their operation is rather resource-intensive. Cell counts could also be performed manually. But especially regarding low cytotoxic effects, the error and bias introduced with the human factor might lead to over- or underestimations of results.

These results confirmed the hypothesis that an ongoing inflammation potentially alters the effects of NMs in the intestine. This certainly stresses the need to include the health conditions at the time of exposure into the safety assessment of NMs. However, other co-cultures mimicking the homeostatic and inflamed intestine failed to show similar outcomes (Susewind et al., 2016). This might be related to the significantly different co-culture structure and pro-inflammatory stressor (IL-1β) (Section 3.4.1.1). Without additional *in vivo* confirmation and validation the results generated here cannot be extrapolated to the potential effects of exposed human patients suffering from inflammatory conditions of the intestine.

The fourth aim of the project was to use the co-culture system to assess the paracellular passage of different sizes of radio-labelled AuNPs. The objective was to quantify and compare the translocation of [^{195}Au]AuNP-associated activity from the AP to the BL compartment between the stable and inflamed co-culture models. The experiments were based on the reports of other groups that AuNPs can translocate across the Caco-2 barrier, with a higher translocation rate for smaller particles (Lin et al., 2011). It was hypothesised that the barrier disruption in the inflamed co-culture would cause an increased paracellular passage compared to the Caco-2 monoculture and the stable co-

culture. However, the experiments did not show any significant translocation of particles independent of the particle size and cell culture health status at the time of exposure. Taking into account that induction of inflammation mainly causes a loosening of the TJ network rather than a disintegration of the Caco-2 barrier these results were, in retrospect, not particularly surprising. In a homeostatic state, the TJ are virtually impermeable to molecules larger than 15 Å (van Meer and Simons, 1986). Hence, a paracellular transport in the stable co-culture would have been an indication for cytotoxic effects induced by either the particles or by the co-culture conditions. It could have been possible that the cytokine-induced disruption of the TJs induced a widening of the paracellular space, which might allow for the translocation of larger structures. However, even if the size selectivity of the TJs was disrupted the passage of AuNPs would have most likely been prevented by their negative charge, as was observed with LY.

Nevertheless, an interesting observation was made concerning the increased sedimentation and accumulation of [^{195}Au]AuNPs in the inflamed co-culture, which was in line with *in vivo* and other *in vitro* studies (Sections 1.5.2 & 6.4.4). Identifying these significantly different effects between the inflamed and stable co-culture that coincide with results obtained in human patients and animal models further strengthened the model's closeness to reality and applicability.

Studying the effects of different types of NMs in the two co-culture models showed that also the third hypothesis ('The two co-culture conditions are suitable to study the effects of NMs in relation to the health status at the time of exposure.') could only partially be supported. On the one hand, significant differences regarding the effects of NMs were observed between the homeostatic and inflamed co-cultures for which the assessment of barrier integrity by means of TEER turned out to be the most sensitive and reliable method. On the other hand, several limitations of both the model and applied methods became visible, which narrow the applicability of the co-culture conditions. These include for instance the uncertain usefulness of the stable co-culture to study the pro-inflammatory potential of NMs and the quantification of cytotoxicity.

7.2 Theoretical outlook

A number of gaps remain and potential improvements of the model are possible.

The overall goal of the project was to challenge the current status quo of *in vitro* research of the intestine with the development of a reliable, reproducible, and versatile co-culture model based on human cell lines. The representation of the immune system using a monocytic cell line improves the model's applicability and closeness to a biological system. Nevertheless, it remains but a sketch of the complex construct that is the intestine.

Even though the project generated many inputs for additional research it left several questions unanswered. For example, it remains inconclusive how the barrier integrity of the inflamed model was restored. This knowledge is important to determine whether the inflammatory process is resolving or on-going. To elucidate this, the Caco-2 barriers should be subject to additional analyses regarding apoptotic and necrotic cell death markers over the course of the co-culture. The cells' morphology could be investigated using flow cytometry or TEM to detect cell shrinkage, compartmentalisation, and chromatin condensation for apoptosis, or cell swelling and membrane rupture for necrotic cell death. Furthermore, the activation of the caspase cascade could be monitored, as well as the expression of apoptosis-related cell surface markers like phosphatidylserine using annexin V (Krysko et al., 2008). In this context, also the paracellular permeability in the co-culture conditions should be addressed again using other markers than LY. Furthermore, the induction of anti-inflammatory or barrier-protective processes, e.g. the release of IL-10 (Madsen et al., 1997), should receive more attention. In parallel, studying the dynamics of the Caco-2 barrier integrity requires a more thorough analysis of the changes in expression of TJ proteins.

Another major question mark is the applicability of the stable co-culture to study the pro-inflammatory potentials of NMs (Section 3.4.2). Before continuing to use the model for such purposes a more thorough testing has to be executed. This includes the assessment of another stressor that does not depend on EDTA to disrupt the IEC barrier, for instance pathogenic *Shiga*-toxin. In contrast to *Staphylococcal* enterotoxin, *Shiga*-toxin can induce a barrier disruption in Caco-2 cells after AP exposure (Kwak et al., 2012; Schüller et al., 2004). Since *Shiga*-toxin alone is only inducing a moderate cytokine response in THP-1 cells a combined exposure with LPS would be useful (Harrison et al., 2005). Since the introduction of a new stressor requires a thorough,

time-intensive characterisation of its effects in monocultures of both cell lines this step was not introduced anymore in this project.

The introduction of additional cell types could certainly enhance the model's relevance. For instance the incorporation of neutrophils and DCs could open up possibilities to study the first lines of inflammatory processes, as well as recruitment of leukocytes and initiation of healing mechanisms. To do so it might be interesting to combine this paracrine co-culture with the collagen-embedded approach chosen by Susewind et al. (2015) and Leonard et al. (2010). To induce a physiologically relevant inflammation-like response the stimulation of leukocytes with LPS appears to bear greater potential than the stimulation of IECs with IL-1β (Section 3.4.1.1). It is questionable, whether the direct stimulation of immune cells would be feasible in case they are embedded in a collagen matrix beneath the IEC barrier. Furthermore, culturing leukocytes over an increased period of time, as done in the studies of Susewind et al. (2015) and Leonard et al. (2010), the cells' responsiveness to stressor would likely be reduced or inhibited as was observed here (Section 2.2.4.2). Therefore, the model should not be fully adapted to this approach but integrated. The model might then be suitable to study the effect of the activation of macrophages in the BL compartment on the embedded immune cells and how this might affect the interaction with enterocytes. Embedding immune cells under the IEC barrier allows assessing the migration of leukocytes to the AP side of the cells and a potentially distinct reaction to the exposure to NMs. In the here presented co-culture the NMs have to cross the IEC barrier to interact with the macrophages, whereas they might encounter leukocytes directly on the AP side of the barrier *in vivo*.

Another possibility would be the introduction of other non-enterocytic epithelial cell types. Especially in the context of nanosafety and nanomedical studies the lack of both mucus-producing goblet cells and M-cells is unfortunate. Long underestimated, the mucus layer covering the mucosa presents a major barrier and designing mucus-penetrating NMs remains a challenge (Barua and Mitragotri, 2014). M-cells, on the other hand, seem to be greatly involved in the uptake of NMs from the lumen (des Rieux et al., 2005). Their targeting has, therefore, been the goal to increase the efficiency of orally delivered vaccines (Garinot et al., 2007). The introduction of one, or better both cell types, would further increase the model's application range and potential to extrapolate results to an *in vivo* situation. However, even without these adaptions the model can generate useful information, especially regarding the

potentially increased susceptibility of the inflamed compared to the homeostatic intestine to the exposure to NMs.

7.3 Final conclusions

Altogether, three of four aims of the project, i.e. the development of the co-culture model in homeostatic state, its advancement to an inflamed state, and the application of both conditions to study the effect of NMs could be achieved. As the model is based on cell lines of human origin it is easily established in other laboratories and more applicable to studies on human exposure than models using cells from other mammalian species. It further sets itself apart from available models as it can mimic the intestine in homeostatic and controlled inflamed state. For the inflamed state, a pathophysiological mechanism was used that is has been shown to be involved in IBD. Hence, a highly realistic inflammation-like process was simulated, which is unique in the available *in vitro* intestinal models.

With the application of the model highly interesting results were obtained on the impact of the health status on NMs-induced effects that indicated a significantly increased susceptibility of the epithelial barrier under inflamed conditions. Especially in the context of rising prevalence and incidences of IBD these results underline the importance to consider the health status as part of the safety assessment of NMs. The fourth aim of studying the paracellular passage of NMs was not fulfilled. This can be traced back to unrealistic expectations concerning the disruption of the TJ network, as well as an overestimation of the barrier damage caused throughout the inflammation-like processes. Nevertheless, the use of radio-labelled NMs revealed an interesting, size- and time-dependent accumulation of AuNPs in the inflamed co-cultures, which further supported the model's applicability and closeness to reality.

The here presented model offers a promising basis for the safety assessment of NMs, as well as for further developments, adjustments, and applications beyond nanosafety research.

References

ABBAS, K.; CYDZIK, I.; DEL TORCHIO, R.; et al. 2009. Radiolabelling of TiO_2 nanoparticles for radiotracer studies. *J Nanopart Res,* **12,** 2435-2443.

ABBOTT CHALEW, T.E. & SCHWAB, K.J. 2013. Toxicity of commercially available engineered nanoparticles to Caco-2 and SW480 human intestinal epithelial cells. *Cell Biol Toxicol,* **29,** 101-116.

ABREU, M.T.; VORA, P.; FAURE, E.; et al. 2001. Decreased expression of Toll-like receptor-4 and MD-2 correlates with intestinal epithelial cell protection against dysregulated proinflammatory gene expression in response to bacterial lipopolysaccharide. *J Immunol,* **167,** 1609-1616.

AL-SADI, R.M. & MA, T.Y. 2007. IL-1β causes an increase in intestinal epithelial tight junction permeability. *J Immunol,* **178,** 4641-4649

AL-SADI, R.; YE, D.; SAID, H.M.; et al. 2010. IL-1β-induced increase in intestinal epithelial tight junction permeability is mediated by MEKK-1 activation of canonical NF-κB pathway. *Am J Pathol,* **177,** 2310-2322.

AL-SADI, R.; YE, D.; BOIVIN, M.; et al. 2014. Interleukin-6 modulation of intestinal epithelial tight junction permeability is mediated by JNK pathway activation of claudin-2 gene. *PLoS One,* **9,** DOI: 10.1371/journal.pone.0085345.

ALARIFI, S.; ALI, D.; VERMA, A.; et al. 2013. Cytotoxicity and genotoxicity of copper oxide nanoparticles in human skin keratinocytes cells. *Int J Toxicol,* **32,** 296-307.

ALBANESE, A.; WALKEY, C.D.; OLSEN, J.B.; et al. 2014. Secreted biomolecules alter the biological identity and cellular interactions of nanoparticles. *ACS Nano,* **8,** 5515-5526.

ALDO, P.B.; CRAVEIRO, V.; GULLER, S.; et al. 2013. Effect of culture conditions on the phenotype of THP-1 monocyte cell line. *Am J Reprod Immunol,* **70,** 80-86.

ALEMDAROGLU, F.E.; ALEMDAROGLU, N.C.; LANGGUTH, P.; et al. 2008. Cellular uptake of DNA block copolymer micelles with different shapes. *Macromol Rapid Commun,* **29,** 326-329.

ALFARO-MORENO, E.; NAWROT, T.S.; VANAUDENAERDE, B.M.; et al. 2008. Co-cultures of multiple cell types mimic pulmonary cell communication in response to urban PM10. *European Respiratory Journal,* **32,** 1184-1194.

ALI, H.; COLLNOT, E.-M.; WINDBERGS, M.; et al. 2013. Nanomedicines for the treatment of inflammatory bowel diseases. *Eur J Nanomed,* **5,** 23-38.

ALTWEGG, R. & VINCENT, T. 2014. TNF blocking therapies and immunomonitoring in patients with inflammatory bowel disease. *Mediators Inflamm,* **2014,** DOI: 10.1155/2014/172821.

ANDERSON, J.M. & VAN ITALLIE, C.M. 2009. Physiology and Function of the Tight Junction. *Cold Spring Harbor Perspectives in Biology,* **1,** a002584-a002584.

ANKARCRONA, M.; DYPBUKT, J.M.; BRÜNE, B.; et al. 1994. Interleukin-1β-induced nitric oxide production activates apoptosis in pancreatic RINm5F cells. *Exp Cell Res,* **213,** 172-177.

ANSES 2011. Second French Total Diet Study - Inorganic contaminants, minerals, persistent organic pollutants, mycotoxins and phytoestrogens; French agency for food, environment and occupational health & safety.

ARAUJO, F.; SLIFER, T.; LI, S.; et al. 2004. Gemifloxacin inhibits cytokine secretion by lipopolysaccharide stimulated human monocytes at the post-transcritptional level. *Clin Microbiol Infec,* **10,** 213-219.

ARNIDA; JANÁT-AMSBURY, M.M.; RAY, A.; et al. 2011. Geometry and surface characteristics of gold nanoparticles influence their biodistribution and uptake by macrophages. *Eur J Pharm Biopharm,* **77,** 417-423.

ARORA, S.; RAJWADE, J.M. & PAKNIKAR, K.M. 2012. Nanotoxicology and *in vitro* studies: the need of the hour. *Toxicol Appl Pharmacol,* **258,** 151-65.

ASSIMAKOPOULOS, S.F.; PAPAGEORGIOU, I. & CHARONIS, A. 2011. Enterocytes' tight junctions: From molecules to diseases. *World J Gastrointest Pathophysiol,* **2,** 123-137.

AUEVIRIYAVIT, S.; PHUMMIRATCH, D. & MANIRATANACHOTE, R. 2014. Mechanistic study on the biological effects of silver and gold nanoparticles in Caco-2 cells--induction of the Nrf2/HO-1 pathway by high concentrations of silver nanoparticles. *Toxicol Lett,* **224,** 73-83.

BAIN, C.C.; BRAVO-BLAS, A.; SCOTT, C.L.; et al. 2014. Constant replenishment from circulating monocytes maintains the macrophage pool in the intestine of adult mice. *Nat Immunol,* **15,** 929-37.

BAIN, C.C. & MOWAT, A.M. 2014. The monocyte-macrophage axis in the intestine. *Cell Immunol,* **291,** 41-48.

BAJAK, E.; FABBRI, M.; PONTI, J.; et al. 2015. Changes in Caco-2 cells transcriptome profiles upon exposure to gold nanoparticles. *Toxicol Lett,* **233,** 187-199.

BAMIAS, G.; ARSENEAU, K.O. & COMINELLI, F. 2014. Cytokines and mucosal immunity. *Curr Opin Gastroenterol,* **30,** 547-552.

BANCOS, S.; STEVENS, D.L. & TYNER, K.M. 2015. Effect of silica and gold nanoparticles on macrophage proliferation, activation markers, cytokine production, and phagocytosis *in vitro*. *Int J Nanomedicine,* **10,** 183-206.

BANKS, C.; BATEMAN, A.; PAYNE, R.; et al. 2003. Chemokine expression in IBD. Mucosal chemokine expression is unselectively increased in both ulcerative colitis and Crohn's disease. *J Pathol,* **199,** 28-35.

BANNUNAH, A.M.; VLLASALIU, D.; LORD, J.; et al. 2014. Mechanisms of nanoparticle internalization and transport across an intestinal epithelial cell model: effect of size and surface charge. *Mol Pharm,* **11,** 4363-4373.

BARKER, N. 2014. Adult intestinal stem cells: critical drivers of epithelial homeostasis and regeneration. *Nat Rev Mol Cell Biol,* **15,** 19-33.

BARUA, S. & MITRAGOTRI, S. 2014. Challenges associated with penetration of nanoparticles across cell and tissue barriers: A review of current status and future prospects. *Nano Today,* **9,** 223-243.

BASUROY, S.; SETH, A.; ELIAS, B.; et al. 2006. MAPK interacts with occludin and mediates EGF-induced prevention of tight junction disruption by hydrogen peroxide. *Biochem J,* **393,** 69-77.

BAUERLY, K.A.; KELLEHER, S.L. & LÖNNERDAL, B. 2004. Functional and molecular responses of suckling rat pups and human intestinal Caco-2 cells to copper treatment. *J Nutr Biochem,* **15,** 155-162.

BEER, C.; FOLDBJERG, R.; HAYASHI, Y.; et al. 2012. Toxicity of silver nanoparticles - nanoparticle or silver ion? *Toxicol Lett,* **208,** 286-292.

BERGES, C.; NAUJOKAT, C.; TINAPP, S.; et al. 2005. A cell line model for the differentiation of human dendritic cells. *Biochem Biophys Res Comm,* **333,** 896-907.

BERGIN, I.L. & WITZMANN, F.A. 2013. Nanoparticle toxicity by the gastrointestinal route: evidence and knowledge gaps. *Int J Biomed Nanosci Nanotechnol,* **3,** DOI: 10.1504/IJBNN.2013.054515

BEVINS, C.L. & SALZMAN, N.H. 2011. Paneth cells, antimicrobial peptides and maintenance of intestinal homeostasis. *Nat Rev Microbiol,* **9,** 356-368.

BIMBO, L.M.; SARPARANTA, M.; SANTOS, H.A.; et al. 2010. Biocompatibility of thermally hydrocarbonized porous silicon nanoparticles and their biodistribution in rats. *ACS Nano,* **4,** 3023-3032.

BISPING, G.; LÜGERING, N.; LÜTKE-BRINTRUP, S.; et al. 2001. Patients with inflammatory bowel disease (IBD) reveal increased induction capacity of intracellular interferon-gamma (IFN-γ) in peripheral $CD8^+$ lymphocytes co-cultured with intestinal epithelial cells. *Clin Exp Immunol,* **123,** 15-22.

BLUMBERG, R.S. 2009. Inflammation in the intestinal tract: pathogenesis and treatment. *Dig Dis,* **27,** 455-464.

BO, S.; DURAZZO, M.; GAMBINO, R.; et al. 2008. Associations of dietary and serum copper with inflammation, oxidative stress, and metabolic variables in adult. *J Nutr,* **138,** 305-310.

BODET, C.; CHANDAD, F. & GRENIER, D. 2005. Modulation of cytokine production by *Porphyromonas gingivalis* in a macrophage and epithelial cell co-culture model. *Microbes Infect,* **7,** 448-456.

BÖHMERT, L.; GIROD, M.; HANSEN, U.; et al. 2014. Analytically monitored digestion of silver nanoparticles and their toxicity on human intestinal cells. *Nanotoxicology,* **8,** 631-642.

BÖHMERT, L.; NIEMANN, B.; THÜNEMANN, A.F.; et al. 2012. Cytotoxicity of peptide-coated silver nanoparticles on the human intestinal cell line Caco-2. *Arch Toxicol,* **86,** 1107-1115.

BÖHMERT, L.; NIEMANN, B.; LICHTENSTEIN, D.; et al. 2015. Molecular mechanism of silver nanoparticles in human intestinal cells. *Nanotoxicology,* **9,** 852-860.

BOISSELIER, E. & ASTRUC, D. 2009. Gold nanoparticles in nanomedicine: preparations, imaging, diagnostics, therapies and toxicity. *Chem Soc Rev,* **38,** 1759-1782.

BOLAND, J.J. 2006. nan´o·tech·nol´o·gy n. *Nature Nanotechnology,* **1,** 8-10.

BOLGER, M.B.; FRACZKIEWICZ, R.; ENTZEROTH, M.; et al. 2006. Concepts for *In Vitro* Profiling: Drug Activity, Selectivity and Liability. *In:* BARTLETT, P.A. & ENTZEROTH, M. (eds.) *Exploting Chemical Diversity for Drug Discovery.* Cambridge: RSC Publishing**,** 336-363.

BONDARENKO, O.; JUGANSON, K.; IVASK, A.; et al. 2013. Toxicity of Ag, CuO and ZnO nanoparticles to selected environmentally relevant test organisms and mammalian cells *in vitro*: a critical review. *Arch Toxicol,* **87,** 1181-1200.

BONFOCO, E.; KRAINC, D.; ANKARCRONA, M.; et al. 1995. Apoptosis and necrosis: Two distinct events induced, respectively, by mild and intense insults with *N*-methyl-D-aspartate or nitric oxide/superoxide in cortical cell cultures. *PNAS,* **92,** 7162-7166.

BORKOW, G.; ZATCOFF, R.C. & GABBAY, J. 2009. Reducing the risk of skin pathologies in diabetics by using copper impregnated socks. *Med Hypotheses,* **73,** 883-886.

BORZĘCKA, K.; PLÓCIENNIKOWSKA, A.; BJÖRKELUND, H.; et al. 2013. CD14 mediates binding of high doses of LPS but is dispensable for TNF-α production. *Mediators inflamm,* **2013,** DOI: 10.1155/2013/824919.

BOUWMEESTER, H.; DEKKERS, S.; NOORDAM, M.Y.; et al. 2009. Review of health safety aspects of nanotechnologies in food production. *Regul Toxicol Pharmacol,* **53,** 52-62.

BOUWMEESTER, H.; POORTMAN, J.; PETERS, R.J.; et al. 2011. Characterization of translocation of silver nanoparticles and effects on whole-genome gene expression using an *in vitro* intestinal epithelium coculture Model. *ACS Nano,* **5,** 4091-4103.

BRAAKHUIS, H.M.; GOSENS, I.; KRYSTEK, P.; et al. 2014. Particle size dependent deposition and pulmonary inflammation after short-term inhalation of silver nanoparticles. *Part Fibre Toxicol,* **11,** DOI: 10.1186/s12989-014-0049-1.

BRAUNSTEIN, E.M.; QIAO, X.T.; MADISON, B.; et al. 2002. Villin: A marker for development of the epithelial pyloric border. *Dev Dynam,* **224,** 90-102.

BRETSCHER, A. & WEBER, K. 1979. Villin: The major microfilament-associated protein of the intestinal microvillus. *PNAS,* **76,** 2321-2325.

BRUEWER, M.; LUEGERING, A.; KUCHARZIK, T.; et al. 2003. Proinflammatory cytokines disrupt epithelial barrier function by apoptosis-independent mechanisms. *J Immunol,* **171,** 6164-6172.

BURGUERA, E.F.; BITAR, M. & BRUININK, A. 2010. Novel *in vitro* co-culture methodology to investigate heterotypic cell-cell interactions. *Euro Cell Mater,* **19,** 166-179.

CALATAYUD, M.; GIMENO-ALCAÑIZ, J.V.; VÉLEZ, D.; et al. 2014. Trivalent arsenic species induce changes in expression and levels of proinflammatory cytokines in intestinal epithelial cells. *Toxicol Lett,* **224,** 40-46.

CAO, M.; WANG, P.; SUN, C.; et al. 2013. Amelioration of IFN-γ and TNF-α-induced intestinal epithelial barrier dysfunction by berberine via suppression of MLCK-MLC phosphorylation signaling pathway. *PLoS One,* **8,** DOI: 10.1371/journal.pone.0061944.

CAPALDO, C.T. & NUSRAT, A. 2009. Cytokine regulation of tight junctions. *Biochim Biophys Acta,* **1788,** 864-871.

CAPALDO, C.T.; FARKAS, A.E.; HILGARTH, R.S.; et al. 2014. Proinflammatory cytokine-induced tight junction remodeling through dynamic self-assembly of claudins. *Mol Biol Cell,* **25,** 2710-2719.

CARIO, E. & PODOLSKY, D.K. 2000. Differential alteration in intestinal epithelial cell expression of Toll-like receptor 3 (TLR3) and TLR4 in inflammatory bowel disease. *Infect Immun,* **68,** 7010-7017.

CARIO, E.; GERKEN, G. & PODOLSKY, D.K. 2004. Toll-like receptor 2 enhances ZO-1-associated intestinal epithelial barrier integrity via protein kinase C. *Gastroenterology,* **127,** 224-238.

CASTELLANOS-GONZALEZ, A.; CABADA, M.M.; NICHOLS, J.; et al. 2013. Human primary intestinal epithelial cells as an improved *in vitro* model for *Cryptosporidium parvum* infection. *Infect Immun,* **81,** 1996-2001.

CERQUETELLA, M. 2010. Inflammatory bowel disease in the dog: Differences and similarities with humans. *World J Gastroenterol,* **16,** 1050-1056.

CHAN, F.K.; MORIWAKI, K. & DE ROSA, M.J. 2013. Detection of necrosis by release of lactate dehydrogenase activity. *Methods Mol Biol,* **979,** 65-70.

CHANANA, M.; RIVERA-GIL, P.; CORREA-DUARTE, M.A.; et al. 2013. Physicochemical properties of protein-coated gold nanoparticles in biological fluids and cells before and after proteolytic digestion. *Angew Chem Int Ed Engl,* **52,** 4179-4183.

CHANG, J.-S.; CHANG, K.L.B.; HWANG, D.-F.; et al. 2007. *In vitro* cytotoxicitiy of silica nanoparticles at high concentrations strongly depends on the metabolic activity type of the cell line. *Environ Sci Technol,* **41,** 2064-2068.

CHANG, M.-H.; LIU, H.-S. & TAI, C.Y. 2011. Preparation of copper oxide nanoparticles and its application in nanofluid. *Powder Technol,* **207,** 378-386.

CHANTRET, I.; BARBAT, A.; DUSSAULX, E.; et al. 1988. Epithelial polarity, villin expression, and enterocytic differentiation of cultured human colon carcinoma cells: A survey of twenty cell lines. *Cancer Res,* **48,** 1936-1942.

CHEN, C.; WANG, P.; SU, Q.; et al. 2012. Myosin light chain kinase mediates intestinal barrier disruption following burn injury. *PloS one,* **7,** e34946.

CHEN, F.; KUHN, D.C.; GAYDOS, L.J.; et al. 1996. Induction of nitric oxide and nitric oxide synthase mRNA by silica and lipopolysaccharide in PMA-primed THP-1 cells. *Acta PathMicro Im,* **104,** 176-182.

CHEN, G.; LIANQIN, Z.; FENGHUA, Z.; et al. 2015a. Comparative evaluation of nano-CuO crossing Caco-2 cell monolayers and cellular uptake. *J Nanopart Res,* **17,** DOI: 10.1007/s11051-015-3005-6.

CHEN, X.M. & KITTS, D.D. 2008. Determining conditions for nitric oxide synthesis in Caco-2 cells using Taguchi and factorial experimental designs. *Anal Biochem,* **381,** 185-192.

CHEN, X.M.; ELISIA, I. & KITTS, D.D. 2010. Defining conditions for the co-culture of Caco-2 and HT29-MTX cells using Taguchi design. *J Pharmacol Toxicol,* **61,** 334-342.

CHEN, Y.; LIN, Y.; DAVIS, K.M.; et al. 2015b. Robust bioengineered 3D functional human intestinal epithelium. *Sci Rep,* **5,** DOI: 10.1038/srep13708.

CHEN, Z.; MENG, H.; XING, G.; et al. 2006. Acute toxicological effects of copper nanoparticles *in vivo*. *Toxicol Lett,* **163,** 109-120.

CHENG, X.; TIAN, X.; WU, A.; et al. 2015. Protein corona influences cellular uptake of gold nanoparticles by phagocytic and nonphagocytic cells in a size-dependent manner. *ACS Appl Mater Interfaces,* **7,** 20568-20575.

CHEUNG, Y.F.; O, K.; TAM, S.C.; et al. 2005. Induction of MCP1, CCR2, and iNOS expression in THP-1 macrophages by serum of children late after Kawasaki disease. *Pediatr Res,* **58,** 1306-1310.

CHIBA, H.; OSANAI, M.; MURATA, M.; et al. 2008. Transmembrane proteins of tight junctions. *Biochim Biophys Acta,* **1778,** 588-600.

CHO, W.-S.; DUFFIN, R.; POLAND, C.A.; et al. 2011. Differential pro-inflammatory effects of metal oxide nanoparticles and their soluble ions *in vitro* and *in vivo*; zinc and copper nanoparticles, but not their ions, recruit eosinophils to the lungs. *Nanotoxicology,* **6,** 22-35.

CHO, W.-S.; CHO, M.; JEONG, J.; et al. 2009. Acute toxicity and pharmacokinetics of 13 nm-sized PEG-coated gold nanoparticles. *Toxicol Appl Pharmacol,* **236,** 16-24.

CHO, W.-S.; DUFFIN, R.; BRADLEY, M.; et al. 2013a. Predictive value of *in vitro* assays depends on the mechanism of toxicity of metal oxide nanoparticles. *Part Fibre Toxicol,* **10**, doi:10.1186/1743-8977-10-55.

CHO, W.-S.; KANG, B.-C.; LEE, J.K.; et al. 2013b. Comparative absorption, distribution, and excretion of titanium dioxide and zinc oxide nanoparticles after repeated oral administration. *Part Fibre Toxicol,* **10,** doi:10.1186/1743-8977-10-9.

CHOPRA, D.P.; DOMBKOWSKI, A.A.; STEMMER, P.M.; et al. 2010. Intestinal epithelial cells *in vitro*. *Stem Cells Dev,* **19,** 131-142.

CIABATTINI, A.; CUPPONE, A.M.; PULIMENO, R.; et al. 2006. Stimulation of human monocytes with the gram-positive vaccine vector *Streptococcus gordonii*. *Clin Vaccine immunol,* **13,** 1037-1043.

CLAYBURGH, D.R.; SHEN, L. & TURNER, J.R. 2004. A porous defense: the leaky epithelial barrier in intestinal disease. *Lab Invest,* **84,** 282-291.

COCCIA, M.; HARRISON, O.J.; SCHIERING, C.; et al. 2012. IL-1β mediates chronic intestinal inflammation by promoting the accumulation of IL-17A secreting innate lymphoid cells and $CD4^+$ Th17 cells. *J Exp Med,* **209,** 1595-1609.

COLLINS, J.A.; SCHANDL, C.A.; YOUNG, K.K.; et al. 1997. Major DNA fragmentation is a late event in apoptosis. *J Histochem Cytochem,* **45,** 923-934.

CONSUMER PRODUCTS INVENTORY 2016. The Project on Emerging Nanotechnologies. Consumer Products Inventory. http://www.nanotechproject.org/cpi/

CONWAY, J.R.; HANNA, S.K.; LENIHAN, H.S.; et al. 2014. Effects and implications of trophic transfer and accumulation of CeO_2 nanoparticles in a marine mussel. *Environ Sci Technol,* **48,** 1517-1524.

COOMBES, J.L. & POWRIE, F. 2008. Dendritic cells in intestinal immune regulation. *Nat Rev Immunol,* **8,** 435-446.

CORAZZA, S. & WADE, E.J. 2010. Assay development using primary and primary-like cells. *In:* CHEN, T. (ed.) *A Practical Guide to Assay Development and High-Throughput Screening in Drug Discovery (Critical Reviews in Combinatorial Chemistry).* Boca Raton, FL: CRC Press, Taylor & Francis Group**,** 169-182.

CRATER, J.S. & CARRIER, R.L. 2010. Barrier properties of gastrointestinal mucus to nanoparticle transport. *Macromol Biosci,* **10,** 1473-1483.

CUI, W.; LI, L.X.; SUN, C.M.; et al. 2010. Tumor necrosis factor alpha increases epithelial barrier permeability by disrupting tight junctions in Caco-2 cells. *Braz J Med Biol Res,* **43,** 330-337.

CUILLEL, M.; CHEVALLET, M.; CHARBONNIER, P.; et al. 2014. Interference of CuO nanoparticles with metal homeostasis in hepatocytes under sub-toxic conditions. *Nanoscale,* **6,** 1707-1715.

CUZZOCREA, S.; MAZZON, E.; DE SARRO, A.; et al. 2000. Role of free radicals and poly(ADP-ribose) synthetase in intestinal tight junction permeability. *Mol Med,* **6,** 766-778.

DADOSH, T. 2009. Synthesis of uniform silver nanoparticles with a controllable size. *Mater Lett,* **63,** 2236-2238.

DAIGNEAULT, M.; PRESTON, J.A.; MARRIOTT, H.M.; et al. 2010. The identification of markers of macrophage differentiation in PMA-stimulated

THP-1 cells and monocyte-derived macrophages. *PloS one,* **5,** DOI: 10.1371/journal.pone.0008668.

DE BARROS, A.L.B.; TSOURKAS, A.; SABOURY, B.; et al. 2012. Emerging role of radiolabeled nanoparticles as an effective diagnostic technique. *EJNMMI Research,* **2,** DOI: 10.1186/2191-219X-2-39.

DE JONG, W.H. & BORM, P.J.A. 2008. Drug delivery and nanoparticles: Applications and hazards. *Int J Nanomedicine,* **3,** 133-149.

DE JONG, W.H.; VAN DER VEN, L.T.; SLEIJFFERS, A.; et al. 2013. Systemic and immunotoxicity of silver nanoparticles in an intravenous 28 days repeated dose toxicity study in rats. *Biomaterials,* **34,** 8333-8343.

DEKKERS, S.; KRYSTEK, P.; PETERS, R.J.; et al. 2011. Presence and risks of nanosilica in food products. *Nanotoxicology,* **5,** 393-405.

DEPLANCKE, B. & GASKINS, H.R. 2001. Microbial modulation of innate defense: goblet cells and the intestinal mucus layer. *Am J Clin Nutr,* **73,** 1131S-1141S.

DES RIEUX, A.; RAGNARSSON, E.G.; GULLBERG, E.; et al. 2005. Transport of nanoparticles across an *in vitro* model of the human intestinal follicle associated epithelium. *Eur J Pharm Sci,* **25,** 455-465.

DESAI, M.P.; LABHASETWAR, V.; WALTER, E.; et al. 1997. The Mechanism of Uptake of Biodegradeable Microparticles in Caco-2 Cells is Size Dependent. *Pharmaceut Res,* **14,** 1568-1573.

DETZEL, C.J.; HORGAN, A.; HENDERSON, A.L.; et al. 2015. Bovine immunoglobulin/protein isolate binds pro-inflammatory bacterial compounds and prevents immune activation in an intestinal co-culture model. *PloS one,* **10,** DOI: 10.1371/journal.pone.0120278.

DHILLON, S.S.; MASTROPAOLO, L.A.; MURCHIE, R.; et al. 2014. Higher activity of the inducible nitric oxide synthase contributes to very early onset inflammatory bowel disease. *Clin Transl Gastroenterol,* **5,** DOI: 10.1038/ctg.2013.17.

DI, L. & KERNS, E.H. 2016. Permeability methods. *In*: *Drug-like properties: Concepts, structure design and methods from ADME to toxicity optimization.* Elsevier Inc.**,** 325-338.

DICKINSON, E. 2010. Food emulsions and foams: Stabilization by particles. *Curr Opin Colloid Interface Sci,* **15,** 40-49.

DISILVESTRO, R.A. & MARTEN, J.T. 1990. Effects of inflammation and copper intake on rat liver and erythrocyte Cu-ZN superoxide dismutase activity levels. *J Nutr,* **120,** 1223-1227.

DOCTER, D.; BANTZ, C.; WESTMEIER, D.; et al. 2014. The protein corona protects against size- and dose-dependent toxicity of amorphous silica nanoparticles. *Beilstein J Nanotechnol,* **5,** 1380-1392.

DOURMASHIIN, R.R.; DAVIES, H.; WELLS, C.; et al. 1983. Epithelial patchy necrosis in Crohn's disease. *Hum Pathol,* **14,** 643-648.

DUELL, B.L.; CRIPPS, A.W.; SCHEMBRI, M.A.; et al. 2011. Epithelial cell coculture models for studying infectious diseases: benefits and limitations. *J biomed biotechnol,* **2011,** DOI: 10.1038/ctg.2013.17.

DUNCAN, T.V. 2011. Applications of nanotechnology in food packaging and food safety: barrier materials, antimicrobials and sensors. *J Colloid Interface Sci,* **363,** 1-24.

DZIENDZIKOWSKA, K.; GROMADZKA-OSTROWSKA, J.; LANKOFF, A.; et al. 2012. Time-dependent biodistribution and excretion of silver nanoparticles in male Wistar rats. *J Appl Toxicol,* **32,** 920-928.

EBABE ELLE, R.; GAILLET, S.; VIDÉ, J.; et al. 2013. Dietary exposure to silver nanoparticles in Sprague-Dawley rats: effects on oxidative stress and inflammation. *Food Chem Toxicol,* **60,** 297-301.

ECKMANN, L.; LAURENT, F.; LANGFORD, T.D.; et al. 2000. Nitric oxide production by human intestinal epithelial cells and competition for arginine as potential determinants of host defense against the lumen-dwelling pathogen *Giardia lamblia*. *J Immunol,* **164,** 1478-1487.

EDELBLUM, K.L. & TURNER, J.R. 2009. The tight junction in inflammatory disease: communication breakdown. *Curr Opin Pharmacol,* **9,** 715-720.

EDELMANN, M.J.; SHACK, L.A.; NASKE, C.D.; et al. 2014. SILAC-based quantitative proteomic analysis of human lung cell response to copper oxide nanoparticles. *PLoS One,* **9,** DOI: 10.1371/journal.pone.0114390.

ELSAESSER, A. & HOWARD, C.V. 2012. Toxicology of nanoparticles. *Adv Drug Deliv Rev,* **64,** 129-137.

ENSIGN, L.M.; CONE, R. & HANES, J. 2012. Oral drug delivery with polymeric nanoparticles: the gastrointestinal mucus barriers. *Adv Drug Deliv Rev,* **64,** 557-570.

EUROPEAN COMMISSION 2011. Commission Recommendation of the definition of nanomaterial. *Official Journal of the European Union,* **L 275,** 38-40.

EVANOFF, D.D., JR. & CHUMANOV, G. 2005. Synthesis and optical properties of silver nanoparticles and arrays. *Chemphyschem,* **6,** 1221-1231.

FAHMY, B. & CORMIER, S.A. 2009. Copper oxide nanoparticles induce oxidative stress and cytotoxicity in airway epithelial cells. *Toxicol In Vitro,* **23,** 1365-1371.

FANG, F.C. & VAZQUEZ-TORRES, A. 2002. Nitric oxide production by human macrophages: there's NO doubt about it. *Am J Physiol,* **282,** L941-L943.

FANNINGS, A.S.; KAMESON, B.J.; JESAITIS, L.A.; et al. 1998. The tight junction protein ZO-1 establishes a link between the transmembrane protein occludin and the actin cytoskeleton. *J Biol Chem,* **273,** 29745-29753.

FAROKHZAD, O.C. & LANGER, R. 2006. Nanomedicine: developing smarter therapeutic and diagnostic modalities. *Adv Drug Deliv Rev,* **58,** 1456-1459.

FERNÁNDEZ-BANARES, F.; MINGORANCE, M.D.; ESTEVE, M.; et al. 1990. Serum zinc, copper, and selenium levels in inflammatory bowel disease: Effect of total enteral nutrition on trace element status. *Am J Gastroenterol,* **85,** 1584-1589.

FERRUZZA, S.; ROSSI, C.; SCARINO, M.L.; et al. 2012. A protocol for differentiation of human intestinal Caco-2 cells in asymmetric serum-containing medium. *Toxicol In Vitro,* **26,** 1252-1255.

FINLAY, S.B.B.A.F. 1990. *Salmonella* Interactions with polarized human intestinal Caco-2 epithelial cells. *J Infect Dis,* **162,** 1096-1106.

FIORENTINO, M.; LEVINE, M.M.; SZTEIN, M.B.; et al. 2014. Effect of wild-type *Shigella* species and attenuated *Shigella* vaccine candidates on small intestinal barrier function, antigen trafficking, and cytokine release. *PLoS One,* **9,** DOI: 10.1371/journal.pone.0085211.

FISICHELLA, M.; BERENGUER, F.; STEINMETZ, G.; et al. 2012. Intestinal toxicity evaluation of TiO_2 degraded surface-treated nanoparticles: a combined

physico-chemical and toxicogenomics approach in Caco-2 cells. *Part Fibre Toxicol,* **9,** doi:10.1186/1743-8977-9-18.

FLEISCHER, D. 1999. Biological transport phenomena in the gastrointestinal tract: cellular mechanisms. *In:* AMIDON, G.L.; LEE, P.I. and TOPP, E.M. (ed.): *Transport Processes in Pharmaceutical Systems.* New York / Basel: Marcel Dekker, Inc.**,** 147-184.

FLORENCE, A.T. 2005. Nanoparticle uptake by the oral route: Fulfilling its potential? *Drug Discov Today Technol,* **2,** 75-81.

FOLDBJERG, R.; OLESEN, P.; HOUGAARD, M.; et al. 2009. PVP-coated silver nanoparticles and silver ions induce reactive oxygen species, apoptosis and necrosis in THP-1 monocytes. *Toxicol Lett,* **190,** 156-162.

FOLDBJERG, R.; DANG, D.A. & AUTRUP, H. 2011. Cytotoxicity and genotoxicity of silver nanoparticles in the human lung cancer cell line, A549. *Arch Toxicol,* **85,** 743-750.

FORAKER, A.B.; WALCZAK, R.J.; COHEN, M.H.; et al. 2003. Microfabricated porous silicon particles enhance paracellular delivery of insulin across intestinal Caco-2 cell monolayers. *Pharmaceut Res,* **20,** 110-116.

FORSTERMANN, U. & SESSA, W.C. 2012. Nitric oxide synthases: regulation and function. *Eur Heart J,* **33,** 829-37, 837a-837d.

FOSTER, A.W.; OSMAN, D. & ROBINSON, N.J. 2014. Metal preferences and metallation. *J Biol Chem,* **289,** 28095-28103.

FOSTER, J.A. & MCVEY NEUFELD, K.A. 2013. Gut-brain axis: how the microbiome influences anxiety and depression. *Trends Neurosci,* **36,** 305-312.

FOURNIER, B.M. & PARKOS, C.A. 2012. The role of neutrophils during intestinal inflammation. *Mucosal Immunol,* **5,** 354-366.

FREESE, C.; UBOLDI, C.; GIBSON, M.I.; et al. 2012. Uptake and cytotoxicity of citrate-coated gold nanospheres: Comparative studies on human endothelial and epithelial cells. *Part Fibre Toxicol,* **9,** doi:10.1186/1743-8977-9-23.

FREIBERGER, E.B.; KAUFMANN, K.C.; BONA, E.; et al. 2015. Encapsulation of roasted coffee oil in biocompatible nanoparticles. *LWT-Food sci technol,* **64,** 381-389.

FRÖHLICH, E. & ROBLEGG, E. 2012. Models for oral uptake of nanoparticles in consumer products. *Toxicology,* **291,** 10-17.

FUNDA, D.P.; TUCKOVA, L.; FARRE, M.A.; et al. 2001. CD14 is expressed and released as soluble CD14 by human intestinal epithelial cells *in vitro*: lipopolysaccharide activation of epithelial cells revisited. *Infect Imm,* **69,** 3772-3781.

GAILLARD, J.-L; Berche, P. ; MOUNIER, J.; et al. 1987. *In vitro* model of penetration and intracellular growth of *Listeria monocytogenes* in the human enterocyte-like cell line Caco-2. *Infect Immun,* **55,** 2822-2829.

GARINOT, M.; FIÉVEZ, V.; POURCELLE, V.; et al. 2007. PEGylated PLGA-based nanoparticles targeting M cells for oral vaccination. *J Controlled Release,* **120,** 195-204.

GASSLER, N.; ROHR, C.; SCHNEIDER, A.; et al. 2001. Inflammatory bowel disease is associated with changes of enterocytic junctions. *Am J Physiol,* **281,** G216-G228.

GENIN, M.; CLEMENT, F.; FATTACCIOLI, A.; et al. 2015. M1 and M2 macrophages derived from THP-1 cells differentially modulate the response of

cancer cells to etoposide. *BMC Cancer,* **15,** 577**,** DOI 10.1186/s12885-015-1546-9.

GEORGANTZOPOULOU, A.; SERCHI, T.; CAMBIER, S.; et al. 2016. Effects of silver nanoparticles and ions on a co-culture model for the gastrointestinal epithelium. *Part Fibre Toxicol,* **13,** DOI 10.1186/s12989-016-0117-9.

GEORGE, R.; MERTEN, S.; WANG, T.T.; et al. 2014. *In vivo* analysis of dermal and systemic absorption of silver nanoparticles through healthy human skin. *Australas J Dermatol,* **55,** 185-190.

GERLOFF, K.; PEREIRA, D.I.; FARIA, N.; et al. 2013. Influence of simulated gastrointestinal conditions on particle-induced cytotoxicity and interleukin-8 regulation in differentiated and undifferentiated Caco-2 cells. *Nanotoxicology,* **7,** 353-366.

GEROVA, V.A.; STOYNOV, S., G.; KATSAROV, D.S.; et al. 2011. Increased intestinal permeability in inflammatory bowel diseases assessed by iohexol test. *World J Gastroenterol,* **17,** 2211-2215.

GIANNASCA, K.T.; GIANNASCA, P.J. & NEUTRA, M.R. 1996. Adherence of *Salmonella typhimurium* to Caco-2 cells: Identification of glycoconjugate receptor. *Infection and immunity,* **64,** 135-145.

GIBSON, N.; HOLZWARTH, U.; ABBAS, K.; et al. 2011. Radiolabelling of engineered nanoparticles for *in vitro* and *in vivo* tracing applications using cyclotron accelerators. *Arch Toxicol,* **85,** 751-773.

GIORIA, S. unpublished results. Influence of 23nm AgNPs on protein expression in Caco-2 cells.

GLIGA, A.R.; SKOGLUND, S.; ODNEVALL WALLINDER, I.; et al. 2014. Size-dependent cytotoxicity of silver nanoparticles in human lung cells: the role of cellular uptake, agglomeration and Ag release. *Part Fibre Toxicol***,** **11**, DOI: 10.1186/1743-8977-11-11.

GNANADHAS, D.P.; THOMAS, M.B.; THOMAS, R.; et al. 2013. Interaction of silver nanoparticles with serum proteins affects their antimicrobial activity *in vivo*. *Antimicrob Agents Chemother,* **57,** 4945-4955.

GOSENS, I.; Cassee, F.R.; ZANELLA, M.; Et al. 2016. Organ burden and pulmonary toxicity of nano-sized copper (II) oxide particles after short-term inhalataion exposure. *Nanotoxicology*. DOI: 10.3109/17435390.2016.1172678.

GOTTARDI, C.J.; ARPIN, M.; FANNING, A.S.; et al. 1996. The junction-associated protein, zonula occludens-1, localizes to the nucleus before the maturation and during the remodeling of cell-cell contacts. *PNAS,* **93,** 10779-10784.

GRABINGER, T.; LUKS, L.; KOSTADINOVA, F.; et al. 2014. *Ex vivo* culture of intestinal crypt organoids as a model system for assessing cell death induction in intestinal epithelial cells and enteropathy. *Cell Death Dis,* **5,** DOI: 10.1038/cddis.2014.183.

GRANT-TSCHUDY, K.S. & WIRA, C.R. 2005. Paracrine mediators of mouse uterine epithelial cell transepithelial resistance in culture. *J Reprod Immunol,* **67,** 1-12.

GREULICH, C.; DIENDORF, J.; GESSMANN, J.; et al. 2011. Cell type-specific responses of peripheral blood mononuclear cells to silver nanoparticles. *Acta Biomater,* **7,** 3505-3514.

GRIFFITHS, S. 2015. Silver nanoparticles extend shelf life of milk. http://fstjournal.org/news/silver-nanoparticles-extend-shelf-life-milk/730. Available: http://fstjournal.org/news/silver-nanoparticles-extend-shelf-life-milk/730 [Accessed 30/06/2016].

GRISHAM, M.B.; JOURD'HEUIL, D. & WINK, D.A. 1999. I. Physiological chemistry of nitric oxide and its metabolites: implications in inflammation. *Am J Physiol: Gastrointest Liver Physiol,* **276,** G315-G321.

GROH, K.J.; DALKVIST, T.; PICCAPIETRA, F.; et al. 2015. Critical influence of chloride ions on silver ion-mediated acute toxicity of silver nanoparticles to zebrafish embryos. *Nanotoxicology,* **9,** 81-91.

GROSELL, M. 2012. Chemical speciation and other factors affecting toxicity in freshwater and seawater. *In:* FARRELL, A.P. & BRAUNER, C.J. (eds.) *Homeostasis and Toxicoloy of Essential Metals* Elsevier Inc.**,** 55-59.

GROSSMANN, J.; MAXSON, J.M.; WHITACRE, C.M.; et al. 1998. New isolation technique to study apoptosis in human intestinal epithelial cells. *Am J Pathol,* **153,** 53-62.

GROSSMANN, J.; WALTHER, K.; ARTINGER, M.; et al. 2001. Apoptotic signaling during initiation of detachment-induced apoptosis ("anoikis") of primary human intestinal epithelial cells. *Cell Growth Differ,* **12,** 147-155.

GÜNTHER, C.; MARTINI, E.; WITTKOPF, N.; et al. 2011. Caspase-8 regulates TNF-α-induced epithelial necroptosis and terminal ileitis. *Nature,* **477,** 335-339.

GUO, S.; AL-SADI, R.; SAID, H.M.; et al. 2013. Lipopolysaccharide causes an increase in intestinal tight junction permeability *in vitro* and *in vivo* by inducing enterocyte membrane expression and localization of TLR-4 and CD14. *Am J Pathol,* **182,** 375-387.

GUO, Z.; JANG, M.H.; OTANI, K.; et al. 2008. $CD4^{+}CD25^{+}$ regulatory T cells in the small intestinal lamina propria show an effector/memory phenotype. *Int Immunol,* **20,** 307-315.

GUTTMAN, J.A. & FINLAY, B.B. 2009. Tight junctions as targets of infectious agents. *Biochim Biophys Acta,* **1788,** 832-841.

HAASE, A.; TENTSCHERT, J.; JUNGNICKEL, H.; et al. 2011. Toxicity of silver nanoparticles in human macrophages: uptake, intracellular distribution and cellular responses. *JPCS,* **304,** DOI: 10.1088/1742-6596/304/1/012030.

HABTEZION, A.; NGUYEN, L.P.; HADEIBA, H.; et al. 2016. Leukocyte trafficking to the small intestine and colon. *Gastroenterol,* **150,** 340-354.

HALAMODA-KENZAOUI, B.; CERIDONO, M.; COLPO, P.; et al. 2015. Dispersion behaviour of silica nanoparticles in biological media and its influence on cellular uptake. *PLoS One,* **10,** DOI: 10.1371/journal.pone0141593.

HALLER, D.; BODE, C.; HAMMES, W.P.; et al. 2000. Non-pathogenic bacteria elicit a differential cytokine response by intestinal epithelial cell/leucocyte co-cultures. *Gut,* **47,** 79-87.

HAN, X.; GELEIN, R.; CORSON, N.; et al. 2011. Validation of an LDH assay for assessing nanoparticle toxicity. *Toxicology,* **287,** 99-104.

HANDY, R.D. & SHAW, B.J. 2007. Toxic effects of nanoparticles and nanomaterials: Implications for public health, risk assessment and the public perception of nanotechnology. *Health Risk Soc,* **9,** 125-144.

HARRISON, L.M.; VAN DEN HOOGEN, C.; VAN HAAFTEN, W.C.; et al. 2005. Chemokine expression in the monocytic cell line THP-1 in response to purified *shiga* toxin 1 and/or lipopolysaccharides. *Infect Immun,* **73,** 403-412.

HARTSOCK, A. & NELSON, W.J. 2008. Adherens and tight junctions: structure, function and connections to the actin cytoskeleton. *Biochim Biophys Acta,* **1778,** 660-669.

HASHIMOTO, K. & SHIMIZU, M. 1993. Epithelial properties of human intestinal Caco-2 cells cultured in serum-free medium. *Cytotechnology,* **13,** 175-184.

HASSANI, S.; PELLEQUER, Y. & LAMPRECHT, A. 2009. Selective adhesion of nanoparticles to inflamed tissue in gastric ulcers. *Pharm Res,* **26,** 1149-1154.

HE, L.; YIN, Y.; LI, T.; et al. 2013. Use of the Ussing chamber technique to study nutrient transport by epithelial tissues. *Front Biosci,* **18,** 1266-1274.

HEBEISH, A.; EL-RAFIE, M.H.; EL-SHEIKH, M.A.; et al. 2014. Antimicrobial wound dressing and anti-inflammatory efficacy of silver nanoparticles. *Int J Biol macromolec,* **65,** 509-515.

HILGENDORF, C.; SPAHN-LANGGUTH, H.; REGARDH, C.G.; et al. 2000. Caco-2 versus Caco-2/HT29-MTX co-cultured cell lines: Permeabilities via diffusion, inside- and outside-directed carrier-mediated transport. *J Pharm Sci,* **89,** 63-75.

HILGERS, A.R.; CONRADI, R.A. & BURTON, P.S. 1990. Caco-2 cell monolayers as a model for drug transport across the intestinal mucosa. *Pharm Res,* **7,** 903-910.

HILLYER, J.F. & ALBRECHT, R.M. 2001. Gastrointestinal persorption and tissue distribution of differently sized colloidal gold nanoparticles. *J Pharm Sci,* **90,** 1927-1936.

HINDERLITER, P.M.; MINARD, K.R.; ORR, G.; et al. 2010. ISDD: A computational model of particle sedimentation, diffusion and target cell dosimetry for *in vitro* toxicity studies. *Part Fibre Toxicol,* **7,** DOI: 10.1186/1743-8977-7-36.

HOET, P.H.; BRUSKE-HOHLFELD, I. & SALATA, O.V. 2004. Nanoparticles - known and unknown health risks. *J Nanobiotechnology,* **2,** DOI: 10.1186/1477-3155-2-12.

HOLZWARTH, U.; BELLIDO, E.; DALMIGLIO, M.; et al. 2014. Be-recoil radiolabelling of industrially manufactured silica nanoparticles. *J Nanopart Res,* **16,** DOI: 10.1007/s11051-014-2574-0.

HOORENS, A.; STANGÉ, G.; PAVLOVIC, D.; et al. 2001. Distinction between interleukin-1-induced necrosis and apoptosis of islet cells. *Diabetes,* **50,** 551-557.

HOWE, K.L.; REARDON, C.; WANG, A.; et al. 2005. Transforming growth factor-*ß* regulation of epithelial tight junction proteins enhances barrier function and blocks enterohemorrhagic *Escherichia coli O157:H7*-induced increased permeability. *Am J Pathol,* **167,** 1587-1597.

HSIAO, I.L.; HSIEH, Y.K.; WANG, C.F.; et al. 2015. Trojan-horse mechanism in the cellular uptake of silver nanoparticles verified by direct intra- and extracellular silver speciation analysis. *Environ Sci Technol,* **49,** 3813-2381.

HUANG, P.L.; HUANG, Z.; MASHIMO, H.; et al. 1995. Hypertension in mice lacking the gene for endothelial nitric oxide synthase. *Nature,* **377,** 239-242.

HUK, A.; IZAK-NAU, E.; REIDY, B.; et al. 2014. Is the toxic potential of nanosilver dependent on its size? *Part Fibre Toxicol,* **11,** DOI: 10.1186/s12989-014-0065-1.

IOANNIDIS, J.P.A. 2012. Exrapolating from animals to humans. *Sci Transl Med,* **4,** DOI: 10.1126/scitranslmed.3004631.

ITO, R.; SHIN-YA, M.; KISHIDA, T.; et al. 2006. Interferon-gamma is causatively involved in experimental inflammatory bowel disease in mice. *Clin Exp Immunol,* **146,** 330-338.

IVERSEN, T.-G.; SKOTLAND, T. & SANDVIG, K. 2011. Endocytosis and intracellular transport of nanoparticles: Present knowledge and need for future studies. *Nano Today,* **6,** 176-185.

IZUMIKAWA, K.; HIRAKATA, Y.; YAMAGUCHI, T.; et al. 1998. *Escherichia coli O157* interactions with human intestinal Caco-2 cells and the influence of fosfomycin. *J Antimicrob Chemother,* **42,** 341-347.

JANI, P.; HALBERT, G.W.; LANGRIDGE, J.; et al. 1990. Nanoparticle uptake by the rat gastrointestinal mucosa: quantitation and particle size dependency. *J Pharm Pharmacol,* **42,** 821-826.

JEONG, G.N.; JO, U.B.; RYU, H.Y.; et al. 2010. Histochemical study of intestinal mucins after administration of silver nanoparticles in Sprague–Dawley rats. *Arch Toxicol,* **84**, 63-69

JI, Z.; JIN, X.; GEORGE, S.; et al. 2010. Dispersion and stability optimization of TiO_2 nanoparticles in cell culture media. *Environ Sci Technol,* **44,** 7309-7314.

JIMINEZ, J.A.; UWIERA, T.C.; DOUGLAS INGLIS, G.; et al. 2015. Animal models to study acute and chronic intestinal inflammation in mammals. *Gut Pathog,* **7,** DOI: 10.1186/s13099-015-0076-y.

JING, X.; PARK, J.H.; PETERS, T.M.; et al. 2015. Toxicity of copper oxide nanoparticles in lung epithelial cells exposed at the air-liquid interface compared with *in vivo* assessment. *Toxicol In Vitro,* **29,** 502-511.

JO, M.-R.; BAE, S.-H.; GO, M.-R.; et al. 2015. Toxicity and biokinetics of colloidal gold nanoparticles. *Nanomaterials,* **5,** 835-850.

JOHANSSON, M.E.; SJOVALL, H. & HANSSON, G.C. 2013. The gastrointestinal mucus system in health and disease. *Nat Rev Gastroenterol Hepatol,* **10,** 352-361.

JOHTATSU, T.; ANDOH, A.; KURIHARA, M.; et al. 2007. Serum concentrations of trace elements in patients with Crohn's disease receiving enteral nutrition. *J Clin Biochem Nutr,* **41,** 197-201.

JUNG, C.; HUGOT, J.P. & BARREAU, F. 2010. Peyer's patches: The immune sensors of the intestine. *Int J Inflam,* **2010,** DOI: 10.4061/2010/823710.

JUNG, L.H.C.E.; YANG, S.-K.; PANJA, A.; et al. 1995. A distinct array of proinflammatory cytokines is expressedn in human colon epithelial cells in response to bacterial invasion. *J Clin Invest,* **95,** 55-65.

JUNG, J.-Y.; MADAN-LALA, R.; GEORGIEVA, M.; et al. 2012. The intracellular environment of human macrophages that produce nitric oxide promotes growth of mycobacteria. *Infect Immun,* **81,** 3198-3209.

KAMADA, N.; HISAMATSU, T.; OKAMOTO, S.; et al. 2008. Unique $CD14^+$ intestinal macrophages contribute to the pathogenesis of Crohn disease via IL-23/IFN-γ axis. *J Clin Invest,* **118,** 2269-2280.

KANAPORIS, G.; BRINK, P.R. & VALIUNAS, V. 2011. Gap junction permeability: selectivity for anionic and cationic probes. *Am J Physiol: Cell Physiology,* **300,** C600-C609.

KANZATO, H.; MANABE, M. & SHIMIZU, M. 2001. An *in vitro* approach to the evaluation of the cross talk between intestinal epithelium and macrophages. *Biosci Biotechnol Biochem,* **65,** 449-451.

KARLSSON, H.L.; CRONHOLM, P.; GUSTAFSSON, J.; et al. 2008. Copper oxide nanoparticles are highly toxic: A comparison between metal oxide nanoparticles and carbon nanotubes. *Chem Res Toxicol,* **27,** 1726-1732.

KASAAI, M.R. 2015. Nanosized particles of silica and its derivatives for applications in various branches of food and nutrition sectors. *J Nanotechnol,* **2015,** DOI: 10.1155/2015/852394.

KASPER, J.Y.; HERMANNS, M.I.; UNGER, R.E.; et al. 2015. A responsive human triple-culture model of the air-blood barrier: incorporation of different macrophage phenotypes. *J Tissue Eng Regen Med,* **15,** DOI: 10.1002/term.2032.

KATZ, K.D.; HOLLANDER, D.; VADHEIM, C.M.; et al. 1989. Intestinal permeability in patients with Crohn's disease and their healthy relatives. *Gastroenterol,* **97,** 927-931.

KAUR, I.P.; KAKKAR, V.; DEOL, P.K.; et al. 2014. Issues and concerns in nanotech product development and its commercialization. *J Control Release,* **193,** 51-62.

KHATRI, M.; BELLO, D.; PAL, A.K.; et al. 2013. Evaluation of cytotoxic, genotoxic and inflammatory responses of nanoparticles from photocopiers in three human cell lines. *Part Fibre Toxicol,* **10,** DOI: 10.1186/1743-8977-10-42.

KIM, H.J.; HUH, D.; HAMILTON, G.; et al. 2012a. Human gut-on-a-chip inhabited by microbial flora that experiences intestinal peristalsis-like motions and flow *Lab Chip,* **12,** 2165-2174.

KIM, J.M.; KIM, J.S.; JUNG, H.C.; et al. 2002. Up-regulation of inducible nitric oxide synthase and nitric oxide in *Helicobacter pylori*-infected human gastric epithelial cells: Possible role of interferon-γ in polarized nitric oxide secretion. *Helicobacter,* **7,** 116-128.

KIM, J.S.; ADAMCAKOVA-DODD, A.; O'SHAUGHNESSY, P.T.; et al. 2011. Effects of copper nanoparticle exposure on host defense in a murine pulmonary infection model. *Part Fibre Toxicol,* **8,** DOI: 10.1186/1743-8977-8-29.

KIM, S.H.; CHI, M.; YI, B.; et al. 2014. Three-dimensional intestinal villi epithelium enhances protection of human intestinal cells from bacterial infection by inducing mucin expression. *Integr Biol,* **6,** 1122-1131.

KIM, T.H.; KIM, M.; PARK, H.S.; et al. 2012b. Size-dependent cellular toxicity of silver nanoparticles. *J Biomed Mater Res A,* **100,** 1033-1043.

KIM, Y.S.; KIM, J.S.; CHO, H.S.; et al. 2008. Twenty-eight-day oral toxicity, genotoxicity, and gender-related tissue distribution of silver nanoparticles in Sprague-Dawley rats. *Inhal Toxicol,* **20,** 575-583.

KIM, Y.S.; SONG, M.Y.; PARK, J.D.; et al. 2010. Subchronic oral toxicity of silver nanoparticles. *Part Fibre Toxicol,* **7,** DOI: 10.1186/1743-8977-7-20.

KINSNER, A.; BOVERI, M.; HARENG, L.; et al. 2006. Highly purified lipoteichoic acid induced pro-inflammatory signalling in primary culture of rat microglia through Toll-like receptor 2: selective potentiation of nitric oxide production by muramyl dipeptide. *J Neurochem,* **99,** 596-607.

KITCHENS, K.M.; FORAKER, A.B.; KOLHATKAR, R.B.; et al. 2007. Endocytosis and interaction of poly (amidoamine) dendrimers with Caco-2 cells. *Pharm Res,* **24,** 2138-2145.

KITTLER, S.; GREULICH, C.; DIENDORF, J.; et al. 2010. Toxicity of silver nanoparticles increases during storage because of slow dissolution under release of silver ions. *Chem Materials,* **22,** 4548-4554.

KLEIN, S.G.; SERCHI, T.; HOFFMANN, L.; et al. 2013. An improved 3D tetraculture system mimicking the cellular organisation at the alveolar barrier to study the potential toxic effects of particles on the lung. *Part Fibre Toxicol,* **10,** DOI: 10.1186/1743-8977-10-31.

KNIPP, G.T.; HO, N.F.; BARSUHN, C.L.; et al. 1997. Paracellular diffusion in Caco-2 cell monolayers: effect of perturbation on the transport of hydrophilic compounds that vary in charge and size. *J Pharm Sci,* **86,** 1105-1110.

KOBAYASHI, K.; KATO, A.; MUKAE, M.; et al. 2012. Adequacy of serum concentrations of vitamin and trace element preparations in treating patients with inflammatory bowel disease receiving long-term, home parenteral nutrition. *The Kitasato Medical Journal,* **42,** 148-155.

KODA, T.; MINAMI, H.; OGAWA, T.; et al. 2003. Higher concentrations of interferon-γ enhances uptake and transport of dietary antigens by human intestinal cells: A study using cultured Caco-2 cells. *J Nutr Sci Vitaminol,* **49,** 179-186.

KOLIOS, G.; VALATAS, V. & WARD, S.G. 2004. Nitric oxide in inflammatory bowel disease: a universal messenger in an unsolved puzzle. *Immunology,* **113,** 427-437.

KOMAI-KOMA, M.; GILCHRIST, D.S. & XU, D. 2009. Direct recognition of LPS by human but not murine $CD8^+$ T cells via TLR4 complex. *Eur J Immunol,* **39,** 1564-1572.

KONSOULA, R. & BARILE, F.A. 2005. Correlation of *in vitro* cytotoxicity with paracellular permeability in Caco-2 cells. *Toxicol In Vitro,* **19,** 675-684.

KORANI, M.; REZAYAT, S.M. & BIDGOLI, S.A. 2013. Sub-chronic dermal toxicity of silver nanoparticles in guinea pig: Special emphasis to heart, bone and kidney toxicities. *Iran J Pharm Res,* **12,** 511-519.

KREMLEV, S.G. & PHELPS, D.S. 1997. Effect of SP-A and surfactant lipids on expression of cell surface markers in the THP-1 monocytic cell line. *Am J Physiol: Lung Cell Mol Physiol,* **272,** L1070-L1077.

KRUG, H.F. 2014. Nanosafety research--are we on the right track? *Angew Chem Int Ed Engl,* **53,** 12304-12319.

KRYSKO, D.V.; VANDEN BERGHE, T.; D'HERDE, K.; et al. 2008. Apoptosis and necrosis: detection, discrimination and phagocytosis. *Methods,* **44,** 205-221.

KRYSTEK, P.; KETTLER, K.; VAN DER WAGT, B.; et al. 2015. Exploring influences on the cellular uptake of medium-sized silver nanoparticles into THP-1 cells. *Microchem J,* **120,** 45-50.

KUCHARZIK, T.; LÜGERING, N.; WINDE, G.; et al. 1997. Colon carcinoma cell lines stimulate monocytes and lamina propria mononuclear cells to produce IL-10. *Clin Experim Immunol,* **110,** 296-302.

KÜHL, A.A.; ERBEN, U.; KREDEL, L.I.; et al. 2015. Diversity of intestinal macrophages in inflammatory bowel diseases. *Front Immunol,* **6,** DOI: 10.3389/fimmu.2015.00613.

KUNZ-SCHUGHART, L.A.; WEBER, A.R., M.; GOTTFRIED, E.; et al. 2003. The "classical" macrophage marker CD68 is strongly expressed in primary human fibroblasts. *Verh Dtsch Ges Pathol,* **87,** 215-223.

KUSWANDI, B.; WICAKSONO, Y.; JAYUS; et al. 2011. Smart packaging: sensors for monitoring of food quality and safety. *Sens Instrum for Food Qual Saf,* **5,** 137-146.

KVIETYS, P.R. & GRANGER, D.N. 2010. Role of intestinal lymphatics in interstitial volume regulation and transmucosal water transport. *Ann N Y Acad Sci,* **1207** Suppl 1**,** E29-43.

KWAK, Y.K.; VIKSTROM, E.; MAGNUSSON, K.E.; et al. 2012. The *Staphylococcus aureus* alpha-toxin perturbs the barrier function in Caco-2 epithelial cell monolayers by altering junctional integrity. *Infect Immun,* **80,** 1670-1680.

KWON, J.-T.; MINAI-TEHRANI, A.; HWANG, S.-K.; et al. 2012. Acute pulmonary toxicity and body distribution of inhaled metallic silver nanoparticles. *Toxicol Res,* **28,** 25-31.

LABBÉ, K. & SALEH, M. 2011. Pyroptosis: A caspase-1-dependent programmed cell death and a barrier to infection. *In*: *The Inflammasomes.* Springer Basel**,** 17-36.

LAI, S.K.; WANG, Y.Y. & HANES, J. 2009. Mucus-penetrating nanoparticles for drug and gene delivery to mucosal tissues. *Adv Drug Deliv Rev,* **61,** 158-171.

LAMPRECHT, A.; UBRICH, N.; YAMAMOTO, H.; et al. 2001. Biodegradable nanoparticles for targeted drug delivery in treatment of inflammatory bowel disease. *J Pharmacol Exp Ther,* **299,** 775-781.

LANKVELD, D.P.K.; OOMEN, A.G.; KRYSTEK, P.; et al. 2010. The kinetics of the tissue distribution of silver nanoparticles of different sizes. *Biomaterials,* **31,** 8350-8361.

LANONE, S.; ROGERIEUX, F.; GEYS, J.; et al. 2009. Comparative toxicity of 24 manufactured nanoparticles in human alveolar epithelial and macrophage cell lines. *Part Fibre Toxicol,* **6,** DOI:10.1186/1743-8977-6-14.

LARA, H.H.; AYALA-NÚÑEZ, N.V.; IXTEPAN TURRENT, L.D.C.; et al. 2009. Bactericidal effect of silver nanoparticles against multidrug-resistant bacteria. *World J Microb Biot,* **26,** 615-621.

LEE, C.M.; JEONG, H.J.; KIM, D.W.; et al. 2012. The effect of fluorination of zinc oxide nanoparticles on evaluation of their biodistribution after oral administration. *Nanotechnology,* **23,** DOI: 10.1088/0957-4484/23/20/205102.

LEE, J.; CHOI, J.H. & KIM, H.J. 2016. Human gut-on-a-chip technology: will this revolutionize our understanding of IBD and future treatments? *Expert Rev Gastroenterol Hepatol,* **1-3,** DOI: 10.1080/17474124.2016.1200466.

LEE, J.A.; KIM, M.K.; PAEK, H.J.; et al. 2014. Tissue distribution and excretion kinetics of orally administered silica nanoparticles in rats. *Int J Nanomedicine,* **9** Suppl 2**,** 251-260.

LEE, J.H.; KIM, Y.S.; SONG, K.S.; et al. 2013. Biopersistence of silver nanoparticles in tissues from Sprague-Dawley rats. *Part Fibre Toxicol,* **10,** DOI: 10.1186/1743-8977-10-36.

LEE, Y.S.; KIM, D.W.; LEE, Y.J.; et al. 2011. Silver nanoparticles induce apoptosis and G2/M arrest via PKCζ-dependent signaling in A549 lung cells. *Inorganic Compounds,* **85,** 1529-1540.

LEFEBVRE, D.E.; VENEMA, K.; GOMBAU, L.; et al. 2015. Utility of models of the gastrointestinal tract for assessment of the digestion and absorption of engineered nanomaterials released from food matrices. *Nanotoxicology,* **9,** 523-542.

LEI, R.; WU, C.; YANG, B.; et al. 2008. Integrated metabolomic analysis of the nano-sized copper particle-induced hepatotoxicity and nephrotoxicity in rats: a rapid *in vivo* screening method for nanotoxicity. *Toxicol Appl Pharmacol,* **232,** 292-301.

LENAERTS, K.; BOUWMAN, F.G.; LAMERS, W.H.; et al. 2007. Comparative proteomic analysis of cell lines and scrapings of the human intestinal epithelium. *BMC Genomics,* **8,** DOI: 10.1186/1471-2164-8-91.

LENNERNAS, H.; PALM, K.; FAGERHOLM, U.; et al. 1996. Comparison between active and passive drug transport in human intestinal epithelial (caco-2) cells *in vitro* and human jejunum *in vivo*. *Int J Pharm,* **127,** 103-107.

LEONARD, F.; COLLNOT, E.-M. & LEHR, C.-M. 2010. A three-dimensional coculture of enterocytes, monocytes and dendritic cells to model inflamed intestinal mucosa *in vitro*. *Mol pharm,* **7,** 2103-2119.

LEVINE, J.S. & BURAKOFF, R. 2011. Extraintestinal manifestations of inflammatory bowel disease. *Gastroenterol Hepatol,* **7,** 235-241.

LI, C.K.F.; SETH, R.; GRAY, T.; et al. 1998. Production of proinflammatory cytokines and inflammatory mediators in human intestinal epithelial cells after invasion by *Trichinella spiralis*. *Infect immun,* **66,** 2200-2206.

LI, Y.; CHEN, D.H.; YAN, J.; et al. 2012. Genotoxicity of silver nanoparticles evaluated using the Ames test and *in vitro* micronucleus assay. *Mutat Res,* **745,** 4-10.

LILIENBLUM, W.; DEKANT, W.; FOTH, H.; et al. 2008. Alternative methods to safety studies in experimental animals: role in the risk assessment of chemicals under the new European Chemicals Legislation (REACH). *Arch toxicol,* **82,** 211-236.

LIM, J.P. & GLEESON, P.A. 2011. Macropinocytosis: an endocytic pathway for internalising large gulps. *Immunol Cell Biol,* **89,** 836-843.

LIN, I.C.; LIANG, M.; LIU, T.Y.; et al. 2011. Interaction of densely polymer-coated gold nanoparticles with epithelial Caco-2 monolayers. *Biomacromolecules,* **12,** 1339-1348.

LIN, I.C.; LIANG, M.; LIU, T.Y.; et al. 2012. Cellular transport pathways of polymer coated gold nanoparticles. *Nanomedicine,* **8,** 8-11.

LIN, F.-C. & YOUNG, H.A. 2013. The talented interferon-gamma. *Adv Biosci Biotech,* **4,** 6-13.

LIU, M.; ZHANG, J.; SHAN, W.; et al. 2015. Developments of mucus penetrating nanoparticles. *AJPS,* **10,** 275-282.

LIU, Q.; CHAN, S.T.F. & MAHENDRAN, R. 2003. Nitric oxide induces cyclooxygenase expression and inhibits cell growth in colon cancer cell lines. *Carcinogenesis,* **24,** 637-642.

LLORENS, A.; LLORET, E.; PICOUET, P.A.; et al. 2012. Metallic-based micro and nanocomposites in food contact materials and active food packaging. *Trends Food Sci Tech,* **24,** 19-29.

LOESCHNER, K.; HADRUP, N.; QVORTRUP, K.; et al. 2011. Distribution of silver in rats following 28 days of repeated oral exposure to silver nanoparticles or silver acetate. *Part Fibre Toxicol,* **8,** DOI: 10.1186/1743-8977-8-18.

LOMER, M.C.E.; THOMPSON, R.P.H.; COMMISSO, J.; et al. 2000. Determination of titanium dioxide in foods using inductively coupled plasma optical emission spectrometry. *The Analyst,* **125,** 2339-2343.

LOMER, M.C.E.; THOMPSON, R.P.H. & POWELL, J.J. 2002. Fine and ultrafine particles of the diet: influence on the mucosal immune response and association with Crohn's disease. *Proc Nutr Soc,* **61,** 123-130.

LÖNDAHL, J.; SWIETLICKI, E.; RISSLER, J.; et al. 2012. Experimental determination of the respiratory tract deposition of diesel combustion particles in patients with chronic obstructive pulmonary disease. *Part Fibre Toxicol,* **9,** DOI: 10.1186/1743-8977-9-30.

LORENZ, R.G. & NEWBERRY, R.D. 2004. Isolated lymphoid follicles can function as sites for induction of mucosal immune responses. *Ann N Y Acad Sci,* **1029,** 44-57.

LU, Y.; ZHANG, Y.; DENG, Y.; et al. 2016. Uptake and accumulation of polystyrene microplastics in zebrafish (*Danio rerio*) and toxic effects in liver. *Environ Sci Technol,* **50,** 4054-4060.

LUBY, A.O.; BREITNER, E.K. & COMFORT, K.K. 2015. Preliminary protein corona formation stabilizes gold nanoparticles and improves deposition efficiency. *Appl Nanosci,***6,** 827-836.

LÜGERING, N.; KUCHARZIK, T.; GOCKEL, H.; et al. 1998. Human intestinal epithelial cells down-regulate IL-8 expression in human intestinal microvascular endothelial cells; role of transforming growth factor-beta 1 (TGF-β1). *Clin Exp Immunol,* **114,** 377-384.

LUNOV, O.; SYROVETS, T.; LOOS, C.; et al. 2011. Differential uptake of functionalized polystyrene nanoparticles by human macrophages and a monocytic cell line. *ACS Nano,* **5,** 1657-1669.

LUO, Y.; TENG, Y. & WANG, Q. 2012. Development of zein nanoparticles coated with carboxymethyl chitosan for encapsulation and controlled release of vitamin D3. *J Agric Food Chem,* **60,** 836-843.

MABBOTT, N.A.; DONALDSON, D.S.; OHNO, H.; et al. 2013. Microfold (M) cells: important immunosurveillance posts in the intestinal epithelium. *Mucosal Immunol,* **6,** 666-677.

MACMICKING, J.D.; NATHAN, C.; HOM, G.; et al. 1995. Altered responses to bacterial infection and endotoxic shock in mice lacking inducible nitric oxide synthase. *Cell,* **81,** 641-650.

MACPHERSON, A.J. & SMITH, K. 2006. Mesenteric lymph nodes at the center of immune anatomy. *J Exp Med,* **203,** 497-500.

MADSEN, K.L.; LEWIS, S.A.; TAVERNINI, M.M.; et al. 1997. Interleukin 10 prevents cytokine-induced disruption of T84 monolayer barrier integrity and limits chloride secretion. *Gastroenterology,* **113,** 151-159.

MAHL, D.; GREULICH, C.; MEYER-ZAIKA, W.; et al. 2010. Gold nanoparticles: dispersibility in biological media and cell-biological effect. *J Mat Chem,* **20,** 6176-6181.

MAISEL, K.; ENSIGN, L.; REDDY, M.; et al. 2015. Effect of surface chemistry on nanoparticle interaction with gastrointestinal mucus and distribution in the gastrointestinal tract following oral and rectal administration in the mouse. *J Control Release,* **197,** 48-57.

MALINSKI, T.; KUBASZEWSKI, E. & KIECHLE, F. 1996. Electrochemical and spectroscopic methods of nitric oxide detection. *In:* MAINES, M.D. (ed.) *Nitric Oxide Synthase, Characterization and Functional Analysis.* San Diego: Academic Press, Inc.**,** 14-33.

MANEERUNG, T.; TOKURA, S. & RUJIRAVANIT, R. 2008. Impregnation of silver nanoparticles into bacterial cellulose for antimicrobial wound dressing. *Carbohydr Polym,* **72,** 43-51.

MANN, E.R. & LI, X. 2014. Intestinal antigen-presenting cells in mucosal immune homeostasis: crosstalk between dendritic cells, macrophages and B-cells. *World J Gastroenterol,* **20,** 9653-9664.

MARCHIANDO, A.M.; SHEN, L.; GRAHAM, W.V.; et al. 2010. Caveolin-1-dependent occludin endocytosis is required for TNF-induced tight junction regulation *in vivo*. *J Cell Biol,* **189,** 111-126.

MARTIN, T.R.; MONGOVING, S.M.; TOBIAS, P.S.; et al. 1994. The CD14 differentiation antigen mediates the development of exdotoxin responsiveness during differentiation of monoculear phagocytes. *J Leukoc Biol,* **56,** 1-9.

MARTIROSYAN, A.; POLET, M.; BAZES, A.; et al. 2012. Food nanoparticles and intestinal inflammation: A real risk? *In*: Szabo, I. (Ed.). Inflammatory Bowel Disease. InTech, DOI: 10.5772/52887.

MARTIROSYAN, A.; BAZES, A. & SCHNEIDER, Y.-J. 2014. *In vitro* toxicity assessment of silver nanoparticles in the presence of phenolic compounds – preventive agents against the harmful effect? *Nanotoxicology,* **8,** 573-582.

MASCETTI, G.; CARRARA, S. & VERGANI, L. 2001. Relationship between chromatin compactness and dye uptake for *in situ* chromatin stained with DAPI. *Cytometry,* **44,** 113-119.

MASHUKOVA, A.; WALD, F.A. & SALAS, P.J. 2011. Tumor necrosis factor alpha and inflammation disrupt the polarity complex in intestinal epithelial cells by a posttranslational mechanism. *Mol Cell Biol,* **31,** 756-765.

MAST, J. & DEMEESTERE, L. 2009. Electron tomography of negatively stained complex viruses: application in their diagnosis. *Diagnostic pathology,* **4,** DOI: 10.1186/1746-1596-4-5.

MATOSIN, N.; FRANK, E.; ENGEL, M.; et al. 2014. Negativity towards negative results: a discussion of the disconnect between scientific worth and scientific culture. *Dis Mod Mech,* **7,** 171-173.

MAZZUCCHELLI, L.; HAUSE, C.; ZGRAGGEN, K.; et al. 1994. Expression of interleukin-8 gene in inflammatory bowel disease is related to the histological grade of active inflammation. *Am J Path,* **144,** 997-1007.

MCCRACKEN, C.; ZANE, A.; KNIGHT, D.A.; et al. 2013. Minimal intestinal epithelial cell toxicity in response to short- and long-term food-relevant inorganic nanoparticle exposure. *Chem Res Toxicol,* **26,** 1514-1525.

MCCRACKEN, C.; ZANE, A.; KNIGHT, D.A.; et al. 2015. Oxidative stress-mediated inhibition of intestinal epithelial cell proliferation by silver nanoparticles. *Toxicol In Vitro,* **29,** 1793-1808.

MCNEIL, E.; CAPALDO, C.T. & MACARA, I.G. 2006. Zonula occludens-1 function in the assembly of tight junctions in Madin-Darby canine kidney epithelial cells. *Mol Biol Cell,* **17,** 1922-1932.

MEDZHITOV, R. 2007. Recognition of microorganisms and activation of the immune response. *Nature*, **449,** 819-826.

MELMED, G.; THOMAS, L.S.; LEE, N.; et al. 2003. Human intestinal epithelial cells are broadly unresponsive to Toll-like receptor 2-dependent bacterial ligands: Implications for host-microbial interactions in the gut. *J Immunol,* **170,** 1406-1415.

MENG, F. & LOWELL, C.A. 1997. Lipopolysaccharide (LPS)-induced macrophage activation and signal transduction in the absence of Src-family kinases Hck, Fgr, and Lyn. *J Exp Med,* **185,** 1661-1670.

MENG, H.; CHEN, Z.; XING, G.; et al. 2007. Ultrahigh reactivity provokes nanotoxicity: explanation of oral toxicity of nano-copper particles. *Toxicol Lett,* **175,** 102-110.

MENG, W. & TAKEICHI, M. 2009. Adherens junction: molecular architecture and regulation. *Cold Spring Harbor perspectives in biology,* **1,** DOI: 10.1101/cshperspect.a002899.

MIETHLING-GRAFF, R.; RUMPKER, R.; RICHTER, M.; et al. 2014. Exposure to silver nanoparticles induces size- and dose-dependent oxidative stress and cytotoxicity in human colon carcinoma cells. *Toxicol In Vitro,* **28,** 1280-1289.

MILANINO, R.; CASSINI, A.; CONFORTI, A.; et al. 1986. Copper and zinc status during acute inflammation: studies on blood, liver and kidneys metal levels in normal and inflamed rats. *Agents Actions,* **19,** 215-223.

MIRON, N. & CRISTEA, V. 2012. Enetrocytes: active cells in tolerance to food and microbial antigens in the gut. *Clin Exp Immunol*. **167,** 405-412.

MISRA, S.K.; NUSEIBEH, S.; DYBOWSKA, A.; et al. 2014. Comparative study using spheres, rods and spindle-shaped nanoplatelets on dispersion stability, dissolution and toxicity of CuO nanomaterials. *Nanotoxicology,* **8,** 422-432.

MIURA, M.; FRIEDLANDER, R.M. & YUAN, J. 1995. Tumor necrosis factor-induced apoptosis is mediated by a CrmA-sensitive cell death pathway. *PNAS,* **92,** 8318-8322.

MOGENSEN, K.B. & KNEIPP, K. 2014. Size-dependent shifts of plasmon resonance in silver nanoparticle films using controlled dissolution: monitoring the onset of surface screening effects. *J Physic Chem C,* **118,** 28075-28083.

MOLLICK, M.M.R.; RANA, D.; DASH, S.K.; et al. 2015. Studies on green synthesized silver nanoparticles using *Abelmoschus esculentus* (L.) pulp extract having anticancer (*in vitro*) and antimicrobial applications. *Arab J Chem***,** DOI: 10.1016/j.arabjc.2015.04.033.

MONCADA, M.; ASTETE, C.; SABLIOV, C.; et al. 2015. Nano spray-dried sodium chloride and its effects on the microbiological and sensory characteristics of surface-salted cheese crackers. *J Dairy Sci,* **98,** 5946-5954.

MOSCHINI, E.; GUALTIERI, M.; COLOMBO, M.; et al. 2013. The modality of cell–particle interactions drives the toxicity of nanosized CuO and TiO_2 in human alveolar epithelial cells. *Toxicol Lett,* **222,** 102-116.

MOULARI, B.; PERTUIT, D.; PELLEQUER, Y.; et al. 2008. The targeting of surface modified silica nanoparticles to inflamed tissue in experimental colitis. *Biomaterials,* **29,** 4554-4560.

MOWAT, A.M. & BAIN, C.C. 2011. Mucosal macrophages in intestinal homeostasis and inflammation. *J Innate Immun,* **3,** 550-564.

MOYES, S.M.; MORRIS, J.F. & CARR, K.E. 2010a. Macrophages increase microparticle uptake by enterocyte-like Caco-2 cell monolayers. *J Anat,* **217,** 740-754.

MUNGER, M.A.; RADWANSKI, P.; HADLOCK, G.C.; et al. 2014. *In vivo* human time-exposure study of orally dosed commercial silver nanoparticles. *Nanomedicine,* **10,** DOI: 10.1016/j.nano.2013.06.010.

MUNIZ, L.R.; KNOSP, C. & YERETSSIAN, G. 2012. Intestinal antimicrobial peptides during homeostasis, infection, and disease. *Front Immunol,* **3,** DOI: 10.3389/fimmu.2012.00310.

MUSTHER, H.; OLIVARES-MORALES, A.; HATLEY, O.J.D.; et al. 2014. Animal versus human oral drug bioavailability: Do they correlate? *Eur J Pharm Sci,* **57,** 280-291.

MÜZES, G.; MOLNAR, B.; TULASSAY, Z.; et al. 2012. Changes of the cytokine profile in inflammatory bowel diseases. *World J Gastroenterol,* **18,** 5848-5861.

NARAI, A.; ARAI, S. & SHIMIZU, M. 1997. Rapid decrease in transepithelial electrical resistance of human intestinal Caco-2 cell monolayers by cytotoxic membrane perturbents. *Toxicol In Vitro,* **11,** 347-354.

NATHENS, A.B.; ROTSTEIN, O.D.; DACKIW, A.P.; et al. 1995. Intestinal epithelial cells down-regulate macrophage tumor necrosis factor-alpha secretion: a mechanism for immune homeostasis in the gut-associated lymphoid tissue. *Surgery,* **118,** 343-350.

NAVA, P.; KOCH, S.; LAUKOETTER, M.G.; et al. 2010. Interferon-γ regulates intestinal epithelial homeostasis through converging β-catenin signaling pathways. *Immunity,* **32,** 392-402.

NEGRONI, A.; CUCCHIARA, S. & STRONATI, L. 2015. Apoptosis, necrosis, and necroptosis in the gut and intestinal homeostasis. *Mediators Inflamm,* **2015,** DOI: 10.1155/2015/250762.

NEURATH, M.F. 2014. Cytokines in inflammatory bowel disease. *Nat Rev Immunol,* **14,** 329-342.

NEUTRA, M.R.; PHILLIPS, T.L.; MAYER, E.L.; et al. 1987. Transport of membrane-bound macromolecules by M cells in follicle-associated epithelium of rabbit Peyer's patch. *Cell Tissue Res,* **247,** 537-546.

NGKELO, A.; MEJA, K.; YEADON, M.; et al. 2012. LPS induced inflammatory response in human peripheral blood mononuclear cells is mediated through NOX4 and Gia dependent PI-3kinase signalling. *J Inflam,* **9,** DOI: 10.1186/1476-9255-9-1.

NGUYEN, K.C.; SELIGY, V.L.; MASSARSKY, A.; et al. 2013. Comparison of toxicity of uncoated and coated silver nanoparticles. *JPCS,* **429,** DOI: 10.1088/1742-6596/429/1/012025.

NGUYEN, K.C.; RICHARDS, L.; MASSARSKY, A.; et al. 2016. Toxicological evaluation of representative silver nanoparticles in macrophages and epithelial cells. *Toxicol In Vitro,* **33,** 163-173.

NISKA, K.; SANTOS-MARTINEZ, M.J.; RADOMSKI, M.W.; et al. 2015. CuO nanoparticles induce apoptosis by impairing the antioxidant defense and detoxification systems in the mouse hippocampal HT22 cell line: protective effect of crocetin. *Toxicol In Vitro,* **29,** 663-671.

NOGUEIRA, C.M.; DE AZEVEDO, W.M.; DAGLI, M.L.; et al. 2012. Titanium dioxide induced inflammation in the small intestine. *World J Gastroenterol,* **18,** 4729-4735.

NOLLEVAUX, G.; DEVILLE, C.; EL MOUALIJ, B.; et al. 2006. Development of a serum-free co-culture of human intestinal epithelium cell-lines (Caco-2/HT29-5M21). *BMC Cell Biol,* **7,** DOI: 10.1186/1471-2121-7-20.

NOMURA, S.; TANDON, N.N.; NAKAMURA, T.; et al. 2001. High-shear-stress-induced activation of platelets and microparticles enhances expression of cell adhesion molecules in THP-1 and endothelial cells. *Atherosclerosis,* **158,** 277-287.

NUNES, T.; BERNARDAZZI, C. & DE SOUZA, H.S. 2014. Cell death and inflammatory bowel diseases: apoptosis, necrosis, and autophagy in the intestinal epithelium. *Biomed Res Int,* **2014,** DOI: 10.1155/2014/218493.

OBEREMM, A.; HANSEN, U.; BÖHMERT, L.; et al. 2016. Proteomic responses of human intestinal Caco-2 cells exposed to silver nanoparticles and ionic silver. *J Appl Toxicol,* **36,** 404-413.

ODZAK, N.; KISTLER, D.; BEHRA, R.; et al. 2014. Dissolution of metal and metal oxide nanoparticles in aqueous media. *Environ Pollut,* **191,** 132-138.

OH, N. & PARK, J.H. 2014. Endocytosis and exocytosis of nanoparticles in mammalian cells. *Int J Nanomedicine,* **9** Suppl 1**,** 51-63.

OH, S.-J.; KIM, H.; LIU, Y.; et al. 2014. Incompatibility of silver nanoparticles with lactate dehydrogenase leakage assay for cellular viability test is attributed to protein binding and reactive oxygen species generation. *Toxicol Lett,* **225,** 422-432.

OJUAWO, A. & KEITH, L. 2002. The serum concentrations of zinc, copper and selenium in children with inflammatory bowel disease. *Cent Afr J Med,* **48,** 116-119.

OLDENBURG, S.J. accessed 2016. *Silver Nanoparticles: Properties and Applications* [Online]. Sigmaaldrich.com. Available: http://www.sigmaaldrich.com/materials-science/nanomaterials/silver-nanoparticles.html [Accessed 29.03. 2016].

OLDENBURG, S.J. & SAUNDERS, A.E. accessed 2016. Silver Nanomaterials for Biological Applications. http://www.sigmaaldrich.com/technical-documents/articles/materials-science/silver-nanomaterials.html. Available: http://www.sigmaaldrich.com/technical-documents/articles/materials-science/silver-nanomaterials.html [Accessed 13.04.2016].

OLSSON, T.; BROBERG, M.; POPE, K.J.; et al. 2006. Cell swelling, seizures and spreading depression: an impedance study. *Neuroscience,* **140,** 505-515.

PAGET, V.; SERGENT, J.A.; GRALL, R.; et al. 2014. Carboxylated nanodiamonds are neither cytotoxic nor genotoxic on liver, kidney, intestine and lung human cell lines. *Nanotoxicology,* **8** Suppl 1**,** 46-56.

PALM, K.; LUTHMAN, K.; ROS, J.; et al. 1999. Effect of molecular charge on intestinal epithelial drug transport: pH-dependent transport of cationic drugs. *J Pharmacol Exp Ther,* **291,** 435-443.

PARK, E.K.; JUNG, H.S.; YANG, H.I.; et al. 2007. Optimized THP-1 differentiation is required for the detection of responses to weak stimuli. *Inflamm Res,* **56,** 45-50.

PARK, E.J.; BAE, E.; YI, J.; et al. 2010a. Repeated-dose toxicity and inflammatory responses in mice by oral administration of silver nanoparticles. *Environ Toxicol Pharmacol,* **30,** 162-168.

PARK, E.J.; YI, J.; KIM, Y.; et al. 2010b. Silver nanoparticles induce cytotoxicity by a Trojan-horse type mechanism. *Toxicol In Vitro,* **24,** 872-878.

PARK, M.V.; NEIGH, A.M.; VERMEULEN, J.P.; et al. 2011. The effect of particle size on the cytotoxicity, inflammation, developmental toxicity and genotoxicity of silver nanoparticles. *Biomaterials,* **32,** 9810-9817.

PARLESAK, A.; HALLER, D.; BRINZ, S.; et al. 2004. Modulation of cytokine release by differentiated Caco-2 cells in a compartmentalized coculture model with mononuclear leucocytes and nonpathogenic bacteria. *Scand J Immunol,* **60,** 477-485.

PARNSAMUT, C. & BRIMSON, S. 2015. Effects of silver nanoparticles and gold nanoparticles on IL-2, IL-6, and TNF-α production via MAPK pathway in leukemic cell lines. *Genet Mol Res,* **14,** 3650-3668.

PASPARAKIS, M. & VANDENABEELE, P. 2015. Necroptosis and its role in inflammation. *Nature,* **517,** 311-320.

PELLETIER, H.; MILLOT, J.-M.; CHAUFFERT, B.; et al. 1990. Mechanisms of resistance of confluent human and rat colon cancer cells to anthracyclines: Alteration of drug passive diffusion. *Cancer Research,* **50,** 6626-6631.

PÉREZ-GARIJO, A.; FUCHS, Y. & STELLER, H. 2013. Apoptotic cells can induce non-autonomous apoptosis through the TNF pathway. *eLIFE,* **2,** DOI: 10.7554/eLife.01004.

PEREZ ESPITIA, P.J.; DE FÁTIMA FERREIRA SOARES, N.; DOS REIS COIMBRA, J.S.; et al. 2012. Zinc oxide nanoparticles: Synthesis, antimicrobial activity and food packaging applications. *Food Bioprocess Tech,* **5,** 1447-1464.

PETERSON, L.W. & ARTIS, D. 2014. Intestinal epithelial cells: regulators of barrier function and immune homeostasis. *Nat Rev Immunol,* **14,** 141-153.

PETTIBONE, J.M.; ADAMCAKOVA-DODD, A.; THORNE, P.S.; et al. 2009. Inflammatory response of mice following inhalation exposure to iron and copper nanoparticles. *Nanotoxicology,* **2,** 189-204.

PHAM, T.N.Q.; BROWN, B.L.; DOBSON, P.R.M.; et al. 2003. Protein kinase C-eta (PKC-η) is required for the development of inducible nitric oxide synthase (iNOS) positive phenotype in human monocytic cells. *Nitric Oxide,* **9,** 123-134.

PHILPOTT, D.J.; ACKERLEY, C.A.; KILIAAN, A.J.; et al. 1997. Translocation of verotoxin-1 across T84 monolayers: mechanism of bacterial toxin penetration of epithelium. *Am J Physiol: Gastroint Liver Physiol,* **273,** G1349-G1358.

PHONG, N.T.P.; THANH, N.V.K. & PHUONG, P.H. 2009. Fabrication of antibacterial water filter by coating silver nanoparticles on flexible polyurethane foams. *J Physics: Conference Series,* **187,** DOI: 10.1088/1742-6596/187/1/012079.

PICHE, T.; BARBARA, G.; AUBERT, P.; et al. 2009. Impaired intestinal barrier integrity in the colon of patients with irritable bowel syndrome: involvement of soluble mediators. *Gut,* **58,** 196-201.

PINTO, M.; ROBINE-LEON, S.; APPAY, M.-D.; et al. 1983. Enterocyte-like differentiation and polarization of the human colon carcinoma cell line Caco-2 in culture. *Biol Cell,* **47,** 323-330.

PIRET, J.P.; JACQUES, D.; AUDINOT, J.N.; et al. 2012a. Copper(II) oxide nanoparticles penetrate into HepG2 cells, exert cytotoxicity via oxidative stress and induce pro-inflammatory response. *Nanoscale,* **4,** 7168-7184.

PIRET, J.P.; VANKONINGSLOO, S.; MEJIA, J.; et al. 2012b. Differential toxicity of copper (II) oxide nanoparticles of similar hydrodynamic diameter on human differentiated intestinal Caco-2 cell monolayers is correlated in part to copper release and shape. *Nanotoxicology,* **6,** 789-803.

PONDER, A. & LONG, M.D. 2013. A clinical review of recent findings in the epidemiology of inflammatory bowel disease. *Clin Epidemiol,* **5,** 237-247.

POWELL, J.J.; FARIA, N.; THOMAS-MCKAY, E.; et al. 2010. Origin and fate of dietary nanoparticles and microparticles in the gastrointestinal tract. *J Autoimmun,* **34,** J226-J233.

PRAST, H. & PHILIPPU, A. 2001. Nitric oxide as modulator of neuronal function. *Prog Neurobiol,* 64**,** 51-68.

PRATSINIS, A.; HERVELLA, P.; LEROUX, J.-C.; et al. 2013. Toxicity of Silver Nanoparticles in Macrophages. *Small,* **9,** 2576-2584.

PRATTIS, S. & JURJUS, A. 2015. Spontaneous and transgenic rodent models of inflammatory bowel disease. *Lab Anim Res,* **31,** 47-68.

PREDKI, P.F. & SARKAR, B. 1994. Metal replacement in "zinc finger" and its effect on DNA binding. *Environ Health Persp,* **102,** 195-198.

PRIVALOVA, L.I.; KATSNELSON, B.A.; LOGINOVA, N.V.; et al. 2014. Subchronic toxicity of copper oxide nanoparticles and its attenuation with the help of a combination of bioprotectors. *Int J Mol Sci,* **15,** 12379-12406.

PUIG-KROGER, A.; SERRANO-GOMEZ, D.; CAPARROS, E.; et al. 2004. Regulated expression of the pathogen receptor dendritic cell-specific

intercellular adhesion molecule 3 (ICAM-3)-grabbing nonintegrin in THP-1 human leukemic cells, monocytes, and macrophages. *J Biol Chem,* **279,** 25680-25688.

QUADRHIRI, Y.; SIBILLE, Y. & TULKENS, P.M. 1999. Modulation of intracellular growth of *Listeria monocytogenes* in human enetrocytes Caco-2 cells by interferon-γ and interleukin-6: Role of nitric oxide and cooperation with antibiotics. *J Infectious Dis,* **180,** 1195-1204.

RAHMAN, M.F.; WANG, J.; PATTERSON, T.A.; et al. 2009. Expression of genes related to oxidative stress in the mouse brain after exposure to silver-25 nanoparticles. *Toxicol Lett,* **187,** 15-21.

RAHNAMA, A. & GHARAGOZLOU, M. 2012. Preparation and properties of semiconductor CuO nanoparticles via a simple precipitation method at different reaction temperatures. *Opt Quant Electron,* **44,** 313-322.

RAKOFF-NAHOUM, S.; PAGLINO, J.; ESLAMI-VARZANEH, F.; et al. 2004. Recognition of commensal microflora by Toll-like receptors is required for intestinal homeostasis. *Cell,* **118,** 229-241.

RANALDI, G.; MARIGLIANO, I.; VESPIGNANI, I.; et al. 2002. The effect of chitosan and other polycations on tight junction permeability in the human intestinal Caco-2 cell line. *J Nutr Biochem,* **13,** 157-167.

RANALDI, G.; CONSALVO, R.; SAMBUY, Y.; et al. 2003. Permeability characteristics of parental and clonal human intestinal Caco-2 cell lines differentiated in serum-supplemented and serum-free media. *Toxicol In Vitro,* **17,** 761-767.

RANI, A.S.; KUMAR, A.K.; KUMAR, C.P.; et al. 2013. Pulmonary toxicity of copper oxide (CuO) nanoparticles in rats. *J Med Sci,* **13,** 571-577.

RAYAMAJHI, M.; ZHANG, Y. & MIAO, E.A. 2013. Detection of pyroptosis by measuring released lactate dehydrogenase activity. *Methods Mol Biol,* **1040,** 85-90.

REN, G.; HU, D.; CHENG, E.W.; et al. 2009. Characterisation of copper oxide nanoparticles for antimicrobial applications. *Int J Antimicrob Agents,* **33,** 587-590.

RESCIGNO, M.; URBANO, M.; VALZASINA, B.; et al. 2001. Dendritic cells express tight junction proteins and penetrate gut epithelial monolayers to sample bacteria. *Nat Immunol,* **2,** 361-367.

RIMOLDI, M.M.C.; SALUCCI, V.; AVOGADRI, F.; et al. 2005. Intestinal immune homeostasis is regulated by the crosstalk between epithelial cells and dendritic cells. *Nat Immunol,* **6,** 507-514.

RIOS, D.; WOOD, M.B.; LI, J.; et al. 2016. Antigen sampling by intestinal M cells is the principal pathway initiating mucosal IgA production to commensal enteric bacteria. *Mucosal Immunol,* **9,** DOI: 10.1038/mi.2015.121.

ROBERTS, J.R.; MCKINNEY, W.; KAN, H.; et al. 2013. Pulmonary and cardiovascular responses of rats to inhalation of silver nanoparticles. *J Toxicol Environ Health A,* **76,** 651-668.

ROE, D.; KARANDIKAR, B.; BONN-SAVAGE, N.; et al. 2008. Antimicrobial surface functionalization of plastic catheters by silver nanoparticles. *J Antimicrob Chemother,* **61,** 869-876.

ROTOLI, B.M.; BUSSOLATI, O.; COSTA, A.L.; et al. 2012. Comparative effects of metal oxide nanoparticles on human airway epithelial cells and macrophages. *J Nanopart Res,* **14,** DOI: 10.1007/s11051-012-1069-0.

ROXAS, J.L.; KOUTSOURIS, A.; BELLMEYER, A.; et al. 2010. Enterohemorrhagic *E. coli* alters murine intestinal epithelial tight junction protein expression and barrier function in a *Shiga* toxin independent manner. *Lab Invest,* **90,** 1152-1168.

RUBAS, W.; JEZYK, N. & GRASS, G.M. 1993. Comparison of the permeability characteristics of a human colonic epithelial (Caco-2) cell line to colon of rabbit, monkey, and dog intestine and human drug absorption. *Pharmaceutical Research,* **10,** 113-118.

SABOURIN, V. & AYANDE, A. 2015. Commercial opportunities and market demand for nanotechnologies in agribusiness sector. *JOTMI,* **10,** 40-51.

SAFI, M.; COURTOIS, J.; SEIGNEURET, M.; et al. 2011. The effects of aggregation and protein corona on the cellular internalization of iron oxide nanoparticles. *Biomaterials,* **32,** 9353-9363.

SÄFSTEN, B. 1993. Duodenal bicarbonate secretion and mucosal protection. Neurohumoral influence and transport mechanisms. *Acta Physiolog Scand. Supplementum,* **613,** 1-43.

SAHU, S.C.; ROY, S.; ZHENG, J.; et al. 2014. Comparative genotoxicity of nanosilver in human liver HepG2 and colon Caco2 cells evaluated by fluorescent microscopy of cytochalasin B-blocked micronucleus formation. *J Appl Toxicol,* **34,** 1200-1208.

SAITOU, M.; FURUSE, M.; SASAKI, H.; et al. 2000. Complex phenotype of mice lacking occludin, a component of tight junction strands. *Mol Biol Cell,* **11,** 4131-4142.

SAMBALE, F.; WAGNER, S.; STAHL, F.; et al. 2015. Investigations of the toxic effect of silver nanoparticles on mammalian cell lines. *J Nanomater,* **2015,** DOI: 10.1155/2015/136765.

SAMBRUY, Y.; FERRUZZA, S.; RANALDI, G.; et al. 2001. Intestinal cell culture models *Cell Biol Toxicol,* **17,** 301-317.

SANCEAU, J.; WIJDENES, J.; REVEL, M.; et al. 1991. IL-6 and IL-6 receptor modulation by IFN-gamma and tumor necrosis factor-alpha in human monocytic cell line (THP-1). Priming effect of IFN-gamma. *J Immunol,* **147,** 2630-2637.

SANDRI, G.; BONFERONI, M.C.; ROSSI, S.; et al. 2007. Nanoparticles based on N-trimethylchitosan: evaluation of absorption properties using *in vitro* (Caco-2 cells) and *ex vivo* (excised rat jejunum) models. *Eur J Pharm Biopharm,* **65,** 68-77.

SANPUI, P.; CHATTOPADHYAY, A. & GHOSH, S.S. 2011. Induction of apoptosis in cancer cells at low silver nanoparticle concentrations using chitosan nanocarrier. *ACS Appl Mater Interfaces,* **3,** 218-228.

SANTOS, I.S.; PONTE, B.M.; BOONME, P.; et al. 2013. Nanoencapsulation of polyphenols for protective effect against colon–rectal cancer. *Biotechnol Adv,* **31,** 514-523.

SARHAN, O.M. & HUSSEIN, R.M. 2014. Effects of intraperitoneally injected silver nanoparticles on histological structures and blood parameters in the albino rat. *Int J Nanomedicine,* **9,** 1505-1517.

SARPARANTA, M.P.; BIMBO, L.M.; MAKILA, E.M.; et al. 2012. The mucoadhesive and gastroretentive properties of hydrophobin-coated porous silicon nanoparticle oral drug delivery systems. *Biomaterials,* **33,** 3353-3362.

SASTRY VENKATESWARA, S.; RAM NYSHADHAM, J. & FIX, J.A. 2000. Recent technological advances in oral drug delivery – a review. *Pharm Sci Tech Today,* **3,** 138-145.

SATAKE, M.; WATANABE, H.; MIYAMOTO, Y.; et al. 2001. Induction of nitric oxide synthase and subsequent production of nitric oxide not involved in interferon-γ-induced hyperpermeability of Caco-2 intestinal epithelial monolayers. *Biosci Biotechnol Biochem,* **65,** 428-430.

SATOH, T.; KAMBE, N. & MATSUE, H. 2013. NLRP3 activation induces ASC-dependent programmed necrotic cell death, which leads to neutrophilic inflammation. *Cell Death Dis,* **4,** DOI: 10.1038/cddis.2013.169.

SATSU, H.; ISHIMOTO, Y.; NAKANO, T.; et al. 2006. Induction by activated macrophage-like THP-1 cells of apoptotic and necrotic cell death in intestinal epithelial Caco-2 monolayers via tumor necrosis factor-alpha. *Exp Cell Res,* 312**,** 3909-3919.

SCHELLER, J.; CHALARIS, A.; SCHMIDT-ARRAS, D.; et al. 2011. The pro- and anti-inflammatory properties of the cytokine interleukin-6. *Biochim Biophys Acta,* **1813,** 878-888.

SCHILLING, J.D.; MARTIN, S.M.; HUNSTAD, D.A.; et al. 2003. CD14- and Toll-like receptor-dependent activation of bladder epithelial cells by lipopolysaccharide and type 1 piliated *Escherichia coli*. *Infect Immun,* **71,** 1470-1480.

SCHIMPEL, C.; TEUBL, B.; ABSENGER, M.; et al. 2014. Development of an advanced intestinal *in vitro* triple culture permeability model to study transport of nanoparticles. *Mol Pharm,* **11,** 808-818.

SCHLEH, C.; SEMMLER-BEHNKE, M.; LIPKA, J.; et al. 2012. Size and surface charge of gold nanoparticles determine absorption across intestinal barriers and accumulation in secondary target organs after oral administration. *Nanotoxicology,* **6,** 36-46.

SCHMIDT, C.; LAUTENSCHLAEGER, C.; COLLNOT, E.M.; et al. 2013. Nano- and microscaled particles for drug targeting to inflamed intestinal mucosa: a first *in vivo* study in human patients. *J Control Release,* **165,** 139-145.

SCHNEEMANN, M.; SCHOEDON, G.; LINSCHEID, P.; et al. 1997. Nitrite generation in interleukin-4-treated human macrophage cultures does not involve the nitric oxide synthase pathway. *J Infect Dis,* **175,** 130-135.

SCHUERER-MALY, C.C.; ECKMANN, L.; KAGNOFF, M.F.; et al. 1994. Colonic epithelial cell lines as a source of interleukin-8: stimulation by inflammatory cytokines and bacterial lipopolysaccharide. *Immunology,* **81,** 85-91.

SCHÜLLER, S.; FRANKEL, G. & PHILLIPS, A.D. 2004. Interaction of *Shiga* toxin from *Escherichia coli* with human intestinal epithelial cell lines and explants: Stx2 induces epithelial damage in organ culture. *Cell Microbiol,* **6,** 289-301.

SCHÜLLER, S.; LUCAS, M.; KAPER, J.B.; et al. 2009. The *ex vivo* response of human intestinal mucosa to enteropathogenic *Escherichia coli* infection. *Cell Microbiol,* **11,** 521-530.

SCHWENDE, H.F., EDITH; AMBS, PETRA; DIETER, PETER 1996. Differences in the state of differentiation of THP-1 cells induced by phorbol ester and 1,25-dihydroxyvitamin D3. *J Leukoc Biol,* **59,** 555-561.

SEGURA, M.; VADEBONCOEUR, N. & GOTTSCHALK, M. 2002. CD14-dependent and -independent cytokine and chemokine production by human THP-1

monocytes stimulated by *Streptococcus suis* capsular type 2. *Clin Exp Immunol,* **127,** 243-254.

SEIFFERT, J.; HUSSAIN, F.; WIEGMAN, C.; et al. 2015. Pulmonary toxicity of instilled silver nanoparticles: influence of size, coating and rat strain. *PLoS One,* **10,** DOI: 10.1371/journal.pone.0119726.

SHANNAHAN, J.H.; PODILA, R.; ALDOSSARI, A.A.; et al. 2015. Formation of a protein corona on silver nanoparticles mediates cellular toxicity via scavenger receptors. *Toxicol Sci,* **143,** 136-146.

SHARMA, V.; SINGH, P.; PANDEY, A.K.; et al. 2012. Induction of oxidative stress, DNA damage and apoptosis in mouse liver after sub-acute oral exposure to zinc oxide nanoparticles. Mutat Res Genet Toxicol Environ Mutagen*,* **745,** 84-91.

SHARMA, V.K.; SISKOVA, K.M.; ZBORIL, R.; et al. 2014. Organic-coated silver nanoparticles in biological and environmental conditions: fate, stability and toxicity. *Adv Colloid Interface Sci,* **204,** 15-34.

SHEN, L. 2012. Tight junctions on the move: molecular mechanisms for epithelial barrier regulation. *Ann N Y Acad Sci,* **1258,** 9-18.

SHI, C. & PAMER, E.G. 2011. Monocyte recruitment during infection and inflammation. *Nat Rev Immunol,* **11,** 762-774.

SHIN, S.H.; YE, M.K.; KIM, H.S.; et al. 2007. The effects of nano-silver on the proliferation and cytokine expression by peripheral blood mononuclear cells. *Int immunopharmacol,* **7,** 1813-1818.

SHINER, M. & BIRBECK, M.S.C. 1961. The microvilli of the small intestinal surface epithelium in coeliac disease and in idiopathic steatorrhoea. *Gut,* **2,** 277-284.

SHINOZAWA, Y.; MATSUMOTO, T.; UCHIDA, K.; et al. 2002. Role of interferon-gamma in inflammatory responses in murine respiratory infection with *Legionella pneumophila*. *J Med Microbiol,* **51,** 225-230.

SHUKLA, R.; VIPUL, B.; CHAUDHARY, M.; et al. 2005. Biocompatibility of gold nanoparticles and their endocytotic fate inside the cellular compartment: A microscopic overview. *Langmuir,* **21,** 10644-10654.

SIDDIQUI, M.A.; ALHADLAQ, H.A.; AHMAD, J.; et al. 2013. Copper oxide nanoparticles induced mitochondria mediated apoptosis in human hepatocarcinoma cells. *PLoS One,* **8,** DOI: 10.1371/journal.pone.0069534.

SILVA, M.T.; DO VALE, A. & DOS SANTOS, N.M. 2008. Secondary necrosis in multicellular animals: an outcome of apoptosis with pathogenic implications. *Apoptosis,* **13,** 463-482.

SILVA, M.T. 2010. Secondary necrosis: the natural outcome of the complete apoptotic program. *FEBS Lett,* **584,** 4491-4499.

SILVESTRE, C.; DURACCIO, D. & CIMMINO, S. 2011. Food packaging based on polymer nanomaterials. *Prog Polym Sci,* **36,** 1766-1782.

SIMARD, J.C.; VALLIERES, F.; DE LIZ, R.; et al. 2015. Silver nanoparticles induce degradation of the endoplasmic reticulum stress sensor activating transcription factor-6 leading to activation of the NLRP-3 inflammasome. *J Biol Chem,* **290,** 5926-5939.

SINGER, I.I.; KAWKA, D.W.; WEIDNER, J.R.; et al. 1996. Expression of inducible nitric oxide synthase and nitrotyrosine in colonic epithelium in inflammatory bowel disease. *Gastroenterology,* **111,** 871-885.

SINGH, P.; DAI, B.; YALLAMPALLI, U.; et al. 1996. Proliferation and differentiation of a human colon cancer cell line (CaCo2) is associated with significant changes in the expression and secretion of insulin-like growth factor

(IGF) IGF-II and IGF binding protein-4: role of IGF-II. *Endocrinology,* **137,** 1764-1774.

SINGH, R.P. & RAMARAO, P. 2012. Cellular uptake, intracellular trafficking and cytotoxicity of silver nanoparticles. *Toxicol Lett,* **213,** 249-259.

SKALSKA, J.; FRONTCZAK-BANIEWICZ, M. & STRUZYNSKA, L. 2015. Synaptic degeneration in rat brain after prolonged oral exposure to silver nanoparticles. *Neurotoxicology,* **46,** 145-154.

SMITH, P.D.; SMYTHIES, L.E.; SHEN, R.; et al. 2011. Intestinal macrophages and response to microbial encroachment. *Mucosal Immunol,* **4,** 31-42.

SMYTHIES, L.E.; SELLERS, M.; CLEMENTS, R.H.; et al. 2005. Human intestinal macrophages display profound inflammatory anergy despite avid phagocytic and bacteriocidal activity. *J Clin Invest,* **115,** 66-75.

SMYTHIES, L.E.; MAHESHWARI, A.; CLEMENTS, R.; et al. 2006. Mucosal IL-8 and TGF-β recruit blood monocytes: evidence for cross-talk between the lamina propria stroma and myeloid cells. *J Leukoc Biol,* **80,** 492-499.

SMYTHIES, L.E.; SHEN, R.; BIMCZOK, D.; et al. 2010. Inflammation anergy in human intestinal macrophages is due to Smad-induced IκBα expression and NF-κB inactivation. *J Biol Chem,* **285,** 19593-19604.

SONDI, I. & SALOPEK-SONDI, B. 2004. Silver nanoparticles as antimicrobial agent: a case study on *E. coli* as a model for Gram-negative bacteria. *J Colloid Interface Sci,* **275,** 177-182.

SONG-ZHAO, G.X.; SRINIVASAN, N.; POTT, J.; et al. 2014. Nlrp3 activation in the intestinal epithelium protects against a mucosal pathogen. *Mucosal Immunol,* **7,** 763-774.

SONG, M.F.; LI, Y.S.; KASAI, H.; et al. 2012. Metal nanoparticle-induced micronuclei and oxidative DNA damage in mice. *J Clin Biochem Nutr,* **50,** 211-216.

SONODA, N.; FURUSE, M.; SASAKI, H.; et al. 1999. *Clostridium perfringens* enterotoxin fragment removes specific claudins from tight junction strands: evidence for direct involvement of claudins in tight junction barrier. *J Cell Biol,* **147,** 195-204.

SOTO, K.; GARZA, K.M. & MURR, L.E. 2007. Cytotoxic effects of aggregated nanomaterials. *Acta Biomater,* **3,** 351-358.

SPERBER, M.; HUPF, C.; LEMBERGER, M.-M.; et al. 2015. Monitoring the impact of nanomaterials on animal cells by impedance analysis: A noninvasive, label-free, and multimodal approach. *In:* WEGENER, J. (ed.) *Measuring Biological Impacts of Nanomaterials.* Springer International Publishing Switzerland**,** 45-108.

STEBOUNOVA, L.; ADAMCAKOVA-DODD, A.; KIM, J.S.; et al. 2011. Nanosilver induces minimal lung toxicity or inflammation in a subacute murine inhalation model. *Part Fibre Toxicol,* **8,** DOI: 10.1186/1743-8977-8-5.

STEFFANSEN, B.N., CARSTEN UHD; BRODIN, BIRGER 2013. Membrane transporters in ADME. *In:* SUGIYAMA, Y.S., BENTE (ed.) *Transporters in Drug Development.* Springer Science+Business**,** 1-22.

STENSBERG, M.C.; WEI, Q.; MCLAMORE, E.S.; et al. 2011. Toxicological studies on silver nanoparticles: challenges and opportunities in assessment, monitoring and imaging. *Nanomedicine (Lond),* **6,** 879-898.

STROBER, W. & FUSS, I.J. 2011. Proinflammatory cytokines in the pathogenesis of inflammatory bowel diseases. *Gastroenterology,* **140,** 1756-1767.

STUDER, A.M.; LIMBACH, L.K.; VAN DUC, L.; et al. 2010. Nanoparticle cytotoxicity depends on intracellular solubility: comparison of stabilized copper metal and degradable copper oxide nanoparticles. *Toxicol Lett,* **197,** 169-174.

SU, X.; YU, Y.; ZHONG, Y.; et al. 2015. Interferon-γ regulates cellular metabolism and mRNA translation to potentiate macrophage activation. *Nat Immunol,* **16,** 838-849.

SUN, J.; WANG, S.; ZHAO, D.; et al. 2011. Cytotoxicity, permeability, and inflammation of metal oxide nanoparticles in human cardiac microvascular endothelial cells: cytotoxicity, permeability, and inflammation of metal oxide nanoparticles. *Cell Biol Toxicol,* **27,** 333-342.

SUN, T.; YAN, Y.; ZHAO, Y.; et al. 2012. Copper oxide nanoparticles induce autophagic cell death in A549 cells. *PLoS One,* **7,** DOI: 10.1371/journal.pone.0043442.

SUNG, J.H.; JI, J.H.; YOON, J.U.; et al. 2008. Lung function changes in Sprague-Dawley rats after prolonged inhalation exposure to silver nanoparticles. *Inhal Toxicol,* **20,** 567-574.

SUNYER, J.; SCHWARTZ, J.; TOBÍAS, A.; et al. 2000. Patients with chronic obstructive pulmonary disease are at increased risk of death associated with urban particle air Ppollution: A case-crossover analysis. *Am J Epidemiol,* **151,** 50-56.

SUSEWIND, J.; DE SOUZA CARVALHO-WODARZ, C.; REPNIK, U.; et al. 2016. A 3D co-culture of three human cell lines to model the inflamed intestinal mucosa for safety testing of nanomaterials. *Nanotoxicology,* **10,** 53-62.

SUZUKI, T.; YOSHINAGA, N. & TANABE, S. 2011. Interleukin-6 (IL-6) regulates claudin-2 expression and tight junction permeability in intestinal epithelium. *J Biol Chem,* **286,** 31263-31271.

SUZUKI, T. 2013. Regulation of intestinal epithelial permeability by tight junctions. *Cell Mol Life Sci,* **70,** 631-659.

SWEENEY, T.E. & MORTON, J.M. 2013. The Human Gut Microbiome: A review of the effect of obesity and surgically induced weight loss. *JAMA Surgery,* **148,** 563-569.

SZCZEPANIK, A.M.; FUNES, S.; PETKO, W.; et al. 2001. IL-4, IL-10 and IL-13 modulate Ab(1–42)-induced cytokine and chemokine production in primary murine microglia and a human monocyte cell line. *J Neuroimmunol,* **113,** 49-62.

TADJALI, M.; SEIDELIN, J.B.; OLSEN, J.; et al. 2002. Transcriptome changes during intestinal cell differentiation. *Biochim Biophy Acta,* **1589,** 160-167.

TAK, Y.K.; PAL, S.; NAOGHARE, P.K.; et al. 2015. Shape-dependent skin penetration of silver nanoparticles: Does it really matter? *Sci Rep,* **5,** DOI: 10.1038/srep16908

TAKASHIBA, S.; VAN DYKE, T.E.; AMAR, S.; et al. 1999. Differentiation of monocytes to macrophages primes cells for lipopolysaccharide stimulation via accumulation of cytoplasmic nuclear factor κB. *Infect Immun,* **67,** 5573-5578.

TAKENAKA, S.; KARG, E.; ROTH, C.; et al. 2001. Pulmonary and systemic distribution of inhaled ultrafine silver particles in rats. *Environ Health Persp,* **109,** 547-551.

TAMAI, R.; SUGAWARA, S.; TAKEUCHI, O.; et al. 2003. Synergistic effects of lipopolysaccharide and interferon-γ in inducing interleukin-8 production in human monocytic THP-1 cells is accompanied by up-regulation of CD14, Toll-like receptor 4, MD-2 and MyD88 expression. *J Endotoxin Res,* **9,** 145-153.

TANG, J.; XIONG, L.; WANG, S.; et al. 2008. Influence of silver nanoparticles on neurons and blood-brain barrier via subcutaneous injection in rats. *Appl Surface Sci,* **255,** 502-504.

TANOUE, T.; NISHITANI, Y.; KANAZAWA, K.; et al. 2008. *In vitro* model to estimate gut inflammation using co-cultured Caco-2 and RAW264.7 cells. *Biochem biophys Res Commun,* **374,** 565-569.

TAPIERO, H.; TOWNSEND, D.M. & TEW, K.D. 2003. Trace elements in human physiology and pathology. Copper. *Biomed Pharmacother,* **57,** 386-398.

TAYLOR, A.; WILSON, K.M.; MURRAY, P.; et al. 2012. Long-term tracking of cells using inorganic nanoparticles as contrast agents: are we there yet? *Chem Soc Rev,* **41,** 2707-2717.

TAYLOR, A.A.; MARCUS, I.M.; GUYSI, R.L.; et al. 2015. Metal oxide nanoparticles induce minimal phenotypic changes in a model colon gut microbiota. *Environ Eng Sci,* **32,** 602-612.

TAYLOR, A.J.; MCCLURE, C.D.; SHIPKOWSKI, K.A.; et al. 2014. Atomic layer deposition coating of carbon nanotubes with aluminum oxide alters pro-fibrogenic cytokine expression by human mononuclear phagocytes *in vitro* and reduces lung fibrosis in mice *in vivo*. *PLoS One,* **9,** DOI: 10.1371/journal.pone.0106870.

TEEGUARDEN, J.G.; HINDERLITER, P.M.; ORR, G.; et al. 2007. Particokinetics *in vitro*: dosimetry considerations for *in vitro* nanoparticle toxicity assessments. *Toxicol Sci,* **95,** 300-312.

TEJAMAYA, M.; ROMER, I.; MERRIFIELD, R.C.; et al. 2012. Stability of citrate, PVP, and PEG coated silver nanoparticles in ecotoxicology media. *Environ Sci Technol,* **46,** 7011-7017.

TENZER, S.; DOCTER, D.; KUHAREV, J.; et al. 2013. Rapid formation of plasma protein corona critically affects nanoparticle pathophysiology. *Nat Nanotechnol,* **8,** 772-781.

THIT, A.; SELCK, H. & BJERREGAARD, H.F. 2013. Toxicity of CuO nanoparticles and Cu ions to tight epithelial cells from *Xenopus laevis* (A6): effects on proliferation, cell cycle progression and cell death. *Toxicol In Vitro,* **27,** 1596-1601.

TOUNEKTI, O.; BELEHRADEK, J. & MIR, L.M. 1995. Relationships between DNA fragmentation, chromatin condensation, and changes in flow cytometry profiles detected during apoptosis. *Exp Cell Res,* **217,** 506-516.

TRIBOULET, S.; AUDE-GARCIA, C.; CARRIÈRE, M.; et al. 2013. Molecular responses of mouse macrophages to copper and copper oxide nanoparticles inferred from proteomic snalyses. *Mol Cell Proteomics,* **12,** 3108-3122.

TRIBOULET, S.; AUDE-GARCIA, C.; ARMAND, L.; et al. 2015. Comparative proteomic analysis of the molecular responses of mouse macrophages to titanium dioxide and copper oxide nanoparticles unravels some toxic mechanisms for copper oxide nanoparticles in macrophages. *PLoS One,* **10,** DOI: 10.1371/journal.pone.0124496.

TSUCHIYA, M.S.Y.; YAMAGUCHI, Y.; KOBAYASHI, Y.; et al. 1980. Establishment and characterization of a human acute monocytic leukemia cell line (THP-1). *Int J Cancer,* **26,** 171-176.

TSUCHIYA, S.Y; KOBAYASHI, Y.; GOTO, Y.; et al. 1982. Induction of maturation in cultured human monocytic leukemia cells by a phorbol diester. *Cancer Research,* **42,** 1530-1536.

TURNER, J.R.; RILL, B.K.; CARLSON, S.L.; et al. 1997. Physiological regulation of epithelial tight junctions is associated with myosin light-chain phosphorylation. *Am J Physiol,* **273,** C1378-C1385.

TYAGI, P.K.; MISHRA, M.; KHAN, N.; et al. 2016. Toxicological study of silver nanoparticles on gut microbial community probiotic. *Environmental Nanotechnology, Monitoring & Management,* **5,** 36-43.

ULLUWISHEWA, D.; ANDERSON, R.C.; MCNABB, W.C.; et al. 2011. Regulation of tight junction permeability by intestinal bacteria and dietary components. *J Nutr,* **141,** 769-776.

UMEDA, K.; MATSUI, T.; NAKAYAMA, M.; et al. 2004. Establishment and characterization of cultured epithelial cells lacking expression of ZO-1. *J Biol Chem,* **279,** 44785-44794.

UMEDA, K.; IKENOUCHI, J.; KATAHIRA-TAYAMA, S.; et al. 2006. ZO-1 and ZO-2 independently determine where claudins are polymerized in tight-junction strand formation. *Cell,* **126,** 741-754.

UNNO, N.; MENCONI, M.; SMITH, M.; et al. 1995. Nitric oxide mediates interferon-gamma-induced hyperpermeability in cultured human intestinal epithelial monolayers. *Crit Care Med,* **23,** 1170-1176.

URBÁN, P. unpublished. Cell surface increase after exposure to cytotoxic concentrations of AgNPs - quantification using the InCell Analyzer.

VAN DE WALLE, J.; HENDRICKX, A.; ROMIER, B.; et al. 2010. Inflammatory parameters in Caco-2 cells: effect of stimuli nature, concentration, combination and cell differentiation. *Toxicol In Vitro,* **24,** 1441-1449.

VAN DEN BERGHE, P.V. & KLOMP, L.W. 2009. New developments in the regulation of intestinal copper absorption. *Nutr Rev,* **67,** 658-672.

VAN DER BRUGGEN, T.; NIJENHUIS, S.; VAN RAAIJ, E.; et al. 1999. Lipopolysaccharide-induced tumor necrosis factor alpha production by human monocytes involves the Raf-1/MEK1-MEK2/ERK1-ERK2 pathway. *Infection and immunity,* **67,** 3824-3829.

VAN DER ZANDE, M.; VANDEBRIEL, R.J.; VAN DOREN, E.; et al. 2012. Distribution, elimination, and toxicity of silver nanoparticles and silver ions in rats after 28-day oral exposure. *ACS Nano,* **6,** 7427-7442.

VAN ELBURG, R.M.; UIL, J.J.; MULDER, C.J.; et al. 1993. Intestinal permeability in patients with coeliac disease and relatives of patients with coeliac disease. *Gut,* **34,** 354-357.

VAN ES, J.H.; JAY, P.; GREGORIEFF, A.; et al. 2005. Wnt signalling induces maturation of Paneth cells in intestinal crypts. *Nat Cell Biol,* **7,** 381-386.

VAN ITALLIE, C.M. & ANDERSON, J.M. 2014. Architecture of tight junctions and principles of molecular composition. *Semin Cell Dev Biol,* **36,** 157-165.

VAN MEER, G. & SIMONS, K. 1986. The function of tight junctions in maintaining differences in lipid composition between the apical and the basolateral cell surface domains of MDCK cells. *EMBO J,* **5,** 1455-1464.

VANDEN BERGHE, T.; VANLANGENAKKER, N.; PARTHOENS, E.; et al. 2010. Necroptosis, necrosis and secondary necrosis converge on similar cellular disintegration features. *Cell Death Differ,* **17,** 922-930.

VANDERROOST, M.; RAGAERT, P.; DEVLIEGHERE, F.; et al. 2014. Intelligent food packaging: The next generation. *Trends Food Sci Tech,* **39,** 47-62.

VIGNOLI, A.L.; SCRIVASTAVA, R.C.; STAMMATI, A.; et al. 2001. Nitric oxide production in Caco-2 cells exposed to different inducers, inhibitors and natural toxins. *Toxicol In Vitro,* **15,** 289-295.

VISSER, J.T.; LAMMERS, K.; HOOGENDIJK, A.; et al. 2010. Restoration of impaired intestinal barrier function by the hydrolysed casein diet contributes to the prevention of type 1 diabetes in the diabetes-prone BioBreeding rat. *Diabetologia,* **53,** 2621-2628.

VON GOETZ, N.; FABRICIUS, L.; GLAUS, R.; et al. 2013. Migration of silver from commercial plastic food containers and implications for consumer exposure assessment. *Food Addit Contam Part A Chem Anal Control Expo Risk Assess,* **30,** 612-620.

WALCZAK, A.P.; KRAMER, E.; HENDRIKSEN, P.J.; et al. 2015. Translocation of differently sized and charged polystyrene nanoparticles in *in vitro* intestinal cell models of increasing complexity. *Nanotoxicology,* **9,** 453-461.

WANG, F.; GRAHAM, W.V.; WANG, Y.; et al. 2005. Interferon-γ and tumor necrosis factor-α synergize to induce intestinal epithelial barrier dysfunction by up-regulating myosin light chain kinase expression. *Am J Pathol,* **166,** 409-419.

WANG, F.; SCHWARZ, B.T.; GRAHAM, W.V.; et al. 2006. IFN-γ-induced TNFR2 upregulation is required for TNF-dependent intestinal epithelial barrier dysfunction. *Gastroenterol,* **131,** 1153-1163.

WANG, L.; NAGESHA, D.K.; SELVARASAH, S.; et al. 2008a. Toxicity of CdSe nanoparticles in Caco-2 cell cultures. *J Nanobiotechnology,* **6,** DOI: 10.1186/1477-3155-6-11.

WANG, N.; LIANG, H. & ZEN, K. 2014. Molecular mechanisms that influence the macrophage m1-m2 polarization balance. *Front Immunol,* **5,** DOI: 10.3389/fimmu.2014.00614.

WANG, Y.Y.; LAI, S.K.; SUK, J.S.; et al. 2008b. Addressing the PEG mucoadhesivity paradox to engineer nanoparticles that "slip" through the human mucus barrier. *Angew Chem Int Ed Engl,* **47,** 9726-9729.

WANG, Z.; LI, N.; ZHAO, J.; et al. 2012. CuO nanoparticle interaction with human epithelial cells: cellular uptake, location, export, and genotoxicity. *Chem Res Toxicol,* **25,** 1512-1521.

WATANABE, F.; SATSU, H.; MOCHIZUKI, T.; et al. 2004. Development of the method for evaluating protective effect of food factors on THP-1-induced damage to human intestinal Caco-2 monolayers. *BioFactors,* **21,** 145-147.

WATSON, C.J.; ROWLAND, M. & WARHURST, G. 2001. Functional modeling of tight junctions in intestnal cell monolayers using polyethylene glycol oligomers. *Am J Physiol - Cell Physiol,* **281,** C388-C397.

WEBER, C.R.; NALLE, S.C.; TRETIAKOVA, M.; et al. 2008. Claudin-1 and claudin-2 expression is elevated in inflammatory bowel disease and may contribute to early neoplastic transformation. *Lab Invest,* **88,** 1110-1120.

WEINBERG, J.B. 1998. Nitric oxide production and nitric oxide synthase type 2 expression by human mononuclear phagocytes: A review. *Mol Med,* **4,** 557-591.

WEIR, A.; WESTERHOFF, P.; FABRICIUS, L.; et al. 2012. Titanium dioxide nanoparticles in food and personal care products. *Environ Sci Technol,* **46,** 2242-2250.

WELLS, C.L.; JECHOREK, R.P.; OLMSTED, S.B.; et al. 1993. Effect of LPS on epithelial integrity and bacterial uptake in the polarized human enterocyte-like cell line Caco-2. *Circ Shock,* **40,** 276-288.

WHITNEY, E. & RADY ROLFES, S. 2008. Digestion, absorption, and transport. *In*: *Understanding Nutrition.* Thomson Learning Inc.**,** 70-99.

WIKMAN-LARHED, A. & ARTURSSON, P. 1995. Co-cultures of human intestinal goblet (HT29-H) and absorptive (Caco-2) cells for studies of drug and peptide absorption. *Eur J Pharm Sci,* **3,** 171-183.

WILDING, L.A.; BASSIS, C.M.; WALACAVAGE, K.; et al. 2016. Repeated dose (28-day) administration of silver nanoparticles of varied size and coating does not significantly alter the indigenous murine gut microbiome. *Nanotoxicology,* **10,** 513-520.

WILLIAMS, K.; MILNER, J.; BOUDREAU, M.D.; et al. 2015. Effects of subchronic exposure of silver nanoparticles on intestinal microbiota and gut-associated immune responses in the ileum of Sprague-Dawley rats. *Nanotoxicology,* **9,** 279-289.

WIN, K.Y. & FENG, S.S. 2005. Effects of particle size and surface coating on cellular uptake of polymeric nanoparticles for oral delivery of anticancer drugs. *Biomaterials,* **26,** 2713-2722.

WINTER, S.E.; WINTER, M.G.; XAVIER, M.N.; et al. 2013. Host-derived nitrate boosts growth of *E. coli* in the inflamed gut. *Science,* **339,** 708-711.

WIRTZ, S.; NEUFERT, C.; WEIGMANN, B.; et al. 2007. Chemically induced mouse models of intestinal inflammation. *Nat Protoc,* **2,** 541-246.

WONG, K.K.Y.; CHEUNG, S.O.F.; HUANG, L.; et al. 2009. Further evidence of the anti-inflammatory effects of silver nanoparticles. *ChemMedChem,* **4,** 1129-1135.

WOTTRICH, R.; DIABATE, S. & KRUG, H.F. 2004. Biological effects of ultrafine model particles in human macrophages and epithelial cells in mono- and co-culture. *Int J Hyg Environ Health,* **207,** 353-361.

WRIGHT, S.D.; RAMOS, R.A.; TOBIAS, P.S.; et al. 1990. CD14, a receptor for complexes of lipopolysaccharide (LPS) and LPS binding protein. *Science,* **249**, 1431-1433.

XIA, T.; HAMILTON, R.F.; BONNER, J.C.; et al. 2013. Interlaboratory evaluation of *in vitro* cytotoxicity and inflammatory responses to engineered nanomaterials: the NIEHS Nano GO Consortium. *Environ Health Perspect,* **121,** 683-690.

XIU, Z.M.; ZHANG, Q.B.; PUPPALA, H.L.; et al. 2012. Negligible particle-specific antibacterial activity of silver nanoparticles. *Nano Lett,* **12,** 4271-4275.

XU, D.-Z.; LU, Q. & DEITCH, E.A. 2002. Nitric oxide directly impairs intestinal barrier function. *Shock,* **17,** 139-145.

XUE, Y.; ZHANG, S.; HUANG, Y.; et al. 2012. Acute toxic effects and gender-related biokinetics of silver nanoparticles following an intravenous injection in mice. *J Appl Toxicol,* **32,** 890-899.

XUE, Y.; ZHANG, T.; ZHANG, B.; et al. 2016. Cytotoxicity and apoptosis induced by silver nanoparticles in human liver HepG2 cells in different dispersion media. *J Appl Toxicol,* **36,** 352-360.

YAMASAKI, Y.C.N.; ZENG, X.-T.; OHMURA, M.; et al. 1999. Induction of cytokines in a human colon epithelial cell line by *Shiga* toxin 1 (Stx1) and Stx2 but not by non-toxic mutant Stx1 which lacks *N*-glycosidase activity. *FEBS Letters,* **442,** 231-234.

YAMAURA, Y.; CHAPRON, B.D.; WANG, Z.; et al. 2016. Functional comparison of human colonic carcinoma cell lines and primary small intestinal epithelial cells for investigations of intestinal drug permeability and first-pass metabolism. *Drug Metab Dispos,* **44,** 329-335.

YANG, E.J.; KIM, S.; KIM, J.S.; et al. 2012. Inflammasome formation and IL-1β release by human blood monocytes in response to silver nanoparticles. *Biomaterials,* **33,** 6858-6867.

YANG, L.; SUNDARESAN, G.; SUN, M.; et al. 2013. Intrinsically radiolabeled multifunctional cerium oxide nanoparticles for *in vivo* studies. *J Mater Chem B,* **1,** 1421-1431.

YANG, Y.; JIANG, G.; ZHANG, P.; et al. 2015. Programmed cell death and its role in inflammation. *Mil Med Res,* **2,** DOI: 10.1186/s40779-015-0039-0.

YANG, Y.; FAUST, J.J.; SCHOEPF, J.; et al. 2016. Survey of food-grade silica dioxide nanomaterial occurrence, characterization, human gut impacts and fate across its lifecycle. *Sci Total Environ,* **565,** 902-912.

YEN, H.-J.; HSU, S.-H. & TSAI, C.-L. 2009. Cytotoxicity and immunological response of gold and silver nanoparticles of different sizes. *Small,* **5,** 1553-1561.

YU, A.S.; CHENG, M.H.; ANGELOW, S.; et al. 2009. Molecular basis for cation selectivity in claudin-2-based paracellular pores: identification of an electrostatic interaction site. *J Gen Physiol,* **133,** 111-127.

YU, L.C.; FLYNN, A.N.; TURNER, J.R.; et al. 2005. SGLT-1-mediated glucose uptake protects intestinal epithelial cells against LPS-induced apoptosis and barrier defects: a novel cellular rescue mechanism? *FASEB J,* **19,** 1822-1835.

ZAREMBER, K.A. & GODOWSKI, P.J. 2002. Tissue expression of human Toll-like receptors and differential regulation of Toll-like receptor mRNAs in leukocytes in response to microbes, their products, and cytokines. *J Immunol,* **168,** 554-561.

ZEIDLER, D.; ZAHRINGER, U.; GERBER, I.; et al. 2004. Innate immunity in *Arabidopsis thaliana*: lipopolysaccharides activate nitric oxide synthase (NOS) and induce defense genes. *PNAS,* **101,** 15811-15816.

ZEISSIG, S.; BÜRGEL, N.; GÜNZEL, D.; et al. 2007. Changes in expression and distribution of claudin 2, 5 and 8 lead to discontinuous tight junctions and barrier dysfunction in active Crohn's disease *Gut,* **56,** 61-72.

ZHANG, G.; ZHANG, H.; LIU, Y.; et al. 2014. CD44 clustering is involved in monocyte differentiation. *Acta Biochim Biophys Sinica,* **46,** 540-547.

ZHANG, J.M. & AN, J. 2007. Cytokines, inflammation, and pain. *Int Anesthesiol Clin,* **45,** 27-37.

ZHOU, J.; ZHU, P.; JIANG, J.L.; et al. 2005. Involvement of CD147 in overexpression of MMP-2 and MMP-9 and enhancement of invasive potential of PMA-differentiated THP-1. *BMC cell biology,* **6,** DOI: 10.1186/1471-2121-6-25.